Freie Universität Berlin
Institute for Chemistry and Biochemistry
Physical & Theoretical Chemistry

Reweighting methods for Molecular Dynamics

Inaugural-Dissertation
to obtain the academic degree
Doctor rerum naturalium (Dr. rer. nat.)
submitted to the Department of Biology, Chemistry and Pharmacy
of Freie Universität Berlin

Luca Donati

First Supervisor:
Prof. Dr. Bettina Keller

Second supervisor:
PD Dr. Marcus Weber

October, 2018

- **First reviewer:**
  Prof. Dr. Bettina G. Keller
  Department of Biology, Chemistry and Pharmacy
  Physical & Theoretical Chemistry
  Frëie Universität Berlin
  Takustraße 3, 14915 Berlin

- **Second reviewer:**
  PD Dr. Marcus Weber
  Computational Molecular Design
  Zuse Institute Berlin (ZIB)
  Takustraße 7, 14915 Berlin

Date of defence: 18.04.2019

List of publications

- L. Donati, C. Hartmann and B. G. Keller, "Girsanov reweighting for path ensembles and Markov state models." *J. Chem. Phys.*, **146** (2017), p. 244112. Included in Chapter 5 of this thesis.
- I. Hassan, L. Donati, B. G. Keller, T. Stensitzk, K. Heyne and P.Imhof "The vibrationalspectrum of the hydrated alanine-leucine peptide in the amide region from ir experiments and first principles calculations." *Chem. Phys. Lett.*, **698** (2018), p. 227. Included in Chapter 4 of this thesis.
- J. Quer, L. Donati, B. G. Keller and M. Weber "An automatic adaptive importance sampling algorithm for molecular dynamics in reaction coordinates." *SIAM J. Sci. Comput.*, **40** (2018), p. A653. Included in Chapter 7 of this thesis.
- L. Donati and B. G. Keller, "Girsanov reweighting for metadynamics simulations." *J. Chem. Phys.*, **149** (2018), p. 072335. Included in Chapter 6 of this thesis.
- L. Donati, M. Heida, B. G. Keller and M. Weber "Estimation of the infinitesimal generator by square-root approximation." *J. Phys. Condens. Matter*, accepted, online 7 september 2018. Included in Chapter 8 of this thesis.
- B. G. Keller, S. Aleksic and L. Donati, "Markov State Models in drug design." In F. L. Gervasio, editor, *Biomolecular Simulations in Structure-based Drug Discovery*, Wiley-VCH, Weinheim (2018), p. 67. Included in Chapter 3 of this thesis.

Contribution to the publications: A description of my contribution to these publications is provided in the preface to the respective chapters.

Zusammenfassung

Eine effiziente Untersuchung solchen Verhaltens ist notwendig, um die Natur von Molekülen besser zu verstehen und die Voraussagbarkeit von Moleküldynamik (MD) Simulationen zu verbessern. In dieser Arbeit schlagen wir ein Umgewichtungs-Schema für Markov Modelle (MSMs) basierend auf dem Girsanov Theorem vor, das es erlaubt, die Rechenkosten der Analyse zu reduzieren, wenn die potentiellen Energie eines Moleküls gestört wird. Die Methode wurde erfolgreich für Metadynamik erweitert und implementiert, um das MSM eines molekularen Systems in einer deutlich kürzeren Rechenzeit im Vergleich zu einer standardisierten MD-Simulation zu erstellen. Wir schlagen auch eine neue Methode zur Diskretisierung des infinitesimalen Generators in eine Ratenmatrix vor, die auch zur effizienten Untersuchung von Hamiltonschen Störungen verwendet werden könnte.

Abstract

The dynamical response of molecular systems, when the potential energy function is perturbed at a microscopic level, is difficult to predict without a numerical or laboratory experiment. This is due to the non-linearity and high-dimensionality of molecular systems. An efficient investigation of such a behaviour is necessary to better understand the nature of molecules and to improve the predictability of Molecular Dynamics simulations. In this thesis we propose a reweighting scheme for Markov State Models (MSMs), based on the Girsanov theorem, that permits to reduce the computational cost of the analysis when the potential energy function of a molecule is perturbed. The method has been successfully extended and implemented with metadynamics, in order to build the MSM of a molecular system in a significantly shorter computational time compared to a standard unbiased MD simulation. We also propose a new method to discretize the infinitesimal generator into a rate matrix, that could be used to efficiently study Hamiltonian perturbations as well.

Acknowledgements

I'm really grateful to my supervisor Prof. Bettina Keller for giving me the opportunity to conduct my doctoral studies in her group and to do high level original scientific research. She first introduced me to Molecular Dynamics and Markov State Models, proposing to me to work on a challenging project in an interdisciplinary field that embraces Chemistry, Physics and Mathematics. She has taught me how to do research, to be creative in the development of new ideas and to always evaluate with a critical eye the results. She always had time to discuss my work, to answer my questions, giving me motivation when difficulties arose.

Next I would like to thank PD. Dr. Marcus Weber for having hosted me at Zuse Institute Berlin in autumn 2016, for having clarified me many theoretical aspects of my project and for having inspired me to pursue also new directions in my PhD studies.

I would like to thank Prof. Castern Hartmann, who initially suggested to me to work on the Girsanov theorem and gave a constant support explaining me the underlying theory.

I would like to thank all the people of the Collaborative Research Centre 1114 for the interesting workshops, the seminars and the scientific discussions. In particular Prof. Petra Imhof, Dr. Martin Heida, Irtaza Hassan and Janner Quer for the collaborations that have produced important results.

I would like to thank the former and present members of the group, in particular Francesca, Stevan and Oliver for the helpful discussions and suggestions.

A special thanks goes to all the friends that I met in Berlin in these four years, but also to my friends from Italy who always supported me.

Last but not the least, I would like to thank my family: my parents and my aunts, who raised me with a love of science and for the encouragement they have given me in these years and in my life. I could not have done it without them.

Contents

Chapter 1

Introduction

Motivation In the last decades, classical Molecular Dynamics (MD) simulations [1, 2] became a fundamental tool for the study of biomolecules, like proteins and RNA/DNA molecules. The general idea is to model a molecule like a system of particles, governed by the Newton's equations of motion, whose reciprocal interactions are approximated by an analytic potential energy function, parametrized in a text file commonly referred to as forcefield. To perform an MD simulation means to solve numerically the equations of motion and to produce a time-discretized molecular trajectory that describes the time evolution of the positions of the atoms in space.

A trajectory can be used to understand several molecular processes, e.g. protein folding processes or the interactions between molecules like ligands and protein [3, 4, 5]. Often MD simulations are used to sample the stationary distribution of molecules and to estimate phase-space ensemble averages of observable functions.

Due to the high-dimensionality and the complexity of the system, molecules are particularly sensitive to external perturbations of the potential energy function. Even a slight modification of the forcefield can have huge consequences on the dynamics of the system, this makes impossible to predict in advance which could be the effect of an arbitrary perturbation.

The high sensitivity and unpredictability of molecular systems has been confirmed also experimentally. There exist indeed several forcefields, for the same molecule, built on the basis of different initial hypotheses or different approximations, which exhibit different dynamical behaviours [6].

Thus, the following questions arise: What is the intrinsic origin of such different dynamic effects? Which components of the forcefield have the largest impact on the dynamics of the molecules? How can we improve the forcefields in order to successfully predict the dynamics of a molecule? But overall, how can we investigate efficiently the differences between similar forcefields?

A naive approach, to study the effect of a modification of the potential energy function, would be to manually edit the file that parametrizes the forcefield, to run an MD simulation and to analyze the new trajectory. On the other hand this approach is time consuming and computationally expensive. Indeed, every time that one desires to study a different modification, one should perform a new simulation.

The aim of this thesis is to present and to discuss new efficient tools, developed in the last years, that could help the scientific community to answer the posed questions.

Markov State Models Although MD simulations are a valid support to laboratory experiments for the investigation of biomolecules, their use is still limited by the com-

putational cost necessary to obtain a long enough trajectory, that well represents the dynamics of the molecule. The transition between conformations can be a very fast or a very slow process, due to the high barriers of the potential energy function that slows the exploration of the phase space. For example, fast oscillations of covalent bonds occur on timescales of femtoseconds, while conformational changes, like slow folding processes, can occur even at timescales of microseconds or milliseconds [7].

Observing rare transitions, can require to run an MD simulation for a long time, causing a sharp growth of the computational cost. For example, the supercomputer Anton [8], specialized in MD simulations, can generate a trajectory of 10 μs of a large protein per day (more than 20,000 atoms, in explicit solvent), then almost three months are necessary to produce a trajectory of 1 ms. Fig. 1.1 shows the unfolding-folding process of the protein gpW realized with Anton [9], that takes about 50 μs, corresponding to approximately 5 days of simulation. In conclusion, MD simulations need very high-efficient computers to capture the slowest timescales that are the most interesting from a biological point of view.

A different approach has been developed in the last years that does not consider only single long trajectories, but ensembles of short trajectories and studies the dynamics of molecules from a statistical point of view. This approach is based on the concept of the propagator [10, 11, 12, 13, 14], a continuous operator that propagates forward in time probability density functions. Because it is not possible to work with a high-dimensional continuous operator, typically, after having discretized the state space in disjoint microsets, one tries to discretize the operator into a matrix on few relevant degrees of freedom. Markov State Models (MSMs) [12, 15, 16, 17, 18, 13, 19, 20, 21] provide a simplified model of the dynamics, easy to build and that uses MD trajectories in a more proficient manner. This tool permits to discretize the propagator in a transition probability matrix, whose elements are estimated as time-lagged correlation functions from MD simulations.

Coming back to the earlier questions, MSMs have been successfully used to analyze the dynamics of molecules [22, 23, 24, 25, 26, 27]. On the other hand, MD simulations are always necessary to build a MSM. If one desires to study the perturbation of a potential energy function through MSM, one cannot avoid to perform an MD simulation with the modified forcefield.

This is the main contribution of this thesis. We discuss a reweighting scheme for MSMs, where the MSM of a biased system is built from the trajectory produced by an unbiased MD simulation.

Dynamical reweighting: state of the art In MD there exist several reweighting schemes for different problems and applications.

Statistical reweighting methods try to recover the correct stationary distribution or the free energy profile of a molecular system from a MD trajectory produced by a biased simulation. For example, weighted histogram analysis method (WHAM) [28] is used when parallel simulations are perturbed by different biases at the same time, like in umbrella sampling [29, 30, 31].

Dynamical reweighting methods attempt to recover the correct information about the dynamics, for example the transition probabilities or the transition rates, from biased simulations as well. On the other hand, dynamical reweighting methods encounter more difficulties and their application is limited to special cases. Schemes for parallel tempering MD simulations [32, 33, 34], can be used to construct the MSM of a biomolecular system, by optimizing the data from MD simulations realized at temperatures different from the

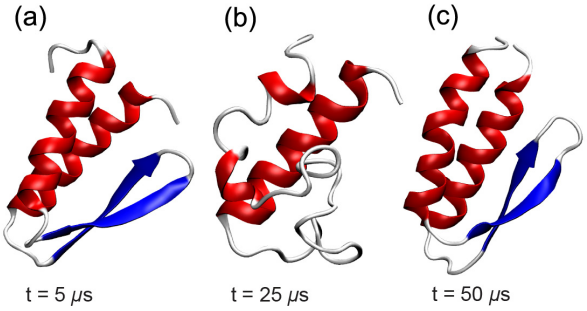

Figure 1.1: Unfolding-folding event of the protein gpW realized with the supercomputer Anton. (A) Folded structure at the beginning of the process. (B) Unfolded structure during the process. (C) Folded structure at the end of the process. Figure taken from reference [9].

environmental one. These schemes imply a reweighting along the time discretized paths, however cannot be extended to the limiting case of continuous paths.

In reference [35, 36], the authors propose a method to recover the rates of transitions between different metastable states in metadynamics simulations, where the Hamiltonian is biased by a time dependent sum of Gaussian functions estimated for few relevant coordinates. The correct escape rate for the unbiased system can be determined from the acceleration given by the bias. On the other hand, the method assumes that no bias is deposited over the transition states, thus the metadynamics potential does not converge to the free energy profile.

Discrete transition-based reweighting analysis method (dTRAM) [37, 38, 39] permits to recover the MSMs of systems subjected to thermostatic and Hamiltonian perturbations, by assuming local equilibrium of the microstates. The reweighiting is performed directly to the transition probabilities, thus it is extremely sensitive to large biasing potentials.

Girsanov reweighting To overcome all these problems and limitations, we have developed a new method [40, 41], based on the Girsanov theorem [42], that permits a correct reweighting of path ensemble averages like the time-lagged correlation functions used to build MSMs. Thus, we need only a simulation, at a single potential energy function, to build different MSMs for several perturbations of the original forcefield, reducing the computational cost and time. The advantage of the method, compared to the above-mentioned, is that we do not need to assume local equilibrium nor we have problems in the limit of continuous paths.

In our experience, the method has shown potentiality also in other research areas. For example, Girsanov reweighting could be useful in combination with enhanced sampling techniques [43, 44, 45, 46, 29], where the potential energy function of a system is perturbed along few relevant coordinates, in order to fill the metastable regions and to facilitate the exploration of the phase space. To test our hypothesis, we have considered metadynamics simulations, which cannot be used directly to build MSMs, because the bias affects significantly the dynamics of the system. Girsanov reweighting, together with metadynamics, permits to recover the proper MSM of the unbiased system, reducing the time necessary to sample the phase space and the rare transitions between metastable

states.

The infinitesimal generator approach Associated to the propagator and the transition probability matrix already mentioned, exist respectively the infinitesimal generator and the rate matrix, which describe the dynamics in terms of transition rates. However, the discretization of the infinitesimal generator is more difficult. We present a new method, named Square Root Approximation (SQRA), which approximates the rates between adjacent microsets as the geometric average of the Boltzmann weight of the microsets. In this way, we provide an algebraic relation between the potential energy function and the rate matrix. The advantage compared to MSMs is that we do not need any more to calculate time-lagged correlation functions.

This method is still at an early stage of development, but a reweighting scheme can be implemented, properly handling the Boltzmann weights of the microsets. Thus, we believe that also SQRA could be helpful to answer the initial posed questions.

Figure 1.2 gives an overview of the methods used and developed in this thesis.

1.1 Outline

The thesis is organized as follows:

- Chapter 2: the main equations of motion used to study molecular dynamics are presented. Afterward the propagator, the closely related transfer operator and MSMs are discussed. Finally the chapter recalls the main steps to derive the Girsanov reweighting and the Square Root Approximation.

- Chapter 3: In the first part, a general introduction to MSMs is given. Then, some useful applications of MSMs in drug design are discussed.

- Chapter 4: MSMs are used in combination with ab-initio simulation, in order to show the high versatility of the method, that is not limited to classical MD simulations.

- Chapter 5: The Girsanov reweighting paper, which treats in detail the method and describes the first results for full atomistic simulations, is presented.

- Chapter 6: Girsanov reweighting is used together with metadynamics and MSMs, exploiting all the advantages offered by these methods.

- Chapter 7: A new algorithm, based on the Girsanov theorem and metadynamics, is used to calculate dynamical estimators with a significant variance reduction compared of the numerical simulation.

- Chapter 8: The theory underlying SQRA and first results for diffusion processes and the Alanine dipeptide is presented.

- Chapter 9: The conclusions of the thesis are drawn and interesting insights for future works are discussed.

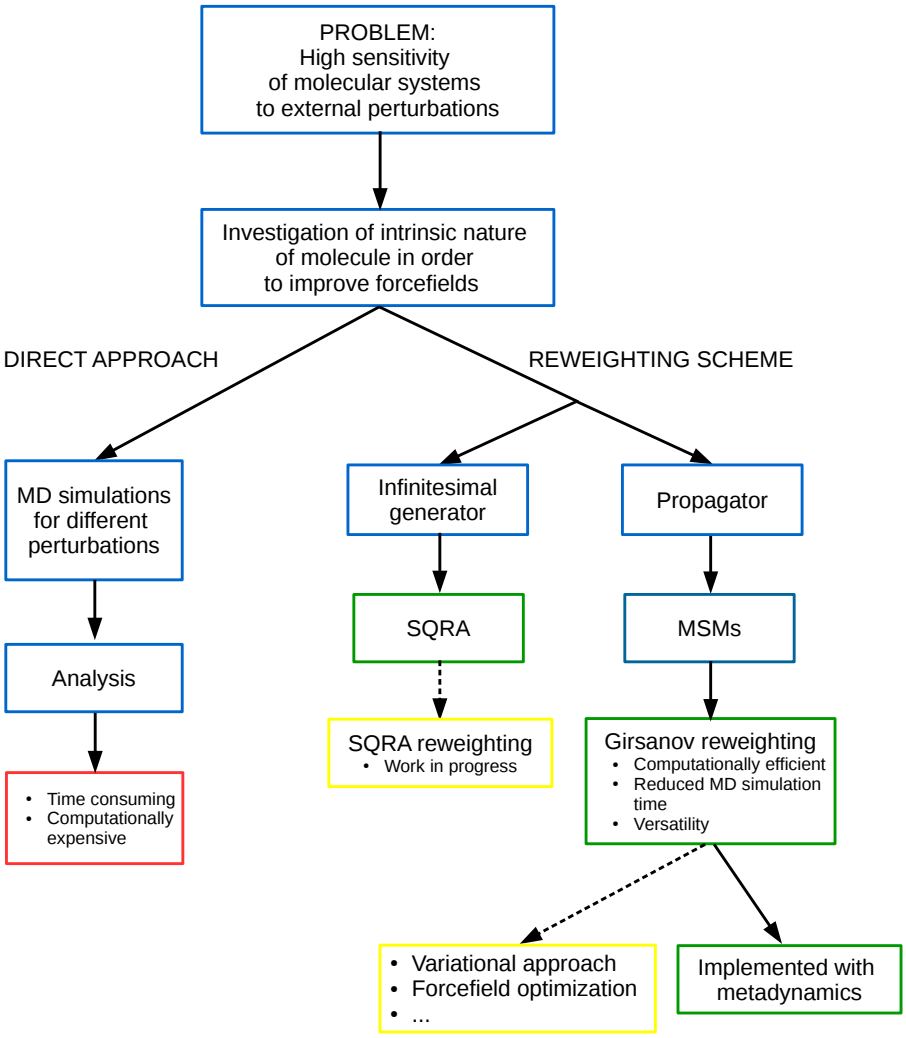

Figure 1.2: Summary of the thesis.

Chapter 2

Theory

2.1 The physical model

Consider a molecular system of N atoms, governed by the equations of motion:

$$\begin{aligned} \dot{q} &= M^{-1}p \\ \dot{p} &= -\nabla V(q) - \gamma(q,p)p + F_{ext}\,, \end{aligned} \tag{2.1}$$

where q and p denote respectively the position and the momentum of the atoms of the system, M is a diagonal matrix $N \times N$, whose entries are the masses of the atoms, $V(q)$ is the potential energy function that governs the interaction between the atoms, $\gamma(q,p)$ is the friction and F_{ext} is any external force acting on the system. The state of the system at time t is represented by $\mathbf{x}(t) = \{q(t), p(t)\} \in \Gamma \subset \mathbf{R}^{6N}$, where Γ is the phase space and can be decomposed in its position and momentum space $\Gamma_q \times \Gamma_p = \Gamma$. The classical Hamiltonian function

$$\mathcal{H}(\mathbf{x}) = H(q,p) = \frac{1}{2}p^T M^{-1} p + V(q) \tag{2.2}$$

is the internal energy of the system. In general, γ and F_{ext} rule the interaction of the system with a thermostat, i.e. a heat bath that keeps the system at constant temperature and at constant volume or pressure. If the thermostat is deterministic, the equation of motion models a *Hamiltonian dynamics* and the internal energy is conserved. For example, the Nosé Hoover thermostat [47, 48, 49] introduces an additional mass, which interacts with the system, simulating a kinetic exchange with a heat bath. If the thermostat is stochastic, the equation of motion models a *Langevin dynamics* and the internal energy is not preserved.

We are interested in experiments performed at constant temperature and volume, thus the system can exchange energy with a thermal bath, but cannot exchange particles. The states that satisfy these conditions, compose the *canonical ensemble* (NVT), characterized by a unique stationary distribution described by the function:

$$\mu_\pi(\mathbf{x}) = \frac{\exp\left(-\beta\mathcal{H}(\mathbf{x})\right)}{Z}\,, \qquad Z = \int_\Gamma \exp\left(-\beta\mathcal{H}(\mathbf{x})\right)\,\mathrm{d}\mathbf{x}\,, \tag{2.3}$$

where $\beta = \frac{1}{k_B T}$, k_B is the Boltzmann's constant, T is the temperature and Z is the canonical partition function. $\mu_\pi(\mathbf{x})$ is a probability density function and defines the probability measure on subsets A of the state space:

$$\pi(A) = \int_A \mu_\pi(\mathbf{x})\,\mathrm{d}\mathbf{x}\,, \quad \forall A \subset \Gamma\,, \tag{2.4}$$

with $\pi(\Gamma) = 1$.

A different approach to study the dynamics of molecular systems, is to consider ensembles of trajectories in the phase space and to study the time evolution of probability density functions $\rho_t(\mathbf{x})$, that denote with which probability the system assumes the state $\mathbf{x}$ at time t. The time evolution of the probability density $\rho_t(\mathbf{x})$ is governed by a continuous operator, called *propagator* $\mathcal{P}(\tau)$, which propagates the probability density from time t to time $t + \tau$. However, depending on the choice of the dynamics the operator $\mathcal{P}(\tau)$ satisfies different properties.

Our aim is to build an operator that well represents an experiment performed under the canonical ensemble conditions (NVT) and that can be discretized in a transition probability matrix, whose entries can be efficiently estimated.

As we will see in the next sections, the dynamics of the process $\mathbf{x}(t)$ should be *Markovian*, *time-homogeneous*, *ergodic* and *reversible*. In this case the propagator has a unique invariant measure, with eigenvalues real, positive and discrete. Moreover, under these conditions, the propagator can be transformed in the transfer operator $\mathcal{T}(\tau)$, which can be easily discretized into a transition probability matrix $\mathbf{T}(\tau)$, whose matrix elements $T_{ij}(\tau)$ can be numerically estimated as time-lagged cross-correlation functions.

In the next sections, we will see which is the best dynamics to obtain the desired properties of the propagator $\mathcal{P}(\tau)$ and how we can derive the transfer operator.

2.2 Hamiltonian dynamics

Consider the case with no friction and no external forces acting on the system, then $\gamma(q, p) = 0$ and $F_{ext} = 0$ in eq. 2.1, then the dynamics of the system is exactly described by the Hamilton's equations of motion [50]:

$$\begin{aligned} \dot{q} &= \frac{\partial H}{\partial p} = M^{-1} p \\ \dot{p} &= -\frac{\partial H}{\partial q} = -\nabla V(q) \end{aligned} \tag{2.5}$$

and the internal energy (eq. 2.2) is a conserved quantity.

The Liouville theorem states that, given the Hamilton's equations (eq. 2.5), then the probability density is locally conserved, i.e. it satisfies the continuity equation[50, 51]:

$$\frac{\partial \rho_t(\mathbf{x})}{\partial t} + \nabla_{\mathbf{x}}(\rho_t \dot{\mathbf{x}}) = 0\,, \tag{2.6}$$

Inserting eq. 2.5 in eq. 2.6, we obtain the Liouville equation [1] [50, 52]:

$$\begin{aligned} \frac{\partial \rho_t(\mathbf{x})}{\partial t} &= \sum_{i=1}^{3N} \left(\frac{\partial \rho_t}{\partial q_i}\frac{\partial H}{\partial p_i} - \frac{\partial \rho_t}{\partial p_i}\frac{\partial H}{\partial q_i} \right) \\ &= \{\rho_t, H\} \\ &= i\mathcal{L}\rho_t\,, \end{aligned} \tag{2.8}$$

where $\{...\}$ denote the Poisson brackets and the imaginary unit i is not more than a convention that makes $\mathcal{L}$ a Hermitian operator.

[1] Eq. 2.8 can be found written also as

$$\partial_t \rho_t(\mathbf{x}) = (-p \cdot \nabla_q + \nabla_q V(q) \cdot \nabla_p)\, \rho_t(\mathbf{x}) = i\mathcal{L}\rho_t(\mathbf{x})\,. \tag{2.7}$$

The solution of the differential eq. 2.8 $\rho_t(\mathbf{x})$ is propagated forward in time by the already mentioned propagator $\mathcal{P}(\tau) : L^1 \to L^1$, also known as Frobenius-Perron operator [10, 11]:

$$\rho_{t+\tau}(\mathbf{y}) = \mathcal{P}(\tau)\rho_t(\mathbf{y}) = \exp(\tau\, i\mathcal{L})\, \rho_t(\mathbf{y})\,. \tag{2.9}$$

For this reason, the Liouville operator $i\mathcal{L}$ is also called *generator* of the propagator.

While the propagator transports probability densities, there exists another operator, the Koopman operator [10, 53] $\mathcal{K}(\tau) : L^\infty \to L^\infty$ which transports observable functions in time:

$$\mathcal{K}(\tau) f_t(\mathbf{y}) = \mathbb{E}[f_{t+\tau}(\mathbf{x}) | \mathbf{x}_t = \mathbf{y}]\,. \tag{2.10}$$

The Koopman operator is the left-adjoint of the propagator:

$$\langle \mathcal{K}(\tau) f\,,\, g \rangle = \langle f\,,\, \mathcal{P}(\tau) g \rangle\,, \tag{2.11}$$

given $f \in L^\infty$ and $g \in L^1$.

The canonical measure defined in eq. 2.4 is an invariant measure, i.e. $\pi(A) = \mathcal{P}(\tau)\pi(A)\,,\ \forall A \subset \Gamma$. However, π is not the only invariant measure. Because the dynamics is purely deterministic, the initial state $\mathbf{x}$ always determines exactly the final state $\mathbf{y}$ after a lag-time τ. An initial state $\mathbf{x}(0)$ determines exactly a closed path in phase-space and the associated invariant measure. It follows that exists an infinite number of invariant measures induced by all possible initial states [11, 12]. In conclusion, Hamiltonian dynamics is not the proper way for building a propagator with the desired characteristics.

2.3 Stochastic dynamics

2.3.1 Langevin dynamics

Consider the equation of motion (eq. 2.1) with a constant friction $\gamma > 0$ and a stochastic external force $F_{ext} = \sigma \dot{B}_t$ [54, 52]:

$$\begin{aligned} \dot{q} &= M^{-1} p \\ \dot{p} &= -\nabla V(q) - \gamma p + \sigma \dot{B}_t\,, \end{aligned} \tag{2.12}$$

where σ is the volatility of the system according to the Einstein relation $\sigma = \sqrt{2 k_B T M \gamma}$. Eq 2.12 describes a closed, but not isolated system that interacts with the environment exchanging energy in order to keep constant the temperature.

Complementary to the stochastic differential equation (eq. 2.12), there exists the Fokker-Planck equation [54, 52], that describes the stochastic process $\mathbf{x}(t)$ as time evolution of the probability density $\rho_t(\mathbf{x})$[2]:

$$\partial_t \rho_t(\mathbf{x}) = \sum_{i=1}^{3N} \left(\sum_{j=1}^{3N} \frac{\sigma^2}{2} \frac{\partial^2 \rho_t}{\partial p_i \partial p_j} - \dot{q}_i \frac{\partial \rho_t}{\partial q_i} + \frac{\partial V(q)}{\partial q_i} \frac{\partial \rho_t}{\partial p_i} - \gamma p_i \frac{\partial \rho_t}{\partial p_i} \right) = \mathcal{A} \rho_t(\mathbf{x})\,. \tag{2.14}$$

This equation is also known as forward Kolmogorov equation. Note that if $\sigma = 0$ and $\gamma = 0$, eq. 2.14 reduces to the Liouville equation.

[2] Eq. 2.14 can be found written also as

$$\partial_t \rho_t(\mathbf{x}) = \left(\frac{\sigma^2}{2} \Delta_p - p \cdot \nabla_q + \nabla_q V(q) \cdot \nabla_p - \gamma p \cdot \nabla_p \right) \rho_t(\mathbf{x}) = \mathcal{A} \rho_t(\mathbf{x})\,. \tag{2.13}$$

In Langevin dynamics, the propagator $\mathcal{P}(\tau)$ takes the form [12, 14]:

$$\rho_{t+\tau}(\mathbf{y}) = \mathcal{P}(\tau)\rho_t(\mathbf{y}) = \exp(\tau\mathcal{A})\rho_t(\mathbf{y}) = \int_\Gamma p(\mathbf{x},\mathbf{y},\tau)\rho_t(\mathbf{x})\,\mathrm{d}\mathbf{x}\,. \tag{2.15}$$

where $p(\mathbf{x},\mathbf{y};\tau)$ is the conditional probability to find the system in state $\mathbf{y}$, at time $t+\tau$, given the state $\mathbf{x}$ at time t. The Koopman operator $\mathcal{K}(\tau) : L^\infty \to L^\infty$ which transports observable functions in time, has the form [12, 14]:

$$\mathcal{K}(\tau)f_t(\mathbf{x}) = \int_\Gamma p(\mathbf{x},\mathbf{y};\tau)f_t(\mathbf{y})\mathrm{d}\mathbf{y} = \mathbb{E}[f_{t+\tau}(\mathbf{x})|\mathbf{x}_t = \mathbf{x}]\,. \tag{2.16}$$

From eq. 2.15 and eq. 2.16 emerges the difference between the propagator and the Koopman operator. The first one is a "forward" operator and averages over the initial states $\mathbf{x}$, the second one is a "backward" operator and averages over the final states $\mathbf{y}$.

The canonical measure defined in eq. 2.3 is the unique invariant measure. However, the molecular conformations are objects in the position space, thus we would prefer an operator defined only on Γ_q instead of Γ [12]. Another problem that arises from Langevin dynamics, is that the friction term is a dissipative process, thus the dynamics is non-reversible. As we will see in the next section, reversibility is important to construct a self-adjoint operator.

2.3.2 Brownian dynamics

Consider the limit case of a stochastic dynamics with high friction, known as over damped Langevin dynamics or Brownian dynamics [54, 52]. Because $\gamma p \gg M\dot{p}$, the inertial forces are neglected and the equation of motion reads

$$\begin{aligned} \dot{q} &= p \\ \gamma p &= -\nabla V(q) + \sigma\dot{B}_t\,. \end{aligned} \tag{2.17}$$

In this case the Fokker-Planck equation reduces to the Smoluchoswki equation [54, 52] [3] :

$$\partial_t\rho_t(q) = \sum_{i=1}^{3N}\left(\sum_{j=1}^{3N}\frac{\sigma^2}{2}\frac{\partial^2\rho_t}{\partial q_i\partial q_j} - \frac{\partial V(q)}{\partial q_i}\frac{\partial\rho_t}{\partial q_i}\right) = \mathcal{S}\rho_t(q)\,, \tag{2.19}$$

where $\mathcal{S}$ is the generator of the propagator $\mathcal{P}(\tau)$ which is defined only in the position space Γ_q:

$$\rho_{t+\tau}(y) = \mathcal{P}(\tau)\rho_t(x) = \exp(\tau\mathcal{S})\rho_t(x) = \int_{\Gamma_q} p(x,y,\tau)\rho_t(x)\,\mathrm{d}x\,, \tag{2.20}$$

where x and y denote conformational states in the space Γ_q. We point out that in Brownian dynamics, the state of the system is fully determined by the position of the atoms in space. In eq. 2.20 x, $y \in \mathbb{R}^{3N}$ denote states in the position space Γ_q, while in eq. 2.15 $\mathbf{x},\mathbf{y} \in \mathbb{R}^{6N}$ denote states in the phase space Γ.

[3] Eq. 2.19 can be found written also as

$$\partial_t\rho_t(q) = \left(\frac{\sigma^2}{2}\Delta_q - \nabla_q V(q)\cdot\nabla_q\right)\rho_t(q) = \mathcal{S}\rho_t(q)\,. \tag{2.18}$$

Likewise, the Koopman operator, adjoint of the propagator, takes the form:

$$\mathcal{K}(\tau)f_t(x) = \int_\Gamma p(x,y;\tau)f_t(y)\mathrm{d}y = \mathbb{E}[f_{t+\tau}(x)|x_t = x]\,. \tag{2.21}$$

The unique invariant measure of the propagator (eq. 2.20) is:

$$\mu_{\pi_q}(x) = \frac{\exp\left(-\beta V(x)\right)}{Z_q}\,, \text{with} \quad Z_q = \int_{\Gamma_q} \exp\left(-\beta V(x)\right)\,\mathrm{d}x\,, \tag{2.22}$$

which is the Boltzmann distribution defined only on the position space Γ_q as requested.

Properties of Brownian dynamics The continuous process $q(t)$, solution of the equation of motion (eq. 2.17), satisfies the following properties [13, 55, 14]:

1. *Markovianity* The time continuous process $q(t)$ is memoryless, i.e. the probability to evolve its state does not depend on the past, but only on the current state. The process is called *Markovian* and satisfies the equation

$$\mathbb{P}[q(t+\tau) = y \,|\, q(s) = x \quad 0 < s < t] = \mathbb{P}[q(t+\tau) = y \,|\, q(t) = x \quad s = t]\,. \tag{2.23}$$

   The process is also *time-homogeneous* if the transition from $q(t)$ to $q(t+\tau)$ does not depend on the time t, then

$$\mathbb{P}[q(t+\tau) = y \,|\, q(t) = x] = \mathbb{P}[q(s+\tau) = y \,|\, q(s) = x \quad 0 < s < t]\,. \tag{2.24}$$

   If the process is Markovian and time-homogeneous, the propagator does not depend on time and the existence of at least one invariant measure $\mu(q)$ is guaranteed.

2. *Ergodicity* If the state space Γ_q does not contain isolated subsets, i.e. each state of the system is reachable from any other state through a continuous path in the state space, then the process $q(t)$ is *ergodic*. Thus, for $t \to \infty$, each state is visited an infinite number of times proportional to the stationary distribution $\mu_{\pi_q}(x)$ (eq. 2.22). This property guarantees also the uniqueness of the invariant measure.

3. *Time-reversibility* The time-continuous process $q(t)$, solution of the eq. 2.17, is time-reversible if we get the same process running the time backward. Thus, the solution $\{q(t),\, 0 \le t < +\infty\}$ has the same probability to be generated as $\{q(-t),\, 0 \le t < +\infty\}$. A time reversible process satisfies the detailed balance condition:

$$\mu_{\pi_q}(x)p(x,y;\tau) = \mu_{\pi_q}(y)p(y,x;\tau)\,. \tag{2.25}$$

   Reversibility guarantees the self-adjointness of the propagator (eq. 2.20) and the Koopman operator (eq. 2.21), respectively with respect to the weighted scalar products $\langle\cdot\,,\cdot\rangle_{\pi_q^{-1}}$ and $\langle\cdot\,,\cdot\rangle_{\pi_q}$:

$$\langle f\,,\, \mathcal{P}(\tau)g\rangle_{\pi_q^{-1}} = \langle \mathcal{P}(\tau)f\,,\, g\rangle_{\pi_q^{-1}}\,, \tag{2.26}$$

   with $f, g \in L^1$ and

$$\langle u\,,\, \mathcal{K}(\tau)v\rangle_{\pi_q} = \langle \mathcal{K}(\tau)u\,,\, v\rangle_{\pi_q}\,, \tag{2.27}$$

   with $u, v \in L^\infty$

In the next sections, we will see that the propagator (eq. 2.20) of a process that satisfies these three properties, can be rewritten in a more convenient operator called transfer operator.

2.4 The dominant eigenspace of the propagator

The operator $\mathcal{P}(\tau)$ is characterized by eigenfunctions l_i associated to eigenvalues $\lambda_i(\tau)$ [12, 13, 55, 14, 56]:

$$\mathcal{P}(\tau)l_i = \lambda_i(\tau)l_i\,. \tag{2.28}$$

The eigenvalues are real valued and $\lambda_i(\tau) \in (0,1]$. Because μ_{π_q} is the unique invariant measure, we have $\mathcal{P}(\tau)\mu_{\pi_q} = \mu_{\pi_q}$. Then μ_{π_q} is the eigenfunction l_1 associated to the eigenvalue $\lambda_1(\tau) = 1$. The other eigenfunctions have both positive and negative values and represent a kinetic exchange between regions with different sign. Self-adjointness of $\mathcal{P}(\tau)$ implies that its eigenfunctions form a complete basis, thus we can decompose any probability density function ρ_t as a combination of eigenfunctions l_i:

$$\rho_t(x) = \sum_{i=1}^{\infty} c_i l_i(x) \tag{2.29}$$

Because of Markovianity of the process, the Chapman-Kolmogorov equation holds:

$$\rho_{t+k\tau}(x) = \mathcal{P}(\tau)^k \rho_t(x) \quad k \in \mathbb{N}\,. \tag{2.30}$$

Inserting eq. 2.29 in eq. 2.30, we have

$$\begin{aligned}\rho_{t+k\tau}(x) =& \mathcal{P}(\tau)^k \sum_{i=1}^{\infty} c_i \lambda_i(\tau) l_i(x) \\ =& \sum_{i=1}^{\infty} c_i \lambda_i(\tau)^k l_i(x) \\ =& \mu_{\pi_q}(x) + \sum_{i=2}^{M} c_i \lambda_i(\tau)^k l_i(x) + \sum_{i=M+1}^{\infty} c_i \lambda_i(\tau)^k l_i(x)\,.\end{aligned} \tag{2.31}$$

Thus we have decomposed the probability density function in the equilibrium distribution, the first $M-1$ slow processes associated to eigenvalues $\lambda_i(\tau) <\approx 1$ and all the other eigenfunctions that represent fast kinetic exchanges associated to eigenvalues $\lambda_i(\tau) >\approx 0$. Since the eigenvalues $\lambda_i(\tau) < 1\,, \forall i > 1$, after a long time, $\rho(t \to \infty) = \mu_{\pi_q}$, indeed all the eigenmodes with $i > 1$ decay exponentially:

$$\lambda_i(\tau)^k = e^{-\frac{k\cdot\tau}{t_i}}\,,$$

where $t_i = -\frac{\tau}{\log \lambda_i(\tau)}$ denotes the implied time scale (or relaxation time scale) at which the contribution of the ith eigenmode is reduced to 36%.

As example, in fig. 2.1, we illustrate the time evolution of the probability density ρ_t of a one dimensional diffusion process governed by a triple-well potential. At time $t = 0$, $\rho_0(x) = \delta_{x_0}(x)$, then the density function evolves into a function with three peaks corresponding to the three minima of the potential energy function. The system is characterized by two slow processes associated to the relaxation timescales $t_2 \approx 450$ timesteps and $t_3 \approx 2100$ timesteps. The other kinetic processes decay after few timesteps. The eigenfunction l_2 represents a kinetic exchange between the right-hand side minimum and the other two minima on the left, while l_3 represents an exchange between the middle minimum and the two on the sides. We observe that when the processes l_2 and l_3 decay, the probability density function converges to the stationary distribution.

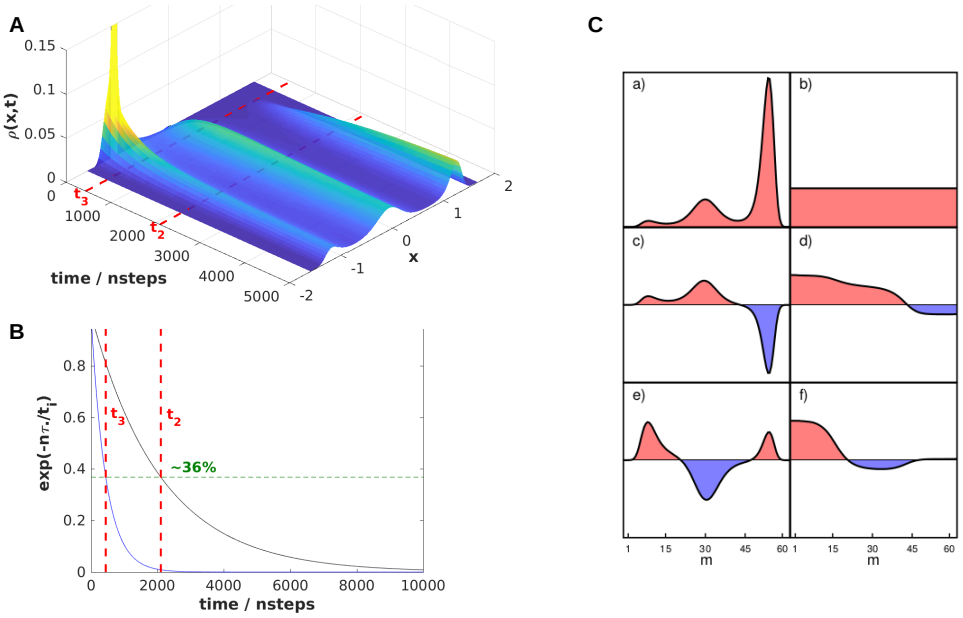

Figure 2.1: Diffusion process with triple-well potential. (A) Time evolution of probability density. (B) Exponential decay of the eigenvalues. (C) First three left and right eigenfunctions, figure taken from reference [56].

2.5 Markov State Models

In Markov State Models (MSMs) [12, 15, 16, 17, 18, 13, 19, 20, 21] the continuous model described by the propagator is converted to a discrete problem and the dynamics is described by a transition probability matrix $\mathbf{T}(\tau)$. On the other hand, building an MSM means also to reduce the dimensionality of the problem. Thus, the first step is to determine a subspace of the state space $X \subset \Gamma_q$, where the relevant dynamics of the system takes place. Afterwards, the space X is discretized into n disjoint microstates A_i such that $\cup A_i = X$.

The transition probability matrix $\mathbf{T}(\tau)$ describes the probability that a Markovian jump from a microstate A_i to A_j occurs:

$$\begin{aligned} T_{ij}(\tau) =& \mathbf{P}\left[q(t+\tau) \in A_j | q(t) \in A_i\right] \\ =& \frac{\mathbf{P}\left[q(t+\tau) \in A_j \text{ AND } q(t) \in A_i\right]}{\mathbf{P}\left[q(t \to \infty) \in A_i\right]} \\ =& \frac{\mathbf{P}\left[q(t+\tau) \in A_j \text{ AND } q(t) \in A_i\right]}{\pi_q\left[A_i\right]} . \end{aligned} \tag{2.32}$$

Note that we have used the classical definition of probability that two dependent events E_1 and E_2 occurs:

$$\mathbf{P}(E_2|E_1) = \frac{\mathbf{P}(E_1 \cap E_2)}{\mathbf{P}(E_1)} . \tag{2.33}$$

The numerator (eq. 2.32) represents the joint probability that $q(t) \in A_i$ and $q(t+\tau) \in A_j$ and reads:

$$\mathbf{P}\left[q(t+\tau) \in A_j \text{ AND } q(t) \in A_i\right] = \int_{A_j} \int_{A_i} p(x, y; \tau) \mu_{\pi_q}(x) \, \mathrm{d}x\mathrm{d}y . \tag{2.34}$$

While the denominator (eq. 2.32) represents the probability distribution of the process at equilibrium:

$$\pi_q\left[q \in A_i\right] = \int_{A_i} \mu_{\pi_q}(x)\,\mathrm{d}x\,. \tag{2.35}$$

2.5.1 From propagator to transfer operator

We now introduce the transfer operator $\mathcal{T}(\tau) : L^1_{\pi_q} \to L^1_{\pi_q}$ that acts on weighted functions $u(x) = \rho(x)/\mu_{\pi_q(x)}$ [11, 12, 15, 13, 55, 14]:

$$u_{t+\tau}(y) = \mathcal{T}(\tau)u_t(y) = \frac{1}{\pi_q(y)}\int_{\Gamma_q} p(x,y;\tau)u_t(x)\mu_{\pi_q}(x)\mathrm{d}x\,. \tag{2.36}$$

Because of reversibility, the transfer operator is self-adjoint with respect to the weighted product scalar $\langle\cdot\,,\cdot\rangle_{\pi_q}$:

$$\langle u\,,\,\mathcal{T}(\tau)v\rangle_{\pi_q} = \langle\mathcal{T}(\tau)u\,,\,v\rangle_{\pi_q}\,, \tag{2.37}$$

with $u, v \in L^1_{\pi_q}$. From a mathematical point of view, the transfer operator is equivalent to the Koopman operator has defined in eq. 2.21.

The advantage of the transfer operator is that it permits to derive the transition probability matrix (eq.2.32) via Galerkin discretization:

$$\begin{aligned}
T_{ij}(\tau) &= \frac{\langle\mathbf{1}_i\,,\,\mathcal{T}(t)\mathbf{1}_j\rangle_{\pi_q}}{\langle\mathbf{1}_i\,,\,\mathbf{1}_i\rangle_{\pi_q}} \\
&= \frac{1}{\int_{\Gamma_q}\mathbf{1}_i(x)\mathbf{1}_i(x)\mu_{\pi_q}(x)\mathrm{d}x}\int_{\Gamma_q}\mathbf{1}_i(y)\left[\frac{1}{\mu_{\pi_q}(y)}\int_{\Gamma_q}p(x,y;\tau)\mathbf{1}_j(x)\mu_{\pi_q}(x)\mathrm{d}x\right]\mu_{\pi_q}(y)\mathrm{d}y \\
&= \frac{1}{\int_{\Gamma_q}\mathbf{1}_i(x)\mu_{\pi_q}(x)\mathrm{d}x}\int_{\Gamma_q}\mathbf{1}_i(y)\left[\int_{\Gamma_q}p(x,y;\tau)\mathbf{1}_j(x)\mu_{\pi_q}(x)\mathrm{d}x\right]\mathrm{d}y \\
&= \frac{1}{\int_{A_i}\mu_{\pi_q}(x)\mathrm{d}x}\int_{A_i}\int_{A_j}p(x,y;\tau)\mu_{\pi_q}(x)\mathrm{d}x\mathrm{d}y \\
&= \frac{1}{\pi_{q_i}}\int_{A_i}\int_{A_j}p(x,y;\tau)\mu_{\pi_q}(x)\mathrm{d}x\mathrm{d}y\,,
\end{aligned} \tag{2.38}$$

where $\mathbf{1}_i$ is the indicator function:

$$\mathbf{1}_i(x) := \begin{cases} 1, & x \in A_i \\ 0, & x \notin A_i \end{cases}\,. \tag{2.39}$$

The transition probability matrix is interpreted as a discretized version of the continuous propagator (eq. 2.20) or of the transfer operator (eq. 2.36). In the first case, it left-multiplicates the vectors $\mathbf{p}(t) = [p_1(t), ..., p_n(t)]^\top$, in the second case, it right-multiplicates the vectors $\mathbf{u}(t) = [u_1(t), ..., u_n(t)]^\top$:

$$\begin{aligned}
\mathbf{p}^\top(t+\tau) &= \mathbf{p}^\top(t)\mathbf{T}(\tau)\,, \\
\mathbf{u}(t+\tau) &= \mathbf{T}(\tau)\mathbf{u}(t)\,,
\end{aligned} \tag{2.40}$$

where $\mathbf{p}(t)$ and $\mathbf{u}(t)$ are respectively the discrete version of the functions ρ_t and u_t.

Note that when the trajectory is projected on the discrete state space, the Markov property is lost [13, 21, 57, 56], then one must choose a fine discretization in order to reduce this systematic error. To test the validity of an MSM, one can plot the implied time scales as a function of the lag time τ. For small values of the lag time, the implied timescales are an increasing monotonic functions. But for a large enough value of τ, the implied timescales are constant, indicating that the Markov property is satisfied.

MSMs from time-correlation functions One advantage of MSMs is that the numerator in eq. 2.32, can be interpreted as a time-lagged correlation function between two observable functions $a(x)$ and $b(x)$:

$$\mathrm{cor}(a,b;\tau) = \int_\Gamma \int_\Gamma a(x)\mu_{\pi_q}(x)p(x,y;\tau)b(y)\,\mathrm{d}x\,\mathrm{d}y\,. \tag{2.41}$$

This quantity can be estimated from long trajectories $q(t)$. The Birkhoff–Khinchin theorem states that, if the process $q(t)$ is ergodic, than the time-average tends to the space average for $t \to +\infty$, then the time correlation function (eq. 2.41) can be written as:

$$\mathrm{cor}(a,b;\tau) = \lim_{t\to+\infty} \frac{1}{t}\int_0^t a(x(s))b(x(s+\tau))\mathrm{d}s\,. \tag{2.42}$$

Replacing $a(x)$ and $b(x)$ respectively with $\mathbf{1}_i$ and $\mathbf{1}_j$, one obtains the correlation matrix $\mathbf{C}(\tau)$:

$$C_{ij}(\tau) = \lim_{t\to+\infty} \frac{1}{t}\int_0^t \mathbf{1}_i(x(s))\mathbf{1}_j(x(s+\tau))\mathrm{d}s\,. \tag{2.43}$$

In MD, a long discretized trajectory can be chopped in m short trajectories of length τ, thus the entries of $\mathbf{C}(\tau)$ can be estimated as

$$C_{ij}(\tau) = \lim_{m\to\infty} \frac{1}{m}\sum_{k=1}^{m} \mathbf{1}_{B_i}([x_0]_k)\cdot\mathbf{1}_{B_j}([x_n]_k) \tag{2.44}$$

where $[x_0]_k$ and $[x_n]_k$ are respectively the initial and the final states of the kth short trajectory. Thus the correlation matrix is a "counting matrix", because given an MD trajectory, $C_{ij}(\tau)$, is the number of transitions between the set A_i to A_j within a time span τ. Finally the entries of the transition probability matrix are

$$T_{ij}(\tau) = \frac{C_{ij}(\tau)}{\pi_{q_i}}\,. \tag{2.45}$$

Note that π_{q_i} can be estimated as sum over the rows of the correlation matrix $\pi_{q_i} = \sum_j C_{ij}(\tau)$.

2.6 Girsanov reweighting

Girsanov reweighting [40, 41] is a technique to reweight the MSM built from a dynamics at potential V_{ref} to the MSM of a modified potential V_{mod}, without re-sampling the dynamics at V_{mod} (fig. 2.2). The method is based on the Girsanov theorem [58, 42], that states the conditions under which a path probability measure can be defined with respect to the Wiener measure and how to reweight path ensemble averages. Because, the correlation functions (eq. 2.41) can be formulated in terms of a path ensemble averages, we could apply the Girsanov theorem successfully to MSMs [40, 41].

We recall here the concept of path space, path probability density and path ensemble average. For more details, see refs. [41, 59], included respectively in chapters 5 and 6.

2.6.1 Path space and path ensemble average

Let $\omega = \{x_0 = x,\, x_1, ...,\, x_n\}$ be a discretized path of length $\tau = n\cdot\Delta t$ in the positional space Γ_q, that is a solution of a Brownian dynamics with drift defined by the gradient of the potential energy function V_{ref} (eq. 2.17) and $x_0 = x$ is the initial state.

The path space, i.e. the set of all possible paths ω of length τ which start in $x_0 = x$, is denoted by $\Omega_{\tau,x} = \Gamma_q^n \subset \mathbf{R}^{3N\cdot n}$.

The path probability density is the probability that a path $\omega \in \Omega_{\tau,x}$ is generated by the equation of motion and is defined as the product of conditional probabilities between consecutive steps:

$$\begin{aligned} \mu_P(\omega) &= \mu_P(x_1, x_2, ..., x_n \,|\, x_0 = x) \\ &= p(x_0, x_1; \Delta t) \cdot p(x_1, x_2; \Delta t) \cdot ... \cdot p(x_{n-1}, x_n; \Delta t)\,. \end{aligned} \tag{2.46}$$

If we assume that the path ω is a solution of a Brownian dynamics (eq. 2.17), with potential energy function V_{ref}, the conditional probability is written

$$p(x_{k-1}, x_k; \Delta t) = \frac{1}{\sqrt{2\pi\Delta t\sigma^2}} \exp\left(-\frac{x_k - x_{k-1} - \nabla V_{\text{ref}}(x_{k-1})}{2\Delta t\sigma^2}\right), \tag{2.47}$$

then the path probability density is strictly dependent on the potential energy function.

Let $f(\omega) = f(x_1, x_2, ..., x_n)$ be a path observable, i.e. a suitable function which assigns a real-valued number to each path ω. The path ensemble average of $f(\omega)$ for dynamics at V_{ref} is the expected value respect to the path probability density $\mu_P(\omega)$:

$$\begin{aligned} \mathbb{E}_P[f \,|\, x_0 = x] &= \int_{\Omega_{\tau,x}} \mu_P(\omega)\, f(\omega)\, \mathrm{d}\omega \\ &= \int_{\Gamma_q}\int_{\Gamma_q} ... \int_{\Gamma_q} \mu_P(x_1, x_2, ..., x_n \,|\, x_0 = x)\, f(x_1, x_2, ..., x_n) \times \\ &\times \quad \mathrm{d}x_1, \mathrm{d}x_2, ..., \mathrm{d}x_n\,. \end{aligned} \tag{2.48}$$

Because the Brownian dynamics is ergodic, the Birkhoff's theorem holds, then, given a set of m paths $S_{\tau,x} = \{\omega_1, \omega_2, ...\omega_m\} \subset \Omega_{\tau,x}$, associated to the dynamics V_{ref}, eq. 2.48 can be written as

$$\mathbb{E}_P[f \,|\, x_0 = x] = \lim_{m\to\infty} \frac{1}{m} \sum_{\omega_k \in S_{\tau,x}} f(\omega_k)\,. \tag{2.49}$$

A different potential energy function V_{mod} would generate a different path probability density $\mu_{\widetilde{P}}(\omega)$ and a different path ensemble average $\mathbb{E}_{\widetilde{P}}[f \,|\, x_0 = x]$. However, if the path probability ratio $M_{\tau,x}(\omega) = \mu_{\widetilde{P}}(\omega)/\mu_P(\omega)$ exists, $\mathbb{E}_{\widetilde{P}}[f \,|\, x_0 = x]$ can be estimated in terms of the path probability density $\mu_P(\omega)$:

$$\mathbb{E}_{\widetilde{P}}[f \,|\, x_0 = x] = \int_{\Omega_{\tau,x}} \widetilde{\mu}_P(\omega)\, f(\omega)\, \mathrm{d}\omega = \int_{\Omega_{\tau,x}} M_{\tau,x}(\omega)\, \mu_P(\omega)\, f(\omega)\, \mathrm{d}\omega\,. \tag{2.50}$$

It follows that given a set of m paths $S_{\tau,x}$ generated by V_{ref},

$$\mathbb{E}_{\widetilde{P}}[f \,|\, x_0 = x] = \lim_{m\to\infty} \frac{1}{m} \sum_{\omega_k \in S_{\tau,x}} M_{\tau,x}(\omega_k) f(\omega_k)\,. \tag{2.51}$$

The Girsanov theorem [58, 42] asserts that, if the path probability measure $\widetilde{P}$ is absolutely continuous with respect to P, i.e.

$$\widetilde{P}(\mathcal{A}) = \int_{\mathcal{A}} \mu_{\widetilde{P}}(\omega)\mathrm{d}\omega = 0 \quad \Rightarrow \quad P(\mathcal{A}) = \int_{\mathcal{A}} \mu_P(\omega)\mathrm{d}\omega = 0 \qquad \forall \mathcal{A} \subset \Omega_{\tau,x}\,, \tag{2.52}$$

then $M_{\tau,x}(\omega)$ exists and in the limit $\Delta t \to 0$, $M_{\tau,x}(\omega)$ is given by

$$M_{\tau,x}(\omega) = \frac{\mu_{\widetilde{P}}(\omega)}{\mu_P(\omega)} = \exp\left\{\sum_{i=1}^{3N}\left[\int_0^\tau \frac{\nabla_i U(x(s))}{\sigma}\mathrm{d}B_s^i - \frac{1}{2}\int_0^\tau \left(\frac{\nabla_i U(x(s))}{\sigma}\right)^2 \mathrm{d}s\right]\right\}, \tag{2.53}$$

where B_s^i is a pure Wiener process in direction i, generated to integrate the equation of motion with V_{ref} and $U = V_{\mathrm{mod}} - V_{\mathrm{ref}}$ is the difference between the two potential energy functions. Note that in eq. 2.53, the path ω is a continuos path.

2.6.2 Girsanov reweighting for MSMs

The correlation function (eq. 2.41) is a double integral, where the integral over the initial state x is a phase-space ensemble average of an observable function $a(x)$, respect to the probability density μ_{π_q} (eq. 2.22):

$$\mathbb{E}_{\pi_q}[\, a(x) \,|\, x_0 = x \,] = \int_{\Gamma_q} a(x)\mu_{\pi_q}(x)\,\mathrm{d}x \tag{2.54}$$

The second integral (eq. 2.41), over the final state y, is an expectation of the function $b(x)$, weighted by the path probability density $\mu_P(\omega)$. Indeed, given a discretized path ω, where $x_0 = x$ and $x_n = y$, the conditional probability between the state x and y, after a lag-time τ, is defined as the integral of the path probability density $\mu_P(\omega)$ over all the intermediate states:

$$p(x,y;\tau) \;=\; \int_{\Gamma_q}\int_{\Gamma_q}\cdots\int_{\Gamma_q} \mu_P(x_1, x_2, ..., x_n \,|\, x_0 = x)\,\mathrm{d}x_1\,\mathrm{d}x_2 \ldots \mathrm{d}x_{n-1}\,. \tag{2.55}$$

The second integral of the correlation function (eq. 2.41), is a path ensemble average of the function $b(x)$ evaluated at the final state x_n of the path:

$$\begin{aligned}
&\mathbb{E}_P[\, b(x_n) \,|\, x_0 = x] \\
=\;& \int_{\Omega_{\tau,x}} \mu_P(\omega)\, b(x_n)\,\mathrm{d}\omega && (2.56)\\
=\;& \int_{\Gamma_q}\left[\int_{\Gamma_q}\int_{\Gamma_q}\cdots\int_{\Gamma_q} \mu_P(x_1, x_2, ..., x_n \,|\, x_0 = x)\,\mathrm{d}x_1\,\mathrm{d}x_2 \ldots \mathrm{d}x_{n-1}\right] b(x_n)\,\mathrm{d}x_n && (2.57)\\
=\;& \int_{\Gamma_q} p(x,y;\tau)\, b(y)\,\mathrm{d}y\,. && (2.58)
\end{aligned}$$

Thus, the correlation function (eq. 2.41) can be written as:

$$\mathrm{corr}(a,b;\tau) = \mathbb{E}_{\pi_q}[a(x)\cdot\mathbb{E}_P[\, b(x_n) \,|\, x_0 = x]]\,. \tag{2.59}$$

If we consider a modified dynamics V_{mod}, with the associated path probability density $\mu_{\widetilde{P}}$ and the stationary probability density $\mu_{\widetilde{\pi}_q}$, the correlation function reads:

$$\widetilde{\mathrm{corr}}(a,b;\tau) = \mathbb{E}_{\widetilde{\pi}_q}[a(x)\cdot\mathbb{E}_{\widetilde{P}}[\, b(x_n) \,|\, x_0 = x]]\,. \tag{2.60}$$

Eq. 2.60 can be written in terms of μ_{π_q} and μ_P, introducing two proper reweighting factors. The first one is the ratio between stationary probability densities:

$$g(x) = \frac{\mu_{\widetilde{\pi}_q}(x)}{\mu_{\pi_q}(x)} = \frac{Z}{\widetilde{Z}}\exp\left(-\beta U(x)\right)\,. \tag{2.61}$$

The second one is the ratio between the two path probability densities $M_{\tau,x}(\omega)$, defined in eq. 2.53 by the Girsanov theorem. Then, eq. 2.60 can be written as

$$\begin{aligned}\widetilde{\mathrm{corr}}(a,b;\tau) &= \mathbb{E}_{\pi_q}[g(x)\cdot a(x)\cdot \mathbb{E}_P[\,M_{\tau,x}(\omega)\cdot b(x_n)\,|\,x_0=x]] &(2.62)\\ &= \int_{\Gamma_q} g(x)\mu_{\pi_q}(x)\,a(x)\int_{\Omega_{\tau,x}} M_{\tau,x}(\omega)\mu_P(\omega)b(x_n)\,\mathrm{d}\omega\,\mathrm{d}x\,. &(2.63)\end{aligned}$$

In MSMs $a(x)=\mathbf{1}_{A_i}(x)$ and $b(x_n)=\mathbf{1}_{B_j}(x_n)$, thus the entries of the counting matrix for the modified dynamics are

$$\begin{aligned}\widetilde{C}_{ij}(\tau) &= \int_{\Gamma_q}\mu_{\widetilde{\pi}_q}(x)\,\mathbf{1}_{A_i}(x)\int_{\Omega_{\tau,x}}\mu_{\widetilde{P}}(\omega)\mathbf{1}_{B_j}(x_n)\,\mathrm{d}\omega\,\mathrm{d}x\\ &= \int_{\Gamma_q} g(x)\mu_{\pi_q}(x)\,\mathbf{1}_{A_i}(x)\int_{\Omega_{\tau,x}} M_{\tau,x}(\omega)\mu_P(\omega)\mathbf{1}_{B_j}(x_n)\,\mathrm{d}\omega\,\mathrm{d}x\\ &= \lim_{m\to\infty}\frac{1}{m}\sum_{\omega_k\in S_{\tau,x}} g([x_0]_k)\mathbf{1}_{A_i}([x_0]_k)\cdot M_{x,\tau}(\omega_k)\mathbf{1}_{B_j}([x_n]_k)\,. &(2.64)\end{aligned}$$

where the last equality holds because of the Birkhoff's theorem and permits to estimate the matrix $\widetilde{\mathbf{C}}(\tau)$ for the modified dynamics V_{mod}, from a set of m paths generated from the reference dynamics V_{ref}.

Finally, the entries of the transition probability matrix between the microset A_i and the microset B_j for the modified dynamics are

$$\widetilde{T}_{ij}(\tau)=\frac{\widetilde{C}_{ij}(\tau)}{\sum_j \widetilde{C}_{ij}(\tau)}\,. \tag{2.65}$$

2.7 The infinitesimal generator

In the previous sections, we have introduced the Liouville operator $\mathcal{L}$ (eq. 2.8), the Fokker-Planck operator $\mathcal{A}$ (eq. 2.14) and the Smoluchowski operator $\mathcal{S}$ (eq. 2.19), which describe how the probability density function ρ_t changes in an infinitesimal time interval. Thus, these operators can be interpreted as time derivatives of the propagator.

In the case of Brownian dynamics, the operator $\mathcal{S}$, also named infinitesimal generator, is defined as [12, 42]

$$\mathcal{S}=\lim_{\tau\downarrow 0}\frac{\mathcal{P}(\tau)-\mathcal{P}(0)}{\tau}\,, \tag{2.66}$$

which acts on suitable functions $\rho(x)\in L^1$.

The eigenfunctions of $\mathcal{S}$ are identical to those of $\mathcal{P}(\tau)$, while the eigenvalues θ_i satisfy

$$\lambda_i(\tau)=\exp(\tau\theta_i)\qquad \forall i\in[1,+\infty]\,, \tag{2.67}$$

with $\theta_i\in[-\infty,0]$ and $\theta_1=0$. It follows that both the operators contain the same information about the dynamics of the system.

Like for MSMs, instead of the operator $\mathcal{S}$, we consider the operator $\mathcal{Q}$, generator of the transfer operator $\mathcal{T}(\tau)$ (eq. 2.36), that acts on weighted functions $u(x)=\rho(x)/\mu_{\pi_q}(x)\in L^1_{\Gamma_q}$:

$$\mathcal{Q}=\lim_{\tau\downarrow 0}\frac{\mathcal{T}(\tau)-\mathcal{T}(0)}{\tau}\,. \tag{2.68}$$

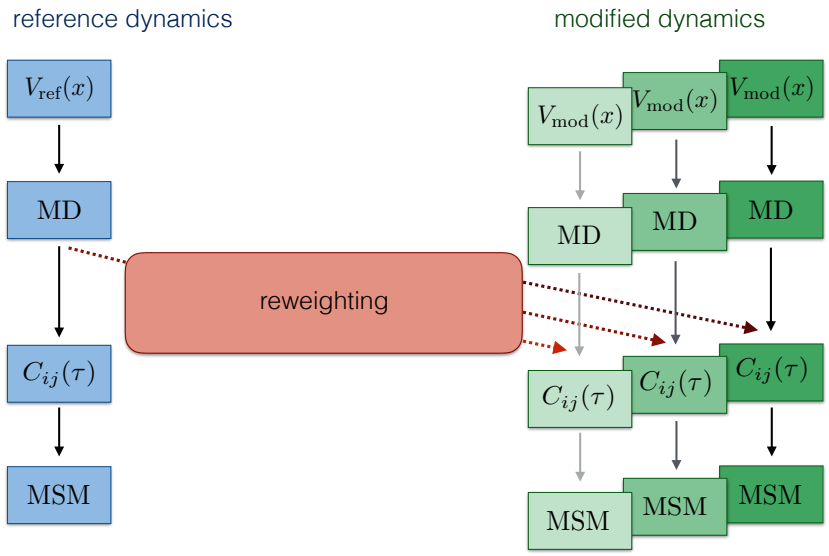

Figure 2.2: Workflow of a reweighting scheme. Given a potential energy function V_{ref}, one needs to run an MD simulation in order to build the counting matrix $\mathbf{C}(\tau)$ and the relative MSM. A new simulation is necessary if one desires to study a modified potential energy function V_{mod}. A dynamical reweighting scheme uses the same trajectory, in order to produce MSMs for different potential energy functions V_{mod}, with no need to run new MD simulations.

Given an arbitrary discretization of the space in disjoint microsets, the entries of the matrix $\mathbf{Q}$, i.e. the Galerikin discretization of $\mathcal{Q}$, read

$$Q_{ij} = \frac{\langle \mathbf{1}_i \,,\, \mathcal{Q}\mathbf{1}_j \rangle_{\pi_q}}{\langle \mathbf{1}_i \,,\, \mathbf{1}_i \rangle_{\pi_q}} \,, \tag{2.69}$$

which fulfill the the master equation for a jump process:

$$\left.\frac{\partial p_i}{\partial \tau}\right|_{\tau=0} = C \sum_{i\sim j} (p_j Q_{ji} - p_i Q_{ij}) \,, \tag{2.70}$$

where p_i, p_j are respectively the ith and jth elements of the vector $\mathbf{p}$, approximation of the probability density function ρ, while C is a normalization constant and the notation $i \sim j$ denotes neighboring microsets. The matrix $\mathbf{Q}$ has the properties of a rate matrix:

1. The diagonal elements satisfy $Q_{ii} = -\sum_{j\neq i} Q_{ij}$
2. The sum of the rows is zero: $\sum_j Q_{ij} = 0$,

thus the entry Q_{ij} describes the transition rate from the set j to the neighbor set i.

2.7.1 Square root approximation of the infinitesimal generator

Square Root Approximation [57] (SQRA) is a technique to discretize the infinitesimal generator $\mathcal{Q}$ (eq. 2.68) for a Brownian dynamics in a rate matrix $\mathbf{Q}$. In this section, we describe the main steps to derive the method assuming a Voronoi tessellation of the conformational space, but we refer the reader to the article included in chapter 8 of this

thesis, where we describe in detail the theory underlying the method and we show that the rate matrix converges to the infinitesimal generator in the limit of infinitely small microsets. The method is presented also in reference [60] and [61, 62], where has been derived from the maximum path entropy principle.

Consider a Voronoi tessellation of the position space $\Gamma_q = \cup_{i=1}^{n} \Omega_i$ in n cells and the transition probability matrix $\mathbf{T}(\tau)$ as defined in eq. 2.32, that describes the transition probability to jump from a cell Ω_i to the cell Ω_j. The rate matrix $\mathbf{Q}$ satisfies the time derivative $\mathbf{Q} := \frac{\partial \mathbf{T}(\tau)}{\partial \tau}\Big|_{\tau=0}$, which can be written in terms of the flux between conformations using the Gauss theorem:

$$Q_{ij} = \frac{1}{\pi_{qi}} \oint_{\partial\Omega_i \partial\Omega_j} \Phi(z)\, \mu_{\pi_q}(z) \mathrm{d}S(z)\,, \tag{2.71}$$

where $\pi_{qi} = \int_{\Omega_i} \mu_{\pi_q}(x)\, \mathrm{d}x$ is the probability that the system assumes a position $x \in \Omega_i$, $\partial\Omega_i\partial\Omega_j$ is the common surface between neighboring cells Ω_i and Ω_j and $\Phi(z)$ denotes the flux of the configurations $z \in \partial\Omega_i\partial\Omega_j$, through the infinitesimal surface $\partial\Omega_i\partial\Omega_j$. The derivation of eq. 2.71 is stated in the appendix A of the article presented in chapter 8.

Multiplying and dividing eq. 2.71 by the Boltzmann density of the intersecting surface:

$$\pi_{ij} = \oint_{\partial\Omega_i \partial\Omega_j} \pi(z)\,, \mathrm{d}S(z)\,, \tag{2.72}$$

one can write

$$\begin{aligned} Q_{ij} =& \frac{\pi_{ij}}{\pi_i} \oint_{\partial\Omega_i \partial\Omega_j} \Phi(z)\ \frac{\mu_{\pi_q}(z)}{\pi_{ij}} \mathrm{d}S(z) \\ =& \frac{\pi_{ij}}{\pi_i} \langle \Phi \rangle_{ij}\,, \end{aligned} \tag{2.73}$$

where $\langle \Phi \rangle_{ij}$ is the mean value of the flux through the surface $\partial\Omega_i\partial\Omega_j$, assuming a constant potential function.

If the Voronoi cells are small enough, the flux through two adjacent cells can assumed to be constant $\hat{\Phi} = \langle \Phi \rangle_{ij}$ and the Boltzmann density of a cell surface is almost equal to the Boltzmann density of the cell itself, i.e. $\pi|_{\Omega_i} \approx \pi_i$. Moreover, the density of the cell Ω_i is almost equal to the density of the cell Ω_j, i.e. $\pi_i \approx \pi_j$, and the Boltzmann weight of the intersecting surface can be estimated as average value. In principle, several mean-value calculations could be used, but only by geometric mean the discretized operator would converge to the continuous infinitesimal generator:

$$\begin{aligned} \pi_{ij} &= \sqrt{\pi_i\, \pi_j} \\ &= \exp\left(-\beta \frac{V(\Omega_i) + V(\Omega_j)}{2} \right)\,. \end{aligned} \tag{2.74}$$

Finally, the entries of the rate matrix are written as

$$Q_{ij} = \frac{\sqrt{\pi_i\, \pi_j}}{\pi_i}\, \hat{\Phi} = \sqrt{\frac{\pi_j}{\pi_i}}\, \hat{\Phi}\,, \tag{2.75}$$

that can be estimated analytically up to the scaling factor $\hat{\Phi}$.

In the work presented in chapter 8 (section II.B), we prove that in the limit of infinitely small Voronoi cells, the rate matrix based on the square root approximation converges to the continuous infinitesimal generator.

Chapter 3

Markov State Models in drug design

In the last decades, ligand-target binding models evolved from the simplistic "lock and key" mechanism [63], where the enzyme active site was assumed to be a rigid lock which can fit only in a single substrate, to modern models like the "conformational selection model" [64] and the "induced fit model" [65], where conformational changes are induced by the binding process. However, these models do not take into account the dynamics of the ligand, which is difficult to characterize from laboratory experiments, and cannot fully explain most of the binding processes.

Molecular Dynamics (MD) simulations [1, 2] can be useful to overcome this problem. In MD simulations, the atoms of a molecule are described as points in the space, moving according to the Newton's equations of motion, where the potential energy function that describes the interactions between atoms, is parametrized in order to fit ab-initio calculations or laboratory experiments. Nowadays, the development of new algorithms and special purpose computers like Anton [8, 9], has permitted a significant improvement in sampling the conformational space and the conformational changes by MD simulations. On the other hand, the time discretized trajectory, produced by an MD simulation, contains the positions of each atom for each time step and analyzing such amount of data to extract only the relevant information, can be a hard task.

Markov State Models (MSMs) [12, 15, 16, 17, 18, 13, 19, 20, 21] are a clever and successful tool that permits to optimize the use of MD simulations. From a set of short trajectories, MSMs capture the relevant dynamics of molecular systems, approximating it as a Markov jump process.

In the work [56] included in this chapter, we present an introduction to MSMs and we explain how can be useful to drug design applications. For example in [66], MSMs have been used to extract representative structures for molecular docking. In other works [67, 68, 69, 70, 71, 25, 72, 73], the transition paths and mean first passage times between the unbound and bound states of a binding process have been estimated by MD simulations and MSMs.

I have contributed writing parts of the theory section and providing the MSM example for a one-dimensional diffusion process.

https://doi.org/10.1002/9783527806836.ch4

Published in *Biomolecular Simulations in Structure-based Drug Discovery*, Wiley-VCH, Weinheim (2018), p. 67

Markov state models in drug design

Bettina G. Keller*[1], Stevan Aleksić[1], and Luca Donati[1]

[1]Department of Biology, Chemistry, Pharmacy, Freie Universität Berlin, Takustr. 3, 14195 Berlin, Germany

1 Introduction

Starting from the lock-and-key model [1], models of ligand-target binding have been extended to acknowledge the role of conformational flexibility. In current models, the targets are assumed to fluctuate between several different conformations. In the conformational selection model [2], one of these conformations is the active state i.e. the conformation which is assumed in complex with the ligand. The ligand then "selects" this conformation from the ensemble and stabilizes it by forming a complex. By contrast, in the induced fit model [3], the active conformation is not sampled by the *apo*-target. Instead, the receptor and the ligand form an unspecific encounter complex. This weak complex then triggers a conformational rearrangement in the receptor which leads to the fully formed complex. While examples of mechanisms have been found [4–7], most binding processes fall somewhere in between these two extremes.

The conformational selection and the induced fit model neglect the conformational dynamics of the ligand, which is justified if the ligand is either rigid or its dynamics is fast compared to the dynamics of the target. However, this is not always a valid assumption. In particular, peptides and peptidomimetics exhibit a complex and often slow conformational dynamics. It is increasingly recognized that the flexibility of the target and the ligand and their mutual interaction are crucial factors in the ligand binding process. Thus, to systematically vary the thermodynamic and kinetic properties of a drug molecule, not only binding affinities but also dynamics need to be taken into account.

Experimentally, it is difficult to characterize the full conformational ensemble and its dynamics. However, an increase in computer power combined with improved algorithms has rendered molecular-dynamics simulations useful tools in structure-based drug design [8]. With progress in distributed computing [9], special purpose computer [10], and GPU devices [11], trajectories of several tens in microseconds are now accessible on a routine basis.

*bettina.keller@fu-berlin.de

A visual inspection of these trajectories is sometimes not feasible, due to the shear size of the data set, and almost always unrewarding, because it does not yield a quantitative description of the system. [1] While statistical analyses of the trajectory for the stationary properties of the system have been used routinely for decades, methods which yield a model of the dynamics have matured only recently. Markov state models (MSMs) [12–17], in which the dynamics is approximated as a Markovian jump process between distinct microstates, are the most widely used dynamic models. MSMs have been used to improve ensemble docking, to optimize a specific conformation in a ligand, to identify cryptic allosteric sites and to characterize ligand-binding processes as well as inactive-to-active transitions in signaling proteins. We do not aim at a comprehensive survey of the literature on this subject, nor do we focus on specific results. Our goal is to explain the different ways in which MSMs can be helpful in structure-based design.

2 Markov state models

MD simulations. Markov state models [12–17] are constructed from time series of the molecular dynamics, which can be generated by classical molecular-dynamics (MD) simulations. In a MD simulation, the molecular system is represented by N particles, where m_i denotes the mass and $\mathbf{r}_i(t) \in \mathbb{R}^3$ the three-dimensional coordinates of the ith particle at time t. The dynamics of the system is governed by a classical equation of motion:

$$m_i \frac{\partial^2 \mathbf{r}_i(t)}{\partial t^2} = -\nabla V\left(\mathbf{r}_1(t), ..., \mathbf{r}_N(t)\right) + \text{ thermostat} \quad \forall i \in [1, N] \tag{1}$$

where $V(\cdot)$ is a pre-defined potential energy function which determines how the particles interact. The thermostat term ensures that the simulation samples the canonical ensemble, and a wide range of algorithms have been proposed to achieve this task [18]. The MD simulation program then generates a trajectory of the particle positions

$$\mathbf{r}(t) = (\mathbf{r}_1(t), \mathbf{r}_2(t), \dots \mathbf{r}_N(t)) \in \mathbb{R}^{3N} \tag{2}$$

by numerically integrating eq. 1 (including the thermostat terms). Often, the momentum $\mathbf{p}_i(t) \in \mathbb{R}^3$ of each particle is additionally calculated yielding a phase space trajectory

$$\mathbf{x}(t) = (\mathbf{r}_1(t), \mathbf{p}_1(t), \dots \mathbf{r}_N(t), \mathbf{p}_N(t)) \in \mathbb{R}^{6N} . \tag{3}$$

where $\Omega \subset \mathbb{R}^{6N}$ is the $6N$-dimensional phase space or, equivalently, state space of the system. For a detailed explanation of the MD simulation technique, see Refs. [19–21]. Ref. [8] gives an overview of the current use of MD simulations in computational drug design.

[1] Nonetheless, any good researcher would have a look at the raw data before proceeding with more complex analyses.

The molecular ensemble. An individual trajectory samples an extremely high-dimensional space and is usually far to complex to be comprehensible by visual inspection. It needs to be further analyzed to transform the trajectory *data* into *information* about the molecular system. To achieve this, one shifts the view point from the dynamics of the individual system to the properties of an ensemble of systems.

In a thermostatted MD simulation, the trajectory samples the Boltzmann distribution

$$\pi(\mathbf{x}) \quad = \quad \frac{1}{Q} \exp\left(-\frac{1}{k_b T} H(\mathbf{x})\right) \tag{4}$$

where Q is the partition function, k_B is the Boltzmann constant, T is the temperature, and $H(\mathbf{x})$ is the classical Hamiltonian of the system. We assume that the dynamics is ergodic, i.e. each region of the state space has to be reachable from any other region of the state space. In practice, this means that the trajectory has to be long enough such that all relevant parts of the state space have been sampled sufficiently. In this case, the ensemble average of any observable $o(\mathbf{x})$ can be replaced by a time integral over the trajectory $\mathbf{x}(t)$

$$\langle o \rangle \quad = \quad \int_\Omega \pi(\mathbf{x}) o(\mathbf{x}) \, \mathrm{d}\mathbf{x} = \lim_{T_{\mathrm{trj}} \to \infty} \frac{1}{T_{\mathrm{trj}}} \int_{t=0}^{T_{\mathrm{trj}}} o(\mathbf{x}(t)) \, \mathrm{d}t \tag{5}$$

where T_{trj} is the length of the trajectory. Eqs. 4 and 5 are the starting point for MD analysis methods, which yield information on the stationary properties of the system.

The propagator. To gain insight into the dynamics of the system, one considers a time-dependent probability density $p_t(\mathbf{x})$ and the transition probability density $p(\mathbf{x}, \mathbf{y}; \tau)$, i.e. the probability density to find the system in state $\mathbf{y}$ at time $t + \tau$, given that it has been in state $\mathbf{x}$ at time t. Note that the transition probability density is parametrized by the lag time τ, which denotes the time interval at which the states of the system are evaluated. Different values of τ yield different transition probability densities. Additionally, the transition probability density relies on two assumptions on the dynamics of the system. First, $p(\mathbf{x}, \mathbf{y}; \tau)$ is independent of t, which is the case if no time-dependent forces act on the system (time-homogeneous dynamics). Second, the transition probability density only depends on the current state $\mathbf{x}$ and not on any of the previous states of the system, i.e. the dynamics need to be Markovian. We make a third assumption, namely that the dynamics fulfill detailed balance

$$\pi(\mathbf{x}) p(\mathbf{x}, \mathbf{y}; \tau) = \pi(\mathbf{y}) p(\mathbf{y}, \mathbf{x}; \tau) \, . \tag{6}$$

That is, in an ensemble which is distributed according to the Boltzmann distribution $\pi(\mathbf{x})$, the number of transitions from state $\mathbf{x}$ to $\mathbf{y}$ within time τ is equal to the number of transitions in the opposite direction.

The transition probability density $p(\mathbf{x}, \mathbf{y}; \tau)$ defines the propagator $\mathcal{P}(\tau)$, a mathematical object that propagates the probability density function $p_t(\mathbf{x})$ forward in time

$$p_{t+\tau}(\mathbf{x}) = \mathcal{P}(\tau) p_t(\mathbf{x}) \,. \tag{7}$$

Because we assumed Markovian dynamics, the probability density at $t + n\tau$ can be obtained by applying the propagator n times

$$p_{t+n\tau}(\mathbf{x}) = \mathcal{P}^n(\tau) p_t(\mathbf{x}) = \mathcal{P}(n\tau) p_t(\mathbf{x}) \,. \tag{8}$$

When $n \to \infty$, the probability density tends to the Boltzmann probability density $\pi(\mathbf{x})$

$$\pi(\mathbf{x}) = \lim_{n\to\infty} \mathcal{P}^n(\tau)\pi(\mathbf{x}) \,. \tag{9}$$

Note that the lag time τ defines the time resolution at which the time-evolution of the probability density can be represented by $\mathcal{P}(\tau)$.

The dominant eigenspace. The advantage of introducing the propagator is that the slow dynamics of the system can be rationalized using a small set of its eigenfunctions $l_i(\mathbf{x})$ and eigenvalues $\lambda_i(\tau)$

$$\mathcal{P}(\tau) l_i(\mathbf{x}) \quad = \quad \lambda_i(\tau) l_i(\mathbf{x}) \,, \tag{10}$$

the so-called dominant eigenspace. For ergodic and detailed-balanced dynamics, the eigenvalues are real-valued and lie on the interval $\lambda_i(\tau) \in]0, 1]$. The largest possible eigenvalue $\lambda_1(\tau)$ is unique and always exists. Its associated eigenfunction $l_1(\mathbf{x})$ is equal to the Boltzmann distribution

$$\pi(\mathbf{x}) \quad = \quad \mathcal{P}(\tau)\pi(\mathbf{x}) = \mathcal{P}(\tau) l_1(\mathbf{x}) \,. \tag{11}$$

The eigenfunctions $l_1(\mathbf{x}), l_2(\mathbf{x}) \ldots$ form a complete basis of the Hilbert space of probability density functions. This means that any probability density function can be expressed as a linear combination of these eigenfunctions

$$p_t(\mathbf{x}) \quad = \quad \sum_{i=1}^{\infty} c_i \, l_i(\mathbf{x}) \,, \tag{12}$$

where the eigenfunctions are ordered according to their associated eigenvalues. Inserting eq. 12 into eq. 8 yields

$$\begin{aligned} p_{t+n\tau}(\mathbf{x}) \quad &= \quad \mathcal{P}^n(\tau) \sum_{i=1}^{\infty} c_i \, l_i(\mathbf{x}) = \sum_{i=1}^{\infty} c_i \, \lambda_i^n(\tau) \, l_i(\mathbf{x}) \\ &\approx \quad \pi(\mathbf{x}) + \sum_{i=1}^{M-1} c_i \, \lambda_i^n(\tau) \, l_i(\mathbf{x}) \,. \end{aligned} \tag{13}$$

The time evolution of a probability density can be regarded as a superposition of dynamic modes $l_i(\mathbf{x})$ with amplitudes $c_i\,\lambda_i^n(\tau)$. Because $\lambda_i(\tau) \in]0,1]$, the factor $\lambda_i^n(\tau)$ decays exponentially

$$\lambda_i^n(\tau) \quad = \quad \exp(n\ln(\lambda_i(\tau))) = \exp\left(-\frac{n\tau}{t_i}\right), \tag{14}$$

where t_i is the implied timescale (its) of the ith mode

$$t_i \quad = \quad -\frac{\tau}{\ln(\lambda_i(\tau))}. \tag{15}$$

Note that, for Markovian dynamics, the implied timescales are independent of τ. The smaller $\lambda_i(\tau)$, the faster $c_i\,\lambda_i^n(\tau)$ decays to zero. Thus, for sufficiently large $n\tau$, the fast decaying modes can be neglected, and the dynamics is determined by the slowest M modes. This works particularly well, if there is gap in the eigenvalue spectrum between $\lambda_M(\tau)$ and $\lambda_{M+1}(\tau)$ (Fig. 1.b). The first mode is the Boltzmann density, for which always $c_1 = 1$. And because $\lambda_1(\tau) = 1$, this mode does not decay ($t_1 = \infty$). Hence, for $n \to \infty$, eq. 13 yields eq. 9.

Fig. 1 illustrates the dominant eigenspace of a diffusion on a one-dimensional potential energy surface (Fig. 1.a). An example trajectory is shown in Fig. 2.a. The eigenvalue spectrum (Fig. 1.b) has a gap between $\lambda_3(\tau)$ and $\lambda_4(\tau)$. Thus, besides the stationary Boltzmann distribution (Fig. 1.c), the system has two slow modes: $l_2(x)$ (Fig. 1.d) and $l_3(x)$ (Fig. 1.e). Note that the number of slow modes coincides with the number of minima in the potential energy surface. The modes represent kinetic exchange processes between regions in which the eigenfunction assumes a negative sign and those regions in which the eigenfunction assumes a positive sign. The mode $l_2(x)$ represents the exchange between the minimum on the right-hand side of the potential energy surface and the two other minima, i.e. the transition across the largest barrier in the system. The equilibration across this barrier takes place on a timescale of approximately $t_2 = 1260$ timesteps. The mode $l_3(x)$ represents the equilibration between the central minimum and the two minima on the left and right side of the potential energy surface, which takes place on a timescale of approximately $t_3 = 300$ timesteps. The modes thus contain a wealth of information on the energy minima of the system and the relative height of the barriers between them.

We remark that the theory of Markov state models is usually not formulated in terms of the propagator, but in terms of the closely related transfer operator. In fact, for detailed-balanced dynamics, the transfer operator is the adjoint of the propagator. The two operators share the same eigenvalues, the eigenfunctions of the transfer operator $r_i(\mathbf{x})$ are related to the eigenfunctions of the propagator by $l_i(\mathbf{x}) = \pi(\mathbf{x})r_i(\mathbf{x})$. For the sake of brevity, we here omit the discussion of the transfer operator and point interested readers to reference [16, 22, 23].

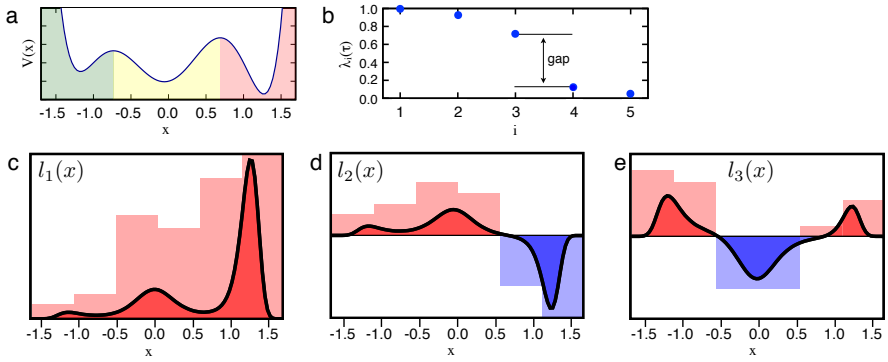

Figure 1: Dominant eigenspace of the propagator. (a) energy function; (b) eigenvalue spectrum at $\tau = 100$ timesteps; (c)-(e) dominant eigenfunctions, continuous lines: true eigenfunctions, histogramm: MSM approximation.

The Markov state model. The analytical expression of the propagator contains the potential energy function and is too complex to be analyzed directly. Instead one approximates the propagator by a transition matrix $\mathbf{T}(\tau)$ whose elements can be estimated from a MD trajectory.

The state space Ω is discretized into a set of m non-overlapping microstates $A_1, A_2 \ldots A_m$, such that $\bigcup_{i=1}^{m} A_i = \Omega$ and $A_i \cap A_j = \emptyset$ for $i \neq j$. The probability density $p_t(\mathbf{x})$ is then approximated as a probability vector $\mathbf{p}_t$ whose elements are obtained by integrating $p_t(\mathbf{x})$ over the individual microstates

$$[\mathbf{p}_t]_i \quad = \quad \int_{A_i} p_t(\mathbf{x})\, \mathrm{d}\mathbf{x}\,. \tag{16}$$

Eq. 7 can then be approximated as

$$\mathbf{p}^\top(t+\tau) = \mathbf{p}^\top(t)\mathbf{T}(\tau)\,. \tag{17}$$

The elements of the transition matrix $\mathbf{T}(\tau)$ represent the transition probabilities between pairs of microstates, i.e the conditional probability of finding the system in state A_i at time $t+\tau$, given that it has been in state A_i at time t

$$T_{ij}(\tau) \quad = \quad \mathbb{P}[\mathbf{x}(t+\tau) \in A_j \mid \mathbf{x}(t) \in A_i]\,. \tag{18}$$

The transition probabilities can be estimated from a MD trajectory $\mathbf{x}(t)$ as

$$\hat{T}_{ij}(\tau) \quad = \quad \frac{\hat{C}_{ij}(\tau)}{\sum_j \hat{C}_{ij}(\tau)}\,. \tag{19}$$

$\hat{C}_{ij}(\tau)$ are the number of transition between state A_i and state A_j within lag time τ which have been sampled by the trajectory. We use the "hat" to denote estimated properties. The transition count $\hat{C}_{ij}(\tau)$ is normalized by the total

number of outgoing transitions from state A_i, thereby yielding a probability. Consequently, the transition matrix $\hat{\mathbf{T}}(\tau)$ is row-normalized, where each row vector $\hat{\mathbf{t}}_i(\tau)$ represents the probability distribution of reaching any microstate A_j in the state space within time τ, starting from state A_i.

Mathematically, $\hat{C}_{ij}(\tau)$ is an estimate of a correlation function

$$C_{ij}(\tau) \quad = \quad \mathrm{cor}(\mathbf{1}_{A_i}, \mathbf{1}_{A_j}; \tau) = \lim_{T_{trj}\to\infty} \int_0^{T_{trj}} \mathbf{1}_{A_i}(t)\, \mathbf{1}_{A_j}(t+\tau)\, \mathrm{d}t\,, \qquad (20)$$

where we used the abbreviated notation $\mathbf{1}_{A_i}(t) = \mathbf{1}_{A_i}(\mathbf{x}(t))$. The function

$$\mathbf{1}_{A_i}(\mathbf{x}) \quad = \quad \begin{cases} 1 & \text{if } \mathbf{x} \in A_i, \\ 0 & \text{if } \mathbf{x} \notin A_i. \end{cases} \qquad (21)$$

is the indicator function of microstate A_i. One can show that $\mathbf{T}_{ij}(\tau) = \frac{C_{ij}(\tau)}{\sum_j C_{ij}(\tau)}$ is a valid discretization of the transfer operator and, by extension, the propagator, and that the discretized operator converges to the true operator if the microstates are infinitesimally small [22, 24].

Fig. 2 illustrates the estimation of an MSM on a trajectory $x(t)$ which samples a one-dimensional potential energy function $V(x)$ (Fig. 2.a). The one-dimensional state space is discretized into six microstates $\{A_1 \dots A_6\}$ and a sliding window of length τ (blue box) is moved across the time axis. The two green dots denote the states at time t and $t+\tau$, in this case $x(t) \in A_6$ and $x(t+\tau) \in A_3$. Consequently, the element $C_{63}(\tau)$ of the transition count matrix is increased by one (Fig. 2.b). Only the state at the beginning and at the end of the sliding window are relevant for the transition. The system might visit other states within the time window τ. The transition matrix can be visualized as a kinetic network, in which the edges correspond to the transition probabilities (Fig. 2.b).

Thus, a MSM replaces a dynamics which is continuous in space by a jump process between discrete microstates. However, the discretization introduces an error. In particular, although the continuous dynamics is Markovian (eq. 8: $\mathcal{P}^n(\tau) = \mathcal{P}(n\tau)$), the discretized dynamics is not

$$\mathbf{T}^n(\tau) \quad \approx \quad \mathbf{T}(n\tau)\,. \qquad (22)$$

It is therefore crucial to validate each MSM.

Two test for the deviation from Markovian behavior are commonly used: the Chapman Kolmogorov test [16] and the implied timescale test [13]. The Chapman Kolmogorov test starts from an initial distribution $\mathbf{p}_0$ which is restricted to a particular set of microstates, e.g. all microstates which belong to the central minimum in Fig. 1 $S = \{A_3, A_4\}$:

$$[\mathbf{p}_0]_i \quad = \quad \begin{cases} \frac{\pi_i}{\sum_{j\in S} \pi_j} & A_i \in S \\ 0 & A_i \notin S \end{cases} \qquad (23)$$

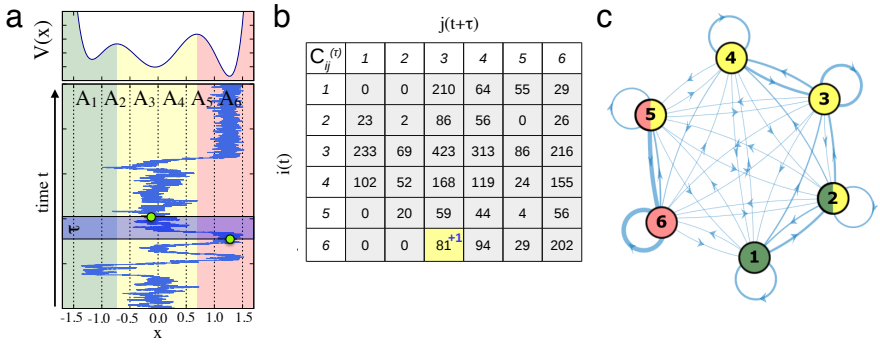

Figure 2: Construction of a MSM. (a) example trajectory; (b) count matrix; (c) network representation of the transition matrix.

where $\pi_i = \int_{A_i} \pi(\mathbf{x})\,\mathrm{d}\mathbf{x}$. This distribution is propagated by a transition matrix $\mathbf{T}(\tau_0)$ n times, and in the resulting probability distribution, the elements corresponding to S are added to find the probability of being in this set of microstates after $n\tau_0$, given that the process has started in S

$$p_{\mathrm{MSM}}(S,S;n\tau_0) \quad = \quad \sum_{i\in S}\left[\mathbf{p}_0^\top \mathbf{T}^n(\tau_0)\right]_i = \sum_{i\in S}\left[\mathbf{p}_{n\tau_0}^\top\right]_i . \tag{24}$$

This probability is compared to the corresponding probability estimated from the trajectory by counting the transitions $S \to S$ within time $n\tau_0$

$$p_{\mathrm{MD}}(S,S;n\tau_0) \quad = \quad \sum_{i\in S}\hat{T}_{ij}(n\tau_0) = \sum_{i\in S}\frac{\hat{C}_{ij}(\tau_0)}{\sum_j \hat{C}_{ij}(\tau_0)} . \tag{25}$$

This test has to be carried out over a wide range of values for n. If the resulting curves $p_{\mathrm{MD}}(S,S,n\tau_0)$ and $p_{\mathrm{MSM}}(S,S,n\tau_0)$ are close enough, the model with lag time τ_0 is a valid model. The advantage of the Chapmann Kolmogorov test is that it directly probes equation 22. The disadvantages are that the test has to be repeated for many values τ_0 and that its results tend to be sensitive to the choice of S.

The implied timescale test probes eq. 15. One estimates MSMs at arange of lag times τ and plots resulting implied timescales as function of τ (Fig. 3). For small values of τ, the implied timescales are an increasing monotonic functions, but after a certain value τ_{Markov}, the implied timescales become approximately constant, thus indicating that for $\tau \geq \tau_{\mathrm{Markov}}$ the MSM is approximately Markovian [24]. Fig. 3 shows the implied timescales associated to the second and third dominant eigenfunction, obtained from a MSM with 100 microstates (solid line) and a MSM with 6 microstates (dashed line). For the fine discretization, the

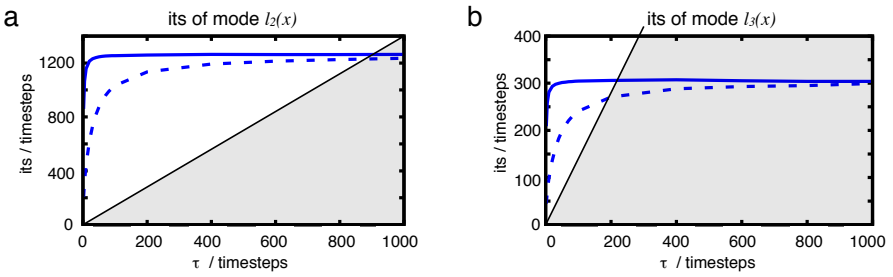

Figure 3: Implied timescale test for the one-dimensional diffusion process (a) its of mode $l_2(x)$, (b) its of mode $l_3(x)$, gray area: its $< \tau$, solid line: MSM with 100 microstates, dashed line: MSM with 6 microstates.

implied timescales converge to a constant function at much smaller values of τ than for the 6-microstate MSM. The approximaton error of the 6-microstate MSM is als demonstrated in Fig. 1.c-e, which shows the MSM eigenvectors as a histogram. As a rule of thumb, the finer the discretization, smaller the approximation error. However, one faces the following trade-off: the larger the number of microstates, the lower the average number of observed counts per transition. Thus, by decreasing the approximation error one tends to increase the statistical uncertainty [25, 26]. The challenge in the construction of MSMs is to balance these two errors.

To summarize, the construction of MSM from a MD simulation consists of three fundamental steps (Fig. 4): (1) discretization of the state space, (2) estimation of the transition probabilities, and (3) validation of the MSM. Several features of the MSMs can be utilized for rational drug desing. From the microstates, one can extract representative structures of the conformational ensemble (section 3). The microstates can be aggregated into long-lived conformations (section 4), and the kinetic network can be analyzed (section 5).

3 Microstates

Structure-based drug design methods, such as molecular docking to a known binding pocket and the detection of new binding pockets, requires high-resolution structures of the target. However, targets are not entirely rigid, and minor fluctuations on the surface of the protein might heavily affect the shape or accessibility of any binding pocket. Using only a single crystal structure arbitrarily limits the predictive power of any structure-based approach. MD simulations in principle cover the entire conformational ensemble of a target, however, using each frame of the trajectory is a starting point for a structure-based design is computationally prohibitive. Thus, a method is needed which extracts meaningful representatives from the conformational ensemble. The discretization of a validated MSM is particularly suited for this task, because the discretization

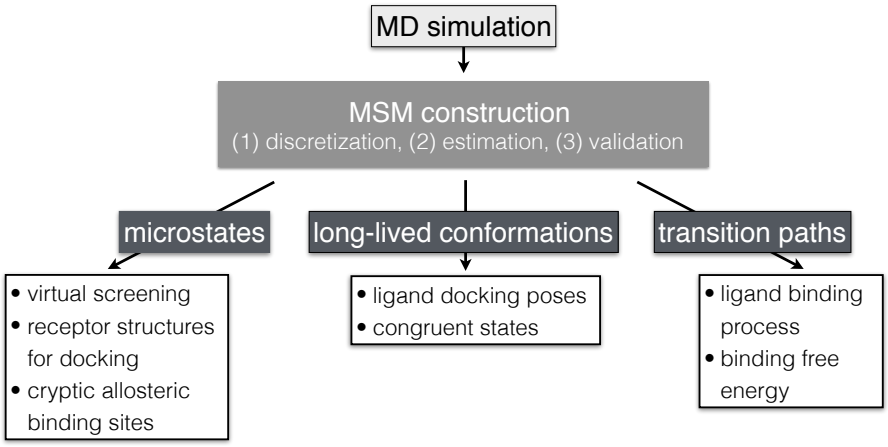

Figure 4: Workflow of MSM analyses for drug design

yields a small number of microstates (compared to the number of frames) and mirrors the features of the free-energy landscape. In particular, it ensures that slowly interconverting structures are assigned to different microstates. From each microstate, a representative structure is extracted and the set of representative structures is processed by the structure-based method of choice. Additionally, the MSM readily provides the relative probability and the life-time of each microstate.

In Ref. [27], this approach has been used for a docking study to MDM2. MDM2 is an interesting target for anti-cancer drugs because it binds to the tumor-suppressor p53 and thereby blocks its activity. Inhibiting MDM2 might thus restore p53 activity in cancer cells. However, the N-terminal lid region of MDM2 transiently covers its binding cleft, making MDM2 a particularly difficult receptor for docking studies. The authors conducted simulations of the *apo*-MDM2 and constructed an MSM with 2000 microstates. A set of ten ligands, for which crystal structures in complex with MDM2 are available, was then docked to representatives of each MDM2 microstate. For each ligand, the twenty docking poses with best docking score were considered as suitable docking poses. This approach recovered the correct docking pose for eight of the ten ligands from the conformational ensemble of the *apo*-MDM2, whereas the success rate of docking the set of ligands to any of the available receptor structures was considerably lower.

Knowledge of the conformational ensemble of the target is also important for the detection of binding sites. The group of G.R. Bowman analyzed MSM microstates to identify cryptic allosteric sites in TEM β-lactamase and two other receptors [28, 29]. Targeting allosteric sites is a promising avenue for several reasons. Allosteric sites drastically increase the range of possible targets,

including proteins which were previously considered undruggable. The allosteric drug might be effective at lower affinities, because they do not have to compete with a natural ligand. Additionally, they might be highly specific, because allosteric sites are less evolutionarily conserved and therefore more unique than orthosteric sites. Finally, with allosteric drugs, one can potentially increase a desired activity of the target. Computational methods for the rational design of allosteric drugs have been reviewed in [30]. Unfortunately, many allosteric sites only open transiently in the conformational ensemble and are often not detectable in a crystal structure of the receptor, hence the adjunct "cryptic".

TEM β-lactamase hydrolyzes β-lactam antibiotics and thereby confers antibiotic resistance. Based on extensive MD simulations, the conformational space of TEM β-lactamase was discretized into 5,152 microstates. Representative structures from each microstate were then screened for pockets using the program LIGSITE [31]. Pockets close to the orthosteric binding site and those visible in the crystal structure were discarded, and the remaining pockets were clustered into merged pockets. The relative probability of a given pocket in the conformational ensemble was estimated as the sum of the relative probabilities π_i of all microstates A_i in which the pocket occurred. This yielded a considerable number of transiently open pockets. The authors then used a mutual-information analysis [32,33] to identify those pockets which are coupled to the orthosteric site. The approach correctly identified a known allosteric binding site as the most accessible transient pocket, with a relative probability of 53% and the strongest coupling to the orthosteric site. Additionally, it yielded a series of previously unknown allosteric sites with sufficient relative probability to be binding pockets. In a subsequent study [34], the group virtually screened a library of compounds against an ensemble of TEM β-lactamase structures which contained the cryptic pockets identified by the MSM analysis. Experimental screening of the hits from the virtual screening identified one inhibitor and two activators of TEM β-lactamase.

4 Long-lived conformations

Peptidomimetics and cyclic peptides mimic the folded structure of a protein and open up a route to inhibiting protein-protein interactions [35,36]. However, their dynamics is complex and often not markedly faster than the dynamics of the target. Moreover, small modifications to the chemical structure can induce startling variations in the affinity or the bioavailability of the drug. To design these ligands, it is paramount to understand the dynamic equilibrium between the targeted long-lived conformation and the competing long-lived conformations.

Long-lived conformations consist of a set microstates which show high transition rates within the set and low transition rates to microstates outside of the set, see for example microstate 5 and 6 in Fig. 2. The relative stability of a long-lived conformation is obtained by summing over Boltzmann populations π_i of each microstate in the set.

The Bayesian agglomerative clustering engine (BACE) algorithm [37] uses the observed transition counts to extract long-lived conformations from an MSM. For each pair of microstates, a Bayes factor is calculated which compares how likely the observed transitions have been generated from the same underlying distribution (i.e. both microstates belong to the same long-lived conformations) or from two different distributions (i.e the microstates belong to different long-lived conformations). By iteratively merging microstates according to the Bayes factor and recalculating the Bayes-factor matrix, the algorithm yields an aggregation of the microstates into long-lived conformations.

The Perron-Cluster Cluster Analysis+ (PCCA+) [38] is based on the insight that the dominant MSM eigenvectors contain information on the slow dynamics and thus on the long-lived conformations. Each microstate corresponds to a point in the M-dimensional space of the dominant eigenvectors. One can show that, for dynamics which exhibits long-lived conformations, the microstates are arranged along a simplex in this space, where each vertex of the simplex corresponds to one long-lived conformation. PCCA+ identifies long-lived conformations by aggregating microstates in the vicinity of each vertex.

Although identifying long-lived conformations from an MSM has become a routine analysis, comparing long-lived conformations of different chemical constructs or in different external conditions remains a challenge. Of course, the long-lived conformations can be compared *a posteriori* by visual inspection or by calculating the RMSD. This, however, amounts to matching conformational sub-ensembles - a task which is often sensitive to the choice of distance measure. On the other hand, comparing single representatives of each conformation tends to be sensitive to the choice of the representative. A direct comparison of the long-lived conformations of two different systems is only possible if the MSMs are built using a common discretization. For this, one concatenates the trajectories of both systems and decides on a discretization based on this combined data set. The count matrices are then estimated on this discretization from each data set separately. As a result, the eigenvectors of the MSMs can be compared directly. For example, a shift in the population of the ith microstate from one system to the other results in a shift in the ith element of the first (left) transition matrix eigenvector. Likewise, if the long-lived conformations change, the set of microstate which defines these long-lived conformations changes. Thus, one can match long-lived conformations in different systems by comparing their sets of microstates.

This approach has been used in Ref. [39] to compare a set of cyclic peptide hairpin mimetics. These peptides were designed to mimic a β-hairpin segment of LapD which forms an interface with LapG and thereby modulates the activity of LapG. The two proteins occur in the bacterium *Pseudomonas fluorescens* and are involved in bacterial biofilm formation. The objective of the study was to identify those molecules in which the hairpin structure was particularly stable, and to rationalize the stability relative to the competing conformations. A prescreening of a larger set of constructs yielded four nine-residues constructs, each of which was covalently cross-linked by two linkers. These constructs had two design switches: a substituent in the terminal linker could be either a hydrogen

(R=H) or a methyl group (R=CH_3), and the N-terminal valine was incorporated either in its D-isomer (D-Val) or its L-isomer (L-isomer), yielding four possible combinations. MSMs with a common discretization were constructed for the D-isomers and L-isomers, respectively, and revealed a native and a near-native conformation, whose populations could now be compared directly. Interestingly, in the D-isomers, the native structure was more for the R=CH_3 construct than for the R=H construct, whereas is was the opposite in the L isomers. This could be rationalized by a steric interaction between the residue R and the valine side chain.

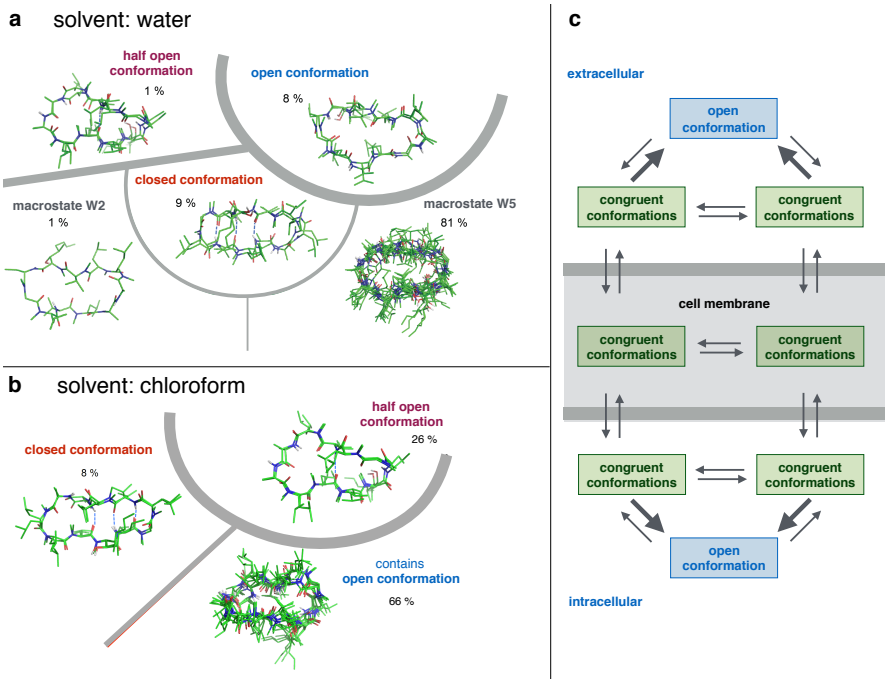

Figure 5: MSMs of Cyclosporin A (a) hierarchy of the free-energy in water, (b) hierarchy of the free-energy in chloroform, (c) updated hypothesis for the diffusion of cyclosporin A across a membrane. Adapted with permission from Ref. [40]. Copyright 2016 American Chemical Society.

In some cases, a crucial feature of a drug molecule relies on a shift in the stability of its long-lived conformations. For example, cyclosporin A, a cyclic peptide, and an immunosuppressive drug, crosses membranes by passive diffusion despite its high molecular weight and lipophilicity. However, the peptide is capable of forming a closed structure in which many backbone hydrogen bond donors and acceptors are engaged in intramolecular hydrogen bonds are thus shielded from the solvent (Fig. 5). It has thus been hypothesized that

cyclosporin A crosses the membrane in the closed conformation and that a suitable design would hence be to stabilize this particular structure. We investigated this hypothesis [40] and simulated cyclosporin A in water and in chloroform as a proxy for the membrane interior. We then constructed MSMs based on a common discretization. The resulting long-lived conformations and hierarchy of the free-energy landscape are shown in Fig. 5.a and b. Both simulations sampled the open and the closed conformation. In water, the closed conformation was neither energetically favorable nor particularly stable: it quickly interconverted with the long-lived conformations W2 and W5 (Fig. 5.a). Intriguingly, we could identify a half-open structure and which was present and long-lived in both ensembles. In water, this structure is energetically more favored and more stable than the closed structure, and it is highly populated and stable in chloroform. The existence of this third conformation was supported by NMR data. We thus proposed that there is actually an ensemble of congruent conformations which occur in polar and apolar solvent and can thus diffuse through a membrane (Fig. 5.a). An appropriate design strategy would then be to stabilize not a single structure but to enable the peptide to form as many congruent conformations as possible.

5 Transition paths

Direct simulation and MSM analysis of ligand binding processes have become available in recent years. Investigated systems include the wide range of target-receptor pairs: serine protease trypsin - benzamidine [41–43], DNA - cisplatin [44], LAO-binding protein - L-arginine [45], choline-binding protein - choline [46], MDM2 - transactivation domain of p53 [47], and GPCR $S1P_1R$ - lipid inhibitor ML056 [48]. Likewise, MSMs of transitions between inactive and active states of signaling proteins have been reported for the GPCR β_2 adrenergic receptor [49, 50], Src kinase [51], and the cyclic nucleotide-binding domain of protein kinase A [52]. What these systems have in common is a clearly defined initial state I, i.e. the unbound state or the inactive state, and an equally well-defined final state F, i.e. the bound state or the active state. Both, the initial and the final state, usually consist of several microstates. MSMs can be used to characterize the transition paths and mean first passage times between I and F.

The mean first passage time (MFPT) [53] of a microstate outside of the final state, $A_i \notin F$, is the average time it takes to get from this microstate to any microstate within the final state, $A_f \in F$. If A_j is a microstate on the way between, A_i and the final state F, and if a transition $A_i \to A_j$ has been made, then $\mathrm{MFPT}(i) = \tau + \mathrm{MFPT}(j)$, i.e. the time τ it took to get to A_j plus the $\mathrm{MFPT}(j)$ from there. All possible transitions $A_i \to A_j$ are accounted for by this equation

$$\mathrm{MFPT}(i) \quad = \quad \sum_j T_{ij}(\tau) \cdot [\tau + \mathrm{MFPT}(j)] \;, \tag{26}$$

where $T_{ij}(\tau)$ is the transition probability from A_i to A_j. We define that, for microstates which belong to the final state,

$$\mathrm{MFPT}(f) = 0 \quad \forall A_f \in F\,. \tag{27}$$

Eq. 26 can be set up for all the microstates. One obtains a system of linear equations which can be solved iteratively. The MFPT from initial to final state is then obtained by summing over the MFPTs of all microstates within I

$$\mathrm{MFPT}(I) \;=\; \frac{1}{\pi_I}\sum_{i\in I}\pi_i\,\mathrm{MFPT}(i) \tag{28}$$

MFPT are particularly useful for binding processes, because they can be converted into association and dissociations rates

$$\begin{aligned} k_{\mathrm{on}} &= \frac{1}{\mathrm{MFPT}(\mathrm{unbound}\to\mathrm{bound})} \\ k_{\mathrm{off}} &= \frac{1}{\mathrm{MFPT}(\mathrm{bound}\to\mathrm{unbound})} \end{aligned} \tag{29}$$

and thus be compared to experiment.

Contrary to rates, transition paths are difficult to elucidate experimentally. Using transition path theory [54, 55], these paths can be extracted. The flux $f_{ij}(\tau)$ between two microstates A_i and A_j is the total probability to observe a transition $A_i \to A_j$ within τ. When considering all possible trajectories, $f_{ij} = \pi_i T_{ij}(\tau)$. From these trajectories, one extracts the reactive trajectories, i.e. those trajectories which go directly from the initial state I to the final state F without hitting I in between. This yields an effective flux,

$$f_{ij}^{\mathrm{effective}} \;=\; q_i^- \cdot \pi_i T_{ij}(\tau)\cdot q_j^+ \tag{30}$$

where q_i^- is the probability that the trajectory came from the initial state I, when it reached A_i, rather than from the final state F, and q_j^+ is the probability that the trajectory will proceed to the final state F after leaving A_j. q_i^- and q_j^+ are the called backward and forward committor, respectively. Both properties can be calculated from the transition matrix by solving a system of linear equations. In the present set of trajectories, many contain recrossing events, i.e. sequences like $A_i \to A_j \to A_i \to A_j \ldots$. This yields a high effective flux between A_i and A_j, which however does not mean that many reactive trajectories pass through A_i and A_j. One therefore reduces the set of trajectories further, and removes all trajectories which contain recrossing events or detours. The probability to observe a transition $A_i \to A_j$ in this set of trajectories is the net flux

$$f_{ij}^+(\tau) \;=\; \max\{0, f_{ij}^{\mathrm{effective}}(\tau) - f_{ji}^{\mathrm{effective}}(\tau)\}\,. \tag{31}$$

For detailed-balanced processes, and if the microstate are arranged such that $q_i^+ \le q_j^+$, eq. 31 can be rearranged as

$$f_{ij}^+(\tau) \;=\; \pi_i T_{ij}(\tau)(q_j^+ - q_i^+)\,. \tag{32}$$

Representing the net flux matrix as network graph usually yields a very intuitive representation of the transition paths from I to F, see Refs. [43, 45]

In addition to mean first passage times and transition paths, many authors have extracted long-lived conformations from their MSMs and have found that ligand binding processes, as well as activation processes are not purely diffusive but proceed via a series of metastable states [41–47,49,51,52]. Also, binding free energies have been estimated from MSMs [41–47]. The results are comparable to or slightly better than the Molecular Mechanics Poisson-Boltzmann Surface Area method (MMPB-SA) [42, 44], but not as good as the estimates from a free-energy perturbation [42].

6 Outlook

In our account, we have not touched on the question of how to find a suitable discretization. In practice, the actual discretization is preceded by a dimensionality reduction of the trajectory, either by manually choosing relevant coordinates or by means of dimensionality reduction method. Many of the studies we mentioned used the time-lagged independent component analysis (tICA) [56, 57] to find a suitable low-dimensional representation of the system. Similar to the principle component analysis, tICA is a coordinate transformation. It yields an optimal slow subspace which decorrelated (at lag time τ) from the remaining coordinates. This subspace is then usually discretized into non-overlapping microstates and a conventional MSM is constructed.

Besides this, several advanced discretizations, such as the core-set method [58, 59] and the variational approach to molecular dynamics [60, 61]. These methods abandon the use of discrete microstates and instead use functions of the conformational space as ansatz functions for the discretization of the transfer operators. This significantly reduces the approximation error of the model and thus yields a more accurate description of the conformational dynamics.

Another important development are dynamical reweighting methods [62–64]. So far, MSMs have been estimated from direct simulations of the conformational transitions. With dynamical reweighting methods, one can estimate a dynamical model from a biased simulation, such as a metadynamics simulation [65] or a replica-exchange MD [63]. This drastically increases the range of molecular time and length scale, for which dynamical models can be contructed.

User-friendly software packages [66, 67] have made MSMs accessible to a wide range academic researchers. This has led to innovative ways to use this technique in structure-based drug design. Currently, the work-flows of an MSM analysis have not been automized to the point where they can be routinely in pharmaceutical companies. However; as the accuracy of dynamics models further improves and the sampling becomes less of an issue, taking the conformational flexibility into account is likely to become the norm structure-based drug design.

Acknowledgements

This research has been funded by Deutsche Forschungsgemeinschaft (DFG) through CRC 765 "Multivalency as a chemical organization and action principle", Project C10, and through CRC1114 "Scaling Cascades in Complex Systems", Project B05.

References

[1] Emil Fischer. Einfluss der configuration auf die wirkung der enzyme. ii. *Ber. Dtsch. Ges.*, 27(3):3479–3483, 1894.

[2] Jacque Monod, Jeffries Wyman, and Jean-Pierre Changeux. On the Nature of Allosteric Transitions: A Plausible Model. *J. Mol. Biol.*, 12:88–118, 1965.

[3] D. E. Koshland, G. Namethy, and D. Filmer. Comparison of experimental binding data and theoretical models in proteins containing subunits. *ACS Biochem.*, 5(1):365–385, 1966.

[4] Christine Berger, Susanne Weber-Bornhauser, Jolanda Eggenberger, Jozef Hanes, Andreas Plckthun, and Hans Rudolf Bosshard. Antigen recognition by conformational selection. *FEBS Lett.*, 450(1-2):149153, 1999.

[5] Yifat Miller, Buyong Ma, and Ruth Nussinov. Polymorphism in Alzheimer Aβ Amyloid Organization Reflects Conformational Selection in a Rugged Energy Landscape. *Chem. Rev.*, 110(8):4820–4838, 2010.

[6] James R Williamson. Induced fit in RNA-protein recognition. *Nat. Struct. Mol. Biol.*, pages 834–837, 2000.

[7] Kenneth A. Johnson. Role of induced fit in enzyme specificity: A molecular forward/reverse switch. *J. Biol. Chem.*, 283(39):26297–26301, 2008.

[8] Marco De Vivo, Matteo Masetti, Giovanni Bottegoni, and Andrea Cavalli. Role of Molecular Dynamics and Related Methods in Drug Discovery. *J. Med. Chem.*, 59(9):4035–4061, 2016.

[9] Michael Shirts and Vijay S Pande. Screen Savers of the World Unite! *Science*, 290(5498):1903–1904, 2000.

[10] David E Shaw, Paul Maragakis, Kresten Lindorff-Larsen, Stefano Piana, Ron O Dror, Michael P Eastwood, Joseph A Bank, John M Jumper, John K Salmon, Yibing Shan, and Willy Wriggers. Atomic-Level Characterization of the Structural Dynamics of Proteins. *Science*, 330(6002):341–346, 2010.

[11] Nathaniel Stanley and Gianni De Fabritiis. High throughput molecular dynamics for drug discovery. *In Silico Pharmacol.*, pages 1–4, 2015.

[12] Ch Schütte, A Fischer, W Huisinga, and P Deuflhard. A Direct Approach to Conformational Dynamics Based on Hybrid Monte Carlo. *J. Comp. Phys.*, 151:146–168, 1999.

[13] William C. Swope, Jed W Pitera, and Frank Suits. Describing Protein Folding Kinetics by Molecular Dynamics Simulations. 1. Theory†. *J. Phys. Chem. B*, 108:6571–6581, 2004.

[14] John D Chodera, Nina Singhal, Vijay S Pande, Ken A Dill, and William C Swope. Automatic discovery of metastable states for the construction of Markov models of macromolecular conformational dynamics. *J. Chem. Phys.*, 126(15):155101, 2007.

[15] Nicolae-Viorel Buchete and Gerhard Hummer. Coarse Master Equations for Peptide Folding Dynamics. *J. Phys. Chem. B*, 112:6057–6069, 2008.

[16] Jan-Hendrik Prinz, Hao Wu, Marco Sarich, Bettina Keller, Martin Senne, Martin Held, John D Chodera, Christof Schütte, and Frank Noé. Markov models of molecular kinetics: generation and validation. *J. Chem. Phys.*, 134:174105, 2011.

[17] Bettina Keller, Philippe Hünenberger, and Wilfred F van Gunsteren. An Analysis of the Validity of Markov State Models for Emulating the Dynamics of Classical Molecular Systems and Ensembles. *J. Chem. Theory Comput.*, 7:1032–1044, 2011.

[18] Philippe H Hünenberger. Thermostat Algorithms for Molecular Dynamics Simulations. In *Adv. Polym. Sci.*, pages 105–149. Springer, Berlin, Heidelberg, Berlin, Heidelberg, 2005.

[19] Daan Frenkel and Berend Smit. *Understanding Molecular Simulation.* Elsevier, 2nd edition, 2001.

[20] Andrew R. Leach. *Molecular Modelling: Principles and Applications.* Pearson Education, 2nd edition, 2001.

[21] Mike P. Allen and Dominic. J. Tildesley. *Computer Simulation of Liquids.* Oxford Science Publications, reprinted edition, 1991 (1987).

[22] Christof Schütte, Wilhelm Huisinga, and Peter Deuflhard. Transfer operator approach to conformational dynamics in biomolecular systems. *ZIB Report*, 36(October):SC 99–36, 1999.

[23] Jan-Hendrik Prinz, Bettina Keller, and Frank Noé. Probing molecular kinetics with markov models: metastable states, transition pathways and spectroscopic observables. *Phys. Chem. Chem. Phys.*, 13:16912–16927, 2011.

[24] Marco Sarich, Frank Noé, and Christof Schütte. On the approximation quality of markov state models. *Multiscale Model. Simul.*, 8:1154–1177, 2010.

[25] Frank Noé. Probability distributions of molecular observables computed from Markov models. *J. Chem. Phys.*, 128(24):244103, 2008.

[26] John D Chodera and Frank Noé. Probability distributions of molecular observables computed from Markov models. II. Uncertainties in observables and their time-evolution. *J. Chem. Phys.*, 133(10):105102, 2010.

[27] Sudipto Mukherjee, George A Pantelopulos, and Vincent A Voelz. Markov models of the apo-MDM2 lid region reveal diffuse yet two-state binding dynamics and receptor poses for computational docking. *Sci. Rep.*, 6(1):1038, 2016.

[28] Gregory R Bowman and Phillip L Geissler. Equilibrium fluctuations of a single folded protein reveal a multitude of potential cryptic allosteric sites. *Proc. Natl. Acad. Sci. U.S.A.*, 109:11681–11686, 2012.

[29] Gregory R Bowman, Eric R Bolin, Kathryn M Hart, Brendan C Maguire, and Susan Marqusee. Discovery of multiple hidden allosteric sites by combining Markov state models and experiments. *Proc. Natl. Acad. Sci. U.S.A.*, 112(9):2734–2739, 2015.

[30] Jeffrey R Wagner, Christopher T Lee, Jacob D Durrant, Robert D Malmstrom, Victoria A Feher, and Rommie E Amaro. Emerging Computational Methods for the Rational Discovery of Allosteric Drugs. *Chem. Rev.*, 116(11):6370–6390, 2016.

[31] Manfred Hendlich, Friedrich Rippmann, and Gerhard Barnickel. LIGSITE: automatic and efficient detection of potential small molecule-binding sites in proteins. *J. Mol. Graph. Model.*, 15(6):359–363, 1997.

[32] Bettina Keller, Zrinka Gattin, and Wilfred F van Gunsteren. What stabilizes the 314-helix in β3-peptides? A conformational analysis using molecular simulation. *PROTEINS: Struct., Funct., and Bioinf.*, 78(7):1677–1690, 2010.

[33] Jonas Hanske, Stevan Aleksić, Martin Ballaschk, Marcel Jurk, Elena Shanina, Monika Beerbaum, Peter Schmieder, Bettina G Keller, and Christoph Rademacher. Intradomain Allosteric Network Modulates Calcium Affinity of the C-Type Lectin Receptor Langerin. *J. Am. Chem. Soc.*, 138:12176–12186, 2016.

[34] Kathryn M Hart, Katelyn E Moeder, Chris M W Ho, Maxwell I Zimmermann, Thomas E Frederick, and Gregory R Bowman. Designing small molecules to target cryptic pockets yields both positive and negative allosteric modulators. *PLOS ONE*, pages 1–13, 2017.

[35] Michelle R Arkin, Yinyan Tang, and James A Wells. Small-Molecule Inhibitors of Protein-Protein Interactions: Progressing toward the Reality. *Chemistry & Biology*, 21(9):1102–1114, 2014.

[36] Christin Rakers, Marcel Bermudez, Bettina G Keller, J r mie Mortier, and Gerhard Wolber. Computational close up on protein-protein interactions: how to unravel the invisible using molecular dynamics simulations? *WIREs Comput. Mol. Sci.*, 5(5):345–359, 2015.

[37] Gregory R Bowman. Improved coarse-graining of Markov state models via explicit consideration of statistical uncertainty. *J. Chem. Phys.*, 137(13):134111, 2012.

[38] Peter Deuflhard and Marcus Weber. Robust Perron cluster analysis in conformation dynamics. *Linear Algebra Appl.*, 398:161–184, 2005.

[39] Asghar M Razavi, William M Wuest, and Vincent A Voelz. Computational Screening and Selection of Cyclic Peptide Hairpin Mimetics by Molecular Simulation and Kinetic Network Models. *J. Chem. Inf. Model.*, 54(5):1425–1432, 2014.

[40] Jagna Witek, Bettina G Keller, Markus Blatter, Axel Meissner, Trixie Wagner, and Sereina Riniker. Kinetic Models of Cyclosporin A in Polar and Apolar Environments Reveal Multiple Congruent Conformational States. *J. Chem. Inf. Model.*, 56(8):1547–1562, 2016.

[41] Ignasi Buch, Toni Giorgino, and Gianni De Fabritiis. Complete reconstruction of an enzyme-inhibitor binding process by molecular dynamics simulations. *Proc. Natl. Acad. Sci. U.S.A.*, 108(25):10184–10189, 2011.

[42] Ryoji Takahashi, Víctor A Gil, and Víctor Guallar. Monte Carlo Free Ligand Diffusion with Markov State Model Analysis and Absolute Binding Free Energy Calculations. *J. Chem. Theory Comput.*, 10(1):282–288, 2013.

[43] Nuria Plattner and Frank Noé. Protein conformational plasticity and complex ligand-binding kinetics explored by atomistic simulations and Markov models. *Nat. Commun.*, 6:7653–10, 2015.

[44] Maria F Lucas, Israel Cabeza de Vaca, Ryoji Takahashi, Jaime Rubio-Martínez, and Víctor Guallar. Atomic Level Rendering of DNA-Drug Encounter. *Biophys. J.*, 106(2):421–429, 2014.

[45] Daniel-Adriano Silva, Gregory R Bowman, Alejandro Sosa-Peinado, and Xuhui Huang. A Role for Both Conformational Selection and Induced Fit in Ligand Binding by the LAO Protein. *PLoS Comput. Biol.*, 7(5):e1002054, 2011.

[46] Shuo Gu, Daniel-Adriano Silva, Luming Meng, Alexander Yue, and Xuhui Huang. Quantitatively Characterizing the Ligand Binding Mechanisms of Choline Binding Protein Using Markov State Model Analysis. *PLoS Comput. Biol.*, 10(8):e1003767, 2014.

[47] Guangfeng Zhou, George A Pantelopulos, Sudipto Mukherjee, and Vincent A Voelz. Bridging microscopic and macroscopic mechanisms of p53-MDM2 binding using molecular simulations and kinetic network models. *Biophys. J.*, 113(4):785–793, 2017.

[48] Nathaniel Stanley, Leonardo Pardo, and Gianni De Fabritiis. The pathway of ligand entry from the membrane bilayer to a lipid G protein-coupled receptor. *Sci. Rep.*, pages 1–8, 2016.

[49] Qifeng Bai, Horacio Pérez-Sánchez, Yang Zhang, Yonghua Shao, Danfeng Shi, Huanxiang Liu, and Xiaojun Yao. Ligand induced change of $\beta 2$ adrenergic receptor from active to inactive conformation and its implication for the closed/open state of the water channel: insight from molecular dynamics simulation, free energy calculation and Markov state model analysis. *Phys. Chem. Chem. Phys.*, 16(30):15874–15885, 2014.

[50] Kai J Kohlhoff, Diwakar Shukla, Morgan Lawrenz, Gregory R Bowman, David E Konerding, Dan Belov, Russ B Altman, and Vijay S Pande. Cloud-based simulations on Google Exacycle reveal ligand modulation of GPCR activation pathways. *Nat. Chem.*, 6:15–21, 2014.

[51] Diwakar Shukla, Yilin Meng, Benoît Roux, and Vijay S Pande. Activation pathway of Src kinase reveals intermediate states as novel targets for drug design. *Nat. Commun.*, 5:3397, 2014.

[52] Robert D Malmstrom, Alexandr P Kornev, Susan S Taylor, and Rommie E Amaro. Allostery through the computational microscope: cAMP activation of a canonical signalling domain. *Nat. Commun.*, 6:7588, 2015.

[53] Nina Singhal, Christopher D Snow, and Vijay S Pande. Using path sampling to build better Markovian state models: Predicting the folding rate and mechanism of a tryptophan zipper beta hairpin. *J. Chem. Phys.*, 121(1):415, 2004.

[54] E Vanden-Eijnden. Transition Path Theory. In *Computer Simulations in Condensed Matter Systems: From Materials to Chemical Biology Volume 1*, pages 453–493. Springer Berlin Heidelberg, Berlin, Heidelberg, 2006.

[55] Frank Noé, Christof Schütte, Eric Vanden-Eijnden, Lothar Reich, and Thomas R Weikl. Constructing the equilibrium ensemble of folding pathways from short off-equilibrium simulations. *Proc. Natl. Acad. Sci. U.S.A.*, 106:19011–19016, 2009.

[56] Guillermo Pérez-Hernández, Fabian Paul, Toni Giorgino, Gianni De Fabritiis, and Frank Noé. Identification of slow molecular order parameters for Markov model construction. *J. Chem. Phys.*, 139:015102, 2013.

[57] Christian R Schwantes and Vijay S Pande. Improvements in Markov State Model Construction Reveal Many Non-Native Interactions in the Folding of NTL9. *J. Chem. Theory Comput.*, 9(4):2000–2009, 2013.

[58] Christof Schütte, Frank Noé, Jianfeng Lu, Marco Sarich, and Eric Vanden-Eijnden. Markov state models based on milestoning. *J. Chem. Phys.*, 134:204105, 2011.

[59] Oliver Lemke and Bettina G Keller. Density-based cluster algorithms for the identification of core sets. *J. Chem. Phys.*, 145:164104, 2016.

[60] Feliks Nüske, Bettina G Keller, Guillermo Pérez-Hernández, Antonia S J S Mey, and Frank Noé. Variational Approach to Molecular Kinetics. *J. Chem. Theory Comput.*, 10:1739–1752, 2014.

[61] F Vitalini, F Noé, and B G Keller. A Basis Set for Peptides for the Variational Approach to Conformational Kinetics. *J. Chem. Theory Comput.*, 11:3992–4004, 2015.

[62] Pratyush Tiwary and Michele Parrinello. From Metadynamics to Dynamics. *Phys. Rev. Lett.*, 111:230602, 2013.

[63] Hao Wu, Fabian Paul, Christoph Wehmeyer, and Frank Noé. Multiensemble Markov models of molecular thermodynamics and kinetics. *Proc. Natl. Acad. Sci. U.S.A.*, 113:E3221–30, 2016.

[64] L Donati, C Hartmann, and B G Keller. Girsanov reweighting for path ensembles and Markov state models. *J. Chem. Phys.*, 146(24):244112, 2017.

[65] Rodrigo Casasnovas, Vittorio Limongelli, Pratyush Tiwary, Paolo Carloni, and Michele Parrinello. Unbinding Kinetics of a p38 MAP Kinase Type II Inhibitor from Metadynamics Simulations. *J. Am. Chem. Soc.*, 139:4780–4788, 2017.

[66] Matthew P Harrigan, Mohammad M Sultan, Carlos X Hernández, Brooke E Husic, Peter Eastman, Christian R Schwantes, Kyle A Beauchamp, Robert T McGibbon, and Vijay S Pande. MSMBuilder: Statistical Models for Biomolecular Dynamics. *Biophysical Journal*, 112(1):10–15, January 2017.

[67] Martin K Scherer, Benjamin Trendelkamp-Schroer, Fabian Paul, Guillermo Pérez-Hernández, Moritz Hoffmann, Nuria Plattner, Christoph Wehmeyer, Jan-Hendrik Prinz, and Frank Noé. PyEMMA 2: A Software Package for Estimation, Validation, and Analysis of Markov Models. *J. Chem. Theory Comput.*, 11(11):5525–5542, October 2015.

Chapter 4

The Vibrational Spectrum of the hydrated Alanine-Leucine Peptide in the Amide region from IR experiments and First Principles Calculation

The state of a molecular system is described by a wave function, that is a solution of the time-dependent Schrödinger equation. The Born-Oppenheimer approximation separates the Schrödinger equation into two components, the motion of the atomic nuclei and the motion of the electrons. This approximation is possible because the electrons are much lighter than the atomic nuclei and the respective timescales of motion are separated by several orders of magnitude. In the Born-Oppenheimer picture, the energy of the nuclei can also be separated in levels of translational, vibrational and rotational energy, that can be determined by spectroscopy experiments. For example, in infrared spectroscopy (IR spectroscopy or vibrational spectroscopy), one can measure the vibrational modes of chemical structures. Usually a sample of matter (solid, liquid or gas) is passed by a beam of infrared light and according to the absorption spectrum, it is possible to determine the frequencies at which the molecule can vibrate, or in other words which vibrational energy transitions are allowed.

In the last years, IR spectra can be obtained also by computer simulations, complementing the results from laboratory experiments. The measure of IR spectra can be improved by quantum chemical calculation of conformations, like harmonic normal mode analysis. However, typically, ab-initio simulations of big molecules, like polypeptides in explicit solvent are computationally expensive. An alternative solution is to determine the conformations through ab-initio simulations in implicit solvent or in vacuum, but this is an approximation that does not consider the effect of the temperature, anharmonicites and the interaction of the molecule with the solvent.

In collaboration with Irtaza Hassan, from Physics department, Frëie Universität Berlin, to overcome this problem and to improve the measure of IR spectra of polypeptides, we used classical MD simulations in explicit solvent, together with MSMs and PCCA+, to determine the conformations [74].

We have studied the Alanine-Leucine peptide and built the IR spectra, combining the following techniques:

1. Molecular Dynamics (MD) simulations [1, 2]: the molecular system is described by a classical potential energy function governing the interaction between the atoms. A spatial trajectory of each atom is determined by integrating numerically the Newton's equations of motion.

2. Markov State Models (MSMs) [11, 12, 15, 16, 17, 18, 13, 19]: under certain conditions, the dynamics of the system is described as time evolution of a probability density function, that converges to a stationary distribution under the action of a continuous operator called propagator. With MSMs, the state space is discretized into disjoint microstates. Then, an MD trajectory is used to approximate the dynamics of the system as a Markov jump process between microstates and the propagator is discretized into a transition probability matrix, whose eigenvectors the eigenvalues contain the dynamical properties of the system.

3. Reduced Perron Cluster analysis (PCCA+) [75]: from the eigenvectors of the MSM, PCCA+ operates a fuzzy clustering, i.e. determines few metastable macrostates and assigns to each microstate the probability to belong to a macrostate.

4. First-principle simulations (or ab-initio simulations) [76]: chemical properties of molecules are recovered from computer simulations based on the fundamental laws of quantum mechanics. The Schrödinger equation is solved with no need of pre-parametrized forcefield, like in classical MD simulations. On the other hand, first-principle simulations have a significant computational cost and need a large amount of computer capacity, thus simulations are usually limited to small molecules.

We have first performed an MD simulation of Alanine-Leucine, in order to sample the state space and to produce a trajectory to build the MSM. Afterward, the MSM has been reduced with PCCA+ to determine three metastable states and the associated transition probabilities. Finally we have chosen four representative conformations belonging to the metastable states and performed first-principle simulations, starting from each representative conformation, in order to estimate the IR spectrum of the peptide. All the computed spectra are in good agreement with the experiments.

My contribution was to construct the MSM of the Alanine-Leucine and to find the metastable states by PCCA+.

https://doi.org/10.1016/j.cplett.2018.03.026

Chemical Physics Letters 698 (2018) 227–233

Contents lists available at ScienceDirect

Chemical Physics Letters

journal homepage: www.elsevier.com/locate/cplett

Research paper

The vibrational spectrum of the hydrated alanine-leucine peptide in the amide region from IR experiments and first principles calculations

Irtaza Hassan [a], Luca Donati [b], Till Stensitzki [a], Bettina G. Keller [b], Karsten Heyne [a], Petra Imhof [a,*]

[a] Institute of Theoretical Physics, Freie Universität Berlin, Arnimallee 14, 14195 Berlin, Germany
[b] Institute of Chemistry and Biochemistry, Freie Universität Berlin, Takustr. 3, 14195 Berlin, Germany

ARTICLE INFO

Article history:
Received 19 December 2017
In final form 14 March 2018
Available online 15 March 2018

Keywords:
Infrared spectra
Peptide
First-principles molecular dynamics simulations

ABSTRACT

We have combined infrared (IR) experiments with molecular dynamics (MD) simulations in solution at finite temperature to analyse the vibrational signature of the small floppy peptide Alanine-Leucine. IR spectra computed from first-principles MD simulations exhibit no distinct differences between conformational clusters of α-helix or β-sheet-like folds with different orientations of the bulky leucine side chain. All computed spectra show two prominent bands, in good agreement with the experiment, that are assigned to the stretch vibrations of the carbonyl and carboxyl group, respectively. Variations in band widths and exact maxima are likely due to small fluctuations in the backbone torsion angles.

1. Introduction

IR spectroscopy techniques are extensively used in the liquid and gas phase at finite temperature to probe molecular vibrations. This provides information about the chemical structure of a molecule and its interaction with the environment. Vibrational spectroscopy has furthermore been successful in revealing the secondary structure of peptides and proteins and allows to probe conformational dynamics via time-resolved measurements [1].

The dynamics of complex bio-molecules involves characteristics timescales ranging from 10^{-12} to 10^{0} seconds i.e. from structural vibrations to complex conformational transitions. Peptides are frequently used model systems of proteins to study their conformational dynamics because of their reduced complexity and the shorter time-scales (up to milli- or micro-seconds).

Molecular simulations can assist to evaluate the dynamics at atomic level and to find the conformations which are responsible for the vibrational fingerprints observed in experimental IR spectra. Often, the assignment of the measured IR spectra is aided by quantum chemical calculations (harmonic normal mode analysis) of one or few conformations of the respective molecule in vacuum or by using implicit solvent models. The spectra calculated for the different conformations are then matched with experimental spectra to identify which conformation is responsible for the measured vibrational signatures. This approach, albeit straightforward, lacks finite temperature, anharmonicites and usually does not account for the explicit interaction with the solvent. Recently, substantial progress has been made to improve the description of solute–solvent interactions by including specific solvent molecules explicitely into an otherwise implicit-solvent model [2,3] also for the computation of vibrational spectra [4,5]. For small molecules corrections for anharmonic effects in vibrational spectra can be obtained from vibrational self-consistend field approaches augmented by correlated methods [6–13].

Inclusion of explicit solvation, thermal and anharmonic effects altogether is possible by employing molecular-dynamics based approaches which are enjoying increasing popularity and have been used successfully to calculate IR spectra of small peptides [14–16].

The computational expenses of such first-principles simulations, however, prevent the exploration of dynamical processes on time scales beyond 10—100′s of picoseconds, even on density functional theory (DFT) level with generalised-gradient functionals with still limited accuracy. Correlated wave function methods with large basis sets, which would give spectroscopic accuracy, are computationally far too demanding for MD simulations.

On the other hand, classical, force-field based MD simulations are a means to exhaustively sample the conformational space of a molecule. Such MD simulations combined with Markov state models (MSMs) allow describing the conformational dynamics of poly-peptides [17–19]. The fixed point-charge model, typically used in force-field based simulations, does not allow to take any change in electronic density into account and therefore cannot accurately model the changes in dipole moment associated with the vibrational motions.

* Corresponding author.
E-mail address: petra.imhof@fu-berlin.de (P. Imhof).

https://doi.org/10.1016/j.cplett.2018.03.026
0009-2614/

Approaches such as frequency maps [20–22], instantaneous normal mode calculations [23–26], quantum-classical descriptions [27,28], perturbed matrix methods [29], or polarisable force fields [26] all attempt at combining the strengths of quantum chemical calculations (accurate electron densities) with that of classical MD simulations (comprehensive sampling of the conformational space).

In this work, we follow a combined approach by sampling the conformational dynamics of a small floppy peptide in water by classic MD simulations. From these data, we constructed a MSM, identified the meta-stable sets and the time scales associated with the slowest processes. For representative conformations of the meta-stable sets, individual first-principles molecular dynamics simulations were performed. From these simulations the vibrational signatures were then computed in the frequency range that is most sensitive to the peptide conformation, so-called amide bands (1300–1800 cm^{-1}) [30,31]. The experimental IR spectrum of Alanine-Leucine (Ala-Leu) in water was then assigned by using the combined information from all the calculations.

We chose the peptide Ala-Leu because of its size: it is just large enough to exhibit conformational dynamics and small enough to allow for long enough first-principles simulations to compute IR spectra from. The uncapped zwitter-ionic form has the further advantage of one charged carboxyl group and a carbonyl group, absorbing at different frequencies, rather than the similar frequencies of two carbonyl groups in a capped peptide. Furthermore, a transition that, in a longer peptide would correspond to a α-helix/β-sheet transition via a torsion around one of the backbone angles (Ψ_{Leu}), in the short peptide Ala-Leu rotates the carboxyl group. Because of the chemical equivalence of the two carboxyl atoms, this rotation yields two chemically equivalent conformations. The bulky side-chain of the Leucine amino acid furthermore gives rise to richer conformational dynamics.

2. Methods

2.1. Theoretical background

2.1.1. Markov state models

A Markov state model of the long-time conformational dynamics is constructed from discrete partitioning of the conformational space into micro-states[1] (Markov states) [32,18]. To this end, a transition matrix $\mathbf{T}$ is set up that estimates the underlying stochastic process, here transitions between conformational micro-states of the system. The entries of the matrix are

$$T_{ij}(\tau) = P(x_{t+\tau} = j | x_t = i) \tag{1}$$

The elements of the transition matrix represent the conditional probabilities of finding the molecule in state j at time $t+\tau$, given it was in state i at time t. This matrix defines a Markov process in which the propagation of the system is entirely determined by knowing its present state x_t and is independent of its past. The dynamic system furthermore fulfils detailed balance, that is in equilibrium all processes are reversible with the number of transitions $i \to j$ equal to the number of transitions $j \to i$.

The eigenvalues $\lambda_i(\tau)$ and eigenvectors $\mathbf{r}_i, \mathbf{l}_i^T$ (right and left) of the transition matrix are important ingredients to understand the prominent features of the conformational dynamics

$$\begin{aligned} \mathbf{T}(\tau)\mathbf{r}_i &= \mathbf{r}_i\lambda_i(\tau) \\ \mathbf{l}_i^T\mathbf{T}(\tau) &= \lambda_i(\tau)\mathbf{l}_i^T \end{aligned} \tag{2}$$

The transition matrix is row-stochastic

$$\sum_{j=1}^{N} T_{ij}(\tau) = 1 \ \forall \mathrm{i} \tag{3}$$

and for ergodic dynamics its largest eigenvalue $\lambda_1(\tau) = 1$. The corresponding left eigenvector is the stationary distribution.

The other eigenvalues $|\lambda_{i>1}(\tau)| < 1$ define the implied timescales which can be understood as molecular relaxation timescales

$$t_i = -\frac{\tau}{\log|\lambda_i(\tau)|} \tag{4}$$

The corresponding eigenvectors represent the conformational transitions that occur on those timescales [32,33,18].

2.1.2. Theory of Infrared (IR) spectra

According to Fermi's Golden Rule, an infrared spectrum can be calculated through [34]:

$$I(\omega) = 3\sum_i\sum_f \rho_i |\langle f|\vec{\mathcal{E}}\vec{\mu}|i\rangle|^2 \delta(\omega_{fi} - \omega) \tag{5}$$

where $\vec{\mathcal{E}}$ is the applied external field vector, $\vec{\mu}$ is the dipole vector of the molecular system. $I(\omega)$ is the intensity as a function of the reciprocal wavenumber of the radiation, ω (in cm^{-1}) and ω_{fi} is the reciprocal wavenumber associated with the transition between the initial and final vibrational states of the system $|i\rangle$ and $\langle f|$, respectively. ρ_i is the density of the molecules in the initial vibrational state $|i\rangle$. Within Linear Response Theory [35], the above equation can be rewritten as the Fourier transform of the dipole moment autocorrelation:

$$I(\omega) = \frac{2\pi k_B T\omega^2}{3cV}\int_{-\infty}^{\infty} \mathrm{d}t\langle\vec{\mu}(t)\cdot\vec{\mu}(0)\rangle \exp(i\omega t) \tag{6}$$

$$f(\omega) = \frac{2\pi k_B T\omega^2}{3cV}\int_{-\infty}^{\infty} \mathrm{d}t\langle\vec{r}(t)\cdot\vec{r}(0)\rangle \exp(i\omega t) \tag{7}$$

where T is the temperature, k_B the Boltzmann constant, c is the speed of light in vacuum, and V is the volume. The angular brackets represent the statistical average, as sampled by MD simulations, of the autocorrelation of the dipole moment $\vec{\mu}$ of the absorbing molecule. Eq. (6) yields the complete IR spectrum of the molecular system. For the assignment to vibrations of molecular groups, power spectra are computed from the Fourier transform of the autocorrelation of the velocities (Eq. (7)) of individual groups. See also review [16] on theoretical spectroscopy of floppy peptides at room temperature.

2.2. Molecular simulations and analysis

2.2.1. Markov state model

Using the trajectory of partially deuterated Ala-Leu (see Fig. 1) in deuterated water obtained from classical MD simulations (see supplementary material for details), a Markov state model was constructed on the conformational space spanned by the torsion angles ψ_{Ala}, χ_{Leu} , ϕ_{Leu} and ψ_{Leu} (highlighted in Fig. 1). Such torsion coordinates have proven useful to capture the essential dynamics of small peptides such as Ala-Leu [36,32,37–39].

The conformational space reduced to the four dimensions corresponding to torsion angles was then discretised into micro-states (corresponding to conformational clusters), based on the one-dimensional distribution of the torsion angles ψ_{Ala} and χ_{Leu} and the two-dimensional joint distribution (the ramachandran plot) of the torsion angles ϕ_{Leu} and ψ_{Leu} (see Fig. 2). Two states for the torsion angles ψ_{Ala} and χ_{Leu}, respectively, were found, while the ramachandran plot was divided into four conformational states. All the possible combinations define $2 \times 2 \times 4 = 16$ micro-states onto which the MD trajectory was projected. Based on the

[1] Please not that a micro-state in the context of this work refers to a set of conformations and not to a point in phase space.

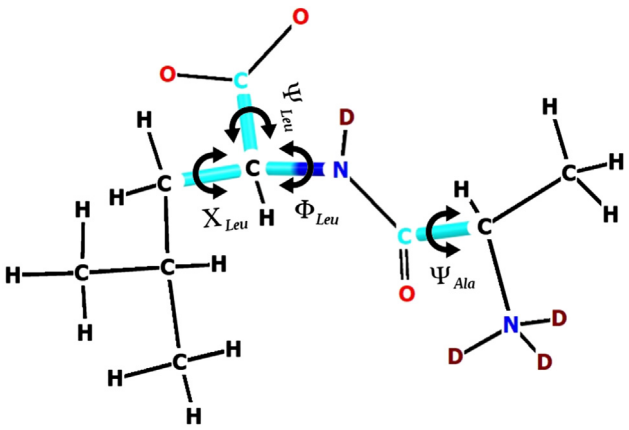

Fig. 1. Scheme of the Ala-Leu peptide and the torsion angles ψ_{Ala}, χ_{Leu}, ϕ_{Leu} , and ψ_{Leu} used for discretisation of the conformational space. Note that ψ_{Leu} is a pseudo-backbone dihedral angle since there is no nitrogen atom of a subsequent amino acid, but a second oxygen atom of the carboxyl terminus. That is, in the short peptide there is no nitrogen atom of the next amino acid but an oxygen atom of the C-teminus instead. Note that Ψ_{Leu} is a pseudo-backbone dihedral angle. A 180° torsion around Ψ_{Leu}, thus does not mean an actual conformational change, but rather an inter-conversion of two chemically equivalent structures. "D" denotes a deuterium atom.

transition probabilities between them, micro-states were merged into three meta-stable sets and a coarse-grained transition matrix was constructed (see section Markov state models in the supplementary material).

2.2.2. First-principles molecular dynamics simulations

For one representative conformation of each micro-state, we performed first-principles molecular dynamics simulations in explicit water at 300 K. The same deuteration (ND_3 and ND in the peptide and D_2O water) as for the classical force field simulations (see Molecular mechanics simulations in supplementary material) was applied. For each of the four representative conformations of Ala-Leu three to four individual first-principles simulations were run for 20–80 ps (see Fig. S5 for individual runs) from which spectra were calculated. For further details please see the supplementary material.

2.3. Experimental setup

Infrared absorption spectra were taken with an Equinox 55 FTIR device (Bruker). Ala-Leu (Sigma–Aldrich, CAS 3303-34-2) was dissolved in D_2O and placed between two CaF_2 windows with a spacer thickness of 0.05 mm. Absorption of D_2O was subtracted in Fig. 4 to stress the absorption signals of Ala-Leu. Note, in D_2O the exchangeable protons will exchange to deuterons. However, a residual amount of partially or undeuterated Ala-Leu remains to be present in the sample.

3. Results

3.1. Markov state model

Fig. 3 shows the coarse-grained model as a transition graph between meta-stable sets, together with representative conformations of the most probable micro-states in the set. Meta-stable set I consists of micro-states with a left-handed helix conformation and has the lowest probability. The transition into this set, corresponding to a torsion around Φ_{Leu}, is the slowest process. The two other meta-stable sets, II and III, have similar probability and are dominated by micro-states, labelled 0 and 4, and 2 and 6, respectively (see Table S1 in section Markov-state-model in the supplementary material for the complete list of micro-states in each meta-stable set and for further details).

The transition between the conformations in the two meta-stable sets II and III corresponds mainly to a torsion around Ψ_{Leu}. Transitions between micro-states within the same set, i.e. between 0 and 4, and between 2 and 6, respectively, both correspond to a torsion of the leucine side chain χ_{Leu}.

3.2. Infrared spectrum

In the course of the individual first-principles simulations initiated from conformations representing micro-states 0, 4, 2, and 6, respectively, the system occasionally undergoes changes in the torsion angles ψ_{Ala}, χ_{Leu} , ϕ_{Leu} and ψ_{Leu} that correspond to transitions between micro-states. Hence, an individual simulation can be composed of parts that belong to different micro-states, e.g. 0 and 4. In most simulations, there are only a few jumps between micro-states. In order to analyse the vibrational fingerprint for individual micro-states, we have partitioned the first-principle trajectories by the micro-states 0, 4, 2, and 6 and computed spectra from the respective parts of the trajectories. For the time series of torsion angles and the assigned micro-state see supplementary Fig. S5.

The experimental infrared spectrum of Ala-Leu in water is presented in Fig. 4 together with the spectra computed from the first-principles MD simulations. The assignment (given as labels in Fig. 4) is based on the computed power spectra with further aid from normal mode calculations (see supplementary material). The most prominent band is the stretch vibration of the carboxyl group (νCOO) at ~1590 cm^{-1}. Note that the most intense band of the νCOO vibration has been used to normalise intensities and therefore shows a relative intensity of one for all spectra. The other

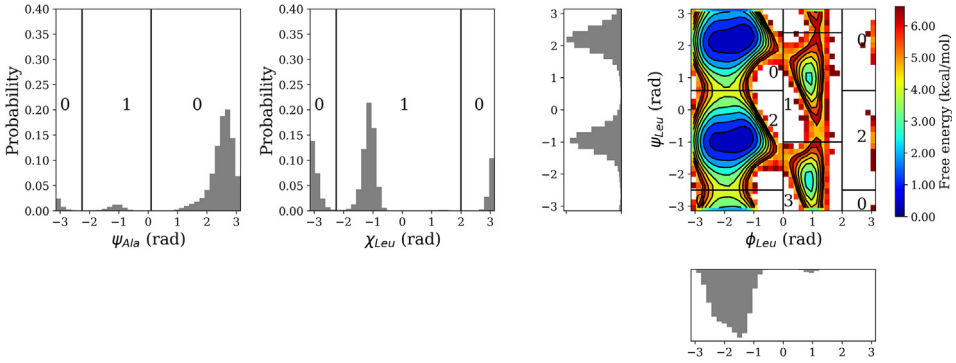

Fig. 2. Distribution of the torsion angles ψ_{Ala}, χ_{Leu} , ϕ_{Leu} and ψ_{Leu} obtained from the classical MD simulation of Ala-Leu in water.

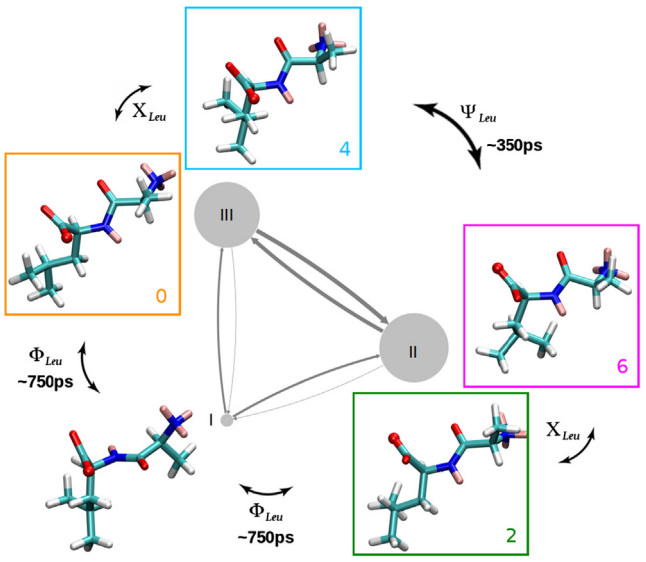

Fig. 3. Coarse-grained model of the conformational dynamics of Ala-Leu in water. The three meta-stable sets, I–III, are represented as circles whose size corresponds to the probability of the respective set. The thickness of the arrows between the circles indicates the transition probability between a pair of meta-stable sets. The molecular structures in the boxes next to the circles are representative conformations of the most probable micro-states in the respective set. See Table S1 for the micro-states that constitute each set. Arrows between the coloured boxes indicate the coordinate of the conformational transition connecting two micro-states. The colour of the boxes correspond to micro-state 0 (orange), 4 (blue), 2 (green), and 6 (magenta), respectively. Carbon atoms are shown in cyan, oxygen atoms in red, nitrogen atoms in blue, hydrogen atoms in white and deuterium atoms in pink. One of the two carboxyl oxygen atoms is shown as sphere to illustrate the change in Ψ_{Leu} between meta-stable set II and III. Note that a Ψ_{Leu}-torsion of 180° inter-converts two chemically equivalent conformations. (For interpretation of the references to colour in this figure legend, the reader is referred to the web version of this article.)

band in the amide I region at ~1660 cm^{-1} contains components of the carbonyl group (νC═O) and the peptide bond (νN—C). The intensity ratio of the two bands, νC═O and νCOO, is well reproduced by the computed spectra. The νC═O band is actually composed of two contributions with varying intensity ratios as can be seen from the spectra computed from the individual micro-states (Fig. 4b) and also indicated in the considerable error in the composed, weighted spectrum (Fig. 4a middle).

The amide II bands at ~1450 cm^{-1} and ~1480 cm^{-1}, assigned to bend (δN—D and δC—H) and stretch (νN—C), with some contribution from the C═O group, are slightly less well reproduced; the higher frequency band is calculated at too high frequency (~1540 cm^{-1}) with too little intensity. The small shoulder at ~1550 cm^{-1} in the experimental spectrum of Ala-Leu is likely due to remains of undeuterated Ala-Leu in the sample. Experiments on N-methylacetamide [40] report the δN-H bend vibration of the undeuterated species at this frequency (~1570 cm^{-1}) and the δN-D at ~1450 cm^{-1} as in our spectrum of Ala-Leu).

The three smaller bands in the amid III region at ~1360 cm^{-1}, ~1390 cm^{-1}, and ~1410 cm^{-1} in the experimental spectrum are computed as one broad band at ~1380 cm^{-1} due to the averaging of several simulations, with also a significant variance in the intensities. The spectra computed individually for the micro-states (Fig. 4b) give rise to two shoulders, albeit with some error, which can be interpreted as corresponding to the lower and higher frequency bands resolved in the experimental spectrum. The main vibrational contribution stems from the terminal ND_3-group and δN—D and νN—C, but there are also COO contributions in varying amounts, depending on the individual simulation. The C═O group does not contribute to the bands in this frequency range. According to Krimm and Bandekar, both amide II and amide III bands are linear combinations of the same group movements, i.e. δN—D and νN—C [41]. In our simulations these bands show different intensity ratios for different simulation runs. As can be seen in the computed power spectra (supplementary Fig. S13) not only do the δN—D and νN—C contributions fluctuate, there are additional contributions by the C═O and COO group to the bands in the amide II and amide III region, respectively, that vary considerably, explaining the different intensities computed for those bands.

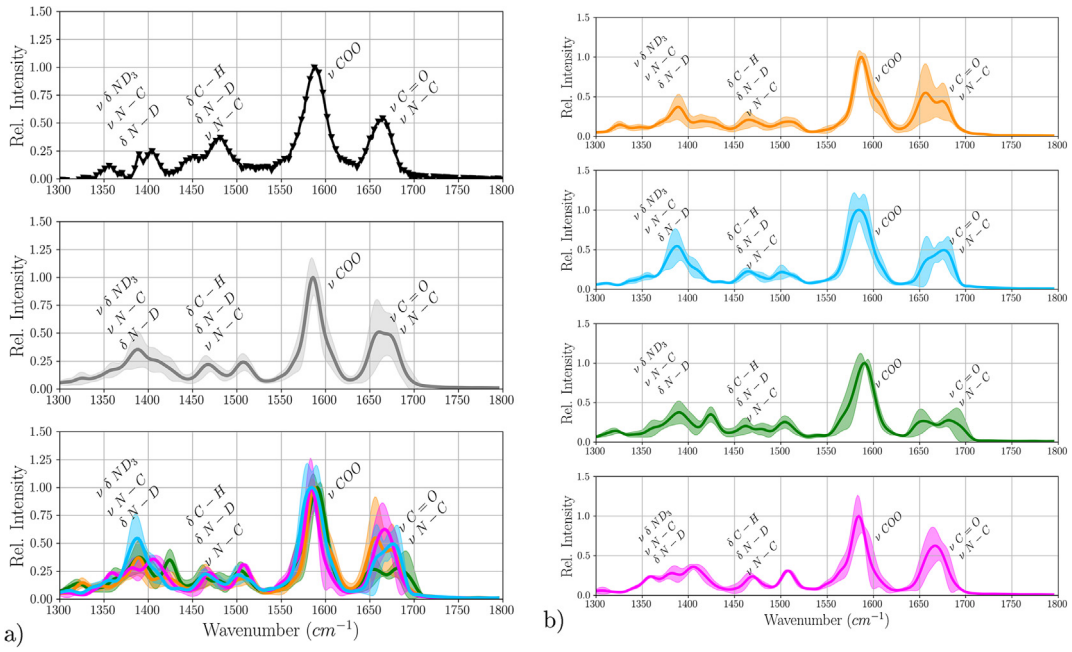

Fig. 4. (a) Experimental (top) and computed (middle) Infrared spectrum of Ala-Leu in water combined from the Boltzmann-weighted average of spectra computed for different micro-states (bottom). (b) Individual computed spectra of micro-states 0 (orange), 4 (blue), 2 (green), and 6 (magenta) (top to bottom). The shaded areas indicate the error as computed from the standard deviation from the mean. (For interpretation of the references to colour in this figure legend, the reader is referred to the web version of this article.)

3.3. Comparison of sampled conformations and resulting spectra

The distribution of the torsion angles within the partitions of trajectories belonging to micro-state 0, 4, 2, or 6, respectively, are shown in supplementary Fig. S13. Within the range of the torsion angles ψ_{Ala}, χ_{Leu}, ϕ_{Leu} and ψ_{Leu}, assigned to the respective micro-states, there are different fluctuations within the individual runs, resulting in wider, narrower, and occasionally almost bimodal distributions.

The computed IR spectra show variations in the band assigned to the νC═O/νN—C stretch vibration, both in intensity and the exact location of the maximum. In many of the simulations, the computed νC═O/νN—C band has a shoulder, others show broadening, and in extreme cases (0-run4, 2-run2 in supplementary Fig. S13), a second band can be observed. Comparison with the distributions of ϕ_{Leu} shows that these correspond to the shape of the νC═O/νN—C band in the IR spectrum in as much as narrow bands are only observed for narrow distributions, and broad distributions, with shoulders, correspond to a broadening or splitting in the νC═O/νN—C peak. This effect is generally more pronounced in the power spectra than in the IR spectra, indicating that the dipole moments are less affected by the variance in torsion angle than the velocities of the C═O and N—C groups.

A similar observation can be made for the distributions of ψ_{Leu} and the shapes of the νCOO bands. Narrow distributions correspond to narrow bands, shoulders in the ψ_{Leu} distribution correspond to shoulders or broadening in the νCOO band.

The two bands in the amide II region are present in almost all computed spectra, albeit with some fluctuation in their intensities. The δC—H contribution, mainly of the Leu sidechain varies in exact frequency, not always matching the computed IR-band at ~1540 cm^{-1}, suggesting only a minor contribution of δC—H to the IR intensity.

The amide III region exhibits considerable variation of the band intensities. Neither amide II nor amide III region show any relation to the torsion angle distributions, likely because the bands in these regions are composed of motions by several groups, N—C, ND, and ND_3 with contributions of the COO group.

Analysis of the distribution of number of hydrogen bonds from the same parts of the first-principles trajectories (Fig. S9 in the supplementary material) shows that all polar groups are almost always engaged in at least one hydrogen-bond with a water molecule. In a few cases, (2-run1, 4-run3, and 6-run1) a second hydrogen bond between C═O and water is counted with $> 30\%$ probability. These are the runs of the respective micro-state with the red-most νC═O band, indicating a slightly higher probability of further weakening of the C═O bond by an additional hydrogen-bond in these cases. Observed and computed broad or even split νC═O/νN—C bands can thus be explained by the C═O group being in different hydrogen-bonded states, resulting in different amounts of red-shift. For the simulation of micro-state 0 with the highest probability of a second hydrogen-bond to C═O, the νC═O band is on the low frequency side, too. This is, however, also the case for other simulations of micro-state 0 with no particular relation to the hydrogen-bond probabilities. More detailed analysis of the hydrogen-bond interactions reveals differences in the hydrogen-bond distances and the distributions of donor-hydrogen-acceptor angles between the different simulations of the micro-states (see Figs. S10 and S11). The impact of water molecules within hydrogen-bond distance on the frequency of the νC═O band, such as a red-shift, is thus further modulated by the orientation within the hydrogen-bond and thus the strength of that interaction.

4. Discussion

The probability distribution of peptide conformations obtained from the classical molecular dynamics simulations suggest a left-handed helix to be very improbable in the Ala-Leu peptide whereas conformations that correspond to a right-handed α-helix or β-sheet dominate. PolyProline (pPII) conformations, which have been suggested to coexist with β- conformers for the dialanine peptide [42], are observed in the classical simulations of Ala-Leu only transiently. Accordingly, such conformations have not been taken into account explicitly in the conformation-specific first-principles simulations. In one first-principle simulation, backbone angles that correspond to pPII-conformations have been observed as transition states between two conformational states (4 and 6) and thus only for short life-times (see Fig. S5 4-run1).

All transitions between meta-stable sets as well as those between the two most probable micro-states in the same meta-stable set ($0 \leftrightarrow 4$ and $2 \leftrightarrow 6$, respectively), equilibrate on time scales that are not accessible in the first-principles dynamics. Still, a few conformational transitions between different micro-states are observed in the course of some of the first-principles simulations. We have therefore dissected the first-principle trajectories into parts that sample only the same micro-state and used these parts for the computation of spectra.

The computed IR spectra show a considerable variance in the band intensities for simulations of the same micro-state. In contrast, there are no (further) differences between spectra computed for the different micro-states. This is to be anticipated for spectra of micro-states 0 and 2, and 4 and 6, respectively, since these correspond to chemically equivalent conformations. The conformational difference between micro-states 0 and 4, and between 2 and 6, is the orientation of the leucine side chain as defined by torsion angle χ_{Leu}. The effect on the amide region, if any, is smaller than or comparable to the variances between spectra from different runs initiated from the same conformation.

The experimental and the computed spectra are dominated by the bands assigned to the carbonyl (νC═O) and carboxyl (νCOO) stretch vibration, respectively. IR spectra of several other small peptides (N-acetyl-Gly-N-methylamide, N-acetyl-Ala-N-methylamide) with capped termini all show only a broad band assigned to the νC═O stretch vibration [43]. Computations of the spectra reveal that the νC═O of Alanine-dipeptide absorbs at almost the same frequency in either the α-helix or polyproline/β-sheet conformation but with a width that corresponds to the experimentally observed spectrum [42,44]. Slightly longer peptides, that can form intramolecular hydrogen bonds and thereby stabilise folds such as turns, Ac-Ph-Pro or trialanine, are reported with νC═O frequencies that differ by ~ 20—$30\ cm^{-1}$ [45–47], giving rise to a shoulder or a double peak. Two-dimensional IR-experiments have furthermore revealed that the two peaks are due to coupled C═O dipoles rather than two conformations [48]. Spectra of $(Ala)_5$, unlabelled and isotope-labelled with $^{13}C{=}O$ and $^{13}C{=}^{18}O$ at individual C═O groups to shift their vibrational frequencies, show dual bands, separated by $\sim 20\ cm^{-1}$, for both, the isotope-shifted and the unshifted groups [49]. Conformational analysis of classical MD simulations, combined with models for transition dipole coupling, reveals the coupling strength, and hence the detailed band shape, to depend on the conformation [49].

In the short peptide Ala-Leu studied in this work, there is only one C═O group. Any coupling would therefore have to be with the COO group. The νCOO band is observed at $1590\ cm^{-1}$, at the same position reported for IR spectra of tripeptides ($(Ala)_3$, $(Ser)_3$, $(Val)_3$) [43]. In Ala-Leu, the two groups, C═O and COO, exhibit two well-separated ($\sim 50\ cm^{-1}$) vibrational signals of rather differ-

ent intensity, suggesting no or only very weak coupling. The νC═O band maximum differs by$\sim$ 20—30 cm^{-1} between simulations, some of which indicate a dual peak also within the same simulation. The width of the frequency fluctuations for the computed νC═O band indicates a relation with the width of the distribution in torsion angle ϕ_{Leu} sampled in that particular simulation. The small differences in this torsion, and similarly of the ψ_{Leu} torsion, give rise to fluctuations in the relative orientation of the C═O and the COO groups (and their corresponding dipoles). Likely, this also leads to fluctuations in the mutual impact of the two groups. Whether and how much the two groups are indeed coupled has to be revealed by future 2D-IR experiments.

5. Conclusions

The slow conformational dynamics of Ala-Leu in water are dominated by torsions around backbone angles ϕ_{Leu} and ψ_{Leu}. The slowest process can be attributed to changes in the ϕ_{Leu} torsion angles that lead to transitions to the least probable conformation, a left-handed helix. The most probable part of the conformational space can be formally assigned to the α-helix and β-sheet regions (as assigned by a discretisation of the relevant torsion angles). The inter-conversion of these two regions along ψ_{Leu} is the second slowest process. In the uncapped peptide, these two conformations are, however, actually chemically equivalent and correspondingly exhibit the same spectral signature. Another subdivision of conformations can be made by the orientation of the leucine side chain, corresponding to a torsion around χ_{Leu}.

The IR spectra computed from the first-principles MD simulations reproduce the experimental spectrum of Ala-Leu in reasonable agreement. In accordance with the chemical equivalence of the conformers with the same absolute ψ_{Leu} value, their spectra are very similar. The orientation of the leucine side chain is not reflected in the amide region of the vibrational spectrum of Ala-Leu as can be seen from comparison of the spectra computed for individual conformations.

The amide I region is very well reproduced by the simulations. The two prominent bands are assigned to the stretch vibrations of the carboxyl group, COO, and the carbonyl group, C═O, respectively. Fluctuations in the backbone torsion angle ψ_{Leu} result in a broadening of the νCOO band. The simulations furthermore reveal the νC═O band to be composed of (at least) two frequency components. The variance in the exact frequency of this band can be attributed to mainly variations in the backbone torsion angle ϕ_{Leu} within the same area of the peptide fold. These small fluctuations occur on short time-scales and are therefore averaged out in the experimental spectrum, explaining the observation of only one broad νC═O band.

Acknowledgement

This research has been funded by Deutsche Forschungsgemeinschaft (DFG) through grant CRC 1114 “Scaling Cascades in Complex Systems”, Project B05 “Origin of scaling cascades in protein dynamics”. We thank the IT support of the Physics department at Freie Universität Berlin. Computational resources provided by the North-German Supercomputing Alliance (HLRN) are gratefully acknowledged.

Appendix A. Supplementary material

Supplementary data associated with this article can be found, in the online version, at https://doi.org/10.1016/j.cplett.2018.03.026.

References

[1] A. Barth, Infrared spectroscopy of proteins, Bioch. Biophys. Acta (BBA)-Bioenerg. 1767 (9) (2007) 1073–1101.
[2] M. Cossi, N. Rega, G. Scalmani, V. Barone, Energies, structures, and electronic properties of molecules in solution with the C-PCM solvation model, J. Comput. Chem. 24 (6) (2003) 669–681.
[3] B. Mennucci, Polarizable continuum model, Wiley Interdiscipl. Rev.: Comput. Mol. Sci. 2 (3) (2012) 386–404.
[4] V. Barone, M. Biczysko, J. Bloino, M. Borkowska-Panek, I. Carnimeo, P. Panek, Toward anharmonic computations of vibrational spectra for large molecular systems, Int. J. Quantum Chem. 112 (9) (2012) 2185–2200.
[5] V. Barone, M. Biczysko, J. Bloino, Fully anharmonic ir and raman spectra of medium-size molecular systems: accuracy and interpretation, PCCP 16 (5) (2014) 1759–1787.
[6] G.M. Chaban, J.O. Jung, R.B. Gerber, Anharmonic vibrational spectroscopy of glycine: testing of ab initio and empirical potentials, J. Phys. Chem. A 104 (44) (2000) 10035–10044.
[7] T.K. Roy, R.B. Gerber, Vibrational self-consistent field calculations for spectroscopy of biological molecules: new algorithmic developments and applications, Phys. Chem. Chem. Phys. 15 (2013) 9468–9492.
[8] E.E. Najbauer, G. Bazso, R. Apostolo, R. Fausto, M. Biczysko, V. Barone, G. Tarczay, Identification of serine conformers by matrix-isolation ir spectroscopy aided by near-infrared laser-induced conformational change, 2d correlation analysis, and quantum mechanical anharmonic computations, J. Phys. Chem. B 119 (33) (2015) 10496–10510.
[9] T.K. Roy, R. Sharma, R.B. Gerber, First-principles anharmonic quantum calculations for peptide spectroscopy: VSCF calculations and comparison with experiments, PCCP 18 (3) (2016) 1607–1614.
[10] P.T. Panek, C.R. Jacob, Anharmonic theoretical vibrational spectroscopy of polypeptides, J. Phys. Chem. Lett. 7 (16) (2016) 3084–3090.
[11] V. Yatsyna, D.J. Bakker, R. Feifel, A.M. Rijs, V. Zhaunerchyk, Far-infrared amide IV-VI spectroscopy of isolated 2-and 4-methylacetanilide, J. Chem. Phys. 145 (10) (2016) 104309.
[12] Q. Yu, J.M. Bowman, Communication: VSCF/VCI vibrational spectroscopy of *H7O3*+ and *H9O4*+ using high-level, many-body potential energy surface and dipole moment surfaces, J. Chem. Phys. 146 (12) (2017) 121102.
[13] M. Faizan, M.J. Alam, Z. Afroz, S.A. Bhat, S. Ahmad, Anharmonic vibrational spectra and mode-mode couplings analysis of 2-aminopyridine, Spectrochim. Acta Part A Mol. Biomol. Spectrosc. 188 (2018) 26–31, https://doi.org/10.1016/j.saa.2017.06.054, URL <http://www.sciencedirect.com/science/article/pii/S1386142517305334>.
[14] M.-P. Gaigeot, R. Vuilleumier, M. Sprik, D. Borgis, Infrared spectroscopy of n-methylacetamide revisited by ab initio molecular dynamics simulations, J. Chem. Theory Comput. 1 (5) (2005) 772–789.
[15] M.-P. Gaigeot, M. Martinez, R. Vuilleumier, Infrared spectroscopy in the gas and liquid phase from first principle molecular dynamics simulations: application to small peptides, Mol. Phys. 105 (19–22) (2007) 2857–2878.
[16] M.-P. Gaigeot, Theoretical spectroscopy of floppy peptides at room temperature. a DFTMD perspective: gas and aqueous phase, PCCP 12 (14) (2010) 3336–3359.
[17] J.D. Chodera, N. Singhal, V.S. Pande, K.A. Dill, W.C. Swope, Automatic discovery of metastable states for the construction of markov models of macromolecular conformational dynamics, J. Chem. Phys. 126 (15) (2007) 155101.
[18] J.-H. Prinz, H. Wu, M. Sarich, B. Keller, M. Senne, M. Held, J.D. Chodera, C. Schütte, F. Noé, Markov models of molecular kinetics: generation and validation, J. Chem. Phys. 134 (17) (2011) 174105.
[19] J.D. Chodera, F. Noé, Markov state models of biomolecular conformational dynamics, Curr. Opin. Struct. Biol. 25 (2014) 135–144.
[20] T. la Cour Jansen, J. Knoester, A transferable electrostatic map for solvation effects on amide I vibrations and its application to linear and two-dimensional spectroscopy, J. Chem. Phys. 124 (4) (2006) 044502.
[21] E. Malolepsza, J.E. Straub, Empirical maps for the calculation of amide I vibrational spectra of proteins from classical molecular dynamics simulations, J. Phys. Chem. B 118 (28) (2014) 7848–7855.
[22] K. Cai, F. Du, X. Zheng, J. Liu, R. Zheng, J. Zhao, J. Wang, General applicable frequency map for the amide-i mode in β-peptides, J. Phys. Chem. B 120 (6) (2016) 1069–1079.
[23] A. Bastida, J. Zúniga, A. Requena, B. Miguel, M.E. Candela, M.A. Soler, Conformational changes of trialanine in water induced by vibrational relaxation of the amide i mode, J. Phys. Chem. B 120 (2) (2016) 348–357.
[24] M.H. Faraq, A. Bastida, M.F. Ruiz-López, G. Monard, F. Ingrosso, Vibrational energy relaxation of the amide i mode of n-methylacetamide in D2O studied through born–oppenheimer molecular dynamics, J. Phys. Chem. B 118 (23) (2014) 6186–6197.
[25] F. Ingrosso, G. Monard, M.H. Farag, A. Bastida, M.F. Ruiz-López, Importance of polarization and charge transfer effects to model the infrared spectra of peptides in solution, J. Chem. Theory Comput. 7 (6) (2011) 1840–1849.
[26] M. Schwörer, C. Wichmann, P. Tavan, A polarizable QM/MM approach to the molecular dynamics of amide groups solvated in water, J. Chem. Phys. 144 (11) (2016) 114504.
[27] R.D. Gorbunov, P.H. Nguyen, M. Kobus, G. Stock, Quantum-classical description of the amide I vibrational spectrum of trialanine, J. Chem. Phys. 126 (2007) 054509.

[28] M. Kobus, P.H. Nguyen, G. Stock, Infrared signatures of the peptide dynamical transition: a molecular dynamics simulation study, J. Chem. Phys. 133 (3) (2010) 034512.
[29] L. Zanetti Polzi, I. Daidone, M. Anselmi, G. Carchini, A. Di Nola, A. Amadei, Analysis of infrared spectra of β-hairpin peptides as derived from molecular dynamics simulations, J. Phys. Chem. B 115 (41) (2011) 11872–11878.
[30] S.Y. Venyaminov, N.N. Kalnin, Quantitative ir spectrophotometry of peptide compounds in water (H2O) solutions. I. Spectral parameters of amino acid residue absorption bands, Biopolymers 30 (13–14) (1990) 1243–1257, https://doi.org/10.1002/bip.360301309.
[31] S.Y. Venyaminov, N.N. Kalnin, Quantitative ir spectrophotometry of peptide compounds in water (H2O) solutions. II. Amide absorption bands of polypeptides and fibrous proteins in α-, β-, and random coil conformations, Biopolymers 30 (13–14) (1990) 1259–1271, https://doi.org/10.1002/bip.360301310.
[32] W.C. Swope, J.W. Pitera, F. Suits, Describing protein folding kinetics by molecular dynamics simulations. 1. Theory, J. Phys. Chem. B 108 (21) (2004) 6571–6581.
[33] N.-V. Buchete, G. Hummer, Coarse master equations for peptide folding dynamics, J. Phys. Chem. B 112 (19) (2008) 6057–6069.
[34] D. McQuarrie, Statistical Mechanics, University Science Books, 2000, URL <https://books.google.de/books?id=itcpPnDnJM0C>.
[35] R. Kubo, M. Toda, N. Hashitsume, Statistical Physics II: Nonequilibrium Statistical Mechanics, vol. 31, Springer Science & Business Media, 2012.
[36] F. Noé, I. Horenko, C. Schütte, J.C. Smith, Hierarchical analysis of conformational dynamics in biomolecules: transition networks of metastable states, J. Chem. Phys. 126 (15) (2007) 155102.
[37] W.C. Swope, J.W. Pitera, F. Suits, M. Pitman, M. Eleftheriou, B.G. Fitch, R.S. Germain, A. Rayshubski, T.J.C. Ward, Y. Zhestkov, R. Zhou, Describing protein folding kinetics by molecular dynamics simulations. 2. Example applications to alanine dipeptide and a β-hairpin peptide, J. Phys. Chem. B 108 (21) (2004) 6582–6594.
[38] B. Strodel, D.J. Wales, Free energy surfaces from an extended harmonic superposition approach and kinetics for alanine dipeptide, Chem. Phys. Lett. 466 (4) (2008) 105–115, https://doi.org/10.1016/j.cplett.2008.10.085, URL <http://www.sciencedirect.com/science/article/pii/S0009261408014796>.
[39] A. Altis, M. Otten, P.H. Nguyen, R. Hegger, G. Stock, Construction of the free energy landscape of biomolecules via dihedral angle principal component analysis, J. Chem. Phys. 128 (24) (2008) 245102.
[40] T. Myazawa, T. Shimanouchi, S.-I. Mizushima, Normal vibrations of N-methylacetamide, J. Chem. Phys. 29 (1958) 611–616.
[41] S. Krimm, J. Bandekar, Vibrational spectroscopy and conformation of peptides, polypeptides, and proteins, Adv. Prot. Chem. 38 (1986) 181–364.
[42] M.-P. Gaigeot, Infrared spectroscopy of the alanine dipeptide analog in liquid water with DFT-MD. direct evidence for PII/β conformations, Phys. Chem. Chem. Phys. 12 (2010) 10198–10209, https://doi.org/10.1039/C003485A.
[43] F. Eker, X. Cao, L. Nafie, R. Schweitzer-Stenner, Tripeptides adopt stable structures in water. a combined polarized visible raman, FTIR, and VCD spectroscopy study, J. Am. Chem. Soc. 124 (48) (2002) 14330–14341.
[44] V. Vitale, J. Dziedzic, S.M.-M. Dubois, H. Fangohr, C.-K. Skylaris, Anharmonic infrared spectroscopy through the fourier transform of time correlation function formalism in ONETEP, J. Chem. Theory Comput. 11 (7) (2015) 3321–3332.
[45] J. Mahe, S. Jaeqx, A.M. Rijs, M.-P. Gaigeot, Can far-ir action spectroscopy combined with bomd simulations be conformation selective?, Phys Chem. Chem. Phys. 17 (2015) 25905–25914, https://doi.org/10.1039/C5CP01518A.
[46] S. Mukherjee, P. Chowdhury, F. Gai, Infrared study of the effect of hydration on the amide I band and aggregation properties of helical peptides, J. Phys. Chem. B 111 (17) (2007) 4596–4602.
[47] M.T. Zanni, M.C. Asplund, R.M. Hochstrasser, Two-dimensional heterodyned and stimulated infrared photon echoes of n-methylacetamide-d, J. Chem. Phys. 114 (10) (2001) 4579–4590.
[48] S. Woutersen, P. Hamm, Structure determination of trialanine in water using polarization sensitive two-dimensional vibrational spectroscopy, J. Phys. Chem. B 104 (47) (2000) 11316–11320.
[49] Y. Feng, J. Huang, S. Kim, J.H. Shim, A.D. MacKerell, N.-H. Ge, Structure of penta-alanine investigated by two-dimensional infrared spectroscopy and molecular dynamics simulation, J. Phys. Chem. B 120 (24) (2016) 5325–5339.

Chapter 5

Girsanov reweighting for path ensembles and Markov state models

In Molecular Dynamics (MD) [1, 2], the time evolution of a molecule, with potential energy function $V(x)$ is studied through computer simulations that solve the equation of motion. The potential energy function is parametrized in a file, called forcefield, that describes the inter- and intra-molecular interactions.

Nowadays, different forcefields have been developed. However, even if they describe the potential energy function of the same molecule, they exhibit different dynamical properties [6]. This behaviour is caused by the high sensitivity of molecular systems to external perturbations. Thus, a deeper investigation of the potential energy functions and the associated dynamical effects is necessary, to improve the forcefields parametrization and to better understand the dynamics of molecules.

In the last years, Markov State Models [11, 12, 15, 16, 17, 18, 13, 19] (MSMs) have become a successful tool to analyze sets of short MD trajectories. MSMs approximate the dynamics of molecular systems through a transition probability matrix $\mathbf{T}(\tau)$, that is the discretized version of the classical propagator. In order to build an MSM, one produces a fully atomistic trajectory by MD simulation, then projects the trajectory on few relevant coordinates and estimates the time-lagged correlation function between Voronoi cells.

To study the effect of a modification of the potential energy function on the dynamics, one should modify the forcefield, to perform a new MD simulation and to analyze the data. But this approach is time consuming and computationally expensive, because for each modification, a new MD simulation and MSM is necessary.

An alternative to reduce the effort and the computational cost, would be to develop a reweighting scheme for dynamic properties of molecules, during the data analysis of MD trajectories.

Thus, a reweighting scheme for MSMs should act on the time-correlation functions. Because time-correlation functions are, from a mathematical point of view, path ensemble averages, the Girsanov theorem [42, 40] can be used to reweight MSMs. The Girsanov theorem states the conditions under which the change of measure is allowed and provides a formula to estimate in practise the ratio between path probability densities.

In the paper [41], included in this chapter, we propose a new method, called Girsanov reweighting that works on full MD simulations. Given a molecular system, described by a reference potential energy function $V(x)$ and an associated time-discretized trajectory x_t, through Girsanov reweighting we can construct the transition probability matrix $\widetilde{\mathbf{T}}(\tau)$ for different perturbed potential energy functions $\widetilde{V}(x)$, using the same trajectory x_t and with no need of further MD simulations.

To explain how to implement the Girsanov theorem in MSMs, we have rewritten the MSMs theory in terms of path probability measures and path ensemble averages. Indeed, as already mentioned, MSMs are built from time-lagged correlation functions, which can be interpreted as path ensemble averages. In this way, it is straightforward to define a reweighting factor as the ratio of the path probability densities associated to the two different dynamics $V(x)$ and $\widetilde{V}(x)$.

Girsanov reweighting can be used in several further applications:

1. To study how each forcefield components modifies the molecular dynamics [77, 78]
2. To reweight the trajectories produced by enhanced sampling simulations (metadynamics [43, 44, 45, 46], Hamiltonian replica exchange [79], umbrella sampling [29, 30]) and to obtain the dynamics of the original unbiased models
3. To optimize the force fields by fitting experimentally measured time correlation functions [6]

I contributed to this paper describing in detail the theory underlying the Girsanov reweighting. Afterward, I discuss practical issues and how the method can be efficiently implemented in real world applications. I carried out all the simulations and the MSMs construction, by Girsanov reweighting, of the systems described in the paper: the two-dimensional process, the high-dimensional diffusion process, the Alanine dipeptide and the Valine dipeptide, in implicit and explicit solvent, including the benchmark test. I also provided a working script for OpenMM simulations [80].

https://doi.org/10.1063/1.4989474

THE JOURNAL OF CHEMICAL PHYSICS **146**, 244112 (2017)

Girsanov reweighting for path ensembles and Markov state models

L. Donati,[1] C. Hartmann,[2] and B. G. Keller[1,a)]
[1]*Department of Biology, Chemistry, Pharmacy, Freie Universität Berlin, Takustraße 3, D-14195 Berlin, Germany*
[2]*Institute of Mathematics, Brandenburgische Technische Universität Cottbus-Senftenberg, Konrad-Wachsmann-Allee 1, D-03046 Cottbus, Germany*

(Received 8 March 2017; accepted 26 May 2017; published online 28 June 2017)

The sensitivity of molecular dynamics on changes in the potential energy function plays an important role in understanding the dynamics and function of complex molecules. We present a method to obtain path ensemble averages of a perturbed dynamics from a set of paths generated by a reference dynamics. It is based on the concept of path probability measure and the Girsanov theorem, a result from stochastic analysis to estimate a change of measure of a path ensemble. Since Markov state models (MSMs) of the molecular dynamics can be formulated as a combined phase-space and path ensemble average, the method can be extended to reweight MSMs by combining it with a reweighting of the Boltzmann distribution. We demonstrate how to efficiently implement the Girsanov reweighting in a molecular dynamics simulation program by calculating parts of the reweighting factor "on the fly" during the simulation, and we benchmark the method on test systems ranging from a two-dimensional diffusion process and an artificial many-body system to alanine dipeptide and valine dipeptide in implicit and explicit water. The method can be used to study the sensitivity of molecular dynamics on external perturbations as well as to reweight trajectories generated by enhanced sampling schemes to the original dynamics. *Published by AIP Publishing.* [http://dx.doi.org/10.1063/1.4989474]

I. INTRODUCTION

Molecular dynamics (MD) simulations with explicit solvent molecules are routinely used as efficient importance sampling algorithms for the Boltzmann distribution of molecular systems. From the conformational snapshots created by MD simulations, one can estimate phase-space ensemble averages and thus interpret experimental data or thermodynamic functions in terms of molecular conformations.

In recent years, the scope of MD simulations has considerably widened, and the method has been increasingly used to construct models of the conformational dynamics.[1–5] Most notably Markov state models (MSMs),[6–14] in which the conformational space is discretized into disjoint states and the dynamics is modeled as a Markov jump process between these states, have become a valuable tool for the analysis of complex molecular dynamics.[15–19]

For the construction of dynamic models, one has to estimate path ensemble averages. For example, in MSMs, the transition probabilities between a pair of states B_i and B_j are estimated by considering a set of paths $S_\tau = \{\omega_1, \omega_2, \ldots \omega_n\}$, each of which has length τ, counting the number of paths which start in B_i and end in B_j and comparing this number to the total number of paths in the set (vertical line of blue boxes in Fig. 1).

Suppose, one would like to compare the dynamics in a reference potential energy function $V(\mathbf{r})$ to the dynamics in a series of perturbed potential energy functions $V(\mathbf{r}) + U(\mathbf{r}, \kappa)$, where $U(\mathbf{r}, \kappa)$ represents the perturbation and κ is a tunable parameter, e.g., a force constant. While for phase-space ensemble averages, numerous methods exist to reweight the samples of the reference conformational ensemble to yield ensemble averages for the perturbed systems,[20–23] similar reweighting schemes have not yet been developed for path ensemble averages of explicit-solvent simulations. This means that currently one would have to re-simulate the dynamics at each parameter value (vertical lines of green boxes in Fig. 1) and then construct a MSM for each simulation separately. This is computationally extremely costly.

An alternative would be to reweight the path ensemble average at the reference potential energy function to obtain path ensemble averages for the perturbed systems (reweighting box in Fig. 1). From measure theory, it is well known that a reweighting factor is given as the ratio between the probability measure associated with the reference potential energy function and the probability measure associated with the perturbed potential energy function. This applies to reweighting phase space ensemble averages as well as to reweighting path ensemble averages. Figure 2 illustrates the idea of a path ensemble reweighting method. The figure shows two sets of paths: one generated by a Brownian dynamics simulation without drift, S_τ [Fig. 2(a)], and the other generated by a Brownian dynamics simulation with drift, $\widetilde{S}_\tau$ [Fig. 2(b)]. Both simulations sample the same path space $\Omega_{\tau,\mathbf{x}}$ but the probability with which a given path is realized differs in the two simulations. In Figs. 2(a) and 2(b), the sets of paths, S_τ and $\widetilde{S}_\tau$, are colored according to their respective path probability density $\mu_P(\omega)$ and $\mu_{\widetilde{P}}(\omega)$. Figures 2(c) and 2(d) show again S_τ; this time however we colored the paths according to the probability density $\mu_{\widetilde{P}}(\omega)$ with which they would have been generated by a

a)Electronic mail: bettina.keller@fu-berlin.de

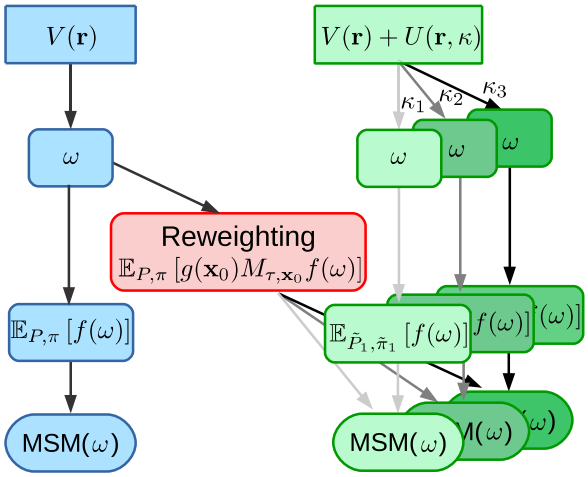

FIG. 1. Workflow of a reweighting scheme. $V(\mathbf{r})$ is the reference potential energy function, $V(\mathbf{r}) + U(\mathbf{r}, \kappa)$ is the perturbed potential energy function, where κ is a tunable parameter, ω is the trajectory generated by a MD simulation at the potential $V(\mathbf{r})$ or $V(\mathbf{r}) + U(\mathbf{r}, \kappa)$ and at a fixed thermodynamic state point. A MSM is an expected value with respect to a path probability measure P and a stationary distribution π, which can be estimated from the trajectory ω. A dynamical reweighting scheme, reweights the path probability measures P and π of the reference dynamics, to the path probability measures of a perturbed potential energy functions $\widetilde{P}$ and $\widetilde{\pi}$. Thus, we can use the trajectory generated at $V(\mathbf{r})$ to estimate dynamical expected value (e.g., MSMs) at the perturbed potential energy functions.

Brownian dynamics with drift. For Brownian dynamics, this probability can be calculated directly [Fig. 2(c)]; for other types of dynamics, a reweighting method has to be used [Fig. 2(d)]. To estimate a path ensemble average for the Brownian dynamics with drift from S_τ, the contribution of each path

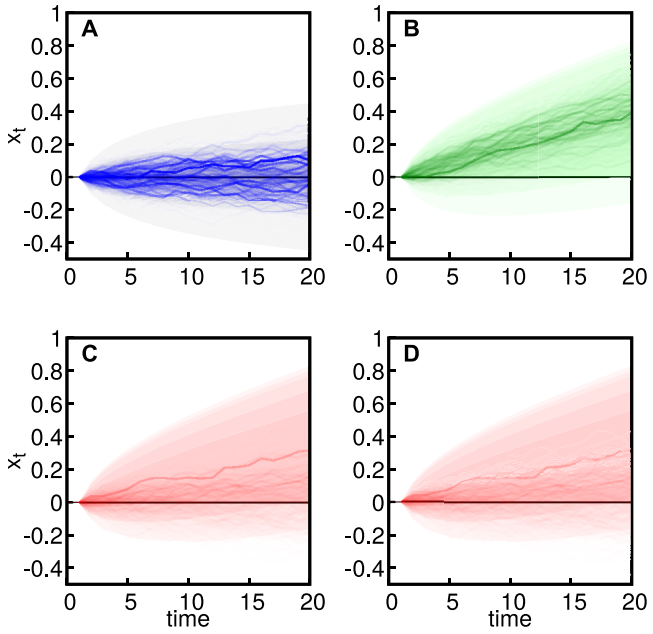

FIG. 2. Two sets of trajectories starting from $x(t = 0) = 0$ with time step $\Delta t = 0.001$. (a) Set S_τ generated by a Brownian motion without drift, associated with path probability measure P. Color intensity represents $\widetilde{P}$. Color intensity represents $\widetilde{P}$. (b) Set $\widetilde{S}_\tau$ generated by a Brownian motion with drift $a = 20$, associated with path probability measure $\widetilde{P}$. (c) Set S_τ, color intensity represents $\widetilde{P}$ (direct calculation). (d) Set S_τ, color intensity represents $\widetilde{P}$ (Girsanov formula).

ω to the estimated value is multiplied by the ratio $M_{\tau,\mathbf{x}}(\omega) = \mu_{\widetilde{P}}(\omega)/\mu_P(\omega)$ (Fig. 1).

Path ensemble reweighting schemes have initially been developed in the field of importance sampling for stochastic differential equations.[24–26] For Langevin dynamics, the Girsanov theorem[27,28] provides us with an expression for the probability ratio, and thus reweighting path ensemble averages become possible for this type of dynamics (Sec. II C). It has recently been demonstrated that the theorem can be applied to reweight Markov state models of Brownian dynamics in one- and two-dimensional potential energy functions.[29]

Here we demonstrate how the Girsanov reweighting scheme can be applied to explicit-solvent all-atom MD simulations. For this, we need to address to critical pillars on which the Girsanov reweighting scheme rests:

- The equation of motion needs to contain a stochastic term which generates random forces drawn from a normal distribution (white noise).
- To calculate the reweighting factor, the random forces need to be accessible for each MD simulation step.

In all-atom MD simulations, the system is propagated by the Newton equations of motion which do not contain a stochastic term. We will discuss how the Girsanov theorem can nonetheless be applied to this type of simulation (Sec. IV B). The second point, in principle, requires that the forces are written out at every MD simulation step, i.e., at a frequency of femtoseconds rather than the usual output rate of several picoseconds. This quickly fills up any hard disc and slows the simulation by orders of magnitudes. We will present a computational efficient implementation of the reweighting scheme (Sec. IV A).

When applying the Girsanov theorem to reweight an MSM, an additional difficulty arises:

- The degrees of freedom which are affected by the perturbation might not be part of the relevant subspace of the MSM.

We found that the reweighting becomes problematic in this case and propose to project the perturbed degrees of freedom onto the relevant subspace during the estimation of the ratio of probability measures (Sec. II E).

The Girsanov reweighting method is demonstrated and benchmarked on several systems, ranging from two-dimensional diffusion processes (Sec. IV C), over molecular model systems which follow a Langevin dynamics (Sec. IV D), to all-atom MD simulations of alanine and valine dipeptides in explicit and implicit solvents (Sec. IV E).

II. THEORY

A. Molecular dynamics

Consider a molecular system with N particles, which evolves in time t according to the Langevin equation

$$M\frac{\mathrm{d}\mathbf{v}(t)}{\mathrm{d}t} = -\nabla V(\mathbf{r}(t)) - \gamma\mathbf{v}(t) + \sigma\eta(t),$$
$$\mathbf{v}(t) = \frac{\mathrm{d}\mathbf{r}(t)}{\mathrm{d}t}, \quad (1)$$

where M is the mass matrix and $\mathbf{r}(t)$ and $\mathbf{v}(t) \in \mathbb{R}^{3N}$ are the position vector and the velocity vector. $V(\mathbf{r})$ is the potential energy function. The interaction with the thermal bath is modelled by the friction coefficient γ, and an uncorrelated Gaussian white noise $\eta(t) \in \mathbb{R}^{3N}$ which is scaled by the volatility σ,

$$\sigma = \sqrt{2k_B T \gamma M}, \tag{2}$$

where k_B is the Boltzmann constant and T is the temperature of the system.

The phase-space vector $\mathbf{x}(t) = \{\mathbf{r}(t), \mathbf{v}(t)\} \in \Gamma$ fully represents the state of the system at time t, where $\Gamma = \mathbb{R}^{6N}$ denotes the phase space of the system. The dynamics in Eq. (1) is associated with an equilibrium probability density

$$\mu_\pi(\mathbf{x}) = \frac{\exp\left[-\beta \mathcal{H}(\mathbf{x})\right]}{Z}, \tag{3}$$

where $\beta = \frac{1}{k_B T}$, $\mathcal{H}(\mathbf{x}) = \frac{1}{2}\mathbf{v}^\top M \mathbf{v} + V(\mathbf{r})$ is the classical Hamiltonian of the system, and $Z = \int_\Gamma \exp\left[-\beta \mathcal{H}(\mathbf{x})\right] \mathrm{d}\mathbf{x}$ is the partition function. The function $\mu_\pi(\mathbf{x})$ is associated with the probability measure

$$\pi(A) = \mathbb{P}(\mathbf{x} \in A) = \int_A \mu_\pi(\mathbf{x}) \mathrm{d}\mathbf{x}\,, \quad \forall A \subset \Gamma, \tag{4}$$

where $\pi(A)$ represents the equilibrium probability of finding the system in a subset A of the phase space Γ. The expected value of a function $a(\mathbf{x}) : \Gamma \to \mathbb{R}$ with respect to the probability density $\mu_\pi(\mathbf{x})$ is given as

$$\mathbb{E}_\pi\left[a\right] = \int_\Gamma a(\mathbf{x}) \mu_\pi(\mathbf{x})\, \mathrm{d}\mathbf{x} = \lim_{n\to\infty} \frac{1}{n} \sum_{\mathbf{x}_k \in S_n} a(\mathbf{x}_k)\,, \tag{5}$$

where $S_n = \{\mathbf{x}_1, \ldots \mathbf{x}_n\}$ is a set of states distributed according to Eq. (3). When the phase space vectors $\mathbf{x}_i$ are generated by numerically integrating Eq. (1), the second equality only holds if the sampling is ergodic. Equation (5) defines a *phase-space ensemble average*. The subscript π indicates the measure for which the expected value is calculated.

B. Path ensembles and MSMs

A path $\omega = \{\mathbf{x}(t=0) = \mathbf{x}_0, \mathbf{x}_1, \mathbf{x}_2, \ldots, \mathbf{x}(\tau) = \mathbf{x}_n\}$ is a time-discretized realization of the dynamics $\mathbf{x}(t)$ on the time interval $[0, \tau = n \cdot \Delta t]$ starting at a particular point $\mathbf{x}_0 \in \Gamma$, where Δt is the time step and $n \in \mathbb{N}$ is the number of time steps. The associated path space is denoted as $\Omega_{\tau,\mathbf{x}} = \mathbb{R}^{6N \cdot n}$. A subset of the path space $\mathcal{A}$ is constructed as a product of subsets $A_i \subset \Gamma$ of the state space $\mathcal{A} = A_1 \times A_2 \cdots \times A_n$, where the subset A_i represents the phase space volume in which $\mathbf{x}_i$ may be found. The probability that by integrating Eq. (1) one obtains a path ω which belongs to the subset $\mathcal{A} \subset \Omega_{\tau,\mathbf{x}}$ is given as

$$\begin{aligned} P(\mathcal{A}) = \mathbb{P}(\omega \in \mathcal{A}) &= \mathbb{P}(\mathbf{x}_1 \in A_1, \mathbf{x}_2 \in A_2, \ldots, \mathbf{x}_\tau \in A_n) \\ &= \int_{A_1}\int_{A_2} \cdots \int_{A_n} p(\mathbf{x}_0, \mathbf{x}_1;\, \Delta t)\, p(\mathbf{x}_1, \mathbf{x}_2;\, \Delta t) \ \ldots \ p \\ &\quad \times (\mathbf{x}_{n-1}, \mathbf{x}_n;\, \Delta t)\, \mathrm{d}\mathbf{x}_1\, \mathrm{d}\mathbf{x}_2 \ \ldots \ \mathrm{d}\mathbf{x}_n\,. \end{aligned} \tag{6}$$

The function $p(\mathbf{x}_i, \mathbf{x}_{i+1};\, \Delta t)$ is the transition probability density, i.e., the conditional probability to be in $\mathbf{x}_{i+1}$ after a time Δt given the initial state $\mathbf{x}_i$. The function P is a path probability measure and is the analogon to π in phase space ensemble averages [Eq. (4)]. The path probability measure is associated with the path probability density function

$$\begin{aligned} \mu_P(\omega) = \mu_P(\mathbf{x}_1, \mathbf{x}_2, \ldots, \mathbf{x}_\tau) = p(\mathbf{x}_0, \mathbf{x}_1;\, \Delta t)\, p(\mathbf{x}_1, \mathbf{x}_2;\, \Delta t) \ \ldots \ p \\ \times (\mathbf{x}_{n-1}, \mathbf{x}_n;\, \Delta t) \end{aligned} \tag{7}$$

and hence the formal analogon to Eq. (4) in the path space is

$$P(\mathcal{A}) = \mathbb{P}(\omega \in \mathcal{A}) = \int_{\mathcal{A}} \mu_P(\omega) \mathrm{d}\omega\,, \quad \forall \mathcal{A} \subset \Omega_{\tau,\mathbf{x}}, \tag{8}$$

where the integration over $\mathrm{d}\omega$ is defined by Eq. (6).

Let $f : \Omega_{\tau,\mathbf{x}} \to \mathbb{R}$ be an integrable function, which assigns a real number to each path. The expected value of this function is

$$\begin{aligned} \mathbb{E}_P[f(\omega)] &= \int_{\Omega_{\tau,\mathbf{x}}} f(\omega)\, \mu_P(\omega)\, \mathrm{d}\omega \\ &= \int_\Gamma \int_\Gamma \cdots \int_\Gamma f(\mathbf{x}_1, \mathbf{x}_2, \ldots, \mathbf{x}_n) \mu_P(\mathbf{x}_1, \mathbf{x}_2, \ldots, \mathbf{x}_n) \\ &\quad \times \mathrm{d}\mathbf{x}_1\, \mathrm{d}\mathbf{x}_2 \ \ldots \ \mathrm{d}\mathbf{x}_n \\ &= \lim_{m\to\infty} \frac{1}{m} \sum_{\omega_k \in S_{\tau,\mathbf{x},m}} f(\omega_k)\,, \end{aligned} \tag{9}$$

where we again assumed that the paths have a common initial state $\mathbf{x}(t=0) = \mathbf{x}_0$, and $S_{\tau,\mathbf{x},m} = \{\omega_1, \omega_2, \ldots \omega_m\}$ corresponds to a set of paths of length τ generated by numerically integrating Eq. (1). When the paths are extracted from a single long trajectory, the last equality only holds if the sampling is ergodic. Equation (9) defines a *path ensemble average*. The subscript P indicates that the expected value is calculated with respect to a path probability measure.

For Markov processes, one can define a transition probability density $p(\mathbf{x}, \mathbf{y}; \tau)$, i.e., the conditional probability to be in $\mathbf{x}_n = \mathbf{y}$ after a time τ given that the path started in $\mathbf{x}_0 = \mathbf{x}$, by integrating the path probability density over all intervening states and applying recursively the Chapman-Kolmogorov equation

$$p(\mathbf{x}, \mathbf{y}, \tau) = \int_\Gamma \int_\Gamma \cdots \int_\Gamma \mu_P(\mathbf{x}_1, \mathbf{x}_2, \ldots, \mathbf{y})\, \mathrm{d}\mathbf{x}_1\, \mathrm{d}\mathbf{x}_2 \ \ldots \ \mathrm{d}\mathbf{x}_{n-1}. \tag{10}$$

Markov processes can be approximated by Markov state models.[6–12,14] In these models, the phase space is discretized into disjoint sets (or microstates) $B_1, B_2, \ldots B_s$ with $\cup_{i=1}^m B_i = \Gamma$, where the indicator function of the ith state is given as

$$\mathbf{1}_{B_i}(\mathbf{x}) := \begin{cases} 1, & \text{if } \mathbf{x} \in B_i, \\ 0, & \text{otherwise.} \end{cases} \tag{11}$$

The associated cross correlation function is

$$C_{ij}(\tau) = \int_\Gamma \mu_\pi(\mathbf{x}) \mathbf{1}_{B_i}(\mathbf{x}) \int_\Gamma p(\mathbf{x}, \mathbf{y}; \tau)\, \mathbf{1}_{B_j}(\mathbf{y})\, \mathrm{d}\mathbf{y}\, \mathrm{d}\mathbf{x}\,, \tag{12}$$

where $\mu_\pi(\mathbf{x})$ is the equilibrium probability density [Eq. (3)]. The transition probability between set B_i and set B_j is

$$T_{ij}(\tau) = \frac{C_{ij}(\tau)}{\sum_{j=1}^s C_{ij}(\tau)}\,. \tag{13}$$

$T_{ij}(\tau)$ are the elements of the transition matrix whose dominant eigenvectors and eigenvalues represent the slow dynamic processes for the system.[6–12,14]

Because of Eq. (10), one can regard the inner integral of the cross correlation function $C_{ij}(\tau)$ [Eq. (12)] as a path ensemble average [Eq. (9)] which depends on the initial state $\mathbf{x}_0 = \mathbf{x}$ of the path ensemble

$$\begin{aligned}\int_\Gamma p(\mathbf{x},\mathbf{y};\tau)\,\mathbf{1}_{B_j}(\mathbf{y})\,\mathrm{d}\mathbf{y} &= \int_\Gamma\int_\Gamma\dots\int_\Gamma \mu_P(\mathbf{x}_1,\mathbf{x}_2,\dots,\mathbf{x}_n)\\ &\quad\times\mathbf{1}_{B_j}(\mathbf{x}_n)\,\mathrm{d}\mathbf{x}_1\,\mathrm{d}\mathbf{x}_2\,\dots\,\mathrm{d}\mathbf{x}_n\\ &= \mathbb{E}_P^{\mathbf{x}_0}[\mathbf{1}_{B_j}(\mathbf{x}_n)]\,. \end{aligned}\tag{14}$$

This expected value is a linear operator and it is called the backward transfer operator. The outer integral in Eq. (12) is a phase space ensemble average, thus we have

$$\begin{aligned}C_{ij}(\tau) &= \int_\Gamma \mu_\pi(\mathbf{x}_0)\,\mathbf{1}_{B_i}(\mathbf{x}_0)\,\mathbb{E}_P^{\mathbf{x}_0}[\mathbf{1}_{B_j}(\mathbf{x}_n)]\mathrm{d}\mathbf{x}_0\\ &= \mathbb{E}_\pi[\mathbf{1}_{B_i}(\mathbf{x}_0)\,\mathbb{E}_P^{\mathbf{x}_0}[\mathbf{1}_{B_j}(\mathbf{x}_n)]]\\ &= \mathbb{E}_{P,\pi}[\mathbf{1}_{B_i}(\mathbf{x}_0)\mathbf{1}_{B_j}(\mathbf{x}_n)],\end{aligned}\tag{15}$$

where the combined phase space and ensemble average is defined as

$$\mathbb{E}_{P,\pi}[f(\omega)] = \int_\Gamma \mu_\pi(\mathbf{x}_0)\int_{\Omega_{\tau,\mathbf{x}}} f(\omega)\,\mu_P(\omega)\,\mathrm{d}\omega\,\mathrm{d}\mathbf{x}_0.\tag{16}$$

Equation (16) extends Eq. (9) to path ensembles with arbitrary initial states. The elements $C_{ij}(\tau)$ can be estimated from a set of paths of length τ, $S_{\tau,m} = \{\nu_1,\nu_2\dots\nu_m\}$, in which the initial states are no longer fixed but are distributed according to $\mu_\pi(\mathbf{x})$,

$$\begin{aligned}C_{ij}(\tau) &= \lim_{m\to\infty}\frac{1}{m}\sum_{\nu_k\in S_\tau}\mathbf{1}_{B_i}([\nu_k]_{t=0})\cdot\mathbf{1}_{B_j}([\nu_k]_{t=n})\\ &= \lim_{m\to\infty}\frac{1}{m}\sum_{k=1}^{m}\mathbf{1}_{B_i}([\mathbf{x}_0]_k)\cdot\mathbf{1}_{B_j}([\mathbf{x}_n]_k),\end{aligned}\tag{17}$$

where $[\nu_k]_{t=i} = [\mathbf{x}_i]_k$ denotes the ith time step of the kth path.

C. Dynamical reweighting

We alter the reference dynamics [Eq. (1)] by adding a perturbation $U(\mathbf{r}) : \Gamma \to \mathbb{R}$ to the potential energy function $V(\mathbf{r})$. Thus, $\widetilde{V}(\mathbf{r}) = V(\mathbf{r}) + U(\mathbf{r})$ is the perturbed potential energy function, and the Langevin equations of motion are

$$\begin{aligned}M\frac{\mathrm{d}\mathbf{v}(t)}{\mathrm{d}t} &= -\nabla\widetilde{V}\,(\mathbf{r}(t)) - \gamma\mathbf{v}(t) + \sigma\eta(t),\\ \mathbf{v}(t) &= \frac{\mathrm{d}\mathbf{r}(t)}{\mathrm{d}t}\,.\end{aligned}\tag{18}$$

The perturbed dynamics is associated with a perturbed stationary probability density

$$\mu_{\widetilde{\pi}}(\mathbf{x}) = \frac{\exp\left[-\beta\widetilde{\mathcal{H}}(\mathbf{x})\right]}{\widetilde{Z}}\,,\tag{19}$$

where $\widetilde{\mathcal{H}}(\mathbf{x}) = \frac{1}{2}\mathbf{v}^\top M\mathbf{v} + \widetilde{V}(\mathbf{r})$ is the Hamiltonian of the perturbed system and $\widetilde{Z}$ is its partition function. The perturbation of the potential energy function also changes the transition probability density $\widetilde{p}(\mathbf{x}_i,\mathbf{x}_{i+1};\Delta t)$, which gives rise to a perturbed path probability density $\mu_{\widetilde{P}}(\omega)$ [Eq. (7)] and a perturbed path measure $\widetilde{P}$ [Eq. (6)].

Reweighting methods compare the probability measure of the perturbed systems to the probability measure of a reference system. We first review the derivation of a reweighting scheme for phase space probability measures before discussing path space probability measures. The perturbed phase-space probability measure $\widetilde{\pi}$ is said to be *absolutely continuous* with respect to the reference phase space probability measure π if

$$\widetilde{\pi}(A) = \int_A \mu_{\widetilde{\pi}}(\mathbf{x})\,\mathrm{d}\mathbf{x} = 0 \;\Rightarrow\; \pi(A) = \int_A \mu_\pi(\mathbf{x})\,\mathrm{d}\mathbf{x} = 0\,.\tag{20}$$

This condition is sufficient and necessary to define the likelihood ratio between probability measures

$$g(\mathbf{x}) = \frac{\mathrm{d}\widetilde{\pi}}{\mathrm{d}\pi} = \frac{\mu_{\widetilde{\pi}}(\mathbf{x})}{\mu_\pi(\mathbf{x})} = \frac{Z}{\widetilde{Z}}\exp\left(-\beta U(\mathbf{x})\right).\tag{21}$$

The function $g(\mathbf{x})$ is also called the Radon-Nikodym derivative (Radon-Nikodym theorem[28]) and can be used to construct the phase-space probability measure of the perturbed system, from the phase-space probability of the reference system,

$$\widetilde{\pi}(A) = \int_A \mu_{\widetilde{\pi}}(\mathbf{x})\mathrm{d}\mathbf{x} = \int_A g(\mathbf{x})\mu_\pi(\mathbf{x})\mathrm{d}\mathbf{x}\,.\tag{22}$$

As a consequence, if $g(\boldsymbol{x})$ can be calculated, one can estimate a phase space ensemble average [Eq. (5)] for the perturbed dynamics [Eq. (18)] from a set of states $S_n = \{\mathbf{x}_1,\dots\mathbf{x}_n\}$ which has been generated by the reference dynamics [Eq. (1)]

$$\begin{aligned}\mathbb{E}_{\widetilde{\pi}}[a] &= \int_\Gamma a(\mathbf{x})\mu_{\widetilde{\pi}}(\mathbf{x})\,\mathrm{d}\mathbf{x} = \int_\Gamma a(\mathbf{x})g(\mathbf{x})\mu_\pi(\mathbf{x})\,\mathrm{d}\mathbf{x}\\ &= \lim_{n\to\infty}\frac{1}{n}\sum_{k=1}^{n}a(\mathbf{x}_k)g(\mathbf{x}_k)\,.\end{aligned}\tag{23}$$

The notion of absolute continuity is valid also for path probability densities,

$$\begin{aligned}\widetilde{P}(\mathcal{A}) = \int_{\mathcal{A}}\mu_{\widetilde{P}}(\omega)\mathrm{d}\omega = 0 \Rightarrow P(\mathcal{A}) = \int_{\mathcal{A}}\mu_P(\omega)\mathrm{d}\omega = 0,\\ \times\forall\mathcal{A}\subset\Omega_{\tau,\mathbf{x}}\,.\end{aligned}\tag{24}$$

Thus we can reweight a path ensemble average, by using the likelihood ratio between the path probability density $\mu_{\widetilde{P}}(\omega)$ and $\mu_P(\omega)$. For diffusion processes like (1) and (18), the likelihood ratio is given as

$$\begin{aligned}M_{\tau,\mathbf{x}}(\omega) = \frac{\mu_{\widetilde{P}}(\omega)}{\mu_P(\omega)} = \exp\left\{\sum_{i=1}^{3N}\left[\sum_{k=0}^{n}\frac{\nabla_i U(\mathbf{r}_k)}{\sigma}\eta_k^i\sqrt{\Delta t}\right.\right.\\ \left.\left. - \frac{1}{2}\sum_{k=0}^{n}\left(\frac{\nabla_i U(\mathbf{r}_k)}{\sigma}\right)^2\Delta t\right]\right\},\end{aligned}\tag{25}$$

where η_k^i are the random numbers, along the dimension i at a time step k, generated to integrate Eq. (1) of the reference dynamics and $\nabla_i U(\mathbf{r}_k)$ is the gradient of the perturbation along the dimension i measured at the position $\mathbf{r}_k$. Note that to evaluate Eq. (25) one needs the positions and the random numbers for every time step of the time-discretized trajectory. Equation (25) is derived in Appendix B. We remark that the quantity $M_{\tau,\mathbf{x}}(\omega)$ exists also for continuous paths ($\Delta t \to 0$). In this case, the existence of the Radon-Nikodym derivative is guaranteed by the Girsanov theorem[27,28] that states the conditions under which a perturbed path probability density $\widetilde{P}$ can be defined with respect to a reference path probability density P. The differences between time-continuous and time-discrete paths are discussed in Appendixes A and B.

Analogous to the reweighting of phase-space ensemble averages [Eq. (23)], we can use $M_{\tau,\mathbf{x}}(\omega)$ to reweight path ensemble averages

$$\begin{aligned}\mathbb{E}_{\widetilde{P}}[f(\omega)] &= \int_{\Omega_{\tau,\mathbf{x}}} f(\omega)\, M_{\tau,\mathbf{x}}(\omega)\, \mu_P(\omega)\, \mathrm{d}\omega \\ &= \lim_{n\to\infty} \frac{1}{n} \sum_{i=1}^{n} M_{\tau,\mathbf{x}}(\omega_i) f(\omega_i)\,. \end{aligned} \tag{26}$$

The second equality shows how to estimate the path ensemble average $\mathbb{E}_{\widetilde{P}}[f(\omega)]$ at the perturbed dynamics [Eq. (18)] from a set of paths $S_{\tau,\mathbf{x},m} = \{\omega_1, \omega_2, \ldots \omega_m\}$ which has been generated by the reference dynamics [Eq. (1)].

D. Reweighting MSMs

When reweighting a MSM, we estimate the cross correlation function $\widetilde{C}_{ij}(\tau)$ for the perturbed dynamics [Eq. (18)], from a set of paths of length τ, $S_{\tau,m} = \{\nu_1, \nu_2 \ldots \nu_m\}$, which has been generated by the reference dynamics [Eq. (1)]. The cross correlation function $\widetilde{C}_{ij}(\tau)$ is a combined phase space and path ensemble average [Eq. (16)]. Thus, both averages have to be reweighted with the appropriated probability ratio,

$$\begin{aligned}\mathbb{E}_{\widetilde{P},\widetilde{\pi}}[a(\mathbf{x}_0)f(\omega)] &= \int_\Gamma a(\mathbf{x}_0)\mu_{\widetilde{\pi}}(\mathbf{x}_0) \int_{\Omega_{\tau,\mathbf{x}}} f(\omega)\, \mu_{\widetilde{P}}(\omega)\, \mathrm{d}\omega\, \mathrm{d}\mathbf{x}_0 \\ &= \int_\Gamma a(\mathbf{x}_0) g(\mathbf{x}_0) \mu_\pi(\mathbf{x}_0) \\ &\quad \times \int_{\Omega_{\tau,\mathbf{x}}} f(\omega)\, M_{\tau,\mathbf{x}}(\omega)\, \mu_P(\omega)\, \mathrm{d}\omega\, \mathrm{d}\mathbf{x}_0\,. \end{aligned} \tag{27}$$

With $a(\mathbf{x}_0) = \mathbf{1}_{B_i}(\mathbf{x}_0)$ and $f(\omega) = \mathbf{1}_{B_j}(\mathbf{x}_n)$, we obtain

$$\begin{aligned}\widetilde{C}_{ij}(\tau) &= \mathbb{E}_{\widetilde{P},\widetilde{\pi}}[\mathbf{1}_{B_i}(\mathbf{x}_0)\mathbf{1}_{B_j}(\mathbf{x}_n)] \\ &= \int_\Gamma \mathbf{1}_{B_i}(\mathbf{x}_0) g(\mathbf{x}_0) \mu_\pi(\mathbf{x}_0) \\ &\quad \times \int_{\Omega_{\tau,\mathbf{x}}} \mathbf{1}_{B_j}(\mathbf{x}_n)\, M_{\tau,\mathbf{x}}(\omega)\, \mu_P(\omega)\, \mathrm{d}\omega\, \mathrm{d}\mathbf{x}_0\,, \end{aligned} \tag{28}$$

which can be estimated from a set of paths $S_{\tau,m} = \{\nu_1, \nu_2 \ldots \nu_m\}$ as

$$\widetilde{C}_{ij}(\tau) = \lim_{m\to\infty} \frac{1}{m} \sum_{\nu_k \in S_{\tau,m}} g([\mathbf{x}_0]_k) \mathbf{1}_{B_i}([\mathbf{x}_0]_k) \cdot M_{\mathbf{x},\tau}(\nu_k) \mathbf{1}_{B_j}([\mathbf{x}_n]_k)\,, \tag{29}$$

where $[\mathbf{x}_i]_k$ is the ith time step of the kth path. As in Eq. (12), the initial states of the paths are not fixed but are distributed according to the equilibrium distribution $\mu_\pi(\mathbf{x})$ of the unperturbed dynamics. Finally, the transition probability between set B_i and set B_j for the perturbed dynamics is obtained as

$$\widetilde{T}_{ij}(\tau) = \frac{\widetilde{C}_{ij}(\tau)}{\sum_j \widetilde{C}_{ij}(\tau)}\,. \tag{30}$$

The Radon-Nikodym derivative for path ensembles $g(\mathbf{x})$ contains the ratio of the partition functions $Z/\widetilde{Z}$ as a multiplicative factor. Since this factor appears both in the numerator and the denominator of Eq. (30), it gets canceled, and the partition functions do not have to be calculated.

$T_{ij}(\tau)$ [and analogously $\widetilde{T}_{ij}(\tau)$] is an element of the $s \times s$ MSM transition matrix $\mathbf{T}(\tau)$, where s is the number of disjoint sets (microstates). We characterize the MSM by plotting and analyzing the dominant left and right eigenvectors of the transition matrix

$$\begin{aligned}\mathbf{T}(\tau)\mathbf{r}_i &= \lambda_i(\tau)\mathbf{r}_i, \\ \mathbf{l}_i^\top \mathbf{T}(\tau) &= \lambda_i(\tau)\mathbf{l}_i^\top, \end{aligned} \tag{31}$$

where $\mathbf{l}_i^\top$ denotes the transpose of vector $\mathbf{l}_i$. We assess the approximation quality of the MSM by checking whether the implied time scales

$$t_i = -\frac{\tau}{\ln(\lambda_i(\tau))} = \text{const}, \quad \forall\, \tau > 0 \tag{32}$$

are constant.[9,12]

E. Projection

We now consider a perturbation $U(\cdot)$ that does not directly affect the relevant coordinates used to construct the MSM. In such a situation, the perturbation acts mainly on the coordinates directly perturbed and has a minor effect on the other degrees of freedom, in particular on the relevant coordinates that do not capture the full effect of the perturbation. Thus the reweighting may become problematic because the reweighting formula (25) is dominated by large, fluctuating gradients. To address this issue, we propose to project the gradient of the perturbation onto the coordinates used to construct the MSM. Let us assume that the MSM has been built on a combination of d coordinates $\chi_1, \ldots \chi_d$, then Eq. (25) is rewritten as

$$\begin{aligned}\hat{M}_{\tau,\mathbf{x}}(\omega) = \frac{\hat{\mu}_{\widetilde{P}}(\omega)}{\mu_P(\omega)} = \exp\Bigg\{ &\sum_{i=1}^{3N} \Bigg[\sum_{k=0}^{n} \frac{\mathbf{c}_{i,k}}{\sigma_i} \eta_k^i \sqrt{\Delta t} \\ &- \frac{1}{2} \sum_{k=0}^{n} \left(\frac{\mathbf{c}_{i,k}}{\sigma_i} \right)^2 \Delta t \Bigg] \Bigg\} \end{aligned} \tag{33}$$

with

$$\mathbf{c}_{i,k} = \sum_{j=1}^{d} \frac{\langle \nabla_i U(\mathbf{r}_k), \chi_{j,k} \rangle}{\langle \chi_{j,k}, \chi_{j,k} \rangle} \chi_{j,k}. \tag{34}$$

To understand why the projection reduces the variance of the estimator, note that $M = M_{\tau,\mathbf{x}}$ admits the decomposition $M = \hat{M}N$, where $\hat{M} = \hat{M}_{\tau,\mathbf{x}}$ denotes the part of the Radon-Nikodym derivative associated with the projected perturbation and $\hat{N} = \hat{N}_{\tau,\mathbf{x}}$ denotes the part corresponding to its orthogonal complement; for simplicity, we will drop the subscripts in the following. We call the relevant coordinates that enter $\hat{M}$ the *resolved* coordinates and call all other coordinates *unresolved*.

Now let Z be any random variable that is independent of the unresolved variables. Then, for a fixed initial condition, the variance of the reweighted estimator is given by

$$\mathrm{Var}[ZM] = \mathbb{E}_P[Z^2M^2] - (\mathbb{E}_P[ZM])^2, \tag{35}$$

where $\mathbb{E}_P[Z^2M^2] = \mathbb{E}_{\widetilde{P}}[Z^2M]$ and $\mathbb{E}_P[\cdot]$ denotes the expectation with respect to the reference measure P. Since the estimators with reweighting factor M or $\hat{M}$ are both unbiased, it follows that the projection decreases the variance if

$$\mathbb{E}_{\widetilde{P}}[Z^2M] \geq \mathbb{E}_{\widetilde{P}}[Z^2\hat{M}]\,. \tag{36}$$

TABLE I. Overview of the notation.

	State: x	Path: ω
Space	$\Gamma \subset \mathbf{R}^{6N}$	$\Omega_{\tau,\mathbf{x}} = \Gamma^n \subset \mathbf{R}^{6N\cdot n}$
Subsets	$A_i \subset \Gamma$	$\mathcal{A} = \left(\prod_{i=1}^n A_i\right) \subset \Omega_{\tau,\mathbf{x}}$
Probability density	$\mu_\pi(\mathbf{x})\,\vert_{t\to\infty}$	$\mu_P(\omega)$
Probability of a state/path	$\pi(A) = \int_A \mu_\pi(\mathbf{x})\mathrm{d}\mathbf{x}$	$P(\mathcal{A}) = \int_{\mathcal{A}} \mu_P(\omega)\mathrm{d}\omega$
Expected value	$\mathbb{E}_\pi[f(\mathbf{x})] = \int_A f(\mathbf{x})\mu_\pi(\mathbf{x})\mathrm{d}\mathbf{x}$	$\mathbb{E}_P[f(\omega)] = \int_{\mathcal{A}} f(\omega)\mu_P(\omega)\mathrm{d}\omega$
Absolute continuity	$\widetilde{\pi}(A) = 0 \Rightarrow \pi(A) = 0$	$\widetilde{P}(\mathcal{A}) = 0 \Rightarrow P(\mathcal{A}) = 0$
Radon-Nikodym derivative	$\frac{\mathrm{d}\widetilde{\pi}}{\mathrm{d}\pi}$, see Eq. (21)	$\frac{\mathrm{d}\widetilde{P}}{\mathrm{d}P}$, see Eq. (25)

In addition to Z being independent of the unresolved variables, we further assume that $\hat{M}$ and N are independent under $\tilde{P}$, an assumption that is at least approximately satisfied in our case as is justified by the numerical experiments. As a consequence,

$$\mathbb{E}_{\tilde{P}}[Z^2 M] = \mathbb{E}_{\tilde{P}}[Z^2\hat{M}]\mathbb{E}_{\tilde{P}}[N]\,, \tag{37}$$

and it follows by Jensen's inequality and $N \geq 0$ that

$$1 = \mathbb{E}_{\tilde{P}}[1/N] \geq 1/\mathbb{E}_{\tilde{P}}[N]\,, \tag{38}$$

which implies that $\mathbb{E}_{\tilde{P}}[N] \geq 1$. Note that $1 = \mathbb{E}_{\tilde{P}}[1/N]$ follows from the fact that $1/N$ is a probability density with respect to $\tilde{P}$. Further note that by the strict convexity of the function $f(x) = 1/x$ for $x \geq 0$, the inequality is strict unless N is $\tilde{P}$-a.s. constant. Hence, assuming that N is not constant, we conclude that (36) holds even strictly, which implies that elimination of the unresolved variables strictly decreases the variance of the estimator.

In Table I we summarize the main notation used in the theory section (Sec. II).

III. METHODS

A. Two-dimensional system

The Brownian dynamics on a two-dimensional potential energy function $V(x, y)$,

$$\begin{cases} \mathrm{d}x_t = -\nabla_x V\,(x_t, y_t) + \sigma \mathrm{d}B_t^x, \\ \mathrm{d}y_t = -\nabla_y V\,(x_t, y_t) + \sigma \mathrm{d}B_t^y, \end{cases} \tag{39}$$

has been solved using the Euler-Maruyama scheme[30] with an integration time step of $\Delta t = 0.001$. The term B_t^i denotes a standard Brownian motion in the direction $i = x, y$, $\sigma = 1$ is the volatility, and the random variables η^i were drawn from a standard Gaussian distribution. The reference potential energy function was

$$V(x, y) = (x^2 - 1)^2 + (y^2 - 1)^2 + |x - y|\,, \tag{40}$$

and the perturbed potential energy function was $\widetilde{V}(x, y,) = V(x, y) + U(y)$ with

$$U(y) = -y. \tag{41}$$

For both potential energy functions, trajectories of 8×10^7 time steps were produced. In both simulations, the path probability ratio $M_{\tau,\mathbf{x}}$ was calculated using Eq. (25). The MSMs have been constructed by discretizing each dimension x and y into 40 bins, yielding 1600 microstates. The chosen lag time was $\tau = 400$ time steps.

B. Many-body system in three-dimensional space

We designed a six-particle system, in which five particles form a chain while the sixth particle branches the chain at the central atom [Fig. 6(a)]. The position of the ith particle is $\mathbf{r}_i \in \mathbb{R}^3$. The potential energy between two directly bonded atoms [blue lines in Fig. 6(a)] was

$$V\left(\mathbf{r}_{ij}\right) = \left(\mathbf{r}_{ij}^2 - 1\right)^2 + 0.6\mathbf{r}_{ij} \tag{42}$$

with $\mathbf{r}_{ij} = \mathbf{r}_j - \mathbf{r}_i$. The bond potential energy function is a tilted double well potential. This ensures that the potential energy function of the complete system has multiple minima with varying depths. No non-bonded interactions were applied. Thus, the reference potential energy function of the complete system was

$$V\,(\mathbf{r}) = \sum_{ij=12,13,14,24,36} V\left(\mathbf{r}_{ij}\right). \tag{43}$$

The Langevin dynamics [Eq. (1)] of this system have been solved using the Brünger-Brooks-Karplus (BBK) integrator[31] with an integration time step of $\Delta t = 0.001$. The masses M of the particles, the temperature T, the friction coefficient γ, and the Boltzmann constant k_B were all set to one. The perturbed potential energy function was $\widetilde{V}(\mathbf{r}) = V(\mathbf{r}) + U(\mathbf{r})$ with

$$U\,(\mathbf{r}) = \frac{1}{2}\mathbf{r}_{24}^2 + \frac{1}{2}\mathbf{r}_{34}^2. \tag{44}$$

The perturbation is a harmonic potential energy along the through-space distance between atoms (2, 4) and (3, 4), respectively [green dashed line in Fig. 6(a)]. For both potential energy functions, trajectories of 3.2×10^8 time steps were produced. The MSMs were constructed on the two-dimensional space spanned by the bond-vectors $\mathbf{r}_{12}$ and $\mathbf{r}_{13}$, i.e., on two coordinates which were not directly perturbed. Each dimension, x and y, has been discretized into 40 bins, yielding 1600 microstates. The chosen lag time was $\tau = 400$ time steps. In both simulations, the path probability ratio $M_{\tau,\mathbf{x}}$ was calculated by projecting the gradient vectors $\nabla U\,(\mathbf{r}_{24})$ and $\nabla U\,(\mathbf{r}_{34})$ on the vectors $\mathbf{r}_{12}$ and $\mathbf{r}_{13}$ and subsequently evaluating Eq. (33).

C. Alanine and valine dipeptides

We performed all-atom MD simulations of acetyl-alanine-methylamide (Ac-A-NHMe, alanine dipeptide) in implicit and explicit water and of acetyl-valine-methylamide (Ac-V-NHMe, valine dipeptide) in implicit water. All simulations

were carried out with the OPENMM 7.01 simulation package,[32] in an NVT ensemble at 300 K. Each system was simulated with the force field AMBER ff-14sb.[33] The water model was chosen according to the simulation, i.e., the Generalized Born Surface Area (GBSA) model[34] for implicit solvent simulation and the TIP3P model[39] for explicit solvent simulation. For each of these setups, the aggregated simulation time was 1 μs and we printed out the positions every nstxout = 100 time steps, corresponding to 0.2 ps. A Langevin thermostat has been applied to control the temperature, and a Langevin leapfrog integrator[35] has been used to integrate Eq. (1). For implicit solvent simulations, interactions beyond 1 nm are truncated. For explicit solvent simulations, periodic boundary conditions are used with the Particle-Mesh Ewald (PME) algorithm[36] to estimate Coulomb interactions.

In the alanine dipeptide simulations, we have perturbed the potential energy function of the backbone dihedral angles ϕ and ψ. The reference potential energy functions were

$$V(\phi) = 0.27\cos(2\phi) + 0.42\cos(3\phi), \tag{45}$$

$$V(\psi) = 0.45\cos(\psi - \pi) + 1.58\cos(2\psi - \pi) + 0.44\cos(3\psi - \pi), \tag{46}$$

where the parameters have been extracted from force field files and π denotes the mathematical constant. The perturbed potential energy function was a harmonic potential along each dihedral angle degree of freedom,

$$U(\phi, \psi) = \frac{1}{2}\kappa_\phi \phi^2 + \frac{1}{2}\kappa_\psi \psi^2, \tag{47}$$

where κ_ϕ and κ_ψ are the force constants, which could be adjusted after the simulation [Figs. 7(a) and 7(b)]. The gradient $\nabla_{\mathbf{r}_i} U(\cdot)$ in Eq. (25) is defined with respect to the Cartesian coordinates. Thus, applying the chain rule, the path probability ratio for the perturbation of the backbone dihedral angles is given as

$$M_\tau = \exp\left\{\sum_i^N \left[\kappa_\phi \int_0^\tau \frac{\phi(s)}{\sigma_i}\frac{\partial\phi(s)}{\partial \mathbf{r}_i} \mathrm{d}B_s^i + \kappa_\psi \int_0^\tau \frac{\psi(s)}{\sigma_i}\frac{\partial\psi(s)}{\partial \mathbf{r}_i} \mathrm{d}B_s^i - \frac{1}{2}\kappa_\phi^2 \int_0^\tau \left(\frac{\phi(s)}{\sigma_i}\frac{\partial\phi(s)}{\partial \mathbf{r}_i}\right)^2 \mathrm{d}s \right.\right.$$
$$\left.\left. - \frac{1}{2}\kappa_\psi^2 \int_0^\tau \left(\frac{\psi(s)}{\sigma_i}\frac{\partial\psi(s)}{\partial \mathbf{r}_i}\right)^2 \mathrm{d}s + \kappa_\phi\kappa_\psi \int_0^\tau \frac{\phi(s)\psi(s)}{\sigma_i^2}\frac{\partial\phi(s)}{\partial \mathbf{r}_i}\frac{\partial\psi(s)}{\partial \mathbf{r}_i}\mathrm{d}s\right]\right\}. \tag{48}$$

In the valine dipeptide simulation, we have perturbed the χ_1 side-chain dihedral angle. The reference potential energy function was

$$V(\chi) = 0.337\cos(\chi) + 0.216\cos(2\chi - \pi) + 0.001\cos(4\chi - \pi) + 0.148\cos(3\chi), \tag{49}$$

where the parameters have been extracted from force field files and π denotes the mathematical constant. The perturbed potential energy function was a harmonic potential,

$$U(\chi) = \frac{1}{2}\kappa_\chi \chi^2, \tag{50}$$

where κ_χ is the force constant, which could be adjusted after the simulation [Fig. 9(a)]. Thus, the path probability ratio is given as

$$M_\tau = \exp\left\{\sum_i^N \left[\kappa_\chi \int_0^\tau \frac{\chi(s)}{\sigma_i}\frac{\partial\chi(s)}{\partial \mathbf{r}_i} \mathrm{d}B_s^i - \frac{1}{2}\kappa_\chi^2 \int_0^\tau \left(\frac{\chi(s)}{\sigma_i}\frac{\partial\chi(s)}{\partial \mathbf{r}_i}\right)^2 \mathrm{d}s\right]\right\}. \tag{51}$$

The MSM, for both alanine dipeptide and valine dipeptide simulations, has been constructed by discretizing the dihedral angles ϕ and ψ into 36 bins each, yielding 1296 microstates. The chosen lag time was 20 ps for both the implicit and explicit solvent simulations.

To study the distribution of the force of the solvent on the solute, we have also performed one all-atom MD simulation of acetyl-alanine-methylamide in explicit water at 300 K, with the GROMACS 5.0.2 simulation package,[37] the force field AMBER ff-99SB-ildn,[38] the TIP3P water model,[39] and the velocity-rescaling scheme.[40] The simulation time was 250 ns. We have printed out the trajectory and the total forces every 1 ps, and afterwards we have rerun the simulation, loading the saved trajectory but excluding the solvent. To obtain the value of the force of the solvent on the solute, we have subtracted the new forces to those initially saved.

IV. RESULTS AND DISCUSSION

A. Efficient implementation

To estimate a MSM at a perturbed potential energy function $V(\mathbf{x}) + U(\mathbf{x}, \kappa)$ with the dynamical reweighting method, one simulates a long trajectory $\mathbf{x}(t)$ at a reference potential energy function $V(\mathbf{x})$ using an integration time step Δt. From this trajectory m, short paths of length $\tau = n\Delta t$ are extracted, yielding a set of paths $S_{\tau,m} = \{\nu_1, \nu_2, \ldots \nu_m\}$, which can subsequently be used to evaluate Eq. (29), where $g([\mathbf{x}_0]_k)$ is given by Eq. (21) and $M_{\mathbf{x},\tau}(\nu_k)$ is given by Eq. (25) or Eq. (33). As discussed in Sec. II C, the factor $Z/\tilde{Z}$ cancels for the estimate of $\widetilde{T}_{ij}(\tau)$ [Eq. (30)] and the partition functions do not need to be calculated.

Let us assume that the simulation integrates the Langevin equations of motion for the reference potential energy function $V(\mathbf{x})$ [Eq. (1)]. To estimate a MSM with transition probabilities $\widetilde{T}_{ij}(\tau)$ for the dynamics in the perturbed potential energy function from a set of paths $S_{\tau,m} = \{\nu_1, \nu_2, \ldots \nu_m\}$, we need to know the value of the perturbation $U([\mathbf{x}_t]_k, \kappa)$,

the gradient of the perturbation $\nabla U([\mathbf{x}_t]_k, \kappa)$ and the random numbers η_k generated at every time step of the simulation of each path ν_k, and the volatility σ. The volatility is determined by the temperature and the friction coefficient [Eq. (2)], both of which are input parameters for the simulation algorithm.

In a naive implementation of the reweighting method, one would hence write out the positions and random numbers at every time step and calculate $g([\mathbf{x}_0]_k)$ and $M_{\mathbf{x},\tau}(\nu_k)$ in a post-analysis step. The advantage of this approach is that the set of paths can be reweighted to the path probability measure of any perturbation $U(\mathbf{x}, \kappa)$, as long as the absolute continuity is respected [Eq. (20)]. On the other hand, this approach is hardly practical because writing out a trajectory at every integration time step quickly fills up any hard disc and slows down the simulation considerably.

We therefore decided to compute the probability ratios $g([\mathbf{x}_0]_k)$ and $M_{\mathbf{x},\tau}(\nu_k)$ "on the fly" during the simulation. In practice, the lag time τ of a MSM can only assume values' integer multiples of the frequency nstxout at which the positions are written to file, i.e., of $\tau = n\Delta t = A \cdot \text{nstxout} \cdot \Delta t$ with $A \in \mathbb{N}$. The discretized Itô integral and the discretized Riemann integral in Eq. (25) are sums from time step $k = 0$ to $k = n$, which can be broken down into A sums of size nstxout,

$$\sum_{k=0}^{n} \cdots = \sum_{k=0}^{\text{nstxout}-1} \cdots + \sum_{k=\text{nstxout}}^{2\cdot\text{nstxout}-1} \cdots + \sum_{k=(A-1)\cdot\text{nstxout}}^{A\cdot\text{nstxout}-1} \cdots . \quad (52)$$

Thus, we calculate the terms

$$I(a) = \sum_{i=1}^{3N} \sum_{k=(a-1)\cdot\text{nstxout}}^{a\cdot\text{nstxout}-1} \frac{\nabla_i U(\mathbf{r}_k)}{\sigma} \eta_k^i \sqrt{\Delta t} \quad (53)$$

and

$$R(a) = -\sum_{i=1}^{3N} \frac{1}{2} \sum_{k=(a-1)\cdot\text{nstxout}}^{a\cdot\text{nstxout}-1} \left(\frac{\nabla_i U(\mathbf{r}_k)}{\sigma} \right)^2 \Delta t \quad (54)$$

"on the fly" and write out the results at the same frequency nstxout as the positions. The path probability ratio is reconstructed after the simulation as

$$M_{\tau,\mathbf{x}}(\omega) = \exp\left\{ \sum_{a=1}^{A} I(a) + R(a) \right\} . \quad (55)$$

The potential energy of the perturbation $U(\mathbf{x}_t)$ is written out at the frequency nstxout, and the complete weight $g([\mathbf{x}_0]_k) \cdot M_{\mathbf{x},\tau}(\nu_k)$ is calculated during the construction of the MSM. The lag time τ can be chosen and varied after the simulation. The modification of the MD integrator can be readily implemented within the MD software package OpenMM.[32] An example script is provided in the supplementary material.

The approach requires that the perturbation potential energy function $U(\mathbf{r}, \kappa)$ is chosen prior to the simulation. Note however that if the perturbation potential energy function depends linearly on the parameter κ, i.e., if κ is a force constant $U(\mathbf{r}, \kappa) = \kappa \cdot U(\mathbf{r})$, then the two integrals are written as $I(a, U(\mathbf{r}, \kappa)) = \kappa \cdot I(a, U(\mathbf{r}))$ and $R(a, U(\mathbf{r}, \kappa)) = \kappa \cdot R(a, U(\mathbf{r}))$. Thus, it is sufficient to calculate $I(a, U(\mathbf{r}))$ and $R(a, U(\mathbf{r}))$ "on the fly" and to scale the integrals after the simulation to any desired value of κ. A single simulation is sufficient to allow for reweighting a whole series of perturbation potential energy functions. Also, the integrator can be modified such that the Itô integrals $I_1(a), I_2(2) \ldots$ and the Riemann integral $R_1(a), R_2(2) \ldots$ of several functionally different perturbation energy functions $U_1(\mathbf{r}), U_2(\mathbf{r}) \ldots$ are calculated. Thus, using a single reference simulation, one can reweight to several functionally different perturbations and scale these perturbations by an arbitrary force constant.

If the perturbation $U(\mathbf{r})$ affects only a small subset of all interactions in the system, the computational cost of calculating of $I_i(a)$ and $R_i(a)$ is modest. The blue line in Fig. 3 shows the computational costs for simulating alanine dipeptide in implicit water with $n = 0, 1, 2, 3, 4, 5$ different perturbations as the number of days required to obtain a trajectory of 1 μs for each perturbation on a small workstation. The red line in Fig. 3 shows the computational cost of implementing the same n perturbations into a single reference simulation. For a single perturbation, 30% of the computational cost is saved by dynamical reweighting, whereas for 5 perturbations more than half of the computational cost is saved. Note that the curve has been obtained by measuring the computational cost and not by extrapolating from the cost of a single perturbation. The gain is even greater, if the dependence on a force constant is to be studied. Moreover, in simulation boxes of larger systems with explicit solvent, the number of interactions affected by a typical perturbation is orders of magnitudes smaller than the total number of all interactions. Thus, the computational cost of calculating the integrals $I_i(a)$ and $R_i(a)$ "on the fly" becomes negligible. We remark that, if $I_i(a)$ and $R_i(a)$ are too large, the Girsanov reweighting method might become numerically intractable. This might be the case if the perturbation is too strong and hence $\nabla_i U(\mathbf{r})$ is large or if $\tau = n\Delta t$ is too large. Thus, a good discretization, which allows for the use of small lag times τ, is crucial in applying the Girsanov reweighting method to MSMs of larger molecules.

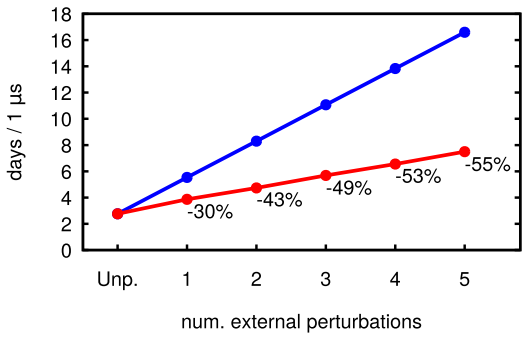

FIG. 3. Number of days needed to product a trajectory of alanine dipeptide in implicit solvent of 1 μs. The system has been perturbed by adding a harmonic potential to different dihedral angles. The blue line denotes the time needed to perform, respectively, 1,...,5 simulations with different potential energy functions (i.e., different perturbations). The red line is the time necessary to perform one single simulation and to compute the Girsanov formula on fly for 1,...,5 different perturbations at the same time. The benchmark test has been realized on a CPU Intel(R) Core(TM) i5-4590 CPU @ 3.30 GHz with 15 GB of RAM.

B. Stochastic forces

The dynamical reweighting method has been derived by using the Langevin equation of motion as the starting point. It relies on the assumption that the random forces are generated by a Wiener process (Appendix B), and it can hence be used directly for MD simulations thermostatted by a Brownian or a Langevin thermostat.

However from a physical perspective, the Langevin dynamics only approximates the Hamiltonian dynamics of the complete system, by splitting the system in a subsystem S and a heat bath B and replacing the interaction of the subsystem with the heat bath by a friction term and a stochastic process. To develop a dynamical reweighting method for a Hamiltonian dynamics simulation, one could split the system into two subsystems S and B, measure the forces which subsystem B exerts on subsystem S, and use these forces as a substitute for the random forces in the path probability ratio. We have tested this on alanine dipeptide by performing a simulation in explicit solvent. We measured the force distribution of the bath degrees of freedom on the heavy atoms of alanine dipeptide and found that they considerably differ from a Gaussian distribution (Fig. 4). Moreover, we would expect that the random forces do not fulfill the usual goodness-criteria of a random number generator. Thus, overall we are skeptical that estimating a substitute for the random forces from a Hamiltonian dynamics simulation, including simulations thermostatted by the Nosé-Hoover or the Berendsen thermostat, will be successful.

Other thermostats, such as the velocity-rescaling or the Andersen thermostat, use random numbers which are however not converted into a Wiener process. For the time-discrete trajectories generated by MD simulations with these thermostats, it is possible to derive reweighting schemes based on the probability of the sequence of random numbers. However, as explained in Appendixes A and B, the path probability ratio would diverge in the limit of continuous paths.

We therefore decided to use the Langevin leapfrog integrator[35] to integrate the Langevin equation of motion for both the implicit and explicit solvent simulations and used the random forces generated by the integrator to reweight the path ensemble.

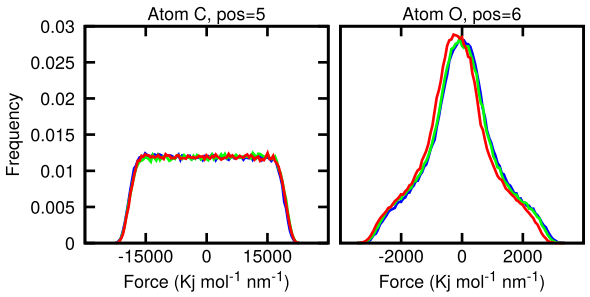

FIG. 4. Distribution of the force of the solvent on the 5th and 6th atoms of the alanine dipeptide. (Blue) Force on the x direction, (green) force on the y direction, and (red) force on the z direction.

C. Two-dimensional system

As a first application, we consider the Brownian dynamics of a particle moving on a two-dimensional potential energy function [Eq. (39)]. The reference potential energy function $V(x, y)$ [Eq. (40), Fig. 5(A)] has two minima at $(-1, -1)$ and $(1, 1)$ which are connected by a transition state at $(0, 0)$. We added a perturbation [Eq. (41)] which tilts the energy function $\widetilde{V}(x, y)$ along the direction y, such that the minimum at $(1, 1)$ becomes much deeper than the minimum at $(-1, -1)$. Figures 5(B) and 5(E) show the dominant left MSM eigenvectors of the two systems (direct MSMs). The first eigenvector corresponds to the equilibrium distribution. In both cases, the second eigenvector represents the transition between the two wells, while the third eigenvector corresponds to an exchange of probability density between the transition state region and the two wells.

Figure 5(C) shows the MSM eigenvectors obtained by reweighting the simulation in $V(x, y)$ to the perturbed potential energy function $V(x, y) + U(y)$ (reweighted MSM). Both eigenvectors [Eq. (31)] and implied time scales [Eq. (32)] are in perfect agreement with Fig. 5(E). This confirms that reweighting MSMs using the Girsanov formula works well for a low-dimensional Brownian dynamics.[29] Note that the simulation in the reference potential energy function $V(x, y)$ exhibits frequent transitions between the two minima, and thus Eq. (24) is certainly fulfilled. By contrast, in the perturbed system $\widetilde{V}(x, y)$, the simulation sampled considerably fewer transitions

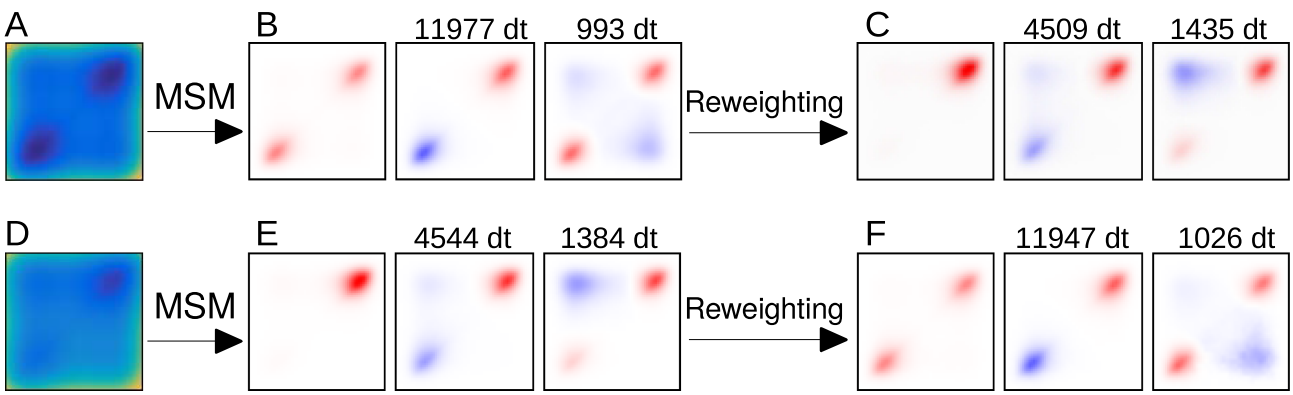

FIG. 5. Two-dimensional system. (A) Reference potential. (B) Dominant left eigenvectors of the reference potential. (C) Dominant left eigenvectors reweighted from the reference dynamics. (D) Perturbed potential. (E) Dominant left eigenvectors of the perturbed potential. (F) Dominant left eigenvectors reweighted from the perturbed dynamics.

between the minima and only a small fraction of the simulation time was spent in the minimum in the lower left corner. Figure 5(F) shows the dominant eigenvectors of a MSM of the reference dynamics constructed by reweighting the perturbed path ensemble. The fact that Fig. 5(C) is in excellent agreement with Fig. 5(B) demonstrates that the reweighting method yields accurate results even for path ensembles with low numbers of transitions across the largest barriers of the system and thus suggests that it can be applied to high-dimensional dynamics on rugged potential energy surfaces.

D. Many-body system in three-dimensional space

As a second example, we studied a six-particle system, in which five particles form a chain while the sixth particle branches the chain at the central atom Fig. 6(a). We constructed the MSM on the central bonds $\mathbf{r}_{12}$ and $\mathbf{r}_{13}$ but applied the perturbation potential energy function along the through-space distances $\mathbf{r}_{24}$ and $\mathbf{r}_{34}$. Thus, the perturbation was projected onto the reaction coordinates $\mathbf{r}_{12}$ and $\mathbf{r}_{13}$ during the reweighting. The reference potential energy function for each bond is a tilted double well potential, such that the reference system exhibits four metastable states [first row of Fig. 6(b)]. The six-particle system and the reference potential energy function are symmetric. Thus the MSM of the reference system has two degenerate dominant eigenvectors with implied time scales of $1.1 \cdot 10^4 \Delta t$.

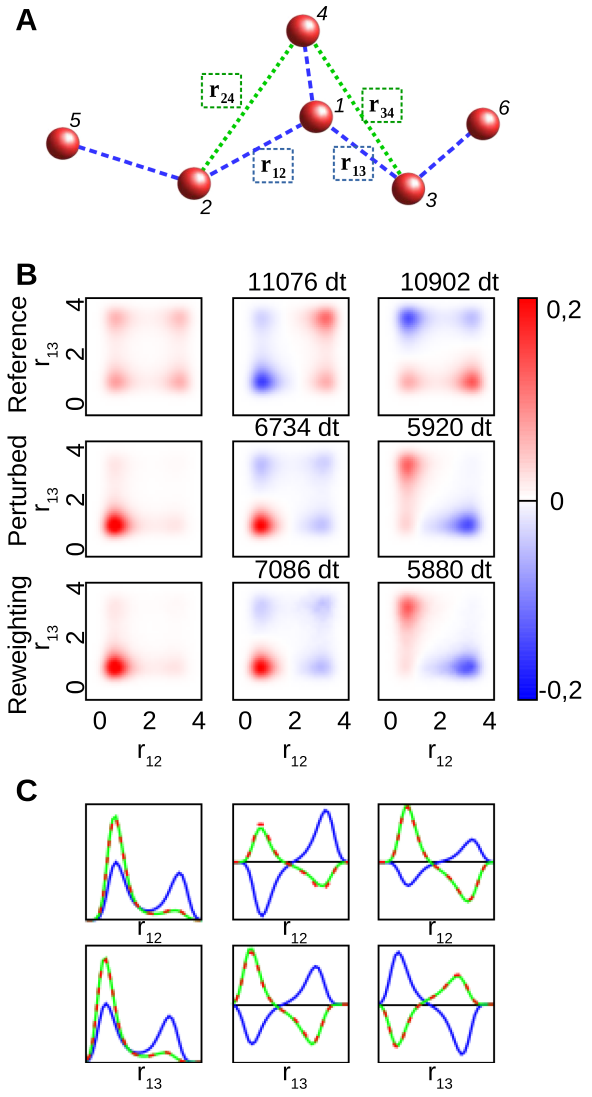

FIG. 6. Many-body system. (a) The perturbation acts on $\mathbf{r}_{24}$ and $\mathbf{r}_{34}$, while the MSM is constructed on the distances $\mathbf{r}_{12}$ and $\mathbf{r}_{13}$. (b) Dominant eigenvectors obtained by direct simulations of the reference and perturbed system and by reweighting the reference simulation. (c) Eigenvectors projected on the coordinates $\mathbf{r}_{12}$ and $\mathbf{r}_{13}$: blue: reference, green: perturbed, and red: reweighted.

The perturbation contracts the bonds, thereby stabilizing the metastable state at the lower left corner in the 1st eigenvector [second row of Fig. 6(b)]. Its effect is to break the symmetry and to accelerate the dynamics, yielding implied time scales of $6.7 \cdot 10^4 \Delta t$ and $5.9 \cdot 10^4 \Delta t$. The third row of Fig. 6(b) shows the eigenvectors and the implied time scales obtained by reweighting the simulation at the reference potential energy function to the perturbed potential energy function. The projection of the eigenvectors [Fig. 6(b)] demonstrates that the direction simulations of the perturbed system and the reweighted model are in almost perfect agreement. The relative error of the implied time scale of the second and third eigenvectors is 5.2% and 0.7%, respectively.

E. Alanine dipeptide and valine dipeptide

Figure 7 shows the results for alanine dipeptide (Ac-A-NHMe) in implicit water. The MSM has been constructed on the ϕ and ψ backbone dihedral angles, and the slow eigenvectors of the unperturbed system are shown in Fig. 7(c). The first eigenvector shows the typical equilibrium distribution in the Ramachandran plane.[41] The second eigenvector represents torsion around the ϕ angle and corresponds to a kinetic exchange between the L_α-minimum ($\phi > 0$) and the α-helix and β-sheet minima ($\phi < 0$). The associated time scale is 2.8 ns. The green arrows in Fig. 7(c) represent the frequency of the transitions, with the transition $L_\alpha \leftrightarrow \beta$-sheet conformation occurring more frequently than the transition $L_\alpha \leftrightarrow \alpha$-helical conformation. The third eigenvector represents a transition β-sheet $\longleftrightarrow$ α-helical conformation, i.e., torsion around ψ, and is associated with a time scale of 27 ps.

We perturbed the dynamics by adding a harmonic potential to the dihedral angle potentials of the ϕ- and ψ-angle [Figs. 7(a) and 7(b), Eq. (47) with $\kappa_\phi = 0.5$ and $\kappa_\psi = 0.5$]. The α-helical region is somewhat stabilized by the perturbation but otherwise the dominant eigenvectors are very similar to the unperturbed system [second row in Fig. 7(c)]. However, the perturbation changes the relative frequency of the two possible transitions (green arrows) in the second eigenvector, resulting in an increased implied time scale of 4.5 ns. The third row of Fig. 7(c) shows the dominant eigenvectors of the perturbed system obtained by reweighting the reference simulations, and Fig. 7(d) shows the projection of the eigenvectors of all three models onto the $\phi-$ and ψ-torsion angle. The reweighted model is in excellent agreement with the direct simulation of the perturbed systems. The relative error of the implied time scale associated with the second eigenvector is 4.1%.

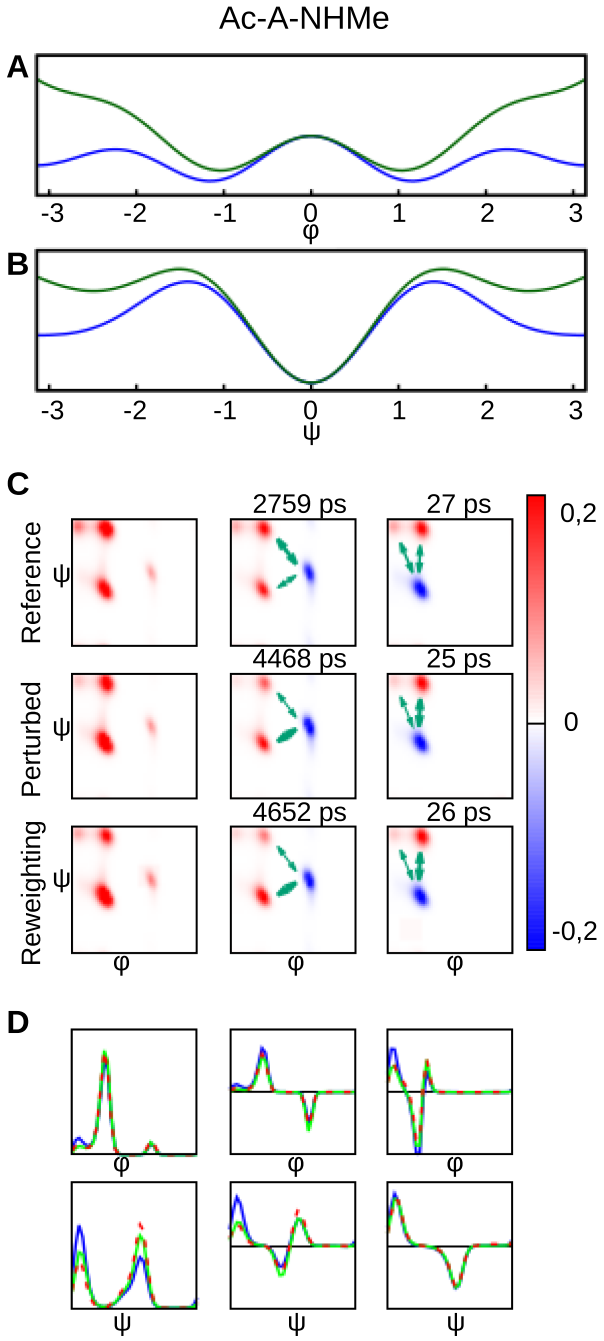

FIG. 7. Alanine dipeptide. (a) Potential energy function along ϕ: blue: reference potential energy function $V(\phi)$ [Eq. (45)], green: perturbed potential energy function $V(\phi) + U(\kappa_\phi = 0.5, \kappa_\psi = 0, \phi, \psi)$ [Eq. (47)]. (b) Potential energy function along ψ: blue: $V(\psi)$ [Eq. (46)], green: $V(\psi) + U(\kappa_\phi = 0, \kappa_\psi = 0.5, \phi, \psi)$ [Eq. (47)]. (c) Dominant MSM eigenvectors of alanine dipeptide. (d) Eigenvectors projected onto the ϕ and ψ backbone torsion angles: blue: reference, green: perturbed, and red: reweighted.

Figure 8(a) shows the implied time scale test [Eq. (32)] for alanine dipeptide in implicit water. All three systems (reference, perturbed, and reweighted) show constant implied time scales, indicating that the MSMs are well converged. Moreover, the graph shows that the reweighting method can recover the implied time scales of the perturbed system over a large range of lag times τ. We have repeated the alanine dipeptide simulations in explicit water. The eigenvectors are very similar to those of alanine dipeptide in implicit water

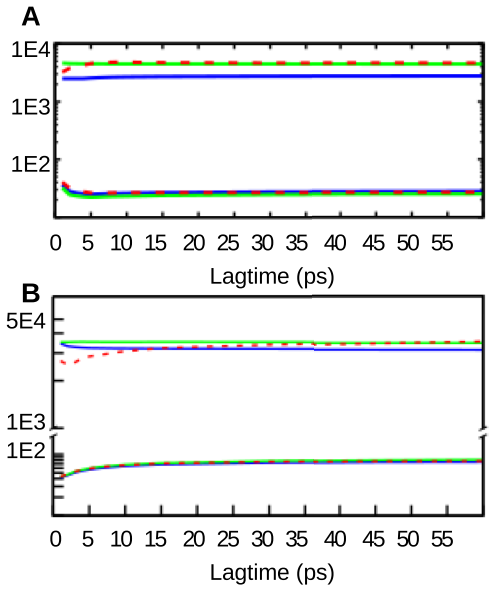

FIG. 8. Alanine dipeptide. (a) Implied time scales in implicit solvent. (b) Implied time scales in explicit solvent. Reference potential (blue line), perturbed potential (green line), and reweighting method (red dashed line).

(data not shown), but the associated implied time scales differ from the implicit solvent simulations [Fig. 8(b)]. In the unperturbed system, the implied time scale of the second eigenvector was 3.1 ns and the implied time scale of the third eigenvector was 75 ps. Perturbing the dihedral angle potentials slightly increased the implied time scale of the second eigenvector to 3.5 ns and left the implied time scale of the third eigenvector unaffected. The implied time scales of the reference simulation and the direct simulation of the perturbed system were constant, whereas we noticed a slight drift in the implied time scale of the second eigenvector for the reweighted MSM. At $\tau = 45$ ps, the measured implied time scale is 3.4 ns which corresponds to a relative error of 2.8%.

We also tested the dynamical reweighting method on valine dipeptide (Fig. 9). Here, however, we perturbed the potential energy function of the χ-side chain dihedral angle [Fig. 9(a)] by adding a harmonic potential, while constructing the MSM on the ϕ and ψ backbone dihedral angles. Thus, the perturbation did not directly act on the variables of the MSM. The perturbation of the χ angle had no effect on the eigenvectors of the MSM [Fig. 9(b)], but it did change the implied time scales. It caused a decrease of the implied time scale of the second eigenvector from 1.3 ns in the reference simulation to 1.0 ns in the perturbed simulation and a slight increase of the implied time scale of the third eigenvector from 159 ps in the reference simulation to 170 ps in the perturbed simulation. Reweighting the reference simulation to the perturbed potential energy function recovered the results of the direct simulation of the perturbed system. The implied time scales obtained by the reweighting calculation were 1.0 ns (relative error: 4.9% before rounding to ns) for the second eigenvector and 179 ps (relative error: 5.3%) for the third eigenvector. This shows that the dynamical reweighting method also works, when the perturbation acts on degrees of freedom which are not part of the relevant coordinates on which the MSM is constructed.

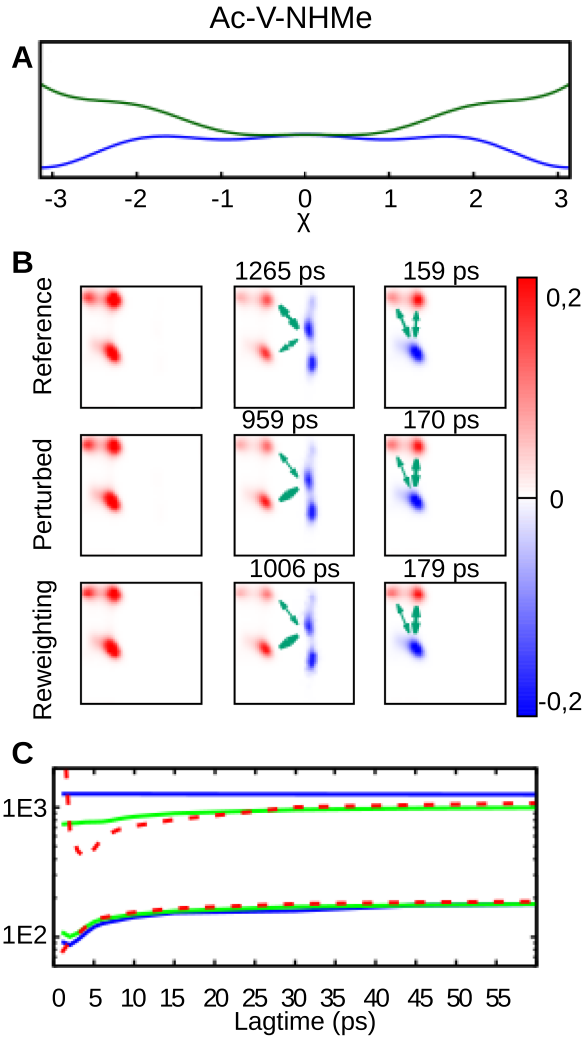

FIG. 9. Valine dipeptide. (a) Reference potential energy function of the side-chain dihedral angle χ, $V(\chi)$ (blue line), and perturbed potential energy function, $V(\chi) + U(\kappa_\chi = 0.5, \chi)$ (green line). (b) First three MSM eigenvectors of the valine dipeptide, where the MSM is constructed in the space spanned by the ϕ- and ψ-backbone dihedral angle. (c) Associated implied time scales as a function of the lag time τ. Reference potential (blue line), perturbed potential (green line), and reweighting method (red dashed line).

Figure 10 illustrates how to use the dynamical reweighting method to study the influence of a force constant on the molecular dynamics. It shows the implied time scale of the second and third MSM eigenvectors of alanine dipeptide in explicit water as a function of the force constant κ_ϕ, where the perturbation potential energy is given by Eqs. (45) and (47). The scan has been repeated with different values of the force constant κ_ψ for the potential energy function of the ψ-backbone dihedral angle [Eqs. (46) and (47)]. The dynamics is more sensitive to a change in the value of κ_ϕ than to a change of κ_ψ, but the overall effect of the perturbation is moderate. It is important to point out that MSMs which are summarized in Fig. 10 have been constructed from a single simulation at the reference potential energy function. During this simulation, the Itô integral $I(a)$ and the Riemann integral $R(a)$ have been calculated for $\kappa_\phi = 1$ and $\kappa_\psi = 1$, and the force constants have been scaled after the simulation during the construction of the MSM, as described in Sec. IV A.

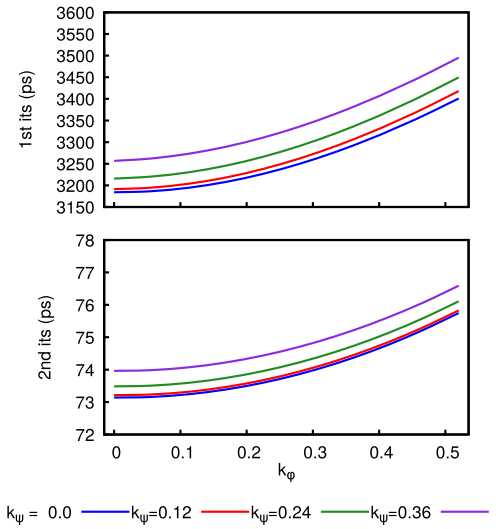

FIG. 10. First and second implied time scales of alanine dipeptide in explicit solvent as a function of the parameters k_ϕ, k_ψ, estimated with the Girsanov reweighting methods.

V. CONCLUSION

We have presented the Girsanov reweighting scheme, which is a method to study the dynamics of a molecular system subject to an (external) perturbation $U(\kappa, \mathbf{x})$ of the (reference) potential energy function $V(\mathbf{x})$. It allows for the estimation of a dynamical model, e.g., a MSM, of the perturbed system from a simulation at the reference potential energy function. The underlying assumption is that the equation of motion generates a path ensemble and that we can define a probability measure on this ensemble. A perturbation of the potential energy function causes modification of the probability measure. The Girsanov theorem guarantees that the probability ratio between these two measures exists (under certain conditions) and leads to an analytical expression for this ratio [Eq. (25)]. By reformulating the MSM transition probabilities as path ensemble averages, we can apply the Girsanov reweighting scheme to obtain the transition probabilities of the perturbed system from a set of paths generated at the reference potential energy function. The method can be extended to the variational approaches,[42,43] milestoning approaches,[44,45] or tensor approaches[46] to molecular dynamics, since in each of these methods the molecular transfer operator is discretized and the resulting matrix elements are estimated as path ensemble averages.

Calculating the path probability ratio requires knowledge of the random forces at each integration time step. For the explicit solvent simulations, we have introduced stochastic forces by using a Langevin thermostat. In an efficient implementation of the method, two terms which are needed to calculate the probability ratio should be calculated "on the fly" during the simulation. We have demonstrated this using the MD simulation toolkit OPENMM.[32]

Two other dynamical reweighting schemes for MSMs have been published in recent years. In the reweighting scheme for parallel tempering simulations,[47,48] the path probability density is defined for time discretized paths at a reference temperature and then reweighted to different temperatures

using statistically optimal estimators.[49,50] Like the Girsanov reweighting scheme, this method relies on the random forces at each integration time step and reweights the contribution of each path to the estimate of the transition probability individually. We remark that the reweighting to different thermodynamic states cannot be extended to the limiting case of continuous paths because for different volatilities the path probability ratio relative to the Wiener process cannot be defined (see Appendix A). This however seems to be of little practical importance. In the Transition-Based Reweighting Analysis Method (TRAM),[51–53] rather than reweighting the probabilities of each individual path, the MSM transition probabilities $T_{ij}(\tau)$ are directly reweighted to a different potential energy function or a different thermodynamic state using a maximum likelihood estimator for the transition counts. This becomes possible, if one additionally assumes that the dynamics is in local equilibrium within each microstate of the MSM, which possibly renders the method more sensitive to the MSM discretization than path-based reweighting methods.

We have tested the Girsanov reweighting method on several systems, ranging from diffusion in a two-dimensional potential energy surface to alanine dipeptide and valine dipeptide in implicit and explicit water. Importantly, the direct simulations of the perturbed potential energy function (Figs. 6, 7, and 9) are only included as a validation for the method. In an actual application, one would only simulate the system at the reference potential energy function and then reweight to the perturbed potential energy function, thus saving the computational time of the direct simulation of the perturbed system.

Girsanov reweighting could be useful in several areas of research. First, one can very efficiently test the influence of a change in the potential energy function on the dynamics of the molecule. The influence of a change in the force constant on the dynamics is particularly easy to study. The Girsanov reweighting method can therefore be applied to improve the dynamical properties of force fields,[41] by, for example, tuning the force constants to match an experimentally measured correlation time. Similarly, one can use Girsanov reweighting to understand the influence of restraining potentials[54,55] on the dynamics of the system. Second, the method can be used to understand which degrees of freedom have the largest influence on the slow modes of the molecule.[56,57] For example, for alanine dipeptide, we showed that the slow dynamic modes are more sensitive to a force field variation in the ϕ-backbone dihedral angle than they are to a variation in the ψ-backbone dihedral angle. Last but not least, Girsanov reweighting can be used to account for the effect of any external potential which has been added to the simulation in order to enhance the sampling. Thus, one can, for example, estimate MSMs from metadynamics simulations,[58,59] Hamilton replica exchange simulations,[60] or umbrella sampling simulations.[61]

SUPPLEMENTARY MATERIAL

See supplementary material for the example script for the implementation of the dynamical reweighting method with OpenMM.[32]

ACKNOWLEDGMENTS

This research has been funded by Deutsche Forschungsgemeinschaft (DFG) through Grant No. CRC 1114 "Scaling Cascades in Complex Systems," Project A05 "Probing scales in equilibrated systems by optimal nonequilibrium forcing," and Project B05 "Origin of the scaling cascades in protein dynamics."

APPENDIX A: TIME-DISCRETE AND CONTINUOUS PATH SPACE MEASURES

Path probability densities of time-discrete paths are derivatives with respect to the Lebesgue measure $\mathrm{d}\omega = \mathrm{d}x_1\mathrm{d}x_2\ldots\mathrm{d}x_n$, i.e., $\mu_P(\omega) = \mathrm{d}P/\mathrm{d}\omega$. Here, we discuss why it is difficult to extend the concept of path probability densities to time-continuous paths. Consider a diffusion process $x_t \in \Gamma \subset \mathbb{R}$ which is a solution of the stochastic differential equation

$$\mathrm{d}x_t = a(x_t)\mathrm{d}t + \sigma\mathrm{d}B_t, \quad 0 \le t \le \tau\,, \tag{A1}$$

where $a(\cdot)$ is a drift, B_t is a Brownian motion, σ is a volatility, and τ is the total time. Discretizing Eq. (A1) using the Euler-Maruyama method yields[62]

$$x_{k+1} = x_k + a_k\Delta t + \eta_k\sigma\sqrt{\Delta t}, \quad 0 \le k \le n\,, \tag{A2}$$

where $a_k = a(x_t)$, Δt is a time step, and η_k is a random number drawn from a standard Gaussian distribution. Iterating Eq. (A2) n times generates a *time-discrete path* as defined in Sec. II B. Likewise, the path space is $\Omega_{\tau,x} = \Gamma^n$. The path probability measure P and the associated path probability density $\mu_P(\omega)$ are given by Eqs. (6) and (7), respectively.

For a Brownian motion with drift, there is an analytical expression for the transition probability density $p(x_k, x_{k+1}; \Delta t)$ of time-discrete paths,

$$p(x_k, x_{k+1}; \Delta t) = \frac{1}{\sqrt{2\pi\Delta t\sigma^2}} \exp\left(-\frac{(x_{k+1} - x_k - a_k\Delta t)^2}{2\Delta t\sigma^2}\right). \tag{A3}$$

The probability density of a path $(x_0, x_1, \ldots, x_n)$ conditional on starting at x_0 is then simply given by the product of the corresponding transition probabilities,

$$\mu_P(x_1, \ldots, x_n; x_0) = \left(\frac{1}{\sqrt{2\pi\Delta t\sigma^2}}\right)^n \times \exp\left(-\frac{\Delta t}{2\sigma^2}\sum_{k=1}^{n}\left(\frac{x_{k+1} - x_k}{\Delta t} - a_k\right)^2\right). \tag{A4}$$

Ideally, one would like to see the continuous path density on the space of, say, continuous curves, to emerge in the limit $\Delta t \to 0$, $n \to \infty$ with $n\Delta t \to \tau$. However, a short moment of reflection convinces us that this cannot be the case: First, the normalization constant, the denominator in (A4), diverges as $\Delta t \to 0$ and $n \to \infty$. Second, the paths of the Brownian motion are nowhere differentiable and, as a consequence, the term $(x_{k+1} - x_k)/\Delta t$ in the path density becomes ill-defined. Third, the reference measure in $\mu_P = \mathrm{d}P/\mathrm{d}\omega$ is the n-dimensional Lebesgue measure $\mathrm{d}\omega$ that has no meaning for $n \to \infty$.

APPENDIX B: DERIVATION OF THE GIRSANOV FORMULA

We now show how the problems described in Appendix A can be solved by considering path densities with respect to reference measure other than the Lebesgue measure, which then gives rise to the Girsanov formula. We note that our short derivation stays purely formal and is given for the reader's convenience. The interested reader may consult standard textbooks on Stochastic Differential Equations (SDEs).[28,63] Analogously to Eqs. (A1) and (A2), we define a second diffusion process with initial conditions $x_0 = x \in \mathbb{R}$ by

$$\mathrm{d}x_t = b(x_t)\,\mathrm{d}t + \sigma \mathrm{d}B_t \tag{B1}$$

and

$$x_{k+1} = x_k + b_k \Delta t + \eta_k \sigma \sqrt{\Delta t}\,. \tag{B2}$$

Given a particular path ω starting at x_0, the likelihood ratio of the corresponding transition probability densities is given by

$$M_{\tau,x}(\omega) = \frac{\mu_{P_b}(\omega)}{\mu_{P_a}(\omega)} = \frac{\prod_{k=1}^{n} \exp\left(-\frac{(x_{k+1}-x_k-b_k\Delta t)^2}{2\Delta t\sigma^2}\right)}{\prod_{k=1}^{n} \exp\left(-\frac{(x_{k+1}-x_k-a_k\Delta t)^2}{2\Delta t\sigma^2}\right)}\,. \tag{B3}$$

In Eq. (B3), the normalization constants get canceled which solves the first problem mentioned in Appendix A. Rearranging the fraction, moving the product into the exponent, and expanding the quadratic terms yield

$$\begin{aligned} M_{\tau,x}(\omega) &= \exp\left(\sum_{k=0}^{n} \frac{-(x_{k+1}-x_k-b_k\Delta t)^2 + (x_{k+1}-x_k-a_k\Delta t)^2}{2\Delta t\sigma^2}\right) \\ &= \exp\left(\sum_{k=0}^{n} -\frac{\left(b_k^2-a_k^2\right)\Delta t^2 - 2x_{k+1}\left(b_k-a_k\right)\Delta t + 2x_k\left(b_k-a_k\right)\Delta t}{2\Delta t\sigma^2}\right) \\ &= \exp\left(\sum_{k=0}^{n} \frac{(x_{k+1}-x_k)\left(b_k-a_k\right)}{\sigma^2}\right) \exp\left(-\sum_{k=0}^{n} \frac{\left(b_k^2-a_k^2\right)\Delta t}{2\sigma^2}\right). \end{aligned} \tag{B4}$$

In the second line, terms which do not contain either $a_k\Delta t$ or $b_k\Delta t$ cancel. Hence, Δt cancels in the overall expression and hence the time derivative of x_t does not appear. This solves the second problem from Appendix A.

The remaining terms have straightforward interpretations: Taking the limit $\Delta t \to 0$ and $n \to \infty$ such that $n\Delta t \to \tau$, the exponent in the second term of (B4) converges to a Riemann integral,

$$\lim_{\Delta t\to 0} \sum_{k=0}^{n} \frac{\left(b_k^2-a_k^2\right)\Delta t}{2\sigma^2} = \frac{1}{2}\int_0^\tau \frac{b(x_s)^2 - a(x_s)^2}{\sigma^2}\mathrm{d}s\,. \tag{B5}$$

The first term converges to an Itô integral, at least formally. More specifically, using (A1),

$$\lim_{\Delta t\to 0} \sum_{k=0}^{n} (b_k-a_k)(x_{k+1}-x_k) = \int_0^\tau (b(x_s)-a(x_s))\mathrm{d}x_s = \int_0^\tau (b(x_s)-a(x_s))\left(a(x_s)\mathrm{d}s + \sigma \mathrm{d}B_s\right). \tag{B6}$$

Inserting (B5) and (B6) into Eq. (B4) yields the Girsanov formula

$$\begin{aligned} \lim_{\Delta t\to 0} M_{\tau,x}(\omega) &= \exp\left(\int_0^\tau \frac{a(x_s)b(x_s)\mathrm{d}s + b(x_s)\sigma\mathrm{d}B_s - a(x_s)^2\mathrm{d}s - a(x_s)\sigma\mathrm{d}B_s}{\sigma^2}\right) \exp\left(-\frac{1}{2}\int_0^\tau \frac{b(x_s)^2-a(x_s)^2}{\sigma^2}\mathrm{d}s\right) \\ &= \exp\left(\int_0^\tau \frac{b(x_s)\sigma\mathrm{d}B_s - a(x_s)\sigma\mathrm{d}B_s}{\sigma^2}\right) \exp\left(\int_0^\tau \frac{a(x_s)b(x_s)-a(x_s)^2}{\sigma^2}\mathrm{d}s - \frac{1}{2}\int_0^\tau \frac{b(x_s)^2-a(x_s)^2}{\sigma^2}\mathrm{d}s\right) \\ &= \exp\left(\int_0^\tau \frac{b(x_s)-a(x_s)}{\sigma}\mathrm{d}B_s\right) \exp\left(-\frac{1}{2}\int_0^\tau \frac{(b(x_s)-a(x_s))^2}{\sigma^2}\mathrm{d}s\right). \end{aligned} \tag{B7}$$

Equation (B7) is an analytical expression for the likelihood ratio of time-continuous paths. In other words, even though the probability densities of the discrete paths have no straightforward extension to the continuous case, their likelihood ratio is always well defined, provided that the two processes are driven by the same Gaussian noise process to yield cancellation of the problematic terms (and further technical integrability conditions).

In this paper, we use the Euler-Maruyama discretization

$$\begin{aligned} M_{\tau,x}(\omega) &= \exp\left(\sum_{k=0}^{n} \frac{(b_k-a_k)\,\eta_k\sqrt{\Delta t}}{\sigma}\right) \\ &\quad\times \exp\left(-\frac{1}{2}\sum_{k=0}^{n} \frac{(b_k-a_k)^2\Delta t}{\sigma^2}\right) \end{aligned} \tag{B8}$$

of the Girsanov formula (B7) which is consistent with the Euler-Maruyama discretization of the corresponding SDEs.

[1]P. G. Bolhuis, D. Chandler, C. Dellago, and P. L. Geissler, Annu. Rev. Phys. Chem. **53**, 291 (2002).
[2]A. K. Faradjian and R. Elber, J. Chem. Phys. **120**, 10880 (2004).
[3]R. B. Best and G. Hummer, Proc. Natl. Acad. Sci. U. S. A. **102**, 6732 (2005).
[4]R. Hegger and G. Stock, J. Chem. Phys. **130**, 034106 (2009).
[5]P. Faccioli, A. Lonardi, and H. Orland, J. Chem. Phys. **133**, 045104 (2010).
[6]C. Schütte, A. Fischer, W. Huisinga, and P. Deuflhard, J. Comput. Phys. **151**, 146 (1999).
[7]C. Schütte, W. Huisinga, and P. Deuflhard, in *Ergodic Theory, Analysis, and Efficient Simulation of Dynamical Systems*, edited by B. Fiedler (Springer, 2001), pp. 191–223.
[8]P. Deuflhard, W. Huisinga, A. Fischer, and C. Schütte, Linear Algebra Appl. **315**, 39 (2000).
[9]W. C. Swope, J. W. Pitera, F. Suits, M. Pitman, M. Eleftheriou, B. G. Fitch, R. S. Germain, A. Rayshubski, T. J. C. Ward, Y. Zhestkov, and R. Zhou, J. Phys. Chem. B **108**, 6582 (2004).
[10]J. D. Chodera, N. Singhal, V. S. Pande, K. A. Dill, and W. C. Swope, J. Chem. Phys. **126**, 155101 (2007).
[11]N.-V. Buchete and G. Hummer, J. Phys. Chem. B **112**, 6057 (2008).
[12]J.-H. Prinz, H. Wu, M. Sarich, B. G. Keller, M. Senne, M. Held, J. D. Chodera, C. Schütte, and F. Noé, J. Chem. Phys. **134**, 174105 (2011).
[13]B. G. Keller, X. Daura, and W. F. Van Gunsteren, J. Chem. Phys. **132**, 074110 (2010).
[14]B. G. Keller, P. Hünenberger, and W. F. van Gunsteren, J. Chem. Theory Comput. **7**, 1032 (2011).
[15]V. A. Voelz, G. R. Bowman, K. A. Beauchamp, and V. S. Pande, J. Am. Chem. Soc. **132**, 1526 (2010).
[16]N. Stanley, S. Esteban-Martin, and G. D. Fabritiis, Nat. Commun. **5**, 5272 (2014).
[17]G. R. Bowman, E. R. Bolin, K. M. Hart, B. C. Maguire, and S. Marqusee, Proc. Natl. Acad. Sci. U. S. A. **112**, 2734 (2015).
[18]N. Plattner and F. Noé, Nat. Commun. **6**, 7653 (2015).
[19]L. Zhang, F. Pardo-Avila, I. C. Unarta, P. P.-H. Cheung, G. Wang, D. Wang, and X. Huang, Acc. Chem. Res. **49**, 687 (2016).
[20]R. Zwanzig, J. Chem. Phys. **22**, 1420 (1954).
[21]C. H. Bennett, J. Comput. Phys. **22**, 245 (1976).
[22]S. Kumar, D. Bouzida, R. H. Swendsen, P. A. Kollman, and J. M. Rosenberger, J. Comput. Chem. **13**, 1011 (1992).
[23]J. Kästner and W. Thiel, J. Chem. Phys. **123**, 144104 (2005).
[24]B. Lapeyre, E. Pardoux, and R. Sentis, *Méthodes de Monte Carlo pour les équations de transport et de diffusion* (Springer, Berlin, 1998).
[25]O. Papaspiliopoulos and G. Roberts, University of Warwick, Centre for Research in Statistical Methodology, Working Papers, No. 28, 2009.
[26]C. Hartmann and C. Schütte, J. Stat. Mech.: Theory Exp. **2012**, P11004.
[27]I. V. Girsanov, Theory Probab. Its Appl. **5**, 285 (1960).
[28]B. Øksendal, *Stochastic Differential Equations: An Introduction with Applications*, 6th ed. (Springer Verlag, Berlin, 2003), pp. 139–167.
[29]C. Schütte, A. Nielsen, and M. Weber, Mol. Phys. **113**, 69 (2015).
[30]E. Platen and N. Bruti-Liberati, *Numerical Solution of Stochastic Differential Equations with Jumps in Finance* (Springer Verlag, Berlin, 2010), p. 246.
[31]A. Brünger, C. L. Brooks III, and M. Karplus, Chem. Phys. Lett. **105**, 495 (1984).
[32]P. Eastman, M. S. Friedrichs, J. D. Chodera, R. J. Radmer, C. M. Bruns, J. P. Ku, K. A. Beauchamp, T. J. Lane, L.-P. Wang, D. Shukla, T. Tye, M. Houston, T. Stich, C. Klein, M. R. Shirts, and V. S. Pande, J. Chem. Theory Comput. **9**, 461 (2013).
[33]J. A. Maier, C. Martinez, K. Kasavajhala, L. Wickstrom, K. E. Hauser, and C. Simmerling, J. Chem. Theory Comput. **11**(8), 3696 (2015).
[34]A. Onufriev, D. Bashford, and D. A. Case, Proteins **55**, 383 (2004).
[35]J. A. Izaguirre, C. R. Sweet, and V. S. Pande, "Multiscale dynamics of macromolecules using normal mode Langevin," in *Pacific Symposium on Biocomputing 2010* (World Scientific, 2010), pp. 240–251.
[36]U. Essmann, L. Perera, M. L. Berkowitz, T. Darden, H. Lee, and L. G. Pedersen, J. Chem. Phys. **103**, 8577 (1995).
[37]D. Van Der Spoel, E. Lindahl, B. Hess, G. Groenhof, A. E. Mark, and H. J. Berendsen, J. Comput. Chem. **26**, 1701 (2005).
[38]K. Lindorff-Larsen, S. Piana, K. Palmo, P. Maragakis, J. Klepeis, R. Dror, and D. E. Shaw, Proteins **78**, 1950 (2010).
[39]W. L. Jorgensen, J. Chandrasekhar, J. D. Madura, R. W. Impey, and M. Klein, J. Chem. Phys. **79**, 926 (1983).
[40]G. Bussi, D. Donadio, and M. Parrinello, J. Chem. Phys. **126**, 014101 (2007).
[41]F. Vitalini, A. S. J. S. Mey, F. Noé, and B. G. Keller, J. Chem. Phys. **142**, 084101 (2015).
[42]F. Nüske, B. G. Keller, G. Pérez-Hernández, A. S. J. S. Mey, and F. Noé, J. Chem. Theory Comput. **10**, 1739 (2014).
[43]F. Vitalini, F. Noé, and B. G. Keller, J. Chem. Theory Comput. **11**, 3992 (2015).
[44]C. Schütte, F. Noé, J. Lu, M. Sarich, and E. Vanden-Eijnden, J. Chem. Phys. **134**, 204105 (2011).
[45]O. Lemke and B. G. Keller, J. Chem. Phys. **145**, 164104 (2016).
[46]F. Nüske, R. Schneider, F. Vitalini, and F. Noé, J. Chem. Phys. **144**, 054105 (2016).
[47]J.-H. Prinz, J. D. Chodera, V. S. Pande, W. C. Swope, J. C. Smith, and F. Noé, J. Chem. Phys. **134**, 244108 (2011).
[48]J. D. Chodera, W. C. Swope, F. Noé, J.-H. Prinz, M. R. Shirts, and V. S. Pande, J. Chem. Phys. **134**, 244107 (2011).
[49]M. R. Shirts and J. D. Chodera, J. Chem. Phys. **129**, 124105 (2008).
[50]D. D. L. Minh and J. D. Chodera, J. Chem. Phys. **131**, 134110 (2009).
[51]A. S. J. S. Mey, H. Wu, and F. Noé, Phys. Rev. X **4**, 041018 (2014).
[52]H. Wu, A. S. J. S. Mey, E. Rosta, and F. Noé, J. Chem. Phys. **141**, 214106 (2014).
[53]H. Wu, F. Paul, C. Wehmeyer, and F. Noé, Proc. Natl. Acad. Sci. U. S. A. **113**, E3221 (2016).
[54]A. Cesari, A. Gil-Ley, and G. Bussi, J. Chem. Theory Comput. **12**, 6192 (2016).
[55]B. G. Keller, M. Christen, C. Oostenbrink, and W. F. van Gunsteren, J. Biomol. NMR **37**, 1 (2007).
[56]A. Tsourtis, Y. Pantazis, M. A. Katsoulakis, and V. Harmandaris, J. Chem. Phys. **143**, 014116 (2015).
[57]G. Arampatzis, M. A. Katsoulakis, and L. Rey-Bellet, J. Chem. Phys. **144**, 104107 (2016).
[58]T. Huber, A. E. Torda, and W. F. van Gunsteren, J. Comput.-Aided Mol. Des. **8**, 695 (1994).
[59]A. Laio and M. Parrinello, Proc. Natl. Acad. Sci. U. S. A. **99**, 12562 (2002).
[60]Y. Sugita and Y. Okamoto, Chem. Phys. Lett. **329**, 261 (2000).
[61]G. Torrie and J. Valleau, J. Comput. Phys. **23**, 187 (1977).
[62]P. E. Kloeden and E. Platen, *Numerical Solution of Stochastic Differential Equations* (Springer Verlag, Berlin, 1992).
[63]L. C. G. Rogers and D. Williams, *Diffusions, Markov Processes and Martingales* (Cambridge University Press, Cambridge, 2000).

Chapter 6

Girsanov reweighting for metadynamics simulations

In the previous chapters we have introduced MSMs, a tool to approximate the dynamics of a molecular system as a jump process between microstates, i.e. small disjoint sets of the state space. To build an MSM, one needs of a time discretized trajectory (or a collection of replicas), that samples the state space and the rare events, i.e. the transitions through the high barriers of the potential energy function. Thus, the quality of the MSM depends on the quality of the trajectory and a system characterized by high barriers, could be difficult to sample, producing a large statistical error of the MSM.

Several enhanced sampling techniques, exist in MD field to solve this problem, e.g. metadynamics [43, 44, 45, 46] or umbrella sampling [29, 30]. The general idea is to add a bias, i.e. a function of relevant coordinates, to the potential energy function, in order to drive the system out of the minima and to force the system to explore rare conformational states. Typically, these tools are used to reconstruct the free energy profile of the system, i.e. the projection of the potential energy function on relevant coordinates.

On the other hand, the bias modifies the Hamiltonian and affects the dynamical properties of the system. It follows that a trajectory produced by a bias potential cannot be used to build a correct MSM describing the dynamics of a molecular system and then, typically, MSMs cannot be used together in combination with enhanced sampling techniques.

A solution to this problem, is offered by Girsanov reweighting [40, 41], a recent technique that permits to reweight path ensemble averages, like the correlation functions used to build the MSMs, when the Hamiltonian of the system is perturbed by an external potential energy function.

In this chapter, we present a recently published paper [59], where Girsanov reweighting has been implemented with metadynamics, in order to reweight the MSMs produced by biased simulations and obtain the correct information about the dynamics of an unbiased molecular system. Thus, Girsanov reweighting closes the missing link between metadynamics and MSMs, providing a tool that exploits the advantages of both the techniques. The combination of these methods can be relevant to study the dynamics of systems with high barriers and reduce the computational cost to build the MSM of a molecular system.

In metadynamics, one chooses a proper set of relevant coordinates, then perturbs the Hamiltonian with a sum of Gaussian functions deposited along the relevant coordinates. After a long time, the time-dependent bias converges to minus the free energy profile. The method is excellent to find the free energy surface of the system, however, the bias

accelerates significantly the dynamics of the system. If a metadynamics trajectory is used to build an MSM, one would obtain smaller timescales respect to the unbiased dynamics.

We use Girsanov reweighting in order to reweight a metadynamics simulation and to build the MSM for the unbiased system. We have developed two protocols:

1. Buildup protocol: The reweighting is applied directly on the time-dependent bias produced during the metadynamics simulation.

2. Rerun protocol: A first simulation is used to build the metadynamics potential, then a second simulation is performed with the bias as constant perturbation. The reweighting is performed on the second simulation.

I contributed to the paper describing the theory of metadynamics, of Girsanov reweighting and how can be used together to construct an MSM. I carried out all the simulations and the MSMs construction, by Girsanov reweighting, of the systems described in the paper: the one-dimensional diffusion process, the Alanine-dipeptide, the VGVAPG hexapeptide and the β-hairpin peptide.

https://doi.org/10.1063/1.5027728

THE JOURNAL OF CHEMICAL PHYSICS **149**, 072335 (2018)

Girsanov reweighting for metadynamics simulations

Luca Donati[a] and Bettina G. Keller[b]
Department of Biology, Chemistry, Pharmacy, Freie Universität Berlin, Takustraße 3, D-14195 Berlin, Germany

(Received 5 March 2018; accepted 10 July 2018; published online 27 July 2018)

Metadynamics is a computational method to explore the phase space of a molecular system. Gaussian functions are added along relevant coordinates on the fly during a molecular-dynamics simulation to force the system to escape from minima in the potential energy function. The dynamics in the resulting trajectory are however unphysical and cannot be used directly to estimate dynamical properties of the system. Girsanov reweighting is a recent method used to construct the Markov State Model (MSM) of a system subjected to an external perturbation. With the combination of these two techniques—metadynamics/Girsanov-reweighting—the unphysical dynamics in a metadynamics simulation can be reweighted to obtain the MSM of the unbiased system. We demonstrate the method on a one-dimensional diffusion process, alanine dipeptide, and the hexapeptide Val-Gly-Val-Ala-Pro-Gly (VGVAPG). The results are in excellent agreement with the MSMs obtained from direct unbiased simulations of these systems. We also apply metadynamics/Girsanov-reweighting to a β-hairpin peptide, whose dynamics is too slow to efficiently explore its phase space by direct simulation. *Published by AIP Publishing.* https://doi.org/10.1063/1.5027728

I. INTRODUCTION

Molecular dynamics (MD) simulations yield a realization, $\mathbf{x}_t$, of the conformational dynamics of a molecular system at atomistic resolution, where $\mathbf{x} \in \Gamma$ is a point in the molecular phase space Γ and t is the time. MD simulations are typically used to estimated phase-space ensemble averages $\mathbb{E}_\Gamma[a]$ of observable functions $a(\mathbf{x})$,

$$\mathbb{E}_\Gamma[a] = \int_\Gamma a(\mathbf{x})\mu_\Gamma(\mathbf{x})\,\mathrm{d}\mathbf{x}, \tag{1}$$

which can then be interpreted in terms of the underlying phase-space probability density $\mu_\Gamma(\mathbf{x})$. Molecular systems are characterized by a vast phase space and high barriers in the potential energy function. Thus, the sampling of the phase-space probability density converges slowly, which renders the estimation of ensemble averages from direct unbiased simulations computationally expensive or even prohibitive for many systems.

A wide range of techniques have been developed to enhance the sampling in MD simulations, such as replica exchange MD,[1] umbrella sampling,[2] and metadynamics.[3–6] These simulations yield unphysical trajectories. However, the phase-space ensemble average of the unbiased molecular system can nonetheless be estimated from these trajectories by comparing the phase-space probability densities of the biased and the unbiased system for each frame in the trajectory (phase-space reweighting). The combination of enhanced sampling and phase-space reweighting techniques has increased the system sizes that can be investigated by MD simulations enormously.

It is important to note that the analysis of phase-space ensemble averages only yields information on the relative population of the various conformations of the molecular system but not on the dynamics with which the system transitions between these conformations. In fact, when estimating phase-space ensemble averages from trajectory data, the time-information is completely neglected. In principle, MD trajectories contain the full information of the molecular dynamics. Yet, extracting any interpretable dynamic properties from these data is an intricate task.[7–11] One property, which can readily be estimated from MD trajectories, is the time-lagged correlation function between two observable functions $a(\mathbf{x})$ and $b(\mathbf{x})$,

$$\mathrm{cor}(a, b; \tau) = \int_\Gamma \int_\Gamma a(\mathbf{x})\mu_\Gamma(\mathbf{x})p(\mathbf{x}, \mathbf{y}; \tau)b(\mathbf{y})\,\mathrm{d}\mathbf{x}\,\mathrm{d}\mathbf{y}, \tag{2}$$

where $p(\mathbf{x}, \mathbf{y}; \tau)$ is the transition probability density, i.e., the probability to find the system at $\mathbf{y}$ after at time $t + \tau$ given that it has been in $\mathbf{x}$ at time t. Markov state models (MSMs)[12–20] make use of cross-correlation functions to build a transition probability matrix of the dynamics. From the dominant eigenvectors and eigenvalues of the transition probability matrix, one obtains a coarse-grained, and thus humanly understandable, representation of the complex and often multiscalar molecular dynamics. MSMs have become an indispensable tool for the elucidation of complex molecular dynamics and have highlighted the importance of dynamic effects in understanding the function and macroscopic properties of molecular systems.[21–26]

When constructing MSMs, one faces a similar sampling problem as for the estimation of phase-space ensemble averages. However until a few years ago, MSMs could not be estimated from enhanced sampling simulations because methods to reweight the transition probability density

[a]Electronic mail: luca.donati@fu-berlin.de
[b]Electronic mail: bettina.keller@fu-berlin.de

$p(\mathbf{x}, \mathbf{y}; \tau)$ from the biased dynamics to the unbiased dynamics were lacking. Although protocols to optimally seed[27] and respawn[28] simulations have been proposed, the limitation to unbiased simulations made MSMs computationally very expensive.

In recent years, several dynamic reweighting schemes[32–36] have been published with which one can reweight a discrete approximation of the transition probability density, namely, $\mathbb{P}[\mathbf{x}_{t+\tau} \in B_j \,|\mathbf{x}_t \in B_i]$, the conditional probability of finding the system within state B_j at time $t + \tau$, given that it has been in state B_i at time t. $B_i, B_j \subset \Gamma$ are discrete states in the phase space of the system. These methods need to assume that the system is in local equilibrium within state B_i before it transitions to state B_j.

An alternative approach is the Girsanov reweighting method for path ensemble averages,[37–39] in which not the transition probability $\mathbb{P}[\mathbf{x}_{t+\tau} \in B_j \,|\mathbf{x}_t \in B_i]$ but the transition probability density $p(\mathbf{x}, \mathbf{y}; \tau)$ is reweighted. One advantage of this approach is that one does not need to assume local equilibrium or even the prior definition of a particular discretization of the molecular phase space. Reweighting $p(\mathbf{x}, \mathbf{y}; \tau)$ becomes possible by considering the ensemble of all possible paths $\omega = \{\mathbf{x}_0, \mathbf{x}_1, \ldots, \mathbf{x}_n\}$ of length τ which start in point $\mathbf{x}_0$ at time t and end in point $\mathbf{x}_n = \mathbf{y}$ at time $t + \tau$. Then, instead of reweighting the transition probability as such, the probability density with which each individual path occurs is reweighted from the biased dynamics to the unbiased dynamics. Integrating over the path ensemble with appropriately reweighted path probability densities ultimately yields the transition probability density of the unbiased system.

We have recently demonstrated the Girsanov reweighting method for all-atom MD simulations and used it to reweight MSMs from a reference potential energy function to a series of perturbed potential energy functions.[39] Since the transition probability density $p(\mathbf{x}, \mathbf{y}; \tau)$ is reweighted, the Girsanov reweighting method can be applied to reweighted arbitrary correlation functions [Eq. (2)] and to obtain the associated dynamic properties, such as, for example, stopping times of trajectories which reach a certain target set.[40]

In this contribution, we ask whether Girsanov reweighting can be used to obtain unbiased MSMs from simulations which are biased by a metadynamics potential. Metadynamics[3–6] is an enhanced sampling method, in which Gaussian functions are deposited along collective variables such that the system is driven out of the minima of the potential energy function. When fully converged, the metadynamics potential compensates the free energy surface in the space of the collective variables. Thus, the bias is quite strong. On the other hand, the variance of the Girsanov reweighting estimator sensitively depends on the gradient of the bias. We choose a heuristic approach and test whether a biasing strength which yields an appreciable speed-up of the simulation is compatible with the Girsanov reweighting method. First, we benchmark the biasing strength and the metadynamics/Girsanov-reweighting method on a one-dimensional diffusion process. Then, we demonstrate the method on two molecular systems for which reference MSMs can be constructed by direct simulation (alanine dipeptide and a hexapeptide). Finally, we use metadynamics/Girsanov-reweighting to obtain a MSM of a β-hairpin peptide whose dynamics is too slow to obtain a MSM by direct simulation.

II. THEORY

A. Molecular dynamics

Consider a molecular system governed by the Langevin equation,

$$\begin{aligned} M\frac{\mathrm{d}\mathbf{v}(t)}{\mathrm{d}t} &= -\nabla V_t(\mathbf{r}(t)) - \gamma\mathbf{v}(t) + \sigma\eta(t), \\ \mathbf{v}(t) &= \frac{\mathrm{d}\mathbf{r}(t)}{\mathrm{d}t}, \end{aligned} \tag{3}$$

where M is the mass matrix, $\mathbf{r}(t)$ and $\mathbf{v}(t) \in \mathbb{R}^{3N}$ are the position and the velocity vector. $V_t(\mathbf{r})$ is the potential energy function, which may be time-dependent. The interaction between the molecular system and the solvent is modeled by the friction coefficient γ and an uncorrelated Gaussian white noise $\eta(t) \in \mathbb{R}^{3N}$, which is scaled by the volatility σ according to the Einstein relation $\sigma = \sqrt{2k_BT\gamma M}$ where k_B is the Boltzmann constant and T is the temperature of the system. The state of the system at time t is represented by the vector $\mathbf{x}(t) = \{\mathbf{r}(t), \mathbf{v}(t)\} \in \Gamma$, where $\Gamma = \mathbb{R}^{6N}$ denotes the phase space of the system.

Numerical integration of Eq. (3) with a time step of Δt for n time steps yields a time-discretized trajectory $\omega = \{\mathbf{x}_0, \mathbf{x}_1, \ldots, \mathbf{x}_n\}$. Note that the numerical integration requires a sequence of normal random numbers for each dimension of the position space $\eta^{(i)} = \{\eta_1^{(i)}, \ldots, \eta_n^{(i)}\}$, with $\eta_k^{(i)} \sim \mathcal{N}(0, 1)$ and $i \in [1, 2, \ldots, \mathbb{R}^{3N}]$.

B. Metadynamics

A recurrent problem in MD simulations is that one needs to generate very long trajectories to exhaustively sample the phase space Γ. Metadynamics[3,4] is a technique used to accelerate the exploration of the phase-space along a few relevant coordinates (also known as collective variables) along which the slowest transitions in the system occur. We consider a set of d collective variables $s = s(\mathbf{r}) = \{s_1(\mathbf{r}), s_2(\mathbf{r}), \ldots, s_d(\mathbf{r})\}$. During the build-up phase in metadynamics, a time-dependent potential $V_{\mathrm{meta}}(s, t)$ is added to a reference potential $V_0(\mathbf{r})$, and Eq. (3) is integrated with

$$V_t(\mathbf{r}) = V_0(\mathbf{r}) + V_{\mathrm{meta}}(s(\mathbf{r}), t). \tag{4}$$

Thus, this build-up phase corresponds to a simulation of Langevin dynamics with a time-dependent potential energy function. The biasing potential is constructed as a growing sum of Gaussian functions on the collective variables s_i as

$$V_{\mathrm{meta}}(s, t) = \sum_{t'=\tau_G, 2\tau_G, \ldots}^{t'<t} W \exp\left(-\sum_i^d \frac{(s_i - s_i(\mathbf{r}(t'))^2}{2\sigma_{s_i}^2}\right), \tag{5}$$

where W is the height of the Gaussian, and σ_s is the variance of the Gaussian function along the collective variable s. At regular intervals τ_G, the biasing potential is updated by adding a Gaussian function of width σ_s, which is centered at the current position $\mathbf{r}(t')$, to the current potential. Note that the parameter τ_G is not related to the Markov model lag-time τ. The effect is that already visited positions are discouraged and the system

is driven out of the minima of the original energy potential. In the long time limit, the biasing potential converges to minus the free energy F profile along the collective variable $V_{\text{meta}}(s, t \to \infty) = -F(s) + C$, where C is a constant.

Well-tempered metadynamics is a variant of metadynamics, in which the height of each Gaussian function W in Eq. (5) is scaled according to

$$W(t') = W_0 \exp\left(-\frac{V_{\text{meta}}(s,t')}{\Delta T}\right), \tag{6}$$

where W_0 is the height of the Gaussian at $V_{\text{meta}}(s,t) = 0$ and ΔT is a temperature-like parameter that controls the decay rate of W. The higher the current metadynamics potential $V_{\text{meta}}(s,t)$ at a position s, the smaller the height of the newly added Gaussian functions. In the long time limit, the well-tempered metadynamics potential [Eq. (5)] does not fully compensate the free energy profile but converges to

$$V_{\text{meta}}(s, t \to \infty) = -\frac{\Delta T}{T + \Delta T} F(s) + C, \tag{7}$$

while the probability distribution on collective variables converges to

$$\pi(s) \propto \exp\left[-\beta\left(\frac{T}{T+\Delta T} F(s)\right)\right]. \tag{8}$$

Note that ΔT controls the extent to which $V_{\text{meta}}(s, t \to \infty)$ compensates the free-energy profile. For $\Delta T \to +\infty$, $W \to W_0$ and the standard metadynamics is retained, while for $\Delta T \to 0$, unbiased MD is recovered.

Various reweighting schemes[41–44] have been developed to estimate phase-space ensemble averages of the reference potential V_0 from the biased simulation. Note, however, that typically the *build-up* phase of a metadynamics simulation, i.e., the part of the simulation in which the metadynamics potential grows, is not analyzed due to the difficulties that arise in analyzing dynamics at time-dependent potential energy functions. Instead, the converged metadynamics potential $V_{\text{meta}}(s(\mathbf{r}))$ is used to construct a time-independent potential energy function

$$V(\mathbf{r}) = V_0(\mathbf{r}) + V_{\text{meta}}(s(\mathbf{r})). \tag{9}$$

MD simulation at this potential is carried out and analyzed by phase-space reweighting methods. We will call this latter type of simulation metadynamics *rerun*.

C. Markov state models

Consider a dynamic process which is Markovian, ergodic, and reversible, such as Eq. (3). The time-evolution of the associated phase-space probability density $p_t(\mathbf{x})$ can be represented by a *propagator* $\mathcal{P}(\tau)$, a continuous operator that transports the probability density forward in time: $p_{t+\tau}(\mathbf{y}) = \mathcal{P}(\tau)p_t(\mathbf{x}) = \int_\Gamma p(\mathbf{x},\mathbf{y};\tau)p_t(\mathbf{x})\,\mathrm{d}\mathbf{x}$. This propagator can be approximated by Markov state models (MSM).[12–18,20]

In MSMs, the phase space is discretized into g disjoint sets (or microstates) $B_1, B_2, \ldots, B_g$ with $\cup_{i=1}^{g} B_i = \Gamma$. Given a lag-time τ, the probability of observing a transition from B_i to B_j, $\mathbb{P}[\mathbf{x}_n \in B_j, \mathbf{x}_0 \in B_i]$, can be represented by a cross-correlation function

$$C_{ij}(\tau) = \int_\Gamma \int_\Gamma \mathbf{1}_{B_i}(\mathbf{x}) \mu_\Gamma(\mathbf{x}) \mathbf{1}_{B_j}(\mathbf{y})\, p(\mathbf{x},\mathbf{y};\tau)\,\mathrm{d}\mathbf{y}\,\mathrm{d}\mathbf{x}, \tag{10}$$

where $\mathbf{1}_{B_i}$ is the indicator function of the ith set

$$\mathbf{1}_{B_i}(\mathbf{x}) := \begin{cases} 1 & \text{if } \mathbf{x} \in B_i \\ 0 & \text{otherwise} \end{cases}, \tag{11}$$

and $\mu_\Gamma(\mathbf{x})$ is the stationary probability density

$$\mu_\Gamma(\mathbf{x}) = \frac{\exp[-\beta\mathcal{H}(\mathbf{x})]}{Z}, \tag{12}$$

where $\beta = \frac{1}{k_B T}$, $\mathcal{H}(\mathbf{x}) = \frac{1}{2}\mathbf{v}^\top M\mathbf{v} + V(\mathbf{r})$ is the classical Hamiltonian of the system, and $Z = \int_\Gamma \exp[-\beta\mathcal{H}(\mathbf{x})]\,\mathrm{d}\mathbf{x}$ is the partition function.

The conditional transition probability $\mathbb{P}[\mathbf{x}_n \in B_j | \mathbf{x}_0 \in B_i]$ of observing the system in B_j at time $t + \tau$, given that it has been in B_i at time t, is

$$T_{ij}(\tau) = \frac{C_{ij}(\tau)}{\sum_{j=1}^{g} C_{ij}(\tau)}. \tag{13}$$

For reversible processes, the resulting transition matrix $\mathbf{T}(\tau)$: $T_{ij}(\tau)$ is a matrix representation (approximation) of the propagator. Its dominant eigenvectors and eigenvalues contain information about the slow processes of the system,[12–18,20]

$$\begin{aligned} \mathbf{T}(\tau)\mathbf{r}_k &= \lambda_k(\tau)\mathbf{r}_k, \\ \mathbf{l}_k^\top \mathbf{T}(\tau) &= \lambda_k(\tau)\mathbf{l}_k^\top, \end{aligned} \tag{14}$$

where $\mathbf{l}_k^\top$ denotes the transpose of vector $\mathbf{l}_k$. If the implied time scales

$$t_k(\tau) = -\frac{\tau}{\ln(\lambda_k(\tau))} = \text{const.} \quad \forall\, \tau > 0 \tag{15}$$

are independent of the lag time τ, the approximation is considered to be valid. In practice, one aims at finding a region of τ, for which the implied time scales are roughly constant.[15,18]

D. Girsanov reweighting

Girsanov reweighting[37] is a method to reweight a path ensemble average $\mathbb{E}_\Omega[f]$ which has been measured for dynamics at potential $V(\mathbf{r})$ to its corresponding value at $V(\mathbf{r}) + U(\mathbf{r})$, without re-sampling the dynamics at $V(\mathbf{r}) + U(\mathbf{r})$. Because Eq. (10) can be formulated in terms of a path ensemble average, Girsanov reweighting can be used to obtain the MSM for dynamics at $V(\mathbf{r}) + U(\mathbf{r})$ by reweighting trajectories sampled at $V(\mathbf{r})$.[38,39] We will explain the method using time-discretized paths ω which are obtained by numerical integrating equation (3). For more details on path spaces and path probabilities and the implications of using time-discrete rather than time-continuous paths, see Ref. 39.

Let $\omega = \{\mathbf{x}_0 = \mathbf{x}, \mathbf{x}_1, \ldots, \mathbf{x}_n\}$ be a path of length $\tau = n \cdot \Delta t$ which starts in a specific state $\mathbf{x}_0 = \mathbf{x}$. The path space, i.e., the set of all possible paths ω of length τ which start in $\mathbf{x}_0 = \mathbf{x}$, is $\Omega_{\tau,\mathbf{x}}$. The path probability density, i.e., the probability of observing a path $\omega \in \Omega_{\tau,\mathbf{x}}$, is $\mu_\Omega(\omega) = \mu_\Omega(\mathbf{x}_1, \mathbf{x}_2, \ldots, \mathbf{x}_n | \mathbf{x}_0 = \mathbf{x})$. Let $S_{\tau,\mathbf{x},m} = \{\omega_1, \omega_2, \ldots, \omega_m\} \subset \Omega_{\tau,\mathbf{x}}$ be a sample of the path space, which has been generated by integrating equation (3) with $V_t(\mathbf{r}) = V(\mathbf{r})$ and $\mathbf{x}_0 = \mathbf{x}$. The probability density that a particular path appears in the set is given by $\mu_\Omega(\omega)$. Let furthermore $f(\omega) = f(\mathbf{x}_1, \mathbf{x}_2, \ldots, \mathbf{x}_n)$ be a path observable, i.e., a function which assigns a real-valued number to each path ω. The path ensemble average of $f(\omega)$ for dynamics at $V(\mathbf{r})$ is

obtained by a weighted integration over all paths, except for the first state $\mathbf{x}_0 = \mathbf{x}$,

$$\begin{aligned}\mathbb{E}_\Omega[f \mid \mathbf{x}_0 = \mathbf{x}] &= \int_{\Omega_{\tau,\mathbf{x}}} \mu_\Omega(\omega) f(\omega)\, \mathrm{d}\omega \\ &= \int_\Gamma \int_\Gamma \cdots \int_\Gamma \mu_\Omega(\mathbf{x}_1, \mathbf{x}_2, \ldots, \mathbf{x}_n \mid \mathbf{x}_0 = \mathbf{x}) \\ &\quad \times f(\mathbf{x}_1, \mathbf{x}_2, \ldots, \mathbf{x}_n)\, \mathrm{d}\mathbf{x}_1, \mathrm{d}\mathbf{x}_2, \ldots, \mathrm{d}\mathbf{x}_n \\ &= \lim_{m\to\infty} \frac{1}{m} \sum_{\omega_k \in S_{\tau,\mathbf{x},m}} f(\omega_k). \end{aligned} \tag{16}$$

The last equality only holds if the sampling is ergodic. Dynamics at an altered potential $V(\mathbf{r}) + U(\mathbf{r})$ generate a different path probability density $\widetilde{\mu}_\Omega(\omega)$ and a different path ensemble average $\widetilde{\mathbb{E}}_\Omega[f \mid \mathbf{x}_0 = \mathbf{x}]$. However, if the path probability ratio $M_{\tau,\mathbf{x}}(\omega) = \widetilde{\mu}_\Omega(\omega)/\mu_\Omega(\omega)$ is defined, $\widetilde{\mathbb{E}}_\Omega[f \mid \mathbf{x}_0 = \mathbf{x}]$ can be estimated from the set of paths $S_{\tau,\mathbf{x},m}$ sampled at $V(\mathbf{r})$,

$$\begin{aligned}\widetilde{\mathbb{E}}_\Omega[f \mid \mathbf{x}_0 = \mathbf{x}] &= \int_{\Omega_{\tau,\mathbf{x}}} \widetilde{\mu}_\Omega(\omega) f(\omega)\, \mathrm{d}\omega \\ &= \int_{\Omega_{\tau,\mathbf{x}}} M_{\tau,\mathbf{x}}(\omega)\, \mu_\Omega(\omega) f(\omega)\, \mathrm{d}\omega \\ &= \lim_{m\to\infty} \frac{1}{m} \sum_{\omega_k \in S_{\tau,\mathbf{x},m}} M_{\tau,\mathbf{x}}(\omega) f(\omega_k). \end{aligned} \tag{17}$$

The Girsanov theorem specifies the conditions under which $M_{\tau,\mathbf{x}}(\omega)$ exists and asserts that

$$\begin{aligned}M_{\tau,\mathbf{x}}(\omega) = \frac{\mu_{\widetilde{\Omega}}(\omega)}{\mu_\Omega(\omega)} = \exp\Bigg\{ &\sum_{i=1}^{3N} \Bigg[\sum_{k=0}^{n} \frac{\nabla_i U(\mathbf{r}_k)}{\sigma} \eta_k^i \sqrt{\Delta t} \\ &- \frac{1}{2} \sum_{k=0}^{n} \left(\frac{\nabla_i U(\mathbf{r}_k)}{\sigma} \right)^2 \Delta t \Bigg] \Bigg\}, \end{aligned} \tag{18}$$

where η_k^i are the random numbers, along dimension i at time step k, generated to integrate equation (3) with $V(\mathbf{r})$, and $\nabla_i U(\mathbf{r}_k)$ is the gradient of $U(\mathbf{r})$ along dimension i measured at the position $\mathbf{r}_k$.

E. Girsanov reweighting for MSMs

To use the Girsanov reweighting method on MSMs, the cross-correlation function [Eq. (10)] has to be reformulated as a path ensemble average. The transition probability $p(\mathbf{x}, \mathbf{y}; \tau)$ in Eq. (10) is obtained from the path probability density $\mu_\Omega(\omega)$ by integrating over all intermediate states between $\mathbf{x}_0 = \mathbf{x}$ and $\mathbf{x}_n = \mathbf{y}$,

$$\begin{aligned}p(\mathbf{x}, \mathbf{y}; \tau) = &\int_\Gamma \int_\Gamma \cdots \int_\Gamma \mu_\Omega(\mathbf{x}_1, \mathbf{x}_2, \ldots, \mathbf{x}_n \mid \mathbf{x}_0 = \mathbf{x}) \\ &\times \mathrm{d}\mathbf{x}_1\, \mathrm{d}\mathbf{x}_2 \ \ldots\ \mathrm{d}\mathbf{x}_{n-1}. \end{aligned} \tag{19}$$

The indicator function of the final set B_j can be regarded as a path observable $f(\omega) = f(\mathbf{x}_n) = \mathbf{1}_{B_j}(\mathbf{x}_n) = \mathbf{1}_{B_j}(\mathbf{y})$. Thus, the integral over the final states $\mathbf{y}$ in Eq. (10) is formally a path ensemble average,

$$\begin{aligned}&\int_\Gamma p(\mathbf{x}, \mathbf{y}; \tau) \mathbf{1}_{B_j}(\mathbf{y})\, \mathrm{d}\mathbf{y} \\ &\quad = \int_\Gamma \Bigg[\int_\Gamma \int_\Gamma \cdots \int_\Gamma \mu_\Omega(\mathbf{x}_1, \mathbf{x}_2, \ldots, \mathbf{x}_n \mid \mathbf{x}_0 = \mathbf{x}) \\ &\qquad \times \mathrm{d}\mathbf{x}_1\, \mathrm{d}\mathbf{x}_2 \ \ldots\ \mathrm{d}\mathbf{x}_{n-1} \Bigg] \mathbf{1}_{B_j}(\mathbf{x}_n)\, \mathrm{d}\mathbf{x}_n, \end{aligned} \tag{20}$$

$$= \mathbb{E}_\Omega[\mathbf{1}_{B_j} \mid \mathbf{x}_0 = \mathbf{x}]. \tag{21}$$

The integral over the initial states in Eq. (10) is then formally a phase-space ensemble average [Eq. (1)] of an observable function $a(\mathbf{x}) = \mathbf{1}_{B_i}(\mathbf{x}) \mathbb{E}_\Omega[\mathbf{1}_{B_j} \mid \mathbf{x}_0 = \mathbf{x}]$,

$$\begin{aligned}C_{ij}(\tau) &= \int_\Gamma \mu_\Gamma(\mathbf{x})\, \mathbf{1}_{B_i}(\mathbf{x}) \int_{\Omega_{\tau,\mathbf{x}}} \mu_\Omega(\omega) \mathbf{1}_{B_j}(\mathbf{x}_n)\, \mathrm{d}\omega\, \mathrm{d}\mathbf{x} \\ &= \mathbb{E}_\Gamma[\mathbf{1}_{B_i}(\mathbf{x}) \mathbb{E}_\Omega[\mathbf{1}_{B_j} \mid \mathbf{x}_0 = \mathbf{x}]]. \end{aligned} \tag{22}$$

The correlation function is thus a nested combination of a path ensemble average and a phase-space ensemble average. To obtain the correlation function $\widetilde{C}_{ij}(\tau)$ at $V(\mathbf{r}) + U(\mathbf{r})$, one needs to reweight the path ensemble average $\mathbb{E}_\Omega[\mathbf{1}_{B_j} \mid \mathbf{x}_0 = \mathbf{x}]$ using Eqs. (17) and (18)and the phase-space ensemble average according to

$$\widetilde{\mathbb{E}}_\Gamma[a] = \int_\Gamma \widetilde{\mu}_\Gamma(\mathbf{x})\, a(\mathbf{x})\, \mathrm{d}\mathbf{x} = \int_\Gamma g(\mathbf{x}) \mu_\Gamma(\mathbf{x})\, a(\mathbf{x})\, \mathrm{d}\mathbf{x}, \tag{23}$$

where

$$g(\mathbf{x}) = \frac{\widetilde{\mu}_\Gamma(\mathbf{x})}{\mu_\Gamma(\mathbf{x})} = \frac{Z}{\widetilde{Z}} \exp(-\beta U(\mathbf{r})). \tag{24}$$

The function $g(\mathbf{x})$ is the probability ratio of the two phase-space probability densities: $\mu_\Gamma(\mathbf{x})$ associated with $V(\mathbf{r})$ and $\widetilde{\mu}_\Gamma(\mathbf{x})$ associated with $V(\mathbf{r}) + U(\mathbf{r})$. Thus,

$$\begin{aligned}\widetilde{C}_{ij}(\tau) &= \int_\Gamma \widetilde{\mu}_\Gamma(\mathbf{x})\, \mathbf{1}_{B_i}(\mathbf{x}) \int_{\Omega_{\tau,\mathbf{x}}} \widetilde{\mu}_\Omega(\omega) \mathbf{1}_{B_j}(\mathbf{x}_n)\, \mathrm{d}\omega\, \mathrm{d}\mathbf{x} \\ &= \int_\Gamma g(\mathbf{x}) \mu_\Gamma(\mathbf{x})\, \mathbf{1}_{B_i}(\mathbf{x}) \int_{\Omega_{\tau,\mathbf{x}}} M_{\tau,\mathbf{x}}(\omega) \mu_\Omega(\omega) \mathbf{1}_{B_j}(\mathbf{x}_n)\, \mathrm{d}\omega\, \mathrm{d}\mathbf{x}. \end{aligned} \tag{25}$$

In praxis, $C_{ij}(\tau)$ is estimated from a set of m paths of length τ, $S_{\tau,m} = \{\nu_1, \nu_2 \ldots, \nu_m\}$, sampled at $V(\mathbf{r})$ with initial states distributed according to Eq. (12) as

$$C_{ij}(\tau) = \lim_{m\to\infty} \frac{1}{m} \sum_{k=1}^{m} \mathbf{1}_{B_i}([\mathbf{x}_0]_k) \cdot \mathbf{1}_{B_j}([\mathbf{x}_n]_k), \tag{26}$$

where $[\mathbf{x}_i]_k$ denotes the ith time step of the kth path. $\widetilde{C}_{ij}(\tau)$ can be estimated from the same set of paths by reweighting Eq. (26) analogously to Eq. (25),

$$\widetilde{C}_{ij}(\tau) = \lim_{m\to\infty} \frac{1}{m} \sum_{\nu_k \in S_{\tau,m}} g([\mathbf{x}_0]_k) \mathbf{1}_{B_i}([\mathbf{x}_0]_k) \cdot M_{\mathbf{x},\tau}(\nu_k) \mathbf{1}_{B_j}([\mathbf{x}_n]_k). \tag{27}$$

Finally, the transition probability between set B_i and set B_j for the perturbed dynamics is obtained as

$$\widetilde{T}_{ij}(\tau) = \frac{\widetilde{C}_{ij}(\tau)}{\sum_j \widetilde{C}_{ij}(\tau)}. \tag{28}$$

The functions $g(\mathbf{x})$ and $M_{\tau,\mathbf{x}}(\omega)$ are two Radon-Nikodym derivatives.[37] In particular, $g(\mathbf{x})$ represents a change of measure on the phase-space, while $M_{\tau,\mathbf{x}}(\omega)$ represents a change of measure on the path-space.

F. Metadynamics/Girsanov reweighting

The metadynamics/Girsanov-reweighting method consists of running metadynamics simulations and constructing MSMs of the unbiased system by reweighting to the molecular reference potential energy function $V_0(\mathbf{r})$. In rerun metadynamics, the paths $S_{\tau,m} = \{\nu_1, \nu_2, \ldots, \nu_m\}$ are sampled at the time-independent potential given by Eq. (9). One would like to reweight the resulting paths to the dynamics at $V(\mathbf{r}) + U(\mathbf{r}) = V_0(\mathbf{r})$. Thus, the perturbation which enters Eq. (18) is

$$U(\mathbf{r}) = V_0(\mathbf{r}) - V(\mathbf{r}) = -V_{\text{meta}}(\mathbf{r}). \tag{29}$$

A different application of the Girsanov reweighting to metadynamics simulations exploits the fact that the Girsanov theorem can also be used to reweight path ensembles generated by time-dependent potential energy functions. Thus, it can be used to reweight the build-up phase of the metadynamics potential. The perturbation which enters Eq. (18) is then time-dependent and is given as

$$U(\mathbf{r}, t) = V_0(\mathbf{r}) - V(\mathbf{r}, t) = -V_{\text{meta}}(\mathbf{r}, t). \tag{30}$$

Additionally, the phase-space probability ratio [Eq. (24)] becomes time-dependent,

$$g(\mathbf{x}, t) = \frac{\widetilde{\mu}_\Gamma(\mathbf{x})}{\mu_\Gamma(\mathbf{x}, t)} = \frac{Z}{\widetilde{Z}} \exp(\beta V_{\text{meta}}(\mathbf{r}, t)). \tag{31}$$

III. METHODS

A. One-dimensional system

We consider a one-dimensional diffusion process x_t which is governed by the stochastic differential equation,

$$\mathrm{d}x_t = -\nabla V(x_t) + \sigma \mathrm{d}B_t, \tag{32}$$

where B_t denotes a standard Brownian motion, $\sigma = 1.5$ is the volatility, and $V(x)$ is a one-dimensional potential energy surface given by the function

$$V(x) = 4\left(x^3 - \frac{3}{2}x\right)^2 - x^3 + x. \tag{33}$$

This function describes a one-dimensional triple-well potential. Equation (32) has been numerically integrated using the Euler-Maruyama scheme

$$x_{n+1} = x_n - \nabla_x V(x_n)\Delta t + \sigma\eta\sqrt{\Delta t}, \tag{34}$$

where $\Delta t = 0.001$ is the integration time step, η are independent and identically distributed random variables drawn from a standard Gaussian distribution, and n is the index of the time step.

Direct simulations. We have first produced trajectories of 4e4, 4e5, 4e6, and 4e7 time steps. For each trajectory, we built an MSM with enforced detailed balance, extracted the dominant eigenvalues and eigenvectors, and estimated the implied time scales [Eq. (15)] in the range of [10 : 500] time steps. The MSMs were built by discretizing the interval $x = -2 : 2$ in 100 bins. The reference MSM is constructed on the trajectory of 4e7 time steps with a lag-time of 50 time steps. To obtain estimates of the uncertainties in the implied time scales, we repeated each numerical experiment, i.e., simulation and MSM construction, 50 times. Thus, for each of the considered simulation lengths (4e4, 4e5, 4e6, and 4e7), we have 50 trajectories and the associated MSMs. The implied time scales in the column "Direct simulation" Table I are given as the average for each sample of 50 MSMs, and the uncertainties are given as the standard deviation.

Metadynamics build-up. The metadynamics potential $V_{\text{meta}}(s(\mathbf{r}))$ [Eq. (5)] was generated with parameters $W = 0.02$, $\sigma_s = 0.2$, and $\tau_G = 2000$, where $s(\mathbf{r}) = x$. Because $V_{\text{meta}}(s(\mathbf{r}))$ is a sum over Gaussians, the gradient calculation becomes computationally demanding as the number of terms in the sum grows. To overcome this problem and keep the efficiency of the simulation constant, we stored the bias at each update, on a grid of 1000 bins between $x = -2.0$ and $x = 2.0$. We terminated the build-up after 4e4 time steps ($V_{\text{meta4e4}}(x)$), 4e5 time steps ($V_{\text{meta4e5}}(x)$), 4e6 time steps ($V_{\text{meta4e6}}(x)$), and 4e7 time steps ($V_{\text{meta4e7}}(x)$) to obtain four different metadynamics potentials for the metadynamics rerun experiments. We reweighted the trajectory from each of the build-up phases using Eqs. (30) and (31)and obtained an MSM of the unbiased potential [Eq. (33)]. The MSMs were constructed analogously to the MSMs of the direct simulation. As before, we repeated

TABLE I. Implied time scales associated with the second and third MSM eigenvector of the one-dimensional diffusion process. The numbers show the average and standard deviation of a sample of 50 numerical experiments (simulation and reweighted MSM).

Simulation		Rerun	Rerun	Rerun	Rerun	
Time steps	Direct simulation	V_{meta4e4}	V_{meta4e5}	V_{meta4e6}	V_{meta4e7}	Build-up
4e4	1.5e3 ± 316	1.5e3 ± 415	1.61e3 ± 433	1.49e3 ± 309	1.74e3 ± 530	1.53e03 ± 142
	345 ± 60	344 ± 60	353 ± 59	346 ± 50	391 ± 174	350 ± 48
4e5	1.53e3 ± 118	1.53e3 ± 107	1.49e3 ± 81	1.51e3 ± 86	1.57e3 ± 581	1.53e3 ± 76
	357 ± 18	357 ± 17	355 ± 15	357 ± 17	381 ± 146	358 ± 16
4e6	1.52e3 ± 32	1.52e3 ± 34	1.52e3 ± 32	1.52e3 ± 21	1.5e3 ± 82	1.52e3 ± 26
	357 ± 6	357 ± 5	357 ± 4	357 ± 4	347 ± 66	358 ± 5
4e7	1.53e3 ± 11	...	...	...	...	...
	358 ± 2	...	...	...	...	...

each numerical experiment, i.e., metadynamics build-up simulation and Girsanov-reweighted MSM, 50 times to obtain averages and standard deviations of the implied time scales (column "Build-up" in Table I).

Metadynamics rerun. We sampled the four metadynamics potentials ($V_{\text{meta4e4}}(x)$, $V_{\text{meta4e5}}(x)$, $V_{\text{meta4e6}}(x)$, $V_{\text{meta4e7}}(x)$) by conducting simulations of 4e4, 4e5, 4e6, and 4e7 time steps for each potential. We reweighted each trajectory using Eq. (29) and obtained an MSM of the unbiased potential [Eq. (33)]. The MSMs were constructed analogously to the MSMs of the direct simulation. In total, this yielded 16 different numerical experiments (metadynamics rerun simulation and Girsanov-reweighted MSM). As before, we repeated each numerical experiment 50 times to obtain averages and standard deviations of the implied time scales (column V_{meta4e4} to V_{meta4e7} in Table I).

To numerically integrate Eq. (32) and to build the MSM, we have written our own software in C++.

B. MD simulations

We performed MD simulations of acetyl-alanine-methylamide (Ac-A-NHMe, alanine dipeptide), VGVAPG hexapeptide, and a β-hairpin structure, in implicit water. All simulations were carried out with the OpenMM 7.01 simulation package[45] in an NVT ensemble at 300 K. Each system was simulated with the force field AMBER ff-14sb[46] and the GBSA model[47] for implicit solvent simulation. A Langevin thermostat has been applied to control the temperature and a Langevin leapfrog integrator[48] has been used to integrate Eq. (3) with a time step of 2 fs. Interactions beyond 1 nm are truncated. Metadynamics has been implemented through the plugin Plumed2.[6]

Girsanov reweighting has been efficiently implemented in OpenMM. We have estimated on the fly the terms of the stochastic and the Riemann integral that appear in Eq. (18), writing out the terms

$$I(a) = \sum_{i=1}^{3N} \sum_{k=(a-1)\cdot\text{nstxout}}^{a\cdot\text{nstxout}-1} \frac{\nabla_i U(\mathbf{r}_k)}{\sigma} \eta_k^i \sqrt{\Delta t} \tag{35}$$

and

$$R(a) = -\sum_{i=1}^{3N} \frac{1}{2} \sum_{k=(a-1)\cdot\text{nstxout}}^{a\cdot\text{nstxout}-1} \left(\frac{\nabla_i U(\mathbf{r}_k)}{\sigma} \right)^2 \Delta t \tag{36}$$

at the same frequency nstxout of the positions. After the simulation, we have reconstructed the complete probability ratio as

$$M_{\tau,\mathbf{x}}(\omega) = \exp\left\{ \sum_{a=1}^{A} I(a) + R(a) \right\}, \tag{37}$$

where $A \in \mathbb{N}$ such that $\tau = n\Delta t = A \cdot \text{nstxout} \cdot \Delta t$. To overcome numerical instabilities caused by Eq. (18), we have used the high precision arithmetic libraries The GNU Multiple Precision Arithmetic Library (GMPLib),[49] The GNU MPFR Library,[50] and Eigen.[51]

1. Alanine dipeptide

For alanine dipeptide, we ran a reference simulation of length 1 μs and we saved the positions every nstxout = 100 time steps, corresponding to 0.2 ps. The selected collective variables were the backbone torsion angles ϕ and ψ.

To test the *rerun* method, we have performed a well-tempered metadynamics with the parameters $W = 1.2$ kJ/mol, $\sigma_\phi = \sigma_\psi = 0.35$ rad, and $\tau_G = 0.2$ ps and bias factor $\lambda = \frac{T+\Delta T}{\Delta T} = 6.0$ of 155 ps. The Gaussian functions were stored on a squared grid with boundaries $-\pi$ and π and a grid spacing of 0.1 for both the torsion angles. We ran simulations of length 20 ns, biased by the metadynamics potential scaled by a factor 0.1, and build an MSM enforcing detailed balance, by discretizing both torsion angles in 36 bins, resulting in $36 \times 36 = 1296$ microstates. The lag-time used for the graphs of the eigenvectors was 100 ps, while the lag-time range for the graphs of the implied time scales was [0: 250] ps. This computational experiment was repeated 20 times to estimate the statistical uncertainty in the implied time scales.

To test the reweighting during the *build-up* phase, we applied a well-tempered metadynamics with the parameters $W = 0.0005$ kJ/mol, $\sigma_\phi = \sigma_\psi = 0.5$ rad, and $\tau_G = 0.2$ ps and bias factor $\lambda = 6.0$. The simulation length was 500 000 time steps corresponding to 100 ns. The MSM was built by discretizing both torsion angles in 36 bins, resulting in $36 \times 36 = 1296$ microstates and enforcing detailed balance. The lag-time used for the graphs of the eigenvectors was 100 ps, while the lag-time range for the graphs of the implied time scales was [0: 250] ps.

2. Hexapeptide Val-Gly-Val-Ala-Pro-Gly

The hexapeptide was obtained by cutting off the residues from 170 to 177 from the crystal structure of the Ca6 site mutant of Pro-SA-subtilisin[52] (PDB ID: 3VHQ). We have performed 20 unbiased replica simulations of length 500 ns to build a reference MSM.

The biased collective variable was the end-to-end distance of the peptide, i.e., the distance between the amine nitrogen of residue 1 and the carbonyl carbon of residue 6.

To test the *rerun* method, we have performed a metadynamics simulation of 2 ns, with the parameters $W = 0.1$ kJ/mol, $\sigma = 0.02$ nm, and $\tau_G = 0.2$ ps to build the bias. Afterward, we have created two sets of simulations biased by the metadynamics potential scaled by a factor 0.1. The first dataset was of ten simulations of length 40 ns and was used to build a single MSM. The second dataset was of ten simulations of length 100 ns and was used to build ten different MSMs.

To test the reweighting during the *build-up* phase, we applied a well-tempered metadynamics with the parameters $W = 0.0005$ kJ/mol, $\sigma = 0.02$ nm, and $\tau_G = 0.2$ ps and bias factor $\lambda = 6.0$. The simulation length was 100 ns.

In both the cases, the bias was stored on a one-dimensional grid between 0.2 nm and 2.2 nm, with a grid-spacing of 0.03 nm.

The MSM have been built, enforcing detailed balance, by discretizing the collective variable in 50 microstates. The lag-time used for the graphs of the eigenvectors was 200 ps, while the lag-time range for the graphs of the implied time scales was [0: 600] ps.

3. β-hairpin peptide

The β-hairpin structure has been extracted from the immunoglobulin binding domain of streptococcal protein G[53] (PDB ID: 1GB1). We have performed 48 simulations of length 350 ns (total simulation time of 16.8 μs).

Metadynamics has been realized by biasing the three hydrogen-bonds, named r_1, r_2, and r_3, connecting, respectively, the residues 2-15, 4-13, and 6-11. The parameters used to build the Gaussian functions are $W = 0.15$ kJ/mol, $\sigma = 0.1$ nm, and $\tau_G = 1$ ps and bias factor $\lambda = 6.0$. The simulation length was 50 ns.

The bias has been stored on a one-dimensional grid between 0.0 nm and 5.2 nm, with a grid-spacing of 0.03 nm. Afterward, we ran 35 parallel simulations of length 40 ns, biased by the metadynamics potential, scaled by a factor 0.1.

In the β-hairpin peptide, we did not use the metadynamics collective variables to construct the Markov state model but instead used the time-structure based Independent Component Analysis (tICA) method to estimate a two-dimensional subspace from the metadynamics rerun simulations. The input coordinates of for tICA were the time series of the minimal atom root-mean-square distances (minRMSD) to a reference structure, i.e., $|\mathbf{x}_i(t) - \mathbf{x}_{i,\mathrm{ref}}|$, where $i = 1, \ldots, N$ is the atom index and $\mathbf{x}_i(t)$ are the Cartesian coordinates of atom i at time t. As a reference structure, we chose the first frame of the trajectory, i.e., $\mathbf{x}_{i,\mathrm{ref}} = \mathbf{x}_i(0)$. The prefix "min" indicates that the atom root-mean-square distances have been measured after a rotational and translational fit has been applied to the structure at time t such that the overall RMSD between the two structures ($\mathrm{RMSD}_{\mathrm{tot}} = \frac{1}{N}\sqrt{\sum_{i=1}^{N}(\mathbf{x}_i(t) - \mathbf{x}_{i,\mathrm{ref}})^2}$) is minimized. Then, we used the k-means algorithm on the two time-independent coordinates with the largest eigenvalues of the tICA matrix and clustered the data in 50 states. The MSM has been stated on a Voronoi discretization which is generated by the 50 cluster centers, enforcing detailed balance. MSM tICA analysis[54,55] has been implement through the package PyEMMA.[56]

IV. RESULTS

A. One-dimensional system

We illustrate the metadynamics/Girsanov-reweighting method on a one-dimensional diffusion process and test how the strength of the bias influences the uncertainty in the reweighted implied time scales. The potential energy function [Eq. (33) and Fig. 1(a)] has three minima at $x = -1.12$, $x = 0.05$, and $x = 1.29$, separated by two barriers located at $x = -0.83$ and $x = 0.61$. The first left MSM eigenvector [Fig. 1(b)] is equal to the Boltzmann distribution. The second eigenvector represents

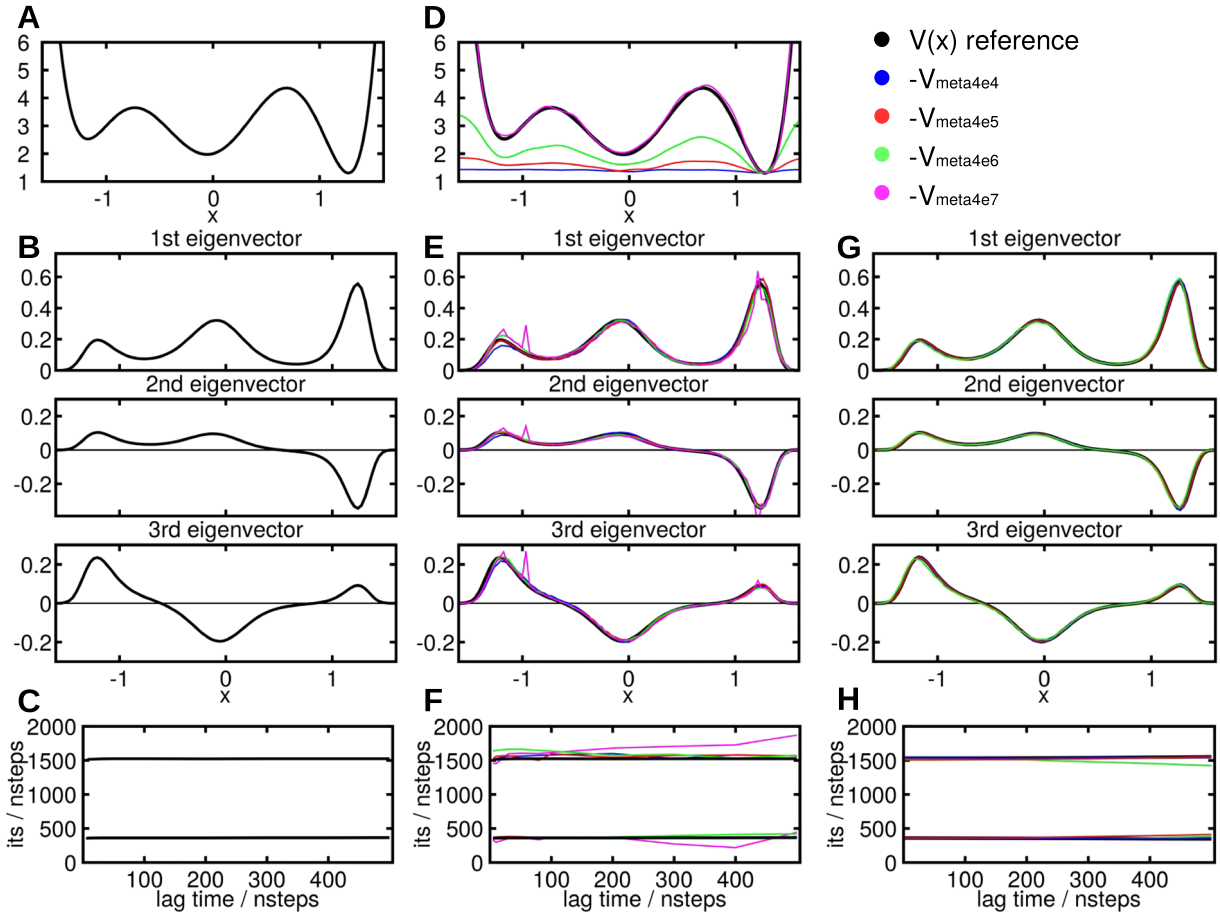

FIG. 1. One-dimensional diffusion process. (a) Potential energy function. (b) First three left MSM eigenvectors. (c) Implied time scales associated with the second and third eigenvector. (d) Free energy profile associated with the metadynamics potential. (e) First three left MSM eigenvectors—rerun. (f) Associated implied time scales—rerun. (g) First three left MSM eigenvectors—build-up. (h) Associated implied time scales—build-up.

the transition across the largest barrier at $x = 0.61$ with an associated implied time scale of 1530 time steps [Figs. 1(b) and 1(c)]. The third eigenvector represents the dynamic exchange between the middle well and the two wells on the sides with an associated implied time scale of 358 time steps [Figs. 1(b) and 1(c)].

The implied-time scale test in Fig. 1(c) shows that the two largest implied time scales of the system are constant, already at very small lag times. This indicates that for the chosen discretization, the discretization error is negligible and the MSM is an excellent approximation of the underlying diffusion process. Thus, any deviation from this reference solution in the metadynamics/Girsanov-reweighting results can be attributed to either statistical uncertainties or to errors due to the reweighting procedure.

Column "Direct simulation" in Table I gives an overview of the statistical uncertainties in the implied time scales for the direct simulation of the process with different simulation lengths: 4e4, 4e5, 4e6, and 4e7 time steps. As expected, increasing the length of the simulation reduces the statistical uncertainties. Note however that the shortest simulation with 4e4 time steps is more than an order of magnitude longer than the slowest implied time scale, yet the statistical uncertainty is still 20%. To decrease the uncertainty to less than 10%, a direct simulation of 4e5 time steps is needed. Due to this slow decrease of the statistical uncertainty with simulation length, statistical uncertainties of 20% and more are quite common in MSMs of molecular systems.[57]

1. Metadynamics/Girsanov reweighting on rerun simulations

We produced four metadynamics potentials V_{meta4e4}, V_{meta4e5}, V_{meta4e6}, and V_{meta4e7} by writing out $V_{\text{meta}}(s,t)$ [Eq. (5)] at t = 4e4, 4e5, 4e6, and 4e7 time steps. We chose a protocol in which the metadynamics potential is build up slowly such that the bias is distributed evenly across the x-axis. Figure 1(d) shows the inverted metadynamics potentials shifted by a constant such that all potentials coincide in the right-hand minimum of the potential energy surface, i.e., $-V_{\text{meta4e4}} + C_{\text{meta4e4}}$, $-V_{\text{meta4e5}} + C_{\text{meta4e5}}$, etc. In the limit of an infinitely long build-up phase, the sum of the metadynamics potential and reference potential should yield a constant potential, i.e., $V(x) + V_{\text{meta}}(x) = C_{\text{meta}}$. Then, up to a constant, the inverted metadynamics potential is equal to the reference potential, i.e., $-V_{\text{meta}}(x) + C_{\text{meta}} = V(x)$. Indeed, the inverted metadynamics potential for a build-up phase of t = 4e7 time steps is almost equal to the reference potential [magenta line in Fig. 1(d)]. The build-up phase of t = 4e4 time steps yields a very weak metadynamics potential, whereas build-up phases of t = 4e5 and t = 4e6 time steps yield metadynamics potentials of intermediate strength.

Each of the four metadynamics potentials was used as a constant bias for a new set of simulations. From these biased simulations, we obtained MSMs of the reference system using the Girsanov-reweighting method. For V_{meta4e4}, V_{meta4e5}, and V_{meta4e6}, the slowest MSM eigenfunctions are in excellent agreement with the reference solution [Fig. 1(e)]. For V_{meta4e7}, the eigenvectors deviate in the region of the first minimum in the potential energy surface from the reference solution. The implied time scale test [Fig. 1(f)] shows that for the reweighted MSMs (as for the reference MSM) the discretization error is negligible for a wide range of lag times. To investigate the statistical uncertainty of the implied time scales, we varied the simulation length of each of the biased simulations between 4e4 and 4e6 time steps (columns "V_{meta4e4}" to "V_{meta4e7}" in Table I). All of the estimates agree within the statistical uncertainty with the corresponding reference values. For each metadynamics potential, increasing the simulation length of the biased simulation decreases the statistical uncertainty, as would be expected.

However, increasing the bias does not necessarily decrease the statistical uncertainty. For a given simulation length, the biases V_{meta4e4} to V_{meta4e6} yield similar statistical uncertainties. By contrast, the largest bias V_{meta4e7} yields much higher statistical uncertainties. The reason for this is that the overall statistical uncertainty is a combination of the number of observed transitions and the variance of the estimator for the path probability ratio $M_{\tau,\mathbf{x}}(\omega)$ [Eq. (18)]. This variance increases with the gradient of the bias $\nabla_i U(\mathbf{r})$. Thus, a larger bias increases the number of observed transitions across the largest barrier in the reference system, which reduces the overall statistical uncertainty. But it also generates a larger gradient, which yields a larger variance in the estimator of $M_{\tau,\mathbf{x}}(\omega)$. In metadynamics/Girsanov-reweighting, these two effects need to be balanced when choosing the optimal bias. We suggest to use a metadynamics potential which partially compensates the free-energy profile along the collective variables. This can, for example, be achieved by rescaling a metadynamics potential. If the metadynamics potential is fully converged, this is equivalent to using a well-tempered metadynamics potential as a bias [Eq. (7)].

Table I seems to indicate that for a given simulation length, metadynamics/Girsanov-reweighting only marginally improves on the statistical uncertainties compared to the direct simulation. This seems to be an artifact of the one-dimensional system. For higher-dimensional systems, biasing a low-dimensional subspace considerably improved the accuracy of the results compared to the direct simulation.

2. Metadynamics/Girsanov reweighting during the build-up phase

Girsanov reweighting can also be applied to time-dependent biasing potentials. Thus, it can be applied directly to the *build-up phase* of the metadynamics potential. With this strategy, one can omit the subsequent rerun simulation. We reweighted build-up phases of t = 4e4, 4e5, and 4e6 time steps to obtain MSMs of the reference system. Both, the reweighted eigenvectors and implied time scales are in excellent agreement with the eigenvectors of the reference system [Fig. 1(g) and Table I]. The uncertainty of the implied time scales is reduced with respect to the direct simulations (Table I).

B. Free energy profile from the reweighted MSM

For a sufficiently long build-up phase, the metadynamics potential converges to minus the free energy F profile along the collective variable $V_{\text{meta}}(s, t \to \infty) = -F(s) + C$. In praxis, converging this estimate of the free energy profile

often requires very long build-up simulations. With metadynamics/Girsanov reweighting, the free energy profile can be obtained from an unconverged metadynamics potential. From a simulation with a constant, but not a fully converged metadynamics biasing potential or from the build-up phase of the metadynamics potential, an MSM of the reference system is constructed in the space of the collective variables using Girsanov reweighting. The first left eigenvector $l_0(s)$ of this MSM represents the Boltzmann distribution of the reference system,

$$l_0(s) = \pi(s) = \frac{1}{Z}\exp(-\beta F(s)). \tag{38}$$

Thus, the free energy profile can be obtained from

$$F(s) = -\frac{1}{\beta}\log(\pi(s)) + C = -\frac{1}{\beta}\log(l_0(s)) + C, \tag{39}$$

where C is an arbitrary constant. We tested this approach on the one-dimensional system with constant bias V_{meta4e6}. Because the position space of the system and the space of the collective variables are identical in this case, $F(s) = V(x)$. In Fig. 2, the red points represent the free energy profile obtained from the first eigenvector of the reweighted MSM, built on the metadynamics trajectory of length 4e6 time steps. The free energy profile obtained in this way fully matches with the expected potential energy function, and it considerably improved the free energy profile obtained by converting the corresponding metadynamics potential V_{meta4e6} (Fig. 2, green line).

C. Alanine dipeptide

As a first molecular test system for the metadynamics/Girsanov-reweighting method, we used alanine dipeptide (Ac-Ala-NHMe). We built an MSM of alanine dipeptide on the space of the backbone torsion angles ϕ and ψ from 1 μs direction simulation of alanine dipeptide in implicit water as a reference. Figure 4(a) (first row) shows the well-known dominant left MSM eigenvectors:[57] the first eigenvector is the stationary distribution with the typical conformational states (β region, L_α region, and R_α region); the second eigenvector represents the transition around the ϕ torsion angle corresponding to a kinetic exchange between the L_α-minimum and the α-helix and β-sheet minima; the third eigenvector represents the torsion around ψ corresponding to a kinetic exchange between the β region and the R_α-helical conformation. The associated time scales of the two transitions are $t_1 = 2.8$ ns and $t_2 = 27$ ps. The implied time scales are approximately constant, indicating that the MSM is a good approximation of the dynamics and that the discretization error is small [Fig. 4(b), green lines].

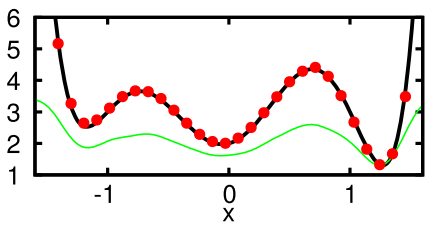

FIG. 2. One-dimensional diffusion process. (Black) Potential energy function; (green) free energy profile associated with V_{meta4e6}; (red dots) free energy profile obtained from the first eigenvector of a reweighted MSM built from a metadynamics simulation of 4e6 time steps.

1. Metadynamics/Girsanov reweighting on rerun simulations

Next, we performed a well-tempered metadynamics simulation of 155 ps, where we chose the ϕ and ψ backbone torsion angles as collective variables. Figure 3(a) shows the build-up of the metadynamics potential for $0 \le t \le 150$ ps. After 150 ps, the metadynamics potential is almost fully converged in the ϕ-torsion angle and reasonably well-converged in the ψ-torsion angle. Note that we use the metadynamics bias to speed up the sampling in the collective variables and not to measure the free-energy profile of the system. Thus, full convergence is not required. On the contrary, our experiments with the one-dimensional diffusion process had shown that a fully converged metadynamics potential causes a large variance in the estimator for path probability ratio $M_{\tau,\mathbf{x}}(\omega)$. We therefore rescaled the final metadynamics potential by a

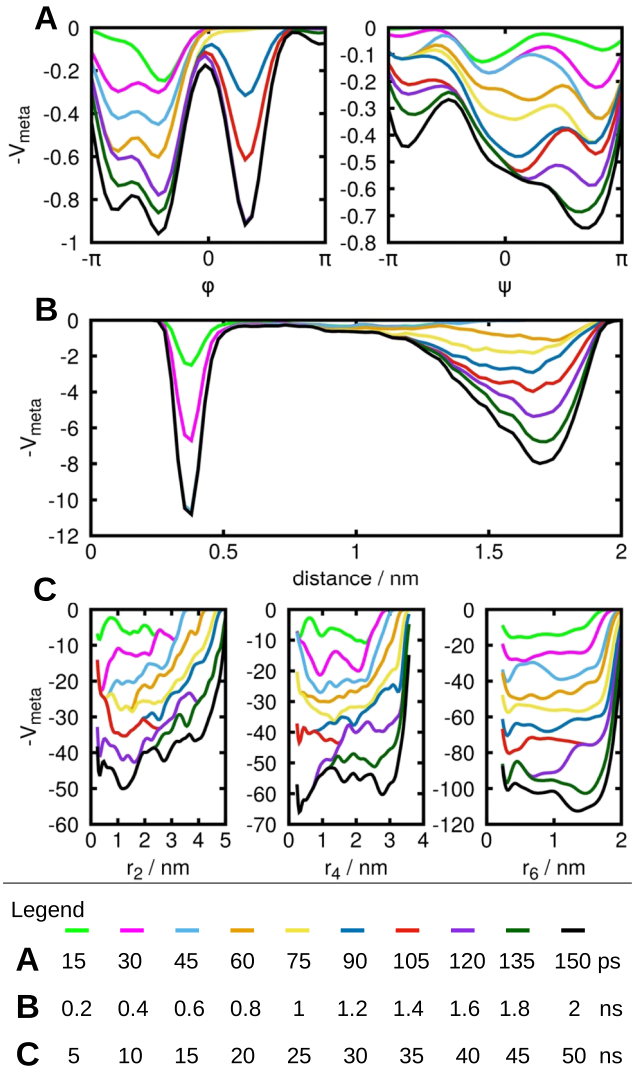

FIG. 3. Time evolution of the metadynamics potentials on the relevant coordinates. (a) Alanine dipeptide, potential every 15 ps, from 0 ps (green) to 150 ps (black). (b) VGVAPG hexapeptide, potential every 200 ps, from 0 ps (green) to 2000 ps (black). (c) β-hairpin, potential every 5 ns, from 0 ns (green) to 50 ns (black).

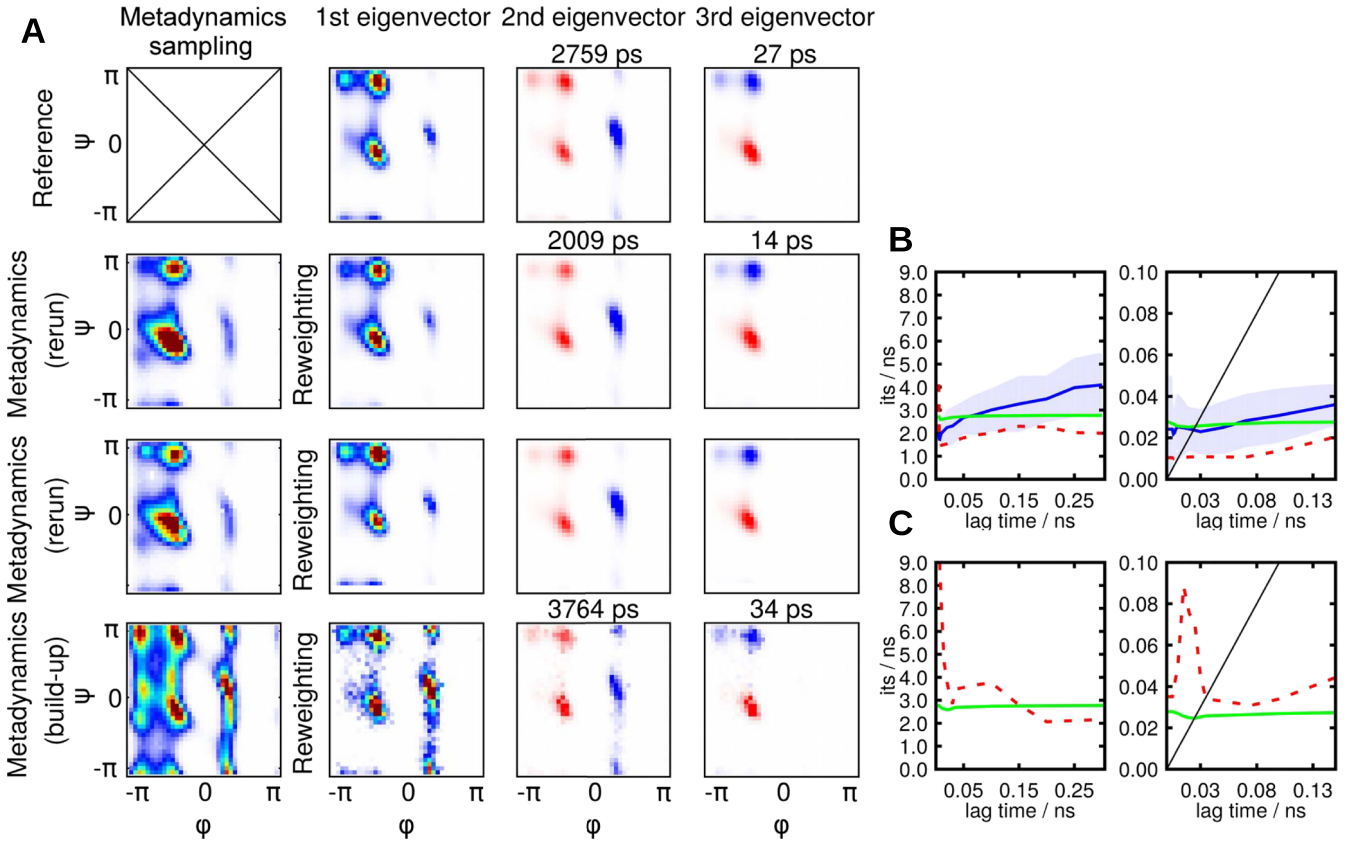

FIG. 4. Alanine dipeptide. (a) First three left MSM eigenvectors. 1st row: reference; 2nd and 3rd rows: reweighting after two independent rerun simulations; 4th row: reweighting during the build-up phase. (b) Implied time scales associated with the second and third eigenvector, rerun method. Green: reference, blue: average and standard deviation over twenty reweighted trajectories red: reweighting of a single trajectory. (c) Implied time scales associated with the second and third eigenvector, build-up method. Green: reference, red: reweighting.

factor 0.1 and produced rerun simulations of 20 ns each at this rescaled potential. This computer experiment was repeated twenty times to account for the statistical uncertainty in the reweighted MSMs. The Boltzmann distribution obtained from the biased simulations is shown in Fig. 4(a) for two different rerun simulations (second and third row, first column). The sampling of the $\phi - \psi$ space is increased [compared to Fig. 4(a), first row, second column], but the overall structure of the underlying reference potential is still clearly visible. To get an estimate of the speed-up of the rerun metadynamics simulation compared to the unbiased simulation, we estimated an MSM from the rerun trajectory without applying Girsanov reweighting. The slowest process is still the torsion around ϕ, but the associated time scale is now 780 ps (data not shown) compared to 2.8 ns in the unbiased simulation. Thus, although we used a moderate bias, we still gain a speed-up by roughly a factor of 4.

Reweighting the rerun metadynamics simulations yielded the dominant left eigenvectors shown in Fig. 4(a) (second and third rows) that are in excellent agreement with the eigenvectors of the reference system. However, the associated implied time scales from single trajectories or aggregated trajectories are lower and less smooth then the implied time scale plot of the direct simulation [Fig. 4(b), red dashed line]. The blue line in Fig. 4(b) shows the average and standard deviation over a set of twenty reweighted MSMs, which is in good agreement with the reference model. Thus, the metadynamics/Girsanov-reweighting yields the correct expected values and the non-smoothness of the implied time scale plots is due to statistical uncertainty, i.e., the variance of the estimator.

2. Metadynamics/Girsanov reweighting during the build-up phase

We also constructed reweighted MSMs from the build-up phase of the metadynamics potential. However, we chose a much smaller height W for the Gaussians [Eq. (5)] such that the growth of the metadynamics potential was slower than the slowest time scale of the unbiased system. The build-up simulation for the metadynamics potential was run for 100 ns. The corresponding sampling of the $\phi - \psi$ space is shown in Fig. 4(a) (third row, first column). Reweighting the build-up metadynamics simulations yielded the dominant left MSM eigenvectors shown in Fig. 4(a) (third row). They are in good agreement with the dominant MSM eigenvectors of the unbiased system; in particular, they correspond to the same conformational transitions. The population of the L_α-region is overestimated, and overall the eigenvectors are "noisier" than those estimated from the metadynamics rerun simulation. The estimated slowest implied time scale is 3.8 ns.

D. Hexapeptide Val-Gly-Val-Ala-Pro-Gly

As non-trivial molecular system for which we can still can generate a reference solution, we chose the hexapeptide

Val-Gly-Val-Ala-Pro-Gly (VGVAPG). The peptide has charged termini and its slowest process is the opening and closing of the salt-bridge between the positively charged N-terminus and the negatively charged C-terminus [Fig. 5(b)]. Correspondingly, we chose the distance between the nitrogen atom of the N-terminus and the carboxyl-carbon of the C-terminus as a collective variable for the metadynamics potential as well as for the MSM.

We performed 10 μs of direct simulations of VGVAPG and constructed a reference MSM. The dominant left MSM eigenvectors are shown as green lines in Figs. 5(c) and 5(e). The first eigenvector represents the Boltzmann distribution along the reaction coordinates, which has two maxima. When the hexapeptide is in the closed conformation, the distance between the nitrogen atom and the carbon atom is around 0.25 nm. When the hexapeptide is in the open conformation, the distance between the backbone termini varies between 0.6 and 1.8 nm. The slowest process is the exchange between these two conformations and is associated with an implied time scale of about 5 ns [Fig. 5(d), green line]. The second slowest process is the exchange between open but relatively compact conformations and conformations at the ends of the distance distribution, i.e., very extended conformations or closed conformations. It is associated with an implied time scale of about 1 ns.

1. Metadynamics/Girsanov reweighting on rerun simulations

We obtained an almost fully converged metadynamics potential after 2 ns of metadynamics build-up simulation [Fig. 3(b)]. As for the one-dimensional case and the alanine-dipeptide, a fully converged metadynamics potential is not the optimal bias for our purpose; thus, we rescaled the bias by a factor 0.1 [blue and green lines in Fig. 5(a)] and then we ran twenty biased simulations of 40 ns to 100 ns. The left eigenvectors of the reweighted MSMs built from single trajectories are in excellent agreement with the eigenvectors of the reference system [Fig. 5(c), respectively, black and green lines]. Also, the reweighted implied time scales, from a MSM built on an aggregated trajectory (400 ns in total), match those of the reference system for lag times of $\tau \leq 300$ ps [Fig. 5(d), red dashed line]. For larger lag times, they drift to large values. The likely reason for this behavior is that the variance of the estimator of $M_{\tau,\mathbf{x}}(\omega)$ increases with the length of τ, i.e., with the number of terms in the sum $\sum_{k=0}^{n} \ldots$ in Eq. (18). The blue line shows the average and standard deviation of a set of ten reweighted MSMs each estimated from a trajectory of 100 ns. As for alanine dipeptide, also here the expected value is in good agreement with the reference model.

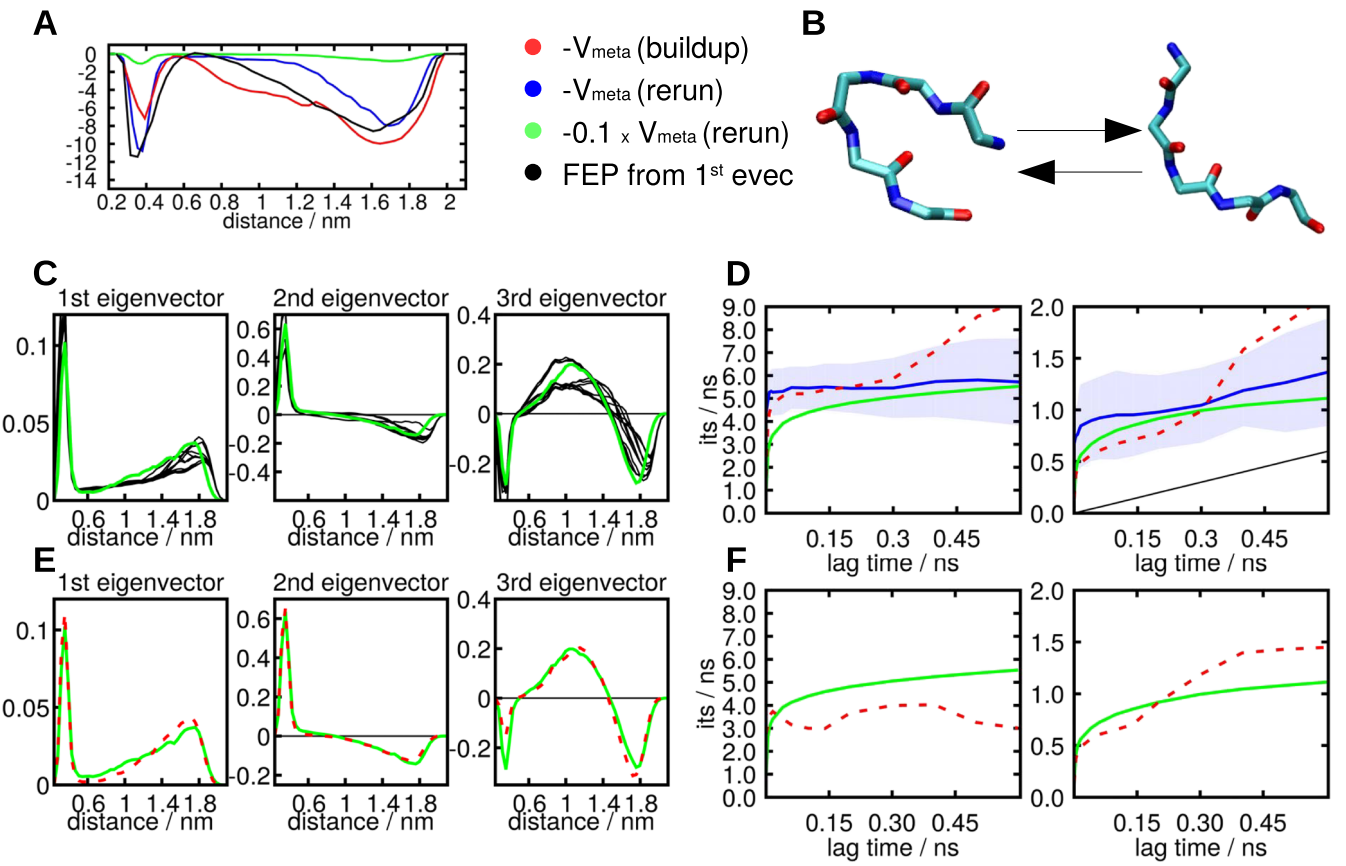

FIG. 5. Hexapeptide VGVAPG. (a) Free energy profiles. (b) Open and closed conformations of VGVAPG. (c) First three left MSM eigenvectors, rerun method. Green: reference, Black: reweighting of ten trajectories. (d) First two implied time scales, rerun method. Green: reference, blue: average over ten reweighted trajectories, red: reweighting of a single trajectory. (e) and (f) First three left MSM eigenvectors and associated implied time scales, build-up method. Green: reference, red: reweighting.

2. Metadynamics/Girsanov reweighting during the build-up phase

To reweight the build-up phase of the metadynamics potential, we chose a slow build-up mode: 100 ns of well-tempered metadynamics simulation. The free-energy profile associated with the final metadynamics potential is shown in red in Fig. 5(a). Girsanov reweighting of this simulation yields eigenvectors which are in very good agreement with the reference MSM [Fig. 5(e)]. Only the population of the closed conformation is slightly under-estimated. The associated implied time scales are in reasonable agreement with the reference solution. Interestingly, the implied time scale plots do not diverge for large lagtimes, as it was the case in the metadynamics/Girsanov-reweighting models of the rerun simulation.

E. β-hairpin peptide

As a last example, we chose the β-hairpin from the immunoglobulin binding domain of streptococcal protein G.[53] The rearrangement of the hydrogen-bond pattern in the β-hairpin is a very slow process. In 16.8 μs of direct simulation of the β-hairpin peptide, we did not observe a single opening event. We nonetheless analyzed the dynamics of this simulation by constructing a MSM in the tICA[54,55] space of the closed peptide (Fig. 6). The most frequent structures are a hairpin laying on a plane and a twisted hairpin along the axis of the H-bonds [Fig. 6(c)]. Thus the only kinetic exchange revealed by the direct simulation is torsion of the closed β-hairpin associated with a time scale of 2.5 ns [Fig. 6(b)]. Note that this MSM is not a reference solution since the slowest process—the rearrangement of the hydrogen bonds—has not been observed in the direct simulation.

1. Metadynamics/Girsanov reweighting on rerun simulations

We have built a metadynamics potential in the space of the distances r_2, r_4, and r_6 [Fig. 6(c)] by conducting 50 ns of well-tempered metadynamics. From the time evolution of the metadynamics potential on the relevant coordinates r_2 and r_4, we deduce that the bias is far from convergence [Fig. 3(c)]. Indeed, the metadynamics potential does not relax toward a constant function, but it is subjected to relevant fluctuations. Moreover, we cannot distinguish basins of metastable states. Only the potential on the distance r_6 relaxed toward an almost stable profile that suggests the existence of two metastable regions. On the other hand, during this build-up phase, the β-hairpin did not only open but in fact sampled completely extended structures. As before, we scaled the obtained potential by a factor of 0.1 and used it as a constant bias in 1.4 μs of metadynamics rerun simulations.

To gauge the sampling in this biased simulation, we constructed tICA-MSMs without reweighting [Fig. 7(a), top row]. Additionally to the planar hairpin (structure *A*) and the twisted hairpin (structure *B*), we found a half-open structure *C* in which the hydrogen bonds toward the end of the β-hairpin are broken [Fig. 7(d)]. The most extended conformation sampled by the metadynamics simulation is the structure *D* [Fig. 7(d)]. The eigenvectors of the reweighted MSMs are shown in the bottom line of Fig. 7(a). The extended structure *D* is now located on a barrier, while structures *A*, *B*, and *C* are still minima. The slowest process is the exchange between the half-open structure *D* and the two fully formed β-hairpin structures. The associated implied time scale is in the range of 100 ns to 1 μs [Fig. 7(b)]. The second slowest process is the exchange between the planar β-hairpin (structure *A*) and the twisted

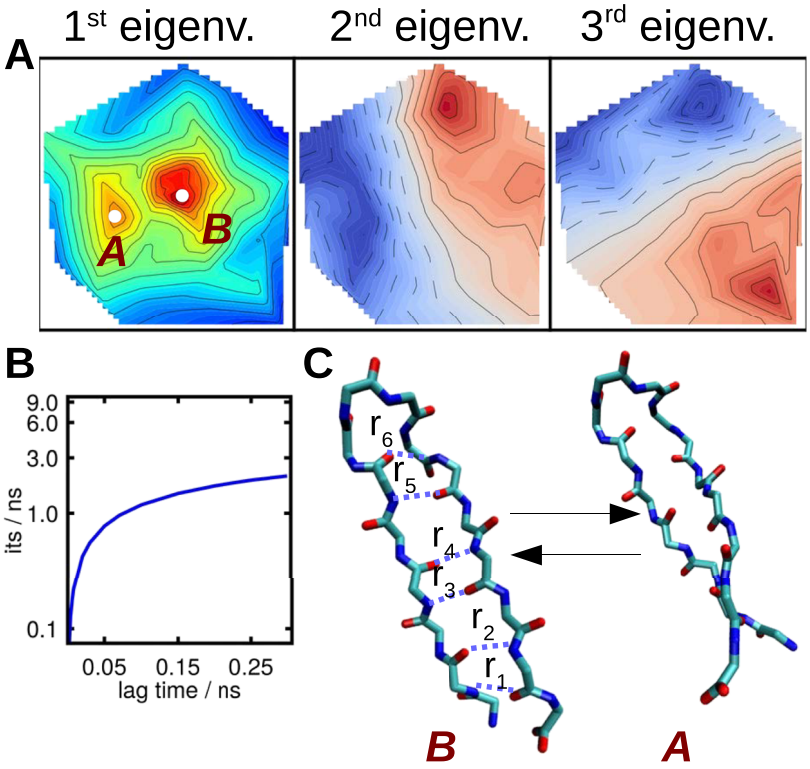

FIG. 6. β-hairpin, reference simulation. (a) First three tICA eigenvectors. (b) Implied time scale associated with the second tICA eigenvector. (c) Conformations A and B.

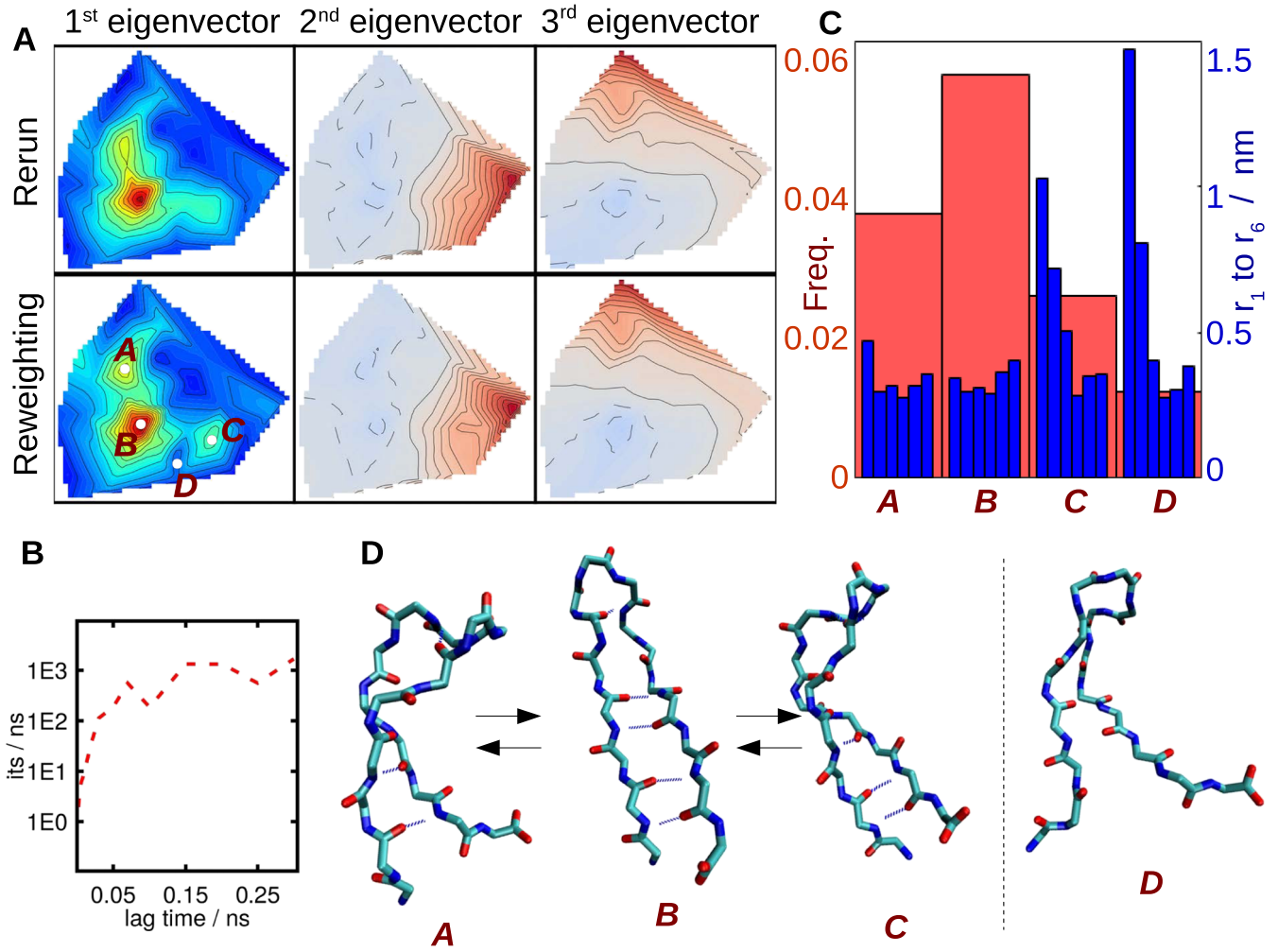

FIG. 7. β-hairpin, metadynamics simulation. (a) First three tICA eigenvectors. First row: rerun simulation, second row: rerun reweighting. (b) Implied time scale associated with the second eigenvector (reweighting). (c) Frequency of the structures A, B, C, and D (red, left axis); r_1 to r_6 distances in nm, blue columns from left to right (right axis). (d) Conformations A, B, C, and D.

hairpin (structure *B*). Figure 6(c) shows the reweighted relative population of the four structures (red bars) and the distance of the hydrogen-bonds r_1, r_2, r_3, r_4, r_5, and r_6 connecting, respectively, the residues 1-16, 2-15, 3-14, 4-13, 5-12, and 6-11 (blue bars).

V. DISCUSSION AND CONCLUSION

We have presented an application of the Girsanov reweighting scheme[38,39] to metadynamics,[3–6] to recover the correct dynamic properties of a molecular system from an enhanced sampling simulation. We have studied two possible strategies. In the first one, that we called *rerun*, we have first built a metadynamics bias, then we have rerun a simulation with the bias as a constant function and we applied the Girsanov reweighting on the trajectory produced by the second simulation. In the second strategy, we have applied the Girsanov reweighting directly during the *build up* phase of the metadynamics simulation, exploiting the validity of the Girsanov theorem for time-dependent perturbations. Both approaches recovered the correct unbiased dynamics for a wide range of systems.

The major difference between the Girsanov reweighting method and other dynamic reweighting methods[32–36] is that the probability density of each possible path of length τ connecting two points $\mathbf{x}_0 = \mathbf{x}$ and $\mathbf{x}_n = \mathbf{y}$ is reweighted and not the MSM transition probability as such. To reweight path probability densities, two prerequisites need to be fulfilled: (*i*) the equation of motion of the molecular systems needs to contain a normal random noise term (Langevin dynamics or Brownian dynamics); (*ii*) the gradient $\nabla_i U(\mathbf{r})$ and the random numbers need to be evaluated for each integration time step to obtain the path probability ratio $M_{\tau,\mathbf{x}}(\omega)$ [Eq. (18)]. The first condition is easily satisfied by using a Langevin thermostat to maintain the temperature. The random forces from this thermostat then serve as the random noise term.[39] The second condition, in principle, requires that the two properties are written to file for each integrator time step, which is not practical. However, if the bias is known for each time step of the simulation, as in metadynamics, two properties can be evaluated on the fly and interim results for $M_{\tau,\mathbf{x}}(\omega)$ are written to file at the same frequency as the coordinates. For this approach, the integrator of the MD simulation program needs to be modified

accordingly,[39] which is unproblematic in modular MD codes, such as OpenMM.[45]

Thus in practice, Girsanov reweighting is not an analysis method that can be used independent of the MD simulation, but it is intertwined with the MD simulation program. This slightly more complex set-up pays off in two ways. First, one does not need to assume that the system is in local equilibrium within a state B_i before it transitions to a state B_j. Second, Girsanov reweighting can be used to reweight arbitrary time-lagged correlation functions [Eq. (2)] and is not limited to transition counts. In particular, it can be used directly to reweight Markov models with advanced discretization methods, such as tICA,[54,55] variational Markov models[58,59] or core-set models.[60,61] Girsanov reweighting is closely related to the Onsager-Machlup action[62–66] and path reweighting methods for parallel tempering simulations.[29–31]

A critical assumption in metadynamics is that the collective variables, along which the metadynamics potential is built up, are aligned with the slow conformational transitions of the system such that the sampling in the degrees of freedom orthogonal to the collective variables is fast. This condition also needs to be fulfilled when applying Girsanov reweighting to a metadynamics simulation. In this contribution, we have therefore chosen systems with known collective variables. Once a suitable set of collective variables for the metadynamics simulations is known, it can be re-used as reaction coordinates for the discretization of the MSM, thus yielding MSMs with a small discretization error.

It is important to point out that the variance of the Girsanov reweighting estimator is a critical factor in the metadynamics/Girsanov reweighting method. It depends on the gradient of the bias, the length of the paths τ (i.e., the MSM lag time), and the number of paths of length τ (i.e., the sampling in the rerun simulations). The gradient of the bias can be controlled by scaling the metadynamics potential. Our results have shown that a fully converged metadynamics potential is usually not the optimal choice but that suitable balance between the speed-up of the simulation and suitable variance of the Girsanov reweighting estimator can be achieved by rescaling the potential by a factor of 0.1. The lag time τ can be decreased by reducing the MSM discretization error. The fact that a metadynamics simulation is only possible if a suitable set of collective variables is known simplifies the search for a good discretization drastically. The lag time could further be reduced by using advanced discretization methods[54,55,58–61] in the space of the collective variables. Finally, the length of the rerun simulation is limited by the available computer resources and by the obvious requirement that computational costs of a rerun simulation should be lower than those of a direct simulation.

In conclusion, metadynamics/Girsanov-reweighting is a valuable tool for obtaining dynamic properties, including MSMs and Markov models with advanced discretizations, from enhanced sampling simulations. Our results show that metadynamics/Girsanov-reweighting considerably decreases the computational costs of Markov models, and we expect that this will make Markov models amenable to a wider circle of scientists.

ACKNOWLEDGMENTS

This research has been funded by Deutsche Forschungsgemeinschaft (DFG) through Grant No. CRC 1114 *Scaling Cascades in Complex Systems*, B05 *Origin of the scaling cascades in protein dynamics*.

[1] Y. Sugita and Y. Okamoto, Chem. Phys. Lett. **329**, 261 (2000).
[2] M. Souaille and B. Roux, Comput. Phys. Commun. **135**, 40–57 (2001).
[3] T. Huber, A. Torda, and W. van Gunsteren, J. Comput.-Aided Mol. Des. **8**, 695 (1994).
[4] A. Laio and M. Parrinello, Proc. Natl. Acad. Sci. U. S. A. **99**, 12562 (2002).
[5] A. Barducci, G. Bussi, and M. Parrinello, Phys. Rev. Lett. **100**, 020603 (2008).
[6] M. Bonomi, D. Branduardi, C. Camilloni, and G. Bussi, Comput. Phys. Commun. **185**, 604 (2014).
[7] P. G. Bolhuis, D. Chandler, C. Dellago, and P. L. Geissler, Annu. Rev. Phys. Chem. **53**, 291 (2002).
[8] A. K. Faradjian and R. Elber, J. Chem. Phys. **120**, 10880 (2004).
[9] R. B. Best and G. Hummer, Proc. Natl. Acad. Sci. U. S. A. **102**, 6732 (2005).
[10] R. Hegger and G. Stock, J. Chem. Phys. **130**, 034106 (2009).
[11] P. Faccioli, A. Lonardi, and H. Orland, J. Chem. Phys. **133**, 045104 (2010).
[12] C. Schütte, A. Fischer, W. Huisinga, and P. Deuflhard, J. Comput. Phys. **151**, 146 (1999).
[13] C. Schütte, W. Huisinga, and P. Deuflhard, ZIB Report SC-99-36, 1999.
[14] P. Deuflhard, W. Huisinga, A. Fischer, and C. Schütte, Linear Algebra Appl. **315**, 39 (2000).
[15] W. C. Swope, J. W. Pitera, F. Suits, M. Pitman, M. Eleftheriou, B. G. Fitch, R. S. Germain, A. Rayshubski, T. J. C. Ward, Y. Zhestkov, and R. Zhou, J. Phys. Chem. B **108**, 6582 (2004).
[16] J. D. Chodera, N. Singhal, V. S. Pande, K. A. Dill, and W. C. Swope, J. Chem. Phys. **126**, 155101 (2007).
[17] N.-V. Buchete and G. Hummer, J. Phys. Chem. B **112**, 6057 (2008).
[18] J.-H. Prinz, H. Wu, M. Sarich, B. Keller, M. Senne, M. Held, J. D. Chodera, C. Schütte, and F. Noé, J. Chem. Phys. **134**, 174105 (2011).
[19] B. Keller, X. Daura, and W. F. Van Gunsteren, J. Chem. Phys. **132**, 074110 (2010).
[20] B. Keller, P. Hünenberger, and W. F. van Gunsteren, J. Chem. Theory Comput. **7**, 1032 (2011).
[21] V. A. Voelz, G. R. Bowman, K. A. Beauchamp, and V. S. Pande, J. Am. Chem. Soc. **132**, 1526 (2010).
[22] G. D. Fabritiis, N. Stanley, and S. Esteban-martín, Nat. Commun. **5**, 5272 (2014).
[23] G. R. Bowman, E. R. Bolin, K. M. Hart, B. C. Maguire, and S. Marqusee, Proc. Natl. Acad. Sci. U. S. A. **112**, 2734 (2015).
[24] N. Plattner and F. Noé, Nat. Commun. **6**, 7653 (2015).
[25] L. Zhang, I. C. Unarta, P. P.-H. Cheung, G. Wang, D. Wang, and X. Huang, Acc. Chem. Res. **49**, 698 (2016).
[26] J. Witek, B. G. Keller, M. Blatter, A. Meissner, T. Wagner, and S. Riniker, J. Chem. Inf. Model. **56**, 1547 (2016).
[27] M. Biswas, B. Lickert, and G. Stock, J. Chem. Phys. B **122**, 5508 (2018).
[28] G. R. Bowman, D. L. Ensign, and V. S. Pande, J. Chem. Theory Comput. **6**, 787–794 (2010).
[29] J.-H. Prinz, J. D. Chodera, V. S. Pande, W. C. Swope, J. C. Smith, and F. Noé, J. Chem. Phys. **134**, 244108 (2011).
[30] J. D. Chodera, W. C. Swope, F. Noé, J.-H. Prinz, M. R. Shirts, and V. S. Pande, J. Chem. Phys. **134**, 244107 (2011).
[31] D. D. L. Minh and J. D. Chodera, J. Chem. Phys. **131**, 134110 (2009).
[32] H. Wu, A. S. J. S. Mey, E. Rosta, and F. Noé, J. Chem. Phys. **141**, 214106 (2014).
[33] H. Wu, F. Paul, C. Wehmeyer, and F. Noé, Proc. Natl. Acad. Sci. U. S. A. **113**, E3221 (2016).
[34] E. Rosta and G. Hummer, J. Chem. Theory Comput. **11**, 276 (2014).
[35] P. Tiwary and M. Parrinello, Phys. Rev. Lett. **111**, 230602 (2013).
[36] R. Casasnovas, V. Limongelli, P. Tiwary, P. Carloni, and M. Parrinello, J. Am. Chem. Soc. **139**, 4780 (2017).
[37] B. Øksendal, *Stochastic Differential Equations: An Introduction with Applications*, 6th ed. (Springer Verlag, Berlin, 2003).
[38] C. Schütte, A. Nielsen, and M. Weber, Mol. Phys. **113**, 69 (2015).

[39]L. Donati, C. Hartmann, and B. G. Keller, J. Chem. Phys. **146**, 244112 (2017).
[40]J. Quer, L. Donati, and B. G. Keller, SIAM J. Sci. Comput. **40**, A653–A670 (2017).
[41]D. Branduardi, G. Bussi, and M. Parrinello, J. Chem. Theory Comput. **8**, 2247–2254 (2002).
[42]F. Marinelli, F. Pietrucci, A. Laio, and S. Piana, PLoS Comput. Biol. **5**, e1000452 (2009).
[43]M. Bonomi, A. Barducci, and M. Parrinello, J. Comput. Chem. **5**, 1 (2009).
[44]P. Tiwary and M. Parrinello, J. Phys. Chem. B **119**, 736–742 (2014).
[45]P. Eastman, M. S. Friedrichs, J. D. Chodera, R. J. Radmer, C. M. Bruns, J. P. Ku, K. A. Beauchamp, T. J. Lane, L.-P. Wang, D. Shukla, T. Tye, M. Houston, T. Stich, C. Klein, M. R. Shirts, and V. S. Pande, J. Chem. Theory Comput. **9**, 461 (2013).
[46]J. A. Maier, C. Martinez, K. Kasavajhala, L. Wickstrom, K. E. Hauser, and C. Simmerling, J. Chem. Theory Comput. **11**, 3696 (2015).
[47]A. Onufriev, D. Bashford, and D. A. Case, Proteins **55**, 383 (2004).
[48]J. A. Izaguirre, C. R. Sweet, and V. S. Pande, Pac. Symp. Biocomput. **15**, 240 (2010).
[49]T. Granlund and GMP Development Team, *GNU MP: The GNU Multiple Precision Arithmetic Library*, 5th ed. (Free Software Foundation, 2012), http://gmplib.org/.
[50]L. Fousse, G. Hanrot, V. Lefèvre, P. Pélissier, and P. Zimmermann, ACM Trans. Math. Software **33**, 13:1 (2007).
[51]G. Guennebaud, J. Benoît *et al.*, Eigen v3, http://eigen.tuxfamily.org, 2010.
[52]R. Uehara, Y. Takeuchi, S. Tanaka, K. Takano, Y. Koga, and S. Kanaya, Biochemistry **51**, 5369 (2012).
[53]A. Gronenborn, D. Filpula, N. Essig, A. Achari, M. Whitlow, P. Wingfield, and G. Clore, Science **253**(5020), 657 (1991).
[54]C. R. Schwantes and V. S. Pande, J. Chem. Theory Comput. **9**, 2000 (2013).
[55]G. Perez-Hernandez, T. Paul Giorgino, G. De Fabritiis, and F. Noé, J. Chem. Phys. **139**, 015102 (2013).
[56]M. K. Scherer, B. Trendelkamp-Schroer, F. Paul, G. Pérez-Hernández, M. Hoffmann, N. Plattner, C. Wehmeyer, J.-H. Prinz, and F. Noé, J. Chem. Theory Comput. **11**, 5525 (2015).
[57]F. Vitalini, A. S. J. S. Mey, F. Noé, B. G. Keller, F. Vitalini, A. S. J. S. Mey, F. Noé, and B. G. Keller, J. Chem. Phys. **142**, 084101 (2015).
[58]F. Nüske, B. Keller, G. Perez-Hernandez, A. S. J. S. Mey, and F. Noé, J. Chem. Theory Comput. **10**, 1739 (2014).
[59]F. Vitalini, F. Noé, and B. G. Keller, J. Chem. Theory Comput. **11**, 3992 (2015).
[60]C. Schütte, F. Noé, J. Lu, M. Sarich, and E. Vanden-Eijnden, J. Chem. Phys. **134**, 204105 (2011).
[61]O. Lemke and B. G. Keller, J. Chem. Phys. **145**, 164104 (2016).
[62]L. Onsager and S. Machlup, Phys. Rev. **91**, 1501 (1953).
[63]T. B. Woolf, Chem. Phys. Lett. **289**, 433 (1998).
[64]D. M. Zuckerman and T. B. Woolf, J. Chem. Phys. **111**, 9475 (1999).
[65]D. M. Zuckerman and T. B. Woolf, Phys. Rev. E **63**, 016702 (2000).
[66]C. Xing and I. Andricioaei, J. Chem. Phys. **124**, 034110 (2006).

Chapter 7

An automatic adaptive importance sampling algorithm for Molecular Dynamics in reaction coordinates

Molecular systems are characterized by metastability and dynamical quantities like exit times (i.e. the time necessary to leave a metastable state) and probabilities to jump between a minimum to another one, are typically estimated by numerical experiments, i.e. performing several simulations and estimating the interested quantities as arithmetic averages. Moreover, as for MSMs, the quality of the estimators depends on the quality of the sampling. Thus, a system characterized by high barriers is difficult to study by MC approach. This approach is not only time consuming, but the results of the analysis are affected by a significant error.

In collaboration with Jannes Quer, from Zuse Institute Berlin, we propose a new algorithm that improves the MC technique, reducing the computational cost and the measurement error [81]. The algorithm relies on two existing methods: i) metadynamics, that is used to drive the system out of the metastable regions o the phase space; ii) Girsanov reweighting, which can be used to reweight path ensembles averages like exit times. The novelty, compared to the previous chapter, is that the reweighting is performed on different quantities than time-lagged correlation functions.

Here we show that, Girsanov theorem not only can be used to reweight correctly path ensemble averages, but that when the bias is built by metadynamics simulation, the error on the measure reduces respect to standard MC simulations. Thus our algorithm permits to obtain the same results that we would obtain with a classic MC approach, but with a significant variance reduction. Furthermore, the use of metadynamics accelerates the exploration of the phase space. This brings to a relevant reduction of the computational cost, because shorter simulations are sufficient to calculate the estimators.

The algorithm is divided in two steps. Firstly, we use metadynamics to construct the free energy profile of the considered metastable region, stopping the simulation when the system is out of the well. Afterward we run a second simulation, with the Hamiltonian perturbed by the bias constructed during the metadynamics simulation, starting at the bottom of the considered well. In this way, the metastable region becomes a flat region, where the gradient of the potential energy function is almost zero and the system drives out quickly from the initial metastable region into the next well. We repeat this biased simulation a significant number of times, in order to be able to estimate the observable functions as arithmetic averages. Of course, the estimators thus calculated, are affected by the bias and do not represent the correct values for the unbiased system. Because

the considered estimators can be interpreted as path ensemble averages respect to a path probability measure, we can exploit the Girsanov theorem to make a dynamical reweighting.

I contributed to the paper taking part to the development of the idea and the algorithm, then I carried out the simulation and the analysis of the Alanine dipeptide projected on the backbone torsion angles ϕ and ψ, Afterward I carried out a benchmark test that shows how the variance of the estimators depends on the choice of metadynamics parameters.

https://doi.org/10.1137/17M1124772

SIAM J. SCI. COMPUT.
Vol. 40, No. 2, pp. A653–A670

AN AUTOMATIC ADAPTIVE IMPORTANCE SAMPLING ALGORITHM FOR MOLECULAR DYNAMICS IN REACTION COORDINATES*

J. QUER†, L. DONATI‡, B. G. KELLER‡, AND M. WEBER†

Abstract. In this article, we propose an adaptive importance sampling scheme for dynamical quantities of complex systems, which are metastable. The main idea of this article is to combine metadynamics, an algorithm from molecular dynamics simulation, with Girsanov's theorem, a result from stochastic analysis. With an assimilated version of the metadynamics algorithm we build a bias to reduce the metastability in the dynamical system. To correct the sampling of the modified system we apply a reweighting strategy based on Girsanov's theorem. The proposed algorithm has two advantages compared to a standard estimator of dynamic quantities: first, it is possible to produce estimators with a lower variance, and second, we speed up the generation of a typical sample.

Key words. adaptive importance sampling, molecular dynamics, metastability, variance reduction, nonequilibrium sampling, metadynamics, Girsanov

AMS subject classifications. 60G99, 68U20, 65C35, 65C60

DOI. 10.1137/17M1124772

1. Introduction and motivation. In molecular dynamics (MD) simulation, dynamical quantities like exit times or transition probabilities play an important role. These quantities of interest can be used to characterize the stability of a certain conformation, which is of importance in, for instance, computational drug design [38]. Often these observables are estimated by averaging over long-term trajectories of some continuous space-time model, which describes the molecular movement, e.g., an overdamped Langevin equation. The sampling of dynamical quantities by MD simulations is often difficult since high barriers impact the system, and thus the sampling of ergodic trajectories is very time consuming. Thus, a molecular system is characterized by metastability, and the transitions between metastable states are rare events. Metastability arises from the multimodality of the stationary distribution of the dynamical system; cf. [23]. For this reason it is often modeled by a Markov jump process, which describes the jump from one metastable state to another; cf. [24, 31]. The estimation of dynamical quantities in such systems can be performed by ensemble averages. We will call these estimators Monte Carlo (MC) estimators. The MC approach for sampling these dynamical quantities is computationally costly and is affected by high variance of the estimator. This problem is known in the computational chemistry community as "the sampling problem."

In this article, we propose a new method to reduce the variance of dynamical

*Submitted to the journal's Methods and Algorithms for Scientific Computing section April 7, 2017; accepted for publication (in revised form) November 17, 2017; published electronically March 1, 2018.

http://www.siam.org/journals/sisc/40-2/M112477.html

Funding: This research has been funded by Deutsche Forschungsgemeinschaft (DFG) through grant CRC 1114 "Scaling Cascades in Complex Systems," A05 ("Probing Scales in Equilibrated Systems by Optimal Nonequilibrium Forcing"), and B05 ("Origin of the Scaling Cascades in Protein Dynamics").

†Zuse Institute Berlin, Berlin, 14195, Germany (quer@zib.de, weber@zib.de, www.zib.de/members/quer).

‡Freie Universität Berlin Department of Biology, Chemistry, Pharmacy, Berlin, 14195, Germany (ldonati@zedat.fu-berlin.de, bettina.keller@fu-berlin.de).

quantities estimated by MD simulations. To achieve this, we combine two strategies: In the first step, we use metadynamics to bias the initial potential energy function, and in the second step, we reweight the estimator of the quantity of interest using Girsanov's theorem.

Several methods have been suggested in the literature in order to solve the sampling problem. Many of these methods are based on ideas from importance sampling [29] or use other enhanced sampling approaches [3]. To sample stationary distributions or free energy profiles of dynamical systems that are characterized by metastability, different methods like metadynamics [21], umbrella sampling [35], adaptive biasing force [9], and Boltzmann reweighting [4] have been proposed. These methods are not designed for the sampling of dynamical quantities, and extending them for this purpose, therefore, is not straightforward.

The methods that have been designed for the sampling of dynamical quantities can be divided into two classes. The first class comprises splitting methods like forward flux sampling [2], adaptive multilevel splitting [6], or milestoning [15]. The second class comprises reweighting methods, sometimes called biased Brownian dynamics, like [10, 40]. Since our approach is a reweighting method we will not discuss splitting methods but refer the reader to [1] and the references therein for a detailed discussion.

Due to the interdisciplinary character of MD, several reweighting methods motivated by physical or mathematical arguments have been proposed. For instance, a physically motivated reweighting technique for the reconstruction of time scales has been proposed in [34]. The authors suggest a method to correct times scales from a metadynamics simulation. For the correction of the time scale, transition path theory is used and the derivation is based on a heuristic argument, which requires that the saddle point is not perturbed.

A mathematical approach to the variance reduction of MC methods was proposed by Milstein in [27]. The author proposes to use Girsanov's theorem and add an additional drift to the stochastic differential equation (SDE). The existence of an optimal drift is derived. This optimal bias satisfies a Bellman equation. The variance of this estimator is zero. Likewise, this work shows the difficulty of constructing a proper sampling scheme. Since the optimal bias is a solution to a nonlinear partial differential equation (PDE), the calculation is very costly or even impossible in high dimensions.

In general the reweighting strategy given by Girsanov's theorem always offers an unbiased estimator for any change of drift. Using this property one can build a suboptimal bias with lower computational cost to achieve the variance reduction.

Motivated by the connection between optimal control and importance sampling, different strategies for a general setting have been suggested by [11, 13, 14]. The authors derive importance sampling schemes for different assumptions based on the Hamilton–Jacobi–Bellman (HJB) equation (continuous version of Bellman's equation) in the large deviation context. These ideas have been developed for the application in MD as well; see [37]. In their work, the authors proposed a technique based on the solution of a deterministic control problem associated with the sampling problem.

Another strategy for situations occurring in MD simulations has been studied in [12]. The authors develop an importance sampling scheme for applications with so-called resting points. The numerical examples of the article show that the importance sampling scheme achieves better results when the resting point is taken into account. In order to build such importance sampling schemes, a lot of knowledge about the dynamical system is necessary, but finally this results in a better variance reduction. In [16], an optimization strategy for building the optimal bias was proposed. To derive

the optimization problem, the solution of the HJB equation is projected to a space of parametrized ansatz functions. Then a stochastic optimization problem needs to be solved to find the best approximation. The main challenge in this approach is to place the ansatz functions such that the algorithm converges quickly. In [33], the author develops a performance measure for an importance sampler related to small noise diffusion processes. This offers the possibility of comparing the different importance sampling schemes analytically.

In [40], an algorithm was proposed to overcome the problem of high dimensions. Motivated by the work of Milstein, the authors developed a variance reduction scheme restricted to reaction coordinates. They used an artificial drift to reduce the variance. The correction terms to reweight the results from the biased sampling, arising due to the artificial drift, are interpreted as weights. Hence, these weights are used to control the influence of different trajectories and are updated according to a stochastic rule, which is essentially the same as the Girsanov weight; cf. [28]. Based on these weights, the authors introduce a split-and-kill strategy of trajectories in order to have a proper sampling of the state space. The bias is placed in some reaction coordinates, which project the dynamics into some manifold of interest. In order to find the optimal bias in these reaction coordinates, they minimize a variational Smoluchowski equation. This expression is written in integral form and uses the stationary density distribution. Thus, the stationary distribution needs to be known a priori or has to be sampled by numerical simulation.

Our approach is distinguished from the above approaches in the following way. We do not try to find the optimal bias because it is computationally too expensive. Instead, we use the fact that the reweighted estimator is unbiased and construct a suboptimal bias, which will lead to a reasonable variance reduction. We use the a priori knowledge that the considered dynamic system is metastable, and this is why the metadynamics algorithm is used to construct the bias. For this, we need an additional sampling but do not have to know the stationary distribution in advance. Moreover, while the authors of [40] considered a very general approach of variance reduction for solving PDEs by path integrals of SDEs, we focus on the special case of metastable dynamical systems with a high energy barrier.

The article is structured as follows: First, we will give a short introduction into importance sampling and the main result from stochastic analysis based on Girsanov's theorem. Then we are going to review the metadynamics algorithm and show how we assimilate the algorithm for our needs. We will prove that Girsanov's theorem can be applied in the considered strategy. In the end we are going to apply our method to different numerical examples followed by a summary and an outlook.

2. Theory. In this section we present the two main ingredients of our algorithm. In the first part, we briefly review the main idea behind importance sampling, supplemented with some necessary tools from stochastic analysis. The second part is a short introduction into metadynamics and how the algorithm is assimilated.

2.1. Importance sampling. In this article we consider a diffusion process $X_t \in \mathbb{R}^n$ governed by the SDE

$$dX_t = -\nabla V(X_t)dt + \sqrt{2\beta^{-1}}dB_t, \quad X_0 = x, \tag{1}$$

where X_t is the state of the system at time $t \geq 0$, $V : \mathbb{R}^n \to \mathbb{R}$ is a sufficiently smooth (e.g., $\mathcal{C}^\infty$) potential energy function, $\beta > 0$ is an arbitrary scaling factor for the noise, often called the inverse temperature, and B_t is a standard n-dimensional Brownian

motion with respect to the probability measure $\mathbb{P}$ on the probability space $(\Omega, \mathbb{P}, \mathcal{F})$. Moreover we assume that the process is trapped in a metastable region $\mathcal{S} \subset \mathbb{R}^n$, which is an open and bounded set with a smooth boundary. Further, we define a target set $\mathcal{T}$ that is an open and bounded set with a smooth boundary as well. Finally, we define the stopping time $\tau = \inf\{t > 0 : X_t \in \mathcal{T}\}$ to be the first time that the process (1) hits the target set $\mathcal{T}$, e.g., when a dihedral angle of a biomolecule reaches a certain value. The presented theory here can be generalized to a state-dependent function prior to the Brownian motion; cf. [28]. But here we will consider the constant case only.

We are interested in expectations of the form

$$\mathbb{E}[e^{-\beta g(X_{0:T})}], \tag{2}$$

where $X_{0:T}$ is a trajectory of (1) until some finite time T and g is some functional on $\mathcal{C}([0,T] : \mathbb{R}^n)$. We consider these types of quantities because they give us information in terms of the temperature of the system. However, a generalization to other quantities expressed as expectations is possible. As pointed out by [37], an interesting case of this quantity arises when $g = 0$ for $X_{0:T} \in \mathcal{A} \subset \mathcal{C}([0,T], \mathbb{R}^n)$ and $g = \infty$ otherwise. Then (2) becomes

$$\mathbb{P}[X_{0:T} \in \mathcal{A}]. \tag{3}$$

Expectations like (2) are integrals over the entire state space and cannot be calculated analytically. But, given an ensemble of paths, they can be approximated by an unbiased MC estimator

$$I = \mathbb{E}[e^{-\beta g(X_{0:T})}] = \lim_{N\to\infty} \frac{1}{N} \sum_{i=1}^{N} e^{-\beta g(X^i_{0:T})}, \tag{4}$$

where $X^i_{0:T}$, $i \in [1, \dots, N]$, are independent paths of length T, all starting at the same point $X_0 = x \in \mathbb{R}^n$, produced, for example, by numerical integration of (1). This estimator is unbiased. Its variance is given by

$$\mathrm{Var}(I) = \frac{1}{N}(\mathbb{E}[e^{-2\beta g(X_{0:T})}] - \mathbb{E}[e^{-\beta g(X_{0:T})}]^2). \tag{5}$$

The relative error is defined by

$$r(I) = \frac{\sqrt{(\mathrm{Var}(I))}}{\mathbb{E}[I]} = \frac{1}{\sqrt{N}} \sqrt{\frac{\mathbb{E}[e^{-2\beta g(X_{0:T})}]}{\mathbb{E}[e^{-\beta g(X_{0:T})}]^2} - 1}; \tag{6}$$

cf. [37].

To build an importance sampling scheme for a metastable diffusion process, one has to decrease the depth of the minima, which cause the metastable behavior. Since the time evolution of the SDE (1) with a low temperature (i.e., large β) is a negative gradient descent perturbed by some Brownian motion, the process X_t will stay in the region around the minimum of V. By filling the metastable region in $V(\cdot)$, we change the metastable behavior, and thus the sampling of the desired quantity of interest gets easier. But this perturbation changes the underlying stationary distribution as well. To compensate for this perturbation, we use Girsanov's theorem to reweight (or correct) the estimators. Another interpretation of this theorem is that it offers

a way to sample equilibrium quantities of some dynamics by sampling the dynamics out of equilibrium. We can construct a bias, which influences the mutimodality of the stationary distribution in such a way that low probability regions are more probable or high barriers are easier to cross. The main advantage of Girsanov's theorem is that it is not necessary to know the stationary distribution a priori.

Next we state the proposition that gives us the correction term for the quantity of interest sampled in a perturbed system. The proposition follows directly from Girsanov's theorem (cf. [28, p. 155]).

PROPOSITION 1. *Let $X_t \in \mathbb{R}^n$ and $Y_t \in \mathbb{R}^n$ be an Itô diffusion and an Itô process of the form*

$$dX_t = b(X_t)dt + \sigma(X_t)dB_t, \quad t \leq T, \quad X_0 = x, \tag{7}$$

$$dY_t = (u(Y_t) + b(Y_t))dt + \sigma(Y_t)dB_t, \quad t \leq T, \quad Y_0 = x, \tag{8}$$

where $b : \mathbb{R}^n \to \mathbb{R}^n$ and $\sigma : \mathbb{R}^n \to \mathbb{R}^{n\times m}$ satisfy some Lipschitz condition such that we can guarantee uniqueness and existence of the solution and the time $T < \infty$. Furthermore, we define for an adapted measurable process $a : \mathbb{R}^n \to \mathbb{R}$ the stochastic process

$$M_t = \exp\left(-\int_0^t a(Y_s)dB_s - \frac{1}{2}\int_0^t a(Y_s)^2 ds\right) \tag{9}$$

for all $t \in [0, T]$ and $\sigma(Y_s)a(Y_s) = u(Y_s)$. Then, given that Novikov's condition

$$\mathbb{E}\left[\exp\left(\frac{1}{2}\int_0^T |a(Y_t)|^2 dt\right)\right] < \infty \tag{10}$$

holds, for any function $f \in \mathcal{C}_0(\mathbb{R}^n)$ and any stopping time τ adapted to the filtration $\mathcal{F}_T$ (the filtration associated to the Brownian motion B in (7) and (8)) we have

$$\mathbb{E}^x_{\mathbb{P}}[f(X_{0:\tau})] = \mathbb{E}^x_{\mathbb{P}}[M_\tau f(Y_{0:\tau})]. \tag{11}$$

Proof. We are going to give a short sketch of the proof here for completeness.

We define a new probability measure

$$d\mathbb{Q} := M_T d\mathbb{P} \quad \text{on } \mathcal{F}_T.$$

Then

$$\hat{B}_t := \int_0^t a(Y_s)ds + B_t, \quad t \leq T,$$

is a Brownian motion with respect to $\mathbb{Q}$, and in terms of $\hat{B}_t$ the process Y_t can be represented by

$$dY_t = b(Y_t)dt + \sigma(Y_t)\hat{B}_t, \quad Y_0 = x,\ t \leq T.$$

Therefore, the $\mathbb{Q}$-law of Y_t with $Y_0 = x$ is the same as the $\mathbb{P}$-law of X_t with $X_0 = x$ for $t \leq T$. This follows directly from the weak uniqueness of solutions of SDEs (see [28, p. 71, Lemma 5.3.1]). Due to the absolute continuity of the two probability measures $\mathbb{Q}$ and $\mathbb{P}$, we can use a change of measure to rewrite the expectation. Thus, for any function $f \in \mathcal{C}_0(\mathbb{R}^n)$ and any stopping time $\tau \leq T$ which is adapted to the filtration $\mathcal{F}_T$ we can write

$$\mathbb{E}_{\mathbb{P}}[f(X_{0:\tau})] = \mathbb{E}_{\mathbb{Q}}[f(Y_{0:\tau})] = \mathbb{E}_{\mathbb{P}}[M_\tau f(Y_{0:\tau})],$$

which gives us the desired result. ∎

By setting $b(\cdot) = -\nabla V(\cdot)$ and $\sigma = \sqrt{2\beta^{-1}}$ we have the metastable SDE model (1) and can use Proposition 1 to reduce the metastability in the dynamical system.

Furthermore, it is possible to derive another reweighting formula (9) if $u(\cdot)$ is of gradient form ($u(\cdot) = \nabla v(\cdot)$). Then one can use Itô's formula and calculate another expression for the stochastic integral term in (9), as it done in [24, p. 838]. Applying Itô's formula to v, we get

$$\begin{aligned} v(Y_T) - v(Y_0) = \int_0^T \frac{1}{\beta}\nabla^2 v(Y_s) - \nabla V(Y_s)\cdot\nabla v(Y_s) + |\nabla v(Y_s)|^2 ds \\ + \sqrt{2\beta^{-1}}\int_0^T \nabla v(Y_s) dB_s, \end{aligned} \tag{12}$$

where ∇^2 is the Laplacian. Now rearranging terms, we get a new expression for the stochastic integral, which can be used in (9) to derive

$$\begin{aligned} M_T = \exp\Bigg(&\frac{1}{2\beta^{-1}}(v(Y_T) - v(Y_0)) \\ &+ \frac{1}{2\beta^{-1}}\int_0^T \Big(\nabla V(Y_s)\cdot\nabla v(Y_s) + \frac{1}{2}|\nabla v(Y_s)|^2 - \beta^{-1}\nabla^2 v(Y_s) ds\Big)\Bigg). \end{aligned} \tag{13}$$

This expression is still stochastic because Y_s is a stochastic process. From the first point of view it seems that this term could be more easily treated numerically compared to the stochastic integral. We will investigate this in the example section.

Focusing on importance sampling, we can use Proposition 1 to rewrite the estimator (4) as

$$\hat{I} = \frac{1}{N}\sum_{i=1}^{N} e^{-\beta g(Y^i_{0:\tau})} M^i_{0:\tau}, \tag{14}$$

where $Y^i_{0:\tau}$ and $M^i_{0:\tau}$ are independent samples from (8) and (9). For $a(Y_t)$ satisfying Novikov's condition and a bounded stopping time, M_τ is a continuous bounded local martingale which yields $\mathbb{E}[M_t] = 1,\ t \in [0, \tau]$. Then the importance sampling estimator is an unbiased estimator with expectation

$$\mathbb{E}[\hat{I}] = \mathbb{E}[e^{-\beta g(X_{0:\tau})}]; \tag{15}$$

cf. [24]. Following [37], we know that the relative error of this estimator is

$$r(\hat{I}) := \frac{1}{\sqrt{N}}\sqrt{\frac{\mathbb{E}[e^{-2\beta g(Y_{0:\tau})}(M_{0:\tau})^2]}{\mathbb{E}[e^{-\beta g(X_{0:\tau})}]^2} - 1}. \tag{16}$$

In order to control the relative error, we have to control the ratio

$$R(\hat{I}) := \sqrt{\frac{\mathbb{E}[e^{-2\beta g(Y_{0:\tau})}(M_{0:\tau})^2]}{\mathbb{E}[e^{-\beta g(X_{0:\tau})}]^2}}. \tag{17}$$

To apply Proposition 1 to dynamic quantities like exit times, we have to guarantee the fulfillment of Novikov's condition. This can be achieved by making different assumptions on the stopping time. We will present two different approaches known from the literature that state how these assumptions can be formulated.

Condition 1. Let $W = \mathcal{C}([0,\infty], \mathbb{R}^n)$ be the space of continuous paths of arbitrary length equipped with the Borel σ-algebra $\sigma(W)$. This σ-algebra is generated by all cylinder sets of the form $\{f \in W : f(t_1) \in E_1, f(t_2) \in E_2, \ldots, f(t_k) \in E_k\}$, where $k \in \mathbb{N}$, $E_i \in \mathcal{B}(\mathbb{R}^n)$, and $0 \le t_1 \le t_2 \le \cdots \le t_k < \infty$. Further, let $\mathcal{F}_t = \sigma(\{w_s : s \le t\})$ denote the σ-algebra generated by the Brownian motion (w_s) up to time $t < \infty$. Then Girsanov's theorem holds on the measurable space $(W, \sigma(W))$ as long as the family $(M_t)_{t\ge 0}$ of random variables

$$M_T = \exp\left(\frac{-1}{\sqrt{2\beta^{-1}}}\int_0^T a(Y_s)dB_s - \frac{1}{2}\int_0^T \frac{1}{2\beta^{-1}}|a(Y_s)|^2 ds\right) \tag{18}$$

is a uniform integrable martingale. By Itô's formula, $(M_t)_{t\ge 0}$ is a nonnegative local martingale, which is uniformly integrable if Novikov's condition (10) holds [28]. This could be achieved by taking an admissible control which is defined up to a random stopping time τ, as done in [17].

Condition 2. Another way to guarantee the applicability of Proposition 1 is to assume that the stopping time is bounded for the specific problem. This assumption is by far nontrivial and can only be shown analytically in a very few situations. Anyhow, from a numerical viewpoint it is impossible to simulate trajectories which have infinite length. One has to stop the simulation after a finite number of steps. The quantity of interest can be approximated by the quantity of interest conditioned on the event happening in a finite simulation time. This assumption can be formalized by considering the stopping time $\hat{\tau} = \min(\tau, T_N)$, where T_N is the length of the numerical simulation. Then Novikov's condition follows for a reasonable function $u(\cdot)$. This treatment has been suggested in [24].

Condition 1 implies that one uses a bias function only up to a certain finite time. Thus, one can guarantee that the integral in the Girsanov weight (9) is bounded. The simulation could continue without the bias function acting on the trajectory. Condition 2 means that the sampling of the quantity of interest has to be finite in time. If the sampling is too long ($t > T_N$), the simulation is stopped.

In conclusion, Proposition 1 gives us an option to sample the dynamic quantity of interest from a different dynamical system without knowing the stationary distribution a priori. The different dynamical system can be changed in such a way that the quantity of interest is observed more often. The main difficulty of applying this strategy to a metastable system is to determine the metastable regions to change it accordingly. For this realization, we are going to use metadynamics. This algorithm is used in MD to sample the free energy surface and can be seen as an adaptive biasing method. In order to use this algorithm for our purposes, we are going to assimilate the algorithm slightly.

2.2. Metadynamics. The method metadynamics was first proposed in [19] under the name *local elevation*. It was reintroduced as metadynamics in [21]. It is an adaptive method for sampling the free energy surface (FES) of high-dimensional molecular systems. Thus, the main interest of this method is to find the stationary distribution. The method combines dynamics in reaction coordinates with adaptive bias potentials. The idea of this approach is to perturb the energy landscape when the simulation is trapped in a metastable region. This is done by locally adding Gaussian functions along a reaction coordinate, which fill up the minima in which the simulation is trapped. In this way, it is possible to explore the energy landscape in a rather short time compared to the plain sampling approach. The convergence of

some certain variants of metadynamics was proven in [8].

In order to apply the method, it is assumed that the high-dimensional system can be projected onto a few relevant collective coordinates. One possible way to find these collective variables for stochastic dynamics is to average out the fast degrees of freedom; see [22] or [39], for example. A more general overview can be found in [7] and the references therein. In general this projection can be written as $s : \mathbb{R}^n \to \mathbb{R}^d$ with $d \ll n$. Only the dependence of these parameters on the free energy $\mathcal{F}(s(x))$ is considered. The exploration of the FES is guided by the forces $F_i^t = -\partial\mathcal{F}(s_i(x))/\partial s_i^t$. The exploration of the FES gets stuck in a local minimum of the FES. In order to sample the FES more efficiently, a bias force is added to the system whenever the simulation is stuck in such a minimum. With metadynamics, one constructs a bias potential $V_{bias} : \mathbb{R}^d \to \mathbb{R}$, which is composed of $K \in \mathbb{N}$ Gaussian functions. The complete bias potential is

$$V_{bias}(x) = \sum_{i=1}^{K} \frac{w_i}{\sqrt{2\pi\lambda_i^2}} \exp\left(-\frac{(x - c_i)^2}{2\lambda_i^2} \right), \tag{19}$$

where $w_i \in \mathbb{R}$ is a weight, $c_i \in \mathbb{R}^d$ is the center of the Gaussian, and $\lambda \in \mathbb{R}$ is the width. These functions are placed along the trajectory to allow for an easy escape from this region, using the derivatives as an artificial force. The method can be parallelized easily since the bias force depends on the history of the individual trajectory only. This makes the method extremely efficient. Additionally, the bias also prevents the trajectory from going back to the visited states.

For simplicity we assume that all considered functions and variables are in the low-dimensional collective variable space and stick with the old notation. Of course, Girsanov's theorem is not restricted to the collective variable space.

2.3. Assimilation of metadynamics. We are going to assimilate the metadynamics algorithm to the sampling of dynamical quantities of interest. For our framework we do not have to calculate the complete FES. We only need a bias, which makes sure the trajectory does not get trapped in the metastable region. This is the reason why we add an additional sampling before we start sampling the quantity of interest to build a bias. In order to build a bias, which decreases the metastability, we use metadynamics in the metastable region only.

The bias is built in the following way: When the trajectory is trapped in a metastable region, we start a metadynamics simulation until the trajectory has left the metastable region. In every kth step, we add a Gaussian function to the potential such that the metastability is reduced. The force is then changed with the gradient of this Gaussian. When the trajectory hits the target set $\mathcal{T}$ for the first time, we save the bias and stop the metadynamics simulation. The bias consists of $\#steps\ needed/k$ bias functions. The choice of k is a compromise between adding as few bias functions as necessary, getting a small hitting time τ, and not perturbing the potential too much. Depending on the choice of the parameters w and λ, a certain number of bias functions is needed. It is obvious that the simulation of metadynamics gets more expensive the more bias functions are added due to the increasing number of function evaluations. That is why all parameters should be adapted to the problem such that the computation does not get too costly.

After having built the bias potential, the sampling of the original trajectory is continued with the bias potential. To correct the quantity of interest at the end of the calculation, we must sample the weights (9) as well. This can be done on the fly.

Remark 1. The construction of the bias potential depends on the history of the trajectory. Since the simulation to get the bias function is done in an additional step, the potential is not time dependent. Furthermore, the discretization of (1) always gives a discrete time Markov process because of the time independence of the Brownian motion. The construction of the bias potential itself is not Markovian because it depends on the history of the trajectory. Since the construction of the bias function and the sampling of the quantity of interest are done independently of each other, the bias does not have any influence on the Markovianity of the perturbed SDE (8). In general, an extension of the proposed method for non-Markovian dynamics should be possible. In this regard, one could use the metadynamics methods proposed in [5] and the general reweighting formula given in [28].

Remark 2. The method is not restricted to the use of metadynamics. Any stochastic approximation algorithm (e.g., adaptive biasing force) or even a deterministic algorithm could be used, provided the bias satisfies Novikov's condition. The method is also not restricted to the case in which the drift term ($b(\cdot)$) of the SDE is of gradient form. Since the Girsanov formula does not use the stationary distribution, all calculations are still valid. However, if the bias is not of gradient form, the alternative Girsanov formula cannot be applied.

3. The algorithm. Now we present the algorithm in pseudocode. We will use the metadynamics algorithm to build a bias in the metastable regions of the potential. Then we sample the quantity of interest in this biased potential N times and reweight the sampling with the weight given by (9).

Algorithm 1. Adaptive importance sampling.

dynamics X_t, Y_t, starting set $\mathcal{S}$, target set $\mathcal{T}$
initialization: $X_0 = Y_0 = x$; w_i, λ_i
Step 1: Build bias potential
while transition has not occurred **do**
  sample the dynamics X_t given in eq. (8);
  every kth steps: add a new bias function to $u(\cdot)$;
end while
save the bias potential;
Step 2: Sample the quantity of interest
for N **do**
  sample the quantity of interest with the additional bias according to eq. (8);
  sample the weights according to eq. (9);
end for
reweight according to eq. (11);
return estimators for quantities of interest

Proof of Novikov's condition. To apply Girsanov's theorem one has to make sure that Novikov's condition is satisfied.

LEMMA 1. *Let $\hat{\tau}$ be the stopping time as given in Condition* 2. *Further, let the bias potential consist of $K < \infty$ bias functions. We choose the weights of the bias function $V_{bias}(\cdot)$ such that the sum is bounded $\sum_{i=1}^{K} w_i < C_w$. If the perturbation potential is uniformly continuous, then the Novikov condition holds and we can use Proposition* 1 *to calculate path-dependent quantities from nonequilibrium sampling for the equilibrium dynamics.*

Proof. Since the bias function is added to the potential V, the resulting SDE is given by

$$dY_t = -\nabla V(Y_t) + \nabla V_{bias}(Y_t; c, w, \lambda)dt + \sqrt{2\beta^{-1}}dB_t, \quad Y_0 = x. \tag{20}$$

We have to verify Novikov's condition for $\nabla V_{bias}(\cdot)$, which states that

$$\mathbb{E}\left[\exp\left(\frac{1}{2}\int_0^{\hat{\tau}} \Big|\frac{\nabla V_{bias}(Y_t; c, w, \lambda)}{\sqrt{2\beta^{-1}}}\Big|^2 dt\right)\right] < \infty. \tag{21}$$

We are going to show that the time integral is bounded, from which we can then conclude that Novikov's condition holds:

$$\begin{aligned}\frac{1}{2}\int_0^{\hat{\tau}} \Big|\frac{\nabla V_{bias}(Y_t; c, w, \lambda)}{\sqrt{2\beta^{-1}}}\Big|^2 dt &= \frac{\beta}{4}\int_0^{\hat{\tau}} \Big\|\nabla V_{bias}(Y_t; c, w, \lambda)\Big\|_2^2 dt \\ &\leq \frac{\beta}{4}\int_0^{\hat{\tau}} \Big\|\nabla V_{bias}(Y_t; c, w, \lambda)\Big\|_\infty^2 dt \\ &\leq \frac{\beta}{4}\hat{\tau}\Big\|\nabla V_{bias}(Y_t; c, w, \lambda)\Big\|_\infty^2 < \infty.\end{aligned}$$

The $\|\cdot\|_\infty$ is bounded because the ansatz functions for the gradient are gradients of Gaussian functions, which are bounded. Furthermore, the stopping time is bounded due to Condition 2. It follows that the whole expression is bounded, and from this we conclude that (21) is satisfied. Therefore Novikov's condition holds. ∎

4. Examples. In the following, we study different numerical examples of the method presented above. We assume that the reaction coordinates are given such that we have a low-dimensional representation of the high-dimensional dynamics. The first 1D example shows the construction of the bias potential with fixed parameters. In the second 1D example we are going to use the alternative reweighting formula (13) to correct the statistics from the nonequilibrium sampling. In the last part of this section we will show a 2D example for alanine-dipeptide in reaction coordinates.

For the first examples we consider the dynamics given by (1) and the potential given by

$$V(x) = \frac{1}{2}(x^2 - 1)^2. \tag{22}$$

This potential has two minima at $x = \pm 1$ and a local maximum at $x = 0$. We are going to calculate two different quantities of interest. The first quantity of interest is the probability of all continuous paths which start at a point x in the metastable region $\mathcal{S}$ and reach the target set in time $\hat{\tau}$. This can be written mathematically as $\mathbb{P}(\mathcal{A})$, where $\mathcal{A} = \{X_{0:\hat{\tau}} \in \mathcal{C}([0, \hat{\tau}], \mathbb{R}^n) | X_0 = x(x \in \mathcal{S}), X_{\hat{\tau}} \in \mathcal{T}\}$. For this quantity of interest, we choose $g(Y_t) = 0$ for $Y_t \in \mathcal{S},\ t \in [0, \hat{\tau}]$, and choose $g(Y_t) = 1$ for $Y_t \in \mathcal{T},\ t \in [0, \hat{\tau}]$. The second quantity of interest is the moment generating function of the stopping $\hat{\tau}$. To sample this, we set $g(Y_{0:\hat{\tau}}) = \hat{\tau}$. The trajectories $Y_{0:\hat{\tau}}$ are realizations of (8) with $b(\cdot) = -\nabla V(\cdot)$, $u(\cdot)$ is the bias constructed by the metadynamics simulation, and $\sigma = \sqrt{2\beta^{-1}}$. We compare our method with the results of a standard MC estimator for the different quantities. We will see that in the first example, our method achieves the variance reduction for both reweighting formulas given in this article. Furthermore, the average transition time was decreased in the biased simulation. For this, we

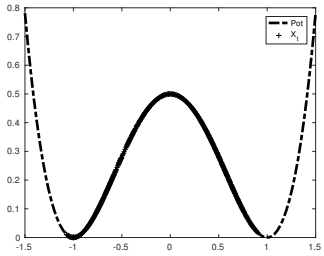

(a) *The dashed-dotted line is the potential function* (22)*, and the black crosses show a realization of* (1) *performing the desired transition we want to sample.*

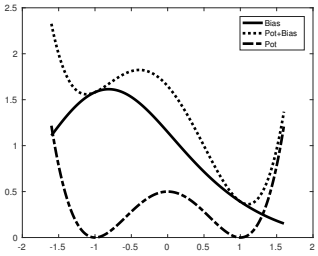

(b) *The dashed-dotted curve shows the original potential* (22)*. The solid black curve shows the bias V_{bias} produced by the metadynamics algorithm, and the dotted curve shows the corresponding biased potential* $(V + V_{bias})$*.*

FIG. 1. (a) *Trajectory of interest in the unperturbed potential.* (b) *Potential, bias, and perturbed potential.*

estimate the mean first hitting time (MFHT) for our experiments. The MFHT is the average time trajectories needed to reach the target set. If the trajectory did not hit the target set, the MFHT is set to T_N.

For the performed 1D experiments, we define the metastable region $\mathcal{S} = [-1.5, 0]$. We choose the starting point of the SDE (1) in the metastable region $X_0 = -1$ and fix $\beta = 3.0$ for all experiments. The stopping time is defined as the first hitting time of the target set $\mathcal{T} = [0.9, 1.1]$. In the first two examples we sampled 100,000 trajectories by using a standard Euler–Maruyama discretization with a time step $\Delta t = 10^{-4}$ in MATLAB; cf. [18]. Our aim was to investigate the variance within the different trajectories. At maximum, we calculated $T_N = 15{,}000$ time steps. The random number generator was fixed at `rng(1,'twister')` in order to have a better comparison within the different examples. Other random number generators have been tested showing similar results.

4.1. Diffusion in a double-well potential with fixed parameters. For this computation we chose $w_i = 0.05$, $\lambda_i = 0.8$ for all bias functions. The c_i of every bias function is chosen as the current value of the trajectory when the new bias function is added. The weights are calculated by (9).

In this example, 79 bias functions have been used; see Figure 1(b) for the calculated bias and the resulting potential energy. The estimators of the MC and the importance sampling are in good agreement for both cases; cf. Table 1. Our results show that the variance of the biased estimator is reduced for both quantities of interest using the reweighting approach. The variance for the transition probability is reduced by 65% and for the moment generating function by 76%. Hence, the automatically generated bias potential by the adjusted metadynamics algorithm is actually a good potential in the sense of importance sampling. Additionally, the MFHT is faster compared to the plain MC approach. This experiment shows that our method achieves the desired goals of variance reduction and computational speedup.

4.2. 1D with alternative reweighting formula. In this example, we use the alternative reweighting formula as shown in (13). In order to calculate the bias, we

TABLE 1
Comparison of the importance sampling estimators and the MC estimators for the simulation with fixed parameters of the biased potential.

	MC	GIR
$P(\mathcal{A})$	4.8470×10^{-2}	4.8323×10^{-2}
Var	4.6121×10^{-2}	1.6404×10^{-2}
$R(I)$	4.4307	2.6504
$\mathbb{E}[e^{-\beta\tau}]$	2.569×10^{-3}	2.4885×10^{-3}
Var	2.5850×10^{-4}	6.9180×10^{-5}
$R(I)$	6.2561	3.3463
MFHT	1.4804	1.4425

TABLE 2
Comparison of the importance sampling estimators and the MC estimators for the simulation with the alternative Girsanov formula.

	MC	AGIR
$P(\mathcal{A})$	4.8470×10^{-2}	4.8329×10^{-2}
Var	4.6121×10^{-2}	1.6407×10^{-2}
$R(I)$	4.4307	2.6504
$\mathbb{E}[e^{-\beta\tau}]$	2.5690×10^{-3}	2.4856×10^{-3}
Var	2.5850×10^{-4}	6.9170×10^{-5}
$R(I)$	6.2561	3.3459
MFHT	1.4804	1.4425

used the same parameters as in the first example. Since the random number generator was fixed, the bias is exactly the same as in the first example; see Figure 1(b).

In order to calculate the Girsanov weights, we need V_{bias}, ∇V_{bias}, and $\nabla^2 V_{bias}$. For V_{bias} as given in (19), the derivatives can be calculated easily.

In this case, the MC estimator and the importance sampling estimator agree very well; cf. Table 2. The variance reduction is very similar to the other reweighting formula. The variance for the transition probability is reduced by 64%, and the variance for the moment generating function is reduced by 73%. These experiments show that the alternative Girsanov formula can be applied as well to correct the biased estimators. The reduction of the MFHT is the same as in the first example since we used the same seed for the random number generator.

4.3. 2D diffusion process. In this example, we consider the dynamics of the molecule alanine-dipeptide (Ac-A-NHMe) in the limit of high friction. We reduced the problem to the motion of the backbone torsion angles ϕ and ψ, modeled by the overdamped Langevin equation:

$$\begin{aligned} \mathrm{d}\phi_t &= -\frac{\nabla V(\phi_t, \psi_t)}{\gamma}\mathrm{d}t + \frac{\sigma}{\gamma}\mathrm{d}B_t, \\ \mathrm{d}\psi_t &= -\frac{\nabla V(\phi_t, \psi_t)}{\gamma}\mathrm{d}t + \frac{\sigma}{\gamma}\mathrm{d}B_t, \end{aligned} \tag{23}$$

where $V(\phi, \psi)$ is the potential energy function of the system, γ is the friction, and B_t is a Brownian motion. The SDE in (23) has been solved using the Euler–Maruyama scheme with the Boltzmann constant $k_B = 0.00831451\,\mathrm{kJ/(mol \cdot K)}$, at temperature $T = 300\,\mathrm{K}$, with friction $\gamma = 1\,\mathrm{ps}^{-1}$ and $\Delta t = 0.002\,\mathrm{ps}$ as integrator time steps.

The constant σ represents the volatility of the Brownian motion and depends on the temperature of the system:

$$\sigma = \sqrt{2k_B T\gamma}. \tag{24}$$

The weights are calculated by (9). The reaction coordinate function $V(\phi, \psi)$ is not known and is therefore estimated from a full atomic MD simulation at high temperature as the FES of the relevant coordinates (ϕ, ψ). We performed an all-atom MD simulation of acetyl-alanine-methylamide (Ac-A-NHMe, alanine-dipeptide) in explicit water at 900 K, with the GROMACS 5.0.2 simulation package [36], the force field AMBER ff-99SB-ildn [25], and the TIP3P water model [20].

If we assume that the distribution of the relevant coordinates is proportional to the true stationary distribution given by the Boltzmann distribution $h(\phi, \psi) \approx \pi(\mathbf{x}) = \exp(-\beta V(\mathbf{x}))/Z$, with Z being the partition function, then the FES can be estimated from the histogram $h(\phi, \psi)$ as

$$V(\phi, \psi) = -\frac{1}{\beta} \log h(\phi, \psi) + \text{const}. \tag{25}$$

Since we need the analytical value of the potential gradient, we have estimated a bicubic spline of $V(\phi, \psi)$ using the ALGLIB [32] package.

In molecular dynamics simulation, the location of the minimum is usually not known. However, it is easy to bring the system into a configuration in a local minimum by optimization algorithms like gradient descent. Thus, instead of estimating the probability of jumping from one minimum to another, we have reformulated the problem and try to estimate the probability of leaving the starting minimum after a certain time. In order to approximate this probability we are going to calculate the probability of all continuous trajectories, which have reached a certain distance after some time. This can be formalized by calculating the probability of the set $\mathcal{A} = \{X_{0:\hat{\tau}} \in \mathcal{C}([0, \hat{\tau}] : \mathbb{R}^n) | X_0 = x(x \in \mathcal{S}), X_{\hat{\tau}} \in \mathcal{T}\}$, where $\mathcal{T} = \{z : |X_0 - z| = \hat{d}\}$.

We have chosen to start all simulations at point $\{\phi_0 = -1.5; \psi_0 = -0.2\}$, i.e., at the bottom of the right α-region of the Ramachandran space [30] and at distance $\hat{d} =$ 0.63, 0.83, 1.0. We have repeated our experiment 100 times, while each experiment is a collection of 10,000 trajectories and the maximum number of time steps for a single trajectory is 50. For each experiment, we estimated the bias by first running a metadynamics simulation and stopping when the trajectory reaches the desired distance $\hat{d}$. The bias is built adaptively with our method. Then we performed the simulations adding the bias to $V(\phi, \psi)$ in the metastable regions.

Figure 2 shows the free energy profile of the system estimated from the full atomic simulation (A), one example of metadynamics potential (B), and the biased potential (C). The effect of the metadynamics potential is to fill the local minimum and accelerate the exit of the trajectory from it.

Figure 3 shows the free energy profile from a different point of view together with two trajectories. While the trajectory spends a lot of time without any dominant direction in the unbiased potential (A), it is forced to leave the local minimum in a northerly direction in the second case (B).

In Table 3, we have collected the results for different experiments. The parameter Δk denotes the frequency at which the metadynamics potential was updated. Since in this kind of experiment the trajectories are quite short, we added a new Gaussian function to the bias potential at every time step, with a new center c_i equal to the last state visited.

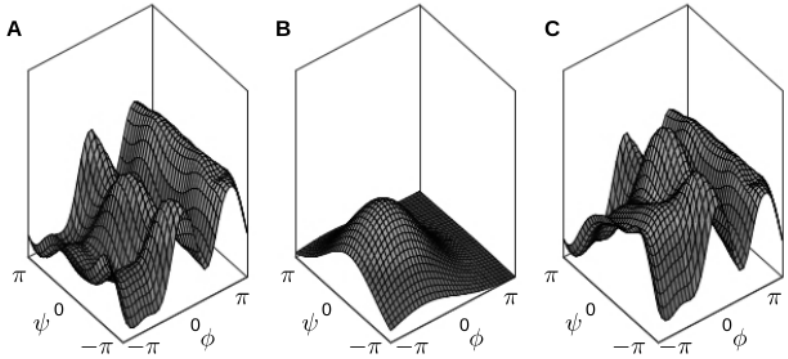

FIG. 2. *Free energy profile* (A), *metadynamics potential* (B), *and free energy profile and metadynamics potential* (C). *To estimate the metadynamics potential, we have used* $w_i = 0.9$, $\lambda_i = 1.6$, *and* $\Delta k = 1$.

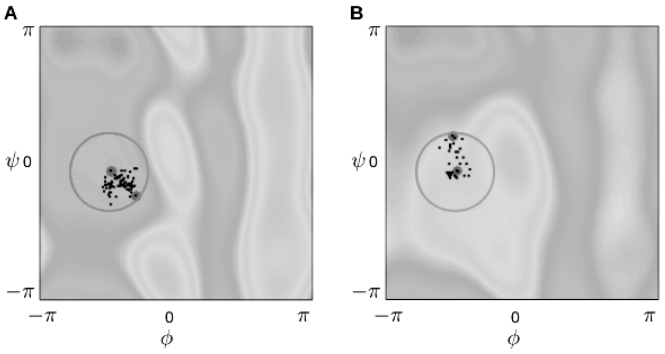

FIG. 3. *FES of alanine-dipeptide* (A), *and biased FES* (B). *The circle* ($\hat{d} = 0.83$) *represents the target that the trajectory has to hit.*

TABLE 3
Table for the numerical examples with alanine-dipeptide.

	MC1	GIR1	MC2	GIR2	GIR3	GIR4	MC5	GIR5
$\hat{d}$	0.63	0.63	0.83	0.83	0.83	0.83	1.0	1.0
w_i	-	0.9	-	0.15	0.9	0.9	-	0.9
λ_i	-	1.6	-	0.5	0.5	1.6	-	2.0
Δk	-	1	-	1	1	1	-	1
$P(\mathcal{A})$	6.46×10^{-1}	6.46×10^{-1}	3.04×10^{-1}	3.04×10^{-1}	2.96×10^{-1}	3.04×10^{-1}	1.53×10^{-1}	1.54×10^{-1}
Var	2.46×10^{-5}	1.97×10^{-5}	2.09×10^{-5}	1.11×10^{-5}	1.36×10^{-3}	1.14×10^{-5}	1.34×10^{-5}	5.21×10^{-6}
$\mathbb{E}[e^{-\beta\tau}]$	6.33×10^{-1}	6.33×10^{-1}	2.97×10^{-1}	2.97×10^{-1}	2.89×10^{-1}	2.97×10^{-1}	1.49×10^{-1}	1.50×10^{-1}
Var	2.37×10^{-5}	1.87×10^{-5}	1.98×10^{-5}	1.06×10^{-5}	1.28×10^{-3}	1.39×10^{-5}	1.27×10^{-5}	4.91×10^{-6}
MFHT	25.42	21.26	30.21	26.47	20.49	25.05	32.82	27.73

In the first two columns (MC1, GIR1), we have considered a short distance $\hat{d} = 0.63$, and the results show that the reweighted estimator allows us to predict the MC estimators with a variance reduction approximatively of 20% and a reduction of the MFHT of 17%.

The next four columns (MC2, GIR2, GIR3, GIR4) report the data for the experiments with $\hat{d} = 0.83$. In the first case (GIR2), we have used $w_i = 0.15$ and $\lambda_i = 0.5$, obtaining a variance reduction of almost 50% and MFHT reduced by 13 %. In the next case (GIR3), we tried to increase the height of the Gaussians to $w_i = 0.9$ with a small variance $\lambda_i = 0.5$. The dynamics is strongly accelerated; thus the trajectory leaves the local minimum quickly, but the precision of the estimators is reduced compared to results obtained by MC estimators. In particular, we observe an increase in the variance of two orders of magnitude. By increasing the variance of the Gaussian functions to $\lambda_i = 1.6$, keeping $w = 0.9$ (GIR4), the results of the reweighted estimators agree with the results obtained by MC simulations again.

The last two columns show the results for $\hat{d} = 1$. In this case, we have increased the variance to $\lambda_i = 2$. We observe a variance reduction of almost 60%. However, in this case the dynamics is slower and the MFHT is reduced only by 14%.

To study the dependence of the method on the metadynamics parameters, we have repeated the last experiment with $\hat{d} = 1.0$ for six values of w_i (the height of the Gaussians) and six values of λ_i (the variance of the Gaussians).

Figure 4 shows the error of the reweighted estimators with respect to the estimators obtained by MC simulations, while Figure 5 shows the variance reduction or increase. The two figures give a heuristic argument for the presented choice of parameters. The success of the method depends on the choice of the initial parameters. If the parameter λ of the Gaussian functions is bigger than the height w, we obtain the best results, i.e., a better value of the estimators and a significant variance reduction. This fact has a heuristic explanation. Thus, if the parameter λ is too small compared to the height w, the bias results in high narrow peaks. Adding this bias leads to a much more rugged potential. On the contrary, a large variance guarantees that the minimum is filled properly.

5. Summary and outlook. In this article, we developed an algorithm for automatic assimilated importance sampling for dynamical quantities in metastable systems. For this, we considered metastable stochastic systems. The main idea is to bias the dynamics in the metastable region. This can be achieved by constructing bias functions raising the region around the minimum of the drift term. To build this bias, we use the metadynamics algorithm, which was adjusted to create a bias decreasing the metastability only. In order to correct the sampling in the perturbed system, we proposed a reweighting scheme based on Girsanov's theorem. We proved that the reweighting scheme can be applied in our situation. We also considered an alternative reweighting formula which can be derived by using Itô's lemma. We tested our approach in different numerical examples. In a 1D example, we showed that this algorithm generates estimators for different quantities of interest with a reduced variance compared to an MC estimator. The bias also reduces the MFHT of the rare events, which results in shorter simulation time. We also tested the alternative reweighting formula. The results of this approach are as good as the results of the original formula. Whether one of the formulas has certain advantages compared to the other is the subject to ongoing research. Recent work shows a deeper mathematical problem with the alternative formula in the long-term limit; cf. [26]. In a 2D example, we also showed that our method works for higher-dimensional reaction coordinates. Further-

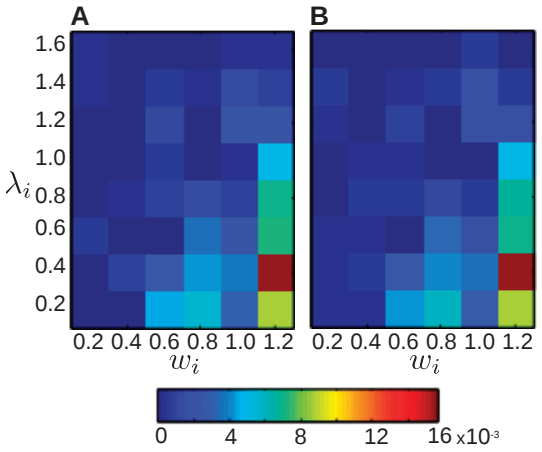

FIG. 4. *Error of $P(\mathcal{A})$ (A) and $\mathbb{E}[e^{-\beta\tau}]$ (B) with respect to the same quantities estimated by MC simulation as a function of the parameters w_i and λ_i.*

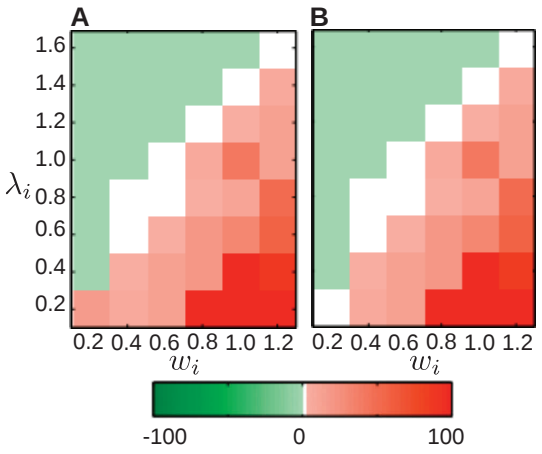

FIG. 5. *Ratio of the variance of $P(\mathcal{A})$ (A) and $\mathbb{E}[e^{-\beta\tau}]$ (B) with respect to variance of the same quantities estimated by MC simulation as a function of the parameters w_i and λ_i. The green color denotes a variance reduction.*

more, the 2D example gave us a heuristic understanding of how to choose the bias parameters in order to achieve appropriate variance reduction. The first impression is that a bigger bias potential is always better. But this is in general not the case for two reasons: First, the numerical treatment of Girsanov's formula is quite delicate, and a higher bias makes this even worse. Second, the analysis of [33] showed that

there is an exponential constant in the decay of the variance involved. A higher bias function will also have an impact on this constant, leading to a slower decay of the variance.

In the next step we aim at analyzing our importance sampling scheme in more detail. One possible direction for this is the analysis of our method in terms of subsolutions of the HJB equation as proposed in [33]. Another direction could be to use log-Sobolev inequalities as proposed in [23]. We are especially interested in discovering under which conditions our proposed method produces subsolutions of the corresponding HJB equation.

Directly perturbing the gradient is another methodological path we are currently following. An approach like this could use adaptive biasing force methods for building the bias instead of metadynamics. First simulations have shown that this leads to an even shorter MFHT because the perturbed gradient of the biased dynamical system is smooth compared to the bias generated by the metadynamics approach. How the variance of the estimator is influenced by this is the subject of ongoing research.

We suggest that our method proposed here serves the generation of an initial guess at solving the optimization problem in [16]. The combination of these two methods could lead to an optimized artificial force, which yields the potential to achieve an even better variance reduction.

The split-and-kill strategy introduced by Zou and Skeel in [40] is a very appealing idea to control the growth of the reweighting factor, which frequently causes numerical issues. We are going to consider this strategy in the future and hope to introduce more stability in the calculations of the reweighting factor.

Acknowledgment. We would like to thank the anonymous reviewers for their very helpful advice and their careful reading.

REFERENCES

[1] R. J. Allen, C. Valeriani, and P. R. ten Wolde, *Forward flux sampling for rare event simulations*, J. Phys. Condensed Matter, 21 (2009), 463102.

[2] R. J. Allen, P. B. Warren, and P. R. ten Wolde, *Sampling rare switching events in biochemical networks*, Phys. Rev. Lett., 94 (2005), 018104.

[3] R. Bernardi, M. Melo, and K. Schulten, *Enhanced sampling techniques in molecular dynamics simulations of biological systems*, Biochim. Biophy. Acta (BBA), 1850 (2015), pp. 872–877.

[4] M. Bonomi, A. Barducci, and M. Parrinello, *Reconstructing the equilibrium Boltzmann distribution from well-tempered metadynamics*, J. Comput. Chem., 30 (2009), pp. 1615–1621.

[5] G. Bussi, A. Laio, and M. Parrinello, *Equilibrium free energies from nonequilibrium metadynamics*, Phys. Rev. Lett., 96 (2006), 090601.

[6] F. Cérou and A. Guyader, *Adaptive multilevel splitting for rare event analysis*, Stoch. Anal. Appl., 25 (2007), pp. 417–443.

[7] C. Chipot and A. Pohorille, *Free Energy Calculations*, Springer Series in Chemical Physics, Springer, Berlin, Heidelberg, 2007.

[8] J. F. Dama, M. Parrinello, and G. A. Voth, *Well-tempered metadynamics converges asymptotically*, Phys. Rev. Lett., 112 (2014), 240602.

[9] E. Darve and A. Pohorille, *Calculating free energy using average forces*, J. Chem. Phys., 115 (2001), pp. 9169–9183.

[10] L. Donati, C. Hartmann, and B. Keller, *Girsanov reweighting for path ensembles and Markov state models*, J. Chem. Phys., 146 (2017).

[11] P. Dupuis, A. D. Sezer, and H. Wang, *Dynamic importance sampling for queueing networks*, Ann. Appl. Probab., 17 (2007), pp. 1306–1346.

[12] P. Dupuis, K. Spiliopoulos, and X. Zhou, *Escaping from an attractor: Importance sampling and rest points* I, Ann. Appl. Probab., 25 (2015), pp. 2909–2958.

[13] P. Dupuis and H. Wang, *Importance sampling, large deviations, and differential games*, Stoch. Stoch. Rep., 76 (2004), pp. 481–508.

[14] P. Dupuis and H. Wang, *Subsolutions of an Isaacs equation and efficient schemes for importance sampling*, Math. Oper. Res., 32 (2007), pp. 723–757.

[15] A. K. Faradjian and R. Elber, *Computing time scales from reaction coordinates by milestoning*, J. Chem. Phys., 120 (2004), 10880.

[16] C. Hartmann and C. Schütte, *Efficient rare event simulation by optimal nonequilibrium forcing*, J. Statist. Mech. Theory Exper., 2012 (2012), P11004.

[17] C. Hartmann, C. Schütte, and W. Zhang, *Model reduction algorithms for optimal control and importance sampling of diffusions*, Nonlinearity, 29 (2016), pp. 2298–2326.

[18] D. J. Higham, *An algorithmic introduction to numerical simulation of stochastic differential equations*, SIAM Rev., 43 (2001), pp. 525–546, https://doi.org/10.1137/S0036144500378302.

[19] T. Huber, A. E. Torda, and W. F. van Gunsteren, *Local elevation: A method for improving the searching properties of molecular dynamics simulation*, J. Computer-Aided Molecular Design, 8 (1994), pp. 695–708.

[20] W. L. Jorgensen, J. Chandrasekhar, J. D. Madura, R. W. Impey, and M. Klein, *Comparison of simple potential functions for simulating liquid water*, J. Chem. Phys., 79 (1983), pp. 926–935.

[21] A. Laio and M. Parrinello, *Escaping free-energy minima*, Proc. Natl. Acad. Sci. USA, 99 (2002), pp. 12562–12566.

[22] F. Legoll, T. Leli'evre, and S. Olla, *Pathwise estimates for an effective dynamics*, Stochastic Process. Appl., 127 (2017), pp. 2841–2863.

[23] T. Leliévre, *Two mathematical tools to analyze metastable stochastic processes*, in Numerical Mathematics and Advanced Applications 2011, Springer, Heidelberg, 2013, pp. 791–810.

[24] T. Lelièvre and G. Stoltz, *Partial differential equations and stochastic methods in molecular dynamics*, Acta Numer., 25 (2016), pp. 681–880.

[25] K. Lindorff-Larsen, S. Piana, K. Palmo, P. Maragakis, J. L. Klepeis, R. O. Dror, and D. E. Shaw, *Improved side-chain torsion potentials for the amber ff99sb protein force field*, Proteins, 78 (2010), pp. 1950–1958.

[26] P. Malsom and F. Pinski, *Pinned Brownian Bridges in the Continuous-Time Limit*, preprint, https://arxiv.org/abs/1704.01991, 2017.

[27] G. N. Milstein, *Numerical Integration of Stochastic Differential Equations*, Math. Appl. 313, Springer Science & Business Media, 1994.

[28] B. Øksendal, *Stochastic Differential Equations: An Introduction with Applications*, Hochschultext/Universitext, Springer, Berlin, 2003.

[29] J. Quer and H. Lie, *Some Connections between Importance Sampling and Enhanced Sampling Methods in Molecular Dynamics*, Tech. report, Zuse Institute Berlin, 2017.

[30] G. Ramachandran, C. Ramakrishnan, and V. Sasisekharan, *Stereochemistry of polypeptide chain configurations*, J. Mol. Biol., 5 (1963), pp. 95–99.

[31] C. Schütte and M. Sarich, *Metastability and Markov State Models in Molecular Dynamics*, AMS, 2013.

[32] B. Sergey, *ALGLIB*, 1999, www.alglib.net.

[33] K. Spiliopoulos, *Nonasymptotic performance analysis of importance sampling schemes for small noise diffusions*, J. Appl. Probab., 52 (2015), pp. 797–810.

[34] P. Tiwary and M. Parrinello, *From metadynamics to dynamics*, Phys. Rev. Lett., 111 (2013), 230602.

[35] G. Torrie and J. Valleau, *Nonphysical sampling distributions in Monte Carlo free-energy estimation: Umbrella sampling*, J. Comput. Phys., 23 (1977), pp. 187–199.

[36] D. Van Der Spoel, E. Lindahl, B. Hess, G. Groenhof, A. E. Mark, and J. Berendsen, H., *GROMACS: Fast, flexible, and free*, J. Comput. Chem., 26 (2005), pp. 1701–1718.

[37] E. Vanden-Eijden and J. Weare, *Rare event simulation of small noise diffusions*, Comm. Pure Appl. Math., 65 (2012), pp. 1770–1803.

[38] M. Weber, C. Zoschke, A. Sedighi, E. Fleige, R. Haag, and M. Schäfer-Korting, *Free energy simulations of cargo-carrier interactions for core-multishell nanotransporters*, J. Nanomedicine Nanotechnology, 5 (2014), 234.

[39] W. Zhang, C. Hartmann, and C. Schütte, *Effective dynamics along given reaction coordinates, and reaction rate theory*, Faraday Discuss., 195 (2016), pp. 365–394.

[40] G. Zou and R. D. Skeel, *Robust variance reduction for random walk methods*, SIAM J. Sci. Comput., 25 (2004), pp. 1964–1981, https://doi.org/10.1137/S1064827503424025.

Chapter 8

Estimation of the infinitesimal generator by square-root approximation

In the previous chapters, the central subject was the transfer operator $\mathcal{T}(\tau)$, i.e. a continuous operator, that we use to study the dynamics of a molecular system as time evolution of probability density functions. Associated to the transfer operator, exists another continuous operator, named infinitesimal generator $\mathcal{Q}$, such that $\mathcal{T}(\tau) = \exp(\tau\mathcal{Q})$, which provides a pattern of the dynamics of the molecular system in terms of transition rates between states. The operators $\mathcal{T}(\tau)$ and $\mathcal{Q}$ have the same eigenfunctions, while the eigenvalues are linked by the relation $\lambda_i(\tau) = \exp(\tau\theta_i)$, where $\lambda_i(\tau)$ and θ_i are respectively the eigenvalues of $\mathcal{T}(\tau)$ and $\mathcal{Q}$. It follows, that the same information about the dynamics, can be recovered both from $\mathcal{T}(\tau)$ and $\mathcal{Q}$.

On the other hand, while MSMs is a consolidated method to discretize the transfer operator in a transition matrix $\mathbf{T}(\tau)$, there is not a valid tool to discetize the infinitesimal generator. Indeed, the elements of the matrix $\mathbf{Q}$ cannot be estimated from time-lagged correlation functions as in MSMs.

In this work [57], we provide a method to discretize the infinitesimal generator into a rate matrix $\mathbf{Q}$, offering a new alternative tool to analyze the dynamical properties of molecular system. The first step is to build a Voronoi tessellation of the state space, that permits a correct discretization of the infinitesimal generator. Using the Gauss theorem, the entries Q_{ij} are written in terms of the Boltzmann weight of the intersecting surface between two adjacent cells and the flux of the configurations through the surface. We now introduce two approximations. Firstly, the flux is assumed to be a constant scalar that does not depend on the potential energy function. Secondly, the Boltzmann weight of the intersecting surface is approximated as geometric average of the Boltzmann weight of the cells.

In this way we provide an algebraic relation between the potential energy function and the rate matrix and we are able to estimate the matrix elements Q_{ij} as the geometric average of the Boltzmann weights of neighboring cells. In the limit of infinitely small Voronoi cells, the relation converges to the Fokker-Planck operator of an over-damped Langevin dynamics, confirming its validity [82]. A sketch of the proof, provided by Martin Heida from Weierstrass Institute Berlin, is included in this work.

In principle, the importance of the method is that it provides a tool to estimate the matrix $\mathbf{Q}$, and then $\mathbf{T}(\tau)$, with no need to perform MD simulations. Indeed, the only information requested is the potential energy function of the system. In practice, a

simulation is always necessary for three reasons:

1. To determine a relevant subset of the state space of the system, discarding those regions that contain unphysical or extremely rare conformations.

2. In case of high-dimensional systems, it is useful to consider only few relevant coordinates and to replace the full dimensional potential energy function with a low dimensional free energy profile, that can be determined by MD simulation.

3. As explained more in detail in the paper, the rates obtained by square root approximation are scaled by an unknown factor $\hat{\Phi}$, i.e. the flux that is assumed to be constant. A strategy to estimate the flux, is to run an MD simulation, to build an MSM, then reduce the matrices $\mathbf{Q}$ and $\mathbf{T}(\tau)$ to the conformational matrices by PCCA+ [75] and to obtain the flux from the eigenvalues.

The method can be improved in future works, by using an enhanced sampling method to obtain in few computational time the free energy profile of the system. Moreover, the square root approximation formula can be modified to study the effect of an Hamiltonian perturbation on the dynamics, providing a new reweighting scheme.

I contributed to the paper providing a detailed explanation of the method and the underlying theory. I carried out all the simulations and the analysis of the systems described in the paper: the two-dimensional diffusion process and the Alanine dipeptide. In particular I studied the sensitivity of the method to the input parameters: the size of Voronoi cells and the environmental temperature. Furthermore, I carried out a test to show that the flux of the configurations $\hat{\Phi}$, between neighboring cells, does not depend on an external perturbation of the potential energy function, according to the initial assumption.

https://doi.org/10.1088/1361-648X/aadfc8

Accepted in Journal of Physics: Condensed Matter, online 7 September 2018

Estimation of the infinitesimal generator by square-root approximation

Luca Donati,[1, a)] Martin Heida,[2, b)] Bettina G. Keller,[1, c)] and Marcus Weber[3, d)]

[1)] *Department of Biology, Chemistry, Pharmacy, Freie Universität Berlin, Takustraße 3, D-14195 Berlin, Germany*

[2)] *Weierstrass Institute for Applied Analysis and Stochastics, Mohrenstr. 39, 10117 Berlin, Germany*

[3)] *Zuse Institute Berlin, Takustr. 7, 14195 Berlin, Germany*

(Dated: 24 September 2018)

In recent years, for the analysis of molecular processes, the estimation of time-scales and transition rates, has become fundamental. Estimating the transition rates between molecular conformations is – from a mathematical point of view – an invariant subspace projection problem. We present a method to project the infinitesimal generator acting on function space to a low-dimensional rate matrix. This projection can be performed in two steps. First, we discretize the conformational space in a Voronoi tessellation, then the transition rates between adjacent cells is approximated by the geometric average of the Boltzmann weights of the Voronoi cells. This method demonstrates that there is a direct relation between the potential energy surface of molecular structures and the transition rates of conformational changes. We will show also that this approximation is correct and converges to the generator of the Smoluchowski equation in the limit of infinitely small Voronoi cells. We present results for a two dimensional diffusion process and Alanine dipeptide as high-dimensional system.

PACS numbers: 02.50.Ga, 05.10.Gg

Keywords: Infinitesimal generator, Markov State Models, transfer operator, molecular kinetics

[a)]Electronic mail: luca.donati@fu-berlin.de

[b)]Electronic mail: martin.heida@wias-berlin.de

[c)]Electronic mail: bettina.keller@fu-berlin.de

[d)]Electronic mail: weber@zib.de

I. INTRODUCTION

In the last decades, molecular processes, like conformational changes or binding processes, have been modeled and studied trough Molecular Dynamics (MD) simulations. In MD simulations, one numerically solves the equation of motion of a molecule, in order to obtain a discretized trajectory, containing the position of each atom at each timestep. From a sufficiently large ammount of MD trajectories, one can recover the Boltzmann distribution and estimate phase-space ensemble averages.

Under certain conditions, the dynamics of a molecular system can be studied as time evolution of probability densities $\rho_t(\mathbf{x})$ governed by the forward propagator, $\mathcal{P}(\tau)\rho_t(\mathbf{x}) = \rho_{t+\tau}(\mathbf{x})$, where τ is called lag time. The propagator has a unique stationary distribution $\pi(\mathbf{x})$, as long as the underlying diffusion process is Markovian, ergodic and aperiodic.

Numerically easier to handle than the propagator is the closely related forward transfer operator[1–3] $\mathcal{T}(\tau)$, which propagates weighted probability densities $u_t(\mathbf{x}) = \rho_t(\mathbf{x})/\pi(\mathbf{x})$ forward in time

$$u_{t+\tau}(\mathbf{x}) = \mathcal{T}(\tau)u_t(\mathbf{x})\,. \tag{1}$$

Both, the propagator and the transfer operator can be projected to finite dimensional matrices by a Galerkin discretization with respect to a set of ansatz functions $(\chi_1(\mathbf{x}), \chi_2(\mathbf{x})...\chi_n(\mathbf{x}))$. If the ansatz functions are orthonormal, the Galerkin discretization of the transfer operator yields the matrix

$$\mathbf{T}(\tau):\ T_{ij}(\tau) = \frac{\langle\chi_i|\mathcal{T}(\tau)\chi_j\rangle_\pi}{\langle\chi_i|\chi_i\rangle_\pi}\,, \tag{2}$$

where $\langle f|g\rangle_\pi = \int_\Gamma f(x)\cdot g(x)\,\pi(\mathbf{x})\mathrm{d}\mathbf{x}$. The denominator and the numerator can be interpreted as (time-lagged correlation) functions, $\langle\chi_i|\mathcal{T}(\tau)\chi_j\rangle_\pi = \mathrm{cor}(\chi_j, \chi_i; \tau)$ and $\langle\chi_i|\chi_i\rangle_\pi = \mathrm{cor}(\chi_i, \chi_i; \tau = 0)$, and can thus be estimated from a realization of the underlying diffusion process, i.e. from a trajectory produced by MD simulations.

A wide collection of methods have been developed to estimate the discretized version of the transfer operator from numerical simulations. The discretization can be carried out with respect to disjoint subsets of the conformational space (Markov state models[1–9]) or with respect to continuous functions of the state space (core-set Markov models[10], variational Markov models[11]). The dominant eigenvectors and associated eigenvalues of a Markov model contain information on long-lived molecular conformations, the kinetic exchange process

between them and the associated equilibration times. This information can in turn be used to derive the hierarchy of barriers and minima of the underlying molecular free-energy surface. Markov models have been largely used in the last years and are now a fundamental tool to study and analyze the dynamics of molecular systems[12–17].

Associated to the transfer operator, there exists another operator called infinitesimal generator[2,18]

$$\mathcal{Q} = \lim_{\tau \downarrow 0} \frac{\mathcal{T}(\tau) - \mathcal{T}(0)}{\tau}\,, \tag{3}$$

that defines the differential equation

$$\frac{\partial}{\partial t} u_t(\mathbf{x}) = \mathcal{Q} u_t(\mathbf{x})\,, \tag{4}$$

with solution

$$\begin{aligned} u_{t+\tau}(\mathbf{x}) &= \exp(\mathcal{Q}\tau) u_t(\mathbf{x}) \\ &= \mathcal{T}(\tau) u_t(\mathbf{x})\,. \end{aligned} \tag{5}$$

$\mathcal{Q}$ and $\mathcal{T}(\tau)$ have the same eigenfunctions, while the eigenvalues of $\lambda_i(\tau)$ of $\mathcal{T}(\tau)$ are related to the eigenvalues θ_i of $\mathcal{Q}$, by

$$\lambda_i(\tau) = \exp(\tau\theta_i)\,. \tag{6}$$

It follows that one can recover the same information about the dynamics of the system, both from the transfer operator and the generator.

The corresponding Galerkin discretization of the infinitesimal generator is called rate matrix, it provides a transition pattern in terms of rates between adjacent disjoint subsets of the conformational space. On the other hand, although several methods for the discretization of transfer operators are available, the discretized infinitesimal generator is more difficult to be estimated numerically, because it is not possible to derive the matrix elements of $\mathbf{Q}$ from correlation functions. Furthermore, we will show in the "Discretization error" section, that there is no analogous relation of eq. 5 for the discretized operators and then $\mathbf{T}(\tau) \neq \exp(\mathbf{Q}\tau)$ (see fig. 1). This means that we cannot estimate $\mathbf{Q}$ from $\tau^{-1}\log(\mathbf{T}(\tau))$.

We propose a method to discretize the infinitesimal generator based on a Voronoi partition of the conformational space. We start from the Galerkin discretization of the generator

$$\mathbf{Q}:\ Q_{ij} = \frac{\langle \chi_i | \mathcal{Q}\chi_j \rangle_\pi}{\langle \chi_i | \chi_i \rangle_\pi}\,, \tag{7}$$

where the ansatz functions are the characteristic functions of the Voronoi cells $\chi_i = \Omega_i$, i.e. a set of orthonormal functions. Then we derive a numerical scheme to estimate $\mathbf{Q}$ that does not rely on correlation functions. Using the Gauss theorem, we write the rate between two neighboring cells in terms of the flux $\hat{\Phi}$ of configurations and of the Boltzmann weight of the intersecting surface between adjacent cells. Assuming that the flux is constant, we approximate the Boltzmann weight of the intersecting surface as the geometric average of the Boltzmann weight of the cells (square root approximation, SQRA), finding a direct algebraic relation between the potential energy function and the matrix elements Q_{ij} (eq. 7).

In principle, different types of averages (e.g. harmonic or arithmetic average) could be used, but a recently published proof[19] showed that the discretization of the generator converges, in the limit of infinitely small Voronoi cells, to the continuous infinitesimal generator $\mathcal{Q}$, if the Boltzmann weight of the intersecting surface is approximated by the geometric average. This SQRA has been used in literature before[20–22]. Interestingly, it cannot only be derived from the transition flux density, but the same result has recently been obtained from the maximum path entropy principle[23].

The SQRA discretization closes an important gap in the discretization methods for dynamical operators. It is fundamentally different from the discretization methods for the transfer operator. The matrix elements Q_{ij} are not estimated from correlation functions, but are calculated from the Boltzmann weights of the cells Ω_i and Ω_j and a constant flux factor $\hat{\Phi}$.

Estimating Boltzmann weights tends to be much easier than estimating correlation functions. While for low-dimensional systems the Boltzmann weights can be estimated directly from the potential energy function, for high-dimensional systems, it is more convenient use the free energy profile on few relevant coordinates, which can be obtained from a wide range of enhanced sampling protocols. However, a method to estimate efficiently the constant flux $\hat{\Phi}$ has so far been lacking.

We are now able to apply the SQRA to realistic systems. Using a two dimensional diffusion process and alanine dipeptide as example of a high-dimensional system, we numerically test the initial assumptions of the method: Does the SQRA approximation yield the correct eigenspace of the system? Does the discretization error decrease in the limit of small Voronoi cells? Is the flux indeed constant and is it independent of the potential? Note that alanine dipeptide is a single amino acid, alanine, capped by two end groups. The end groups are

chosen such that the central backbone torsion angles ϕ and ψ in alanine are subject to the same steric hindrances as an alanine residue within a longer peptide chain. This molecule thus serves as a standard test system for biomolecular dynamics simulations[6,11,24,25].

In this paper, we give a detailed derivation of the SQRA, a summary of the proof that it converges to an infinitesimal generator in the limit of small Voronoi cells and we discuss the relations between operators described in fig. 1. Next, we provide an approach to estimate the flux $\hat{\Phi}$ based on the robust Perron cluster analysis in conformation dynamics (PCCA+)[26].

II. THEORY

We consider ergodic and reversible Markovian processes, whose dynamics can be represented by the forward transfer operator[1–3] $\mathcal{T}(\tau) : L^1_\pi(\Gamma) \to L^1_\pi(\Gamma)$, defined for a certain finite lag-time τ, that acts on relative probability densities $u_t(\mathbf{x}) = \rho_t(\mathbf{x})/\pi(\mathbf{x})$, where $\rho_t(\mathbf{x})$ is the probability density at time t and $\pi(\mathbf{x})$ is the stationary probability density. The transfer operator propagates the functions $u_t(\mathbf{x})$ forward in time according to

$$u_{t+\tau}(\mathbf{y}) = \mathcal{T}(\tau)u_t(\mathbf{y}) = \frac{1}{\pi(\mathbf{y})}\int_\Gamma p(\mathbf{x},\mathbf{y};\tau)\, u_t(\mathbf{x})\, \pi(\mathbf{x})\, \mathrm{d}\mathbf{x}\,, \tag{8}$$

where $p(\mathbf{x},\mathbf{y};\tau)$ is the conditional probability to find the system in state $\mathbf{y}$, at time $t+\tau$, given that it was in the state $\mathbf{x}$ at time t. The basis of our considerations is a discretization of the state space Γ into disjoint subsets Ω_i. The Galerkin discretization $\mathcal{T}(\tau)$ (eq. 2) with respect to these subsets, turns into a row-stochastic transition matrix $\mathbf{T}(\tau)$. Its dominant eigenvectors, approximations of the eigenfunctions of $\mathcal{T}(\tau)$, contain information about the dynamics of the dominant processes of the system[1–7,9], associated with a timescale defined as:

$$t_i(\tau) = -\frac{\tau}{\ln(\lambda_i(\tau))}\,, \quad \forall\, \tau > 0\,, \tag{9}$$

where $\lambda_i(\tau)$ is the i*th* eigenvalue of the matrix $\mathbf{T}(\tau)$. If $t_i(\tau)$ does not depend on the lag time τ, then the matrix $\mathbf{T}(\tau)$ satisfies the Markovian property[3,5] and the discretization is considered valid, i.e. the underlying discretized molecular process can be approximated as a Markov chain with time step τ in this discretized space. In this case t_i is the implied timescale at which the ith dominant process occurs.

Besides the transition matrix $\mathbf{T}(\tau)$, we can also define a rate matrix $\mathbf{Q}$, which is in the same sense a discretization of the infinitesimal generator $\mathcal{Q}$ of the transfer operator. The

infinitesimal generator and the transfer operator are related by

$$\begin{aligned}\mathcal{Q}\, f(\mathbf{x}) &= \left.\frac{\partial \mathcal{T}(\tau)}{\partial \tau}\right|_{\tau=0} f(\mathbf{x}) \\ &= \lim_{\tau \downarrow 0} \frac{\mathcal{T}(\tau) - \mathcal{T}(0)}{\tau} f(\mathbf{x})\,, \end{aligned} \tag{10}$$

whose solution is

$$\mathcal{T}(\tau) = \exp(\mathcal{Q}\tau)\,. \tag{11}$$

Because the eigenvalues of $\mathcal{Q}$ and $\mathcal{T}(\tau)$ are related by eq. 6, the implied timescales of the kinetic processes can be derived also from the eigenvalues θ_i of the rate matrix:

$$t_i = -\frac{1}{\theta_i}\,. \tag{12}$$

Note that the implied timescales derived from the eigenvalues of the rate matrix (eq. 12) do not depend on the lag time. In the next section, we will show how to discretize the infinitesimal generator $\mathcal{Q}$, into a rate matrix $\mathbf{Q}$, following Lie et al.[21].

A. Square Root Approximation

Consider a Voronoi tessellation of the state space $\Gamma = \cup_{i=1}^{n} \Omega_i$, then define the transition probability matrix $\mathbf{T}(\tau)$, via eq. 2, the entries $T_{ij}(\tau)$ describe the probability to jump from the cell Ω_i to the cell Ω_j in a time span τ. The associated infinitesimal generator can be discretized on the basis of the same tessellation (eq. 7). Formally, the transition probability matrix and the rate matrix are related by $\mathbf{Q} := \left.\frac{\partial \mathbf{T}(\tau)}{\partial \tau}\right|_{\tau=0}$. Using the Gauss theorem one can show that the non-diagonal entries of the matrix satisfy

$$Q_{ij} = \frac{1}{\pi_i} \oint_{\partial\Omega_i \partial\Omega_j} \Phi(\mathbf{z})\, \pi(\mathbf{z}) \mathrm{d}S(\mathbf{z})\,, \tag{13}$$

where $\partial\Omega_i \partial\Omega_j$ is the common surface between the cell Ω_i and Ω_j, π_i is the Boltzmann probability of the cell Ω_i and $\Phi(\mathbf{z})$ denotes the flux of the configurations $\mathbf{z}$ through the infinitesimal surface $\partial\Omega_i \partial\Omega_j$. The complete derivation is provided in appendix A.

Multiplying and dividing the matrix entries Q_{ij} (eq. 13) by the Boltzmann density of the intersecting surface $\partial\Omega_i \partial\Omega_j$

$$s_{ij} = \oint_{\partial\Omega_i \partial\Omega_j} \pi(\mathbf{z})\, \mathrm{d}S(\mathbf{z})\,, \tag{14}$$

one obtains

$$\begin{aligned} Q_{ij} =& \frac{s_{ij}}{\pi_i} \oint_{\partial\Omega_i \partial\Omega_j} \Phi(\mathbf{z}) \, \frac{\pi(\mathbf{z})}{s_{ij}} \mathrm{d}S(\mathbf{z}) \\ =& \frac{s_{ij}}{\pi_i} \langle \Phi \rangle_{ij} \,, \end{aligned} \tag{15}$$

where $\langle \Phi \rangle_{ij}$ represents the mean value of the flux through the surface $\partial\Omega_i \partial\Omega_j$.

In what follows, we make the following assumptions

1. The flux $\hat{\Phi}$ is constant and does not depend on the potential energy function, it holds $\hat{\Phi} = \langle \Phi \rangle_{ij}$.

2. The cells are so small such that $\pi(\mathbf{x})$ is almost constant on every cell Ω_i and on every interface $\partial\Omega_i \partial\Omega_j$, i.e. $\pi|_{\Omega_i} \approx \pi_i$ and $\pi|_{\partial\Omega_i \partial\Omega_j} \approx \pi_{ij}$.

Due to assumption 1, the matrix elements of $\mathbf{Q}$ can be rewritten as

$$Q_{ij} = \frac{s_{ij}}{\pi_i} \hat{\Phi} \,. \tag{16}$$

The quantity s_{ij} (eq. 17), i.e. the Boltzmann density of the intersecting surface between two neighboring cells Ω_i and Ω_j, is a surface integral that can be approximated by the Boltzmann density π_{ij} due to assumption 2:

$$\begin{aligned} s_{ij} &= \oint_{\partial\Omega_i \partial\Omega_j} \pi(\mathbf{z}) \mathrm{d}S(\mathbf{z}) \\ &\approx \pi_{ij} \,. \end{aligned} \tag{17}$$

Thus eq. 16 reads

$$Q_{ij} = \frac{\pi_{ij}}{\pi_i} \, \hat{\Phi} \,. \tag{18}$$

A second approximation is necessary to estimate the Boltzmann weight of the intersecting surface π_{ij}. We have chosen to use the geometric mean of the Boltzmann weights of the centers of the cells Ω_i and Ω_j, which corresponds to an arithmetic mean of the corresponding potential energy function of the cells:

$$\begin{aligned} \pi_{ij} &= \sqrt{\pi_i \, \pi_j} \\ &= \exp\left(-\beta \frac{V(\Omega_i) + V(\Omega_j)}{2} \right) \,. \end{aligned} \tag{19}$$

In principle, other mean-value calculations could be used, but as we will show in the next section, only by the geometric mean the discretized operator converges to the continuous infinitesimal generator. Finally, the entries of the rate matrix are written as

$$Q_{ij} = \frac{\sqrt{\pi_i \, \pi_j}}{\pi_i} \, \hat{\Phi} = \sqrt{\frac{\pi_j}{\pi_i}} \, \hat{\Phi} \,. \tag{20}$$

Note that it is not necessary to know the partition function of the system, because it would cancel in the ratio π_j/π_i in eq. 20. Thus the unnormalized Boltzmann weights π_i and π_j can be used.

The matrix $\mathbf{Q}$, as formulated in eq. 20, is a valid approximation of the infinitesimal generator $\mathcal{Q}$ (eq. 10), that satisfies the properties of a rate matrix:

1. The diagonal entries satisfy $Q_{ii} = -\sum_{j\neq i} Q_{ij}$
2. The sum of the rows is zero $\sum_j Q_{ij} = 0$.

Moreover, the matrix $\mathbf{Q}$ defines the master equation for a jump process

$$\left.\frac{\partial \rho_i}{\partial \tau}\right|_{\tau=0} = C \sum_{i\sim j} (\rho_j Q_{ji} - \rho_i Q_{ij}) \,, \tag{21}$$

where ρ is the probability density, C is a normalization constant and the notation $i \sim j$ denotes neighboring cells.

B. Convergence of the rate matrix

The square root approximation of the infinitesimal generator $\mathcal{Q}$ is based on a Voronoi tessellation of the state space. In principle, it is not clear if this kind of approximation has a physically meaningful limit, whenever the number of Voronoi cells tends to infinity. If this limit exists, it is furthermore not clear whether the limit operator is physically reasonable. An arbitrary refinement strategy of increasing the number of Voronoi cells will probably not converge. However, a recent mathematical study[19] which will be published separately, shows that under suitable assumptions on the Voronoi tessellation, the square root approximation converges towards the generator of the Smoluchowski equation, i.e., towards the Langevin dynamics for the limit of high friction.

In what follows, let ε denote the maximal diameter of the cells and for given $\varepsilon > 0$ let $(P_i^\varepsilon)_i$ be the set of points that generate the Voronoi tessellation and let Ω_i^ε be the Voronoi cell that corresponds to P_i^ε. For any continuous function ρ, we write $\rho_i^\varepsilon := \rho(P_i^\varepsilon)$. In particular, for the function $\pi(x) := \exp(-\beta V(x))$ we write $v_i^\varepsilon := \sqrt{\pi_i^\varepsilon}$ and using eq. 20 we denote the right hand side of eq. 21 as

$$(\mathcal{L}^\varepsilon \rho)_i^\varepsilon := C_\varepsilon \sum_{i\sim j} \left(\rho_j^\varepsilon \frac{v_i^\varepsilon}{v_j^\varepsilon} - \rho_i^\varepsilon \frac{v_j^\varepsilon}{v_i^\varepsilon} \right) \,, \tag{22}$$

where $\sum_{i\sim j}$ relates to the sum over all neighboring cells Ω_j^ε of the cell Ω_i^ε and where we interpret $(\mathcal{L}^\varepsilon\rho)_i^\varepsilon$ as a function which is constant on every Ω_i^ε. Written in a formal way, for the scaling factor $C_\varepsilon = \varepsilon^{-2}$ and a suitable positive definite symmetric matrix $A_{\text{hom}} \in \mathbb{R}^{n\times n}$, it holds for twice continuously differentiable functions u that[19]

$$C_\varepsilon \sum_{i\sim j} \left(\rho_j^\varepsilon \frac{v_i^\varepsilon}{v_j^\varepsilon} - \rho_i^\varepsilon \frac{v_j^\varepsilon}{v_i^\varepsilon} \right) \to \nabla\cdot(A_{\text{hom}}\nabla\rho(x)) + \beta\nabla\cdot(\rho(x)A_{\text{hom}}\nabla V(x)) \quad \text{as } \varepsilon\to 0\,, \tag{23}$$

provided that $P_i^\varepsilon \to x$ as $\varepsilon \to 0$. In case that the Voronoi tessellations are isotropic, we find $A_{\text{hom}} = a\mathbb{I}$, where $a > 0$ is a constant and $\mathbb{I}$ is the identity. However, if for some reason the tessellations are systematically anisotropic, the right hand side of eq. 23 can be brought into the form of a classical Fokker-Planck operator via a coordinate transform. Hence, we also call the right hand side of eq. 23 a Fokker-Planck operator. In what follows, we will roughly explain how the convergence 23 can be obtained.

There exists a simpler version of eq. 22 known as *the discrete Laplace operator* $\mathcal{F}^\varepsilon$ having the form

$$(\mathcal{F}^\varepsilon\rho)_i^\varepsilon := C_\varepsilon \sum_{i\sim j} \left(\rho_j^\varepsilon - \rho_i^\varepsilon\right)\,. \tag{24}$$

Note that the use of $\mathcal{L}$ and $\mathcal{F}$ is opposite in[19]. It turns out that the understanding of the asymptotic behavior of $\mathcal{F}^\varepsilon$ is essential for the study of the asymptotic behavior of $\mathcal{L}^\varepsilon$.

In case the point process is a rectangular grid (fig. 2), the operator $\mathcal{F}^\varepsilon$ has been studied intensively and in broad generality from physicists (as generator of a markovian process that models Brownian motion, see the review[27]) and mathematicians (for rigorous results, see the review[28]). The notion of discrete Laplace operator can be understood as follows: On the lattice $\varepsilon\mathbb{Z}^n$ (that consists of all points $x \in \mathbb{R}^n$ such that $(\varepsilon^{-1}x) \in \mathbb{Z}^n$, see fig. 2), the *discrete derivative* in the j-th direction is given by $\mathrm{d}_{j,\varepsilon}\rho(x) := \frac{1}{\varepsilon}\left(\rho(x+\varepsilon e_j) - \rho(x)\right)$, where e_j is the j-th unit vector. The *second order discrete derivative* is given by

$$\begin{aligned}\mathrm{d}_j^2\rho(x) :&= \frac{1}{\varepsilon}\left(\mathrm{d}_j\rho(x) - \mathrm{d}_j\rho(x-\varepsilon e_j)\right)\\ &= \frac{1}{\varepsilon^2}\left[\left(\rho(x+\varepsilon e_j)-\rho(x)\right) + \left(\rho(x-\varepsilon e_j)-\rho(x)\right)\right]\,.\end{aligned} \tag{25}$$

Hence, we obtain for $x_i^\varepsilon \in \varepsilon\mathbb{Z}^n$ that

$$\sum_{j=1}^n \mathrm{d}_j^2\rho(x_i^\varepsilon) = \varepsilon^{-2}\sum_{j\sim i}\left(\rho(x_j^\varepsilon) - \rho(x_i^\varepsilon)\right) = \left(\mathcal{F}^\varepsilon\rho\right)_i\,, \tag{26}$$

where now $i \sim j$ relates to all neighbors $x_j^\varepsilon \in \varepsilon\mathbb{Z}^n$ of x_i^ε s.t. $\left|x_j^\varepsilon - x_i^\varepsilon\right| = \varepsilon$. We now show that for twice continuously differentiable functions u, it holds

$$(\mathcal{F}^\varepsilon \rho)_i^\varepsilon \to \Delta\rho \qquad \text{as } \varepsilon \to 0 \text{ if } x_i^\varepsilon \to x\,. \tag{27}$$

In order to show this, we use Taylor's formula, i.e.

$$\rho(x + \varepsilon e_i) - \rho(x) = \partial_i \rho(x)\varepsilon + \frac{1}{2}\partial_i^2 \rho(x)\varepsilon^2 + \sum_{k=3}^{\infty} \frac{1}{k!}\partial_i^k \rho(x)\varepsilon^k \tag{28}$$

and hence

$$\begin{aligned}
\mathrm{d}_j^2 \rho(x_i^\varepsilon) &= \frac{1}{\varepsilon^2}\left(\partial_j \rho(x_i^\varepsilon)\varepsilon + \frac{1}{2}\partial_j^2 \rho(x_i^\varepsilon)\varepsilon^2 + \sum_{k=3}^{\infty} \frac{1}{k!}\partial_j^k \rho(x_i^\varepsilon)\varepsilon^k\right) \\
&\quad + \frac{1}{\varepsilon^2}\left(-\partial_j \rho(x_i^\varepsilon)\varepsilon + \frac{1}{2}\partial_j^2 \rho(x_i^\varepsilon)\varepsilon^2 + \sum_{k=3}^{\infty} \frac{1}{k!}\partial_j^k \rho(x_i^\varepsilon)\left(-\varepsilon\right)^k\right) \\
&= \partial_j^2 \rho(x_i^\varepsilon) + \mathcal{O}(\varepsilon)\,.
\end{aligned} \tag{29}$$

From this, we obtain that eq. 27 holds.

We will now use the above insights to formally understand the asymptotic behavior of the operator

$$(\mathcal{L}^\varepsilon \rho)_i := \varepsilon^{-2} \sum_{i \sim j} \left(\rho_j^\varepsilon \frac{v_i^\varepsilon}{v_j^\varepsilon} - \rho_i^\varepsilon \frac{v_j^\varepsilon}{v_i^\varepsilon}\right), \qquad \text{where } v_i^\varepsilon = \exp\left(-\frac{1}{2}\beta V(x_i^\varepsilon)\right), \tag{30}$$

on the lattice $\varepsilon\mathbb{Z}^n$. Writing $V_i^\varepsilon := V(x_i^\varepsilon)$ and using the Taylor's formula, we obtain

$$\frac{v_i^\varepsilon}{v_j^\varepsilon} = 1 - \frac{1}{2}\beta\left(V_i^\varepsilon - V_j^\varepsilon\right) + \frac{1}{8}\beta^2\left(V_i^\varepsilon - V_j^\varepsilon\right)^2 - \mathcal{O}\left(\left(V_i^\varepsilon - V_j^\varepsilon\right)^3\right) \tag{31}$$

and inserting this expansion into eq. 30, we obtain

$$\begin{aligned}
(\mathcal{L}^\varepsilon \rho)_i &= \varepsilon^{-2} \sum_{i \sim j} \left(\left(\rho_j^\varepsilon - \rho_i^\varepsilon\right) + \frac{\beta}{2}\left(\rho_j^\varepsilon + \rho_i^\varepsilon\right)\left(V_j^\varepsilon - V_i^\varepsilon\right)\right) \\
&\quad + \varepsilon^{-2} \sum_{i \sim j} \left(\frac{1}{8}\beta^2\left(V_i^\varepsilon - V_j^\varepsilon\right)^2 + \mathcal{O}\left(\left(V_i^\varepsilon - V_j^\varepsilon\right)^4\right)\right)\left(\rho_j^\varepsilon - \rho_i^\varepsilon\right) \\
&\quad + \varepsilon^{-2} \sum_{i \sim j} \left(\rho_j^\varepsilon + \rho_i^\varepsilon\right)\mathcal{O}\left(\left(V_i^\varepsilon - V_j^\varepsilon\right)^3\right).
\end{aligned} \tag{32}$$

We know that for small $\varepsilon \approx 0$, it holds $\left(V_i^\varepsilon - V_j^\varepsilon\right) \approx \varepsilon \nabla V(x_i^\varepsilon) + \mathcal{O}(\varepsilon^2)$ and equivalently $\left(\rho_i^\varepsilon - \rho_j^\varepsilon\right) \approx \varepsilon \nabla \rho(x_i^\varepsilon) + \mathcal{O}(\varepsilon^2)$. Therefore, we obtain

$$(\mathcal{L}^\varepsilon \rho)_i^\varepsilon = \varepsilon^{-2} \sum_{i \sim j} \left(\left(\rho_j^\varepsilon - \rho_i^\varepsilon\right) + \frac{\beta}{2}\left(\rho_j^\varepsilon + \rho_i^\varepsilon\right)\left(V_j^\varepsilon - V_i^\varepsilon\right)\right) + \mathcal{O}(\varepsilon) \tag{33}$$

and using once more the Taylor expansion for u and V in eq. 33, we further obtain

$$\begin{aligned}(\mathcal{L}^\varepsilon\rho)_i^\varepsilon &= \varepsilon^{-2}\sum_{i\sim j}\left(\rho_j^\varepsilon-\rho_i^\varepsilon\right)+\varepsilon^{-2}\rho_i^\varepsilon\sum_{i\sim j}\beta\left(V_j^\varepsilon-V_i^\varepsilon\right)+\varepsilon^{-2}\sum_{i\sim j}\frac{\beta}{2}\left(\rho_j^\varepsilon-\rho_i^\varepsilon\right)\left(V_j^\varepsilon-V_i^\varepsilon\right)+\mathcal{O}(\varepsilon)\\ &= \varepsilon^{-2}\sum_{i\sim j}\left(\rho_j^\varepsilon-\rho_i^\varepsilon\right)+\varepsilon^{-2}\rho_i^\varepsilon\sum_{i\sim j}\beta\left(V_j^\varepsilon-V_i^\varepsilon\right)+\sum_{i\sim j}\frac{\beta}{2}\partial_j\rho(x_i^\varepsilon)\cdot\partial_j V(x_i^\varepsilon)+\mathcal{O}(\varepsilon)\,. \quad (34)\end{aligned}$$

Thus, as $\varepsilon\to 0$ we observe that

$$\begin{aligned}(\mathcal{L}^\varepsilon\rho)_i^\varepsilon &\to \Delta\rho(x)+\beta\rho(x)\Delta V(x)+\beta\nabla\rho(x)\cdot\nabla V(x) \qquad x_i^\varepsilon\to x\\ &= \Delta\rho(x)+\beta\nabla\cdot(\rho(x)\nabla V(x))\end{aligned}$$

on the Grid $\varepsilon\mathbb{Z}^n$. Hence, we recover eq. 23 with $A_{\text{hom}}=1$ for the cubic Voronoi tessellation.

On arbitrary Voronoi tessellations, things become more involved. In particular, the convergence (eq. 27) or calculations like in eq. 29 and 34 do not hold anymore, as they rely on the rectangular structure of $\mathbb{Z}^n$. However, the key ideas of the proof remain the same with the difference that some terms which explicitly cancel out in the above calculation only vanish in a "statistically averaged" sense, using G-convergence.

G-convergence is a concept from early stage in the development of Homogenization theory and is rarely used (refer to[29]), since other concepts are usually much better suited. In the discrete setting, G-convergence can be formulated in the following sense: The operator $\mathcal{F}^\varepsilon$ is called G-convergent if there exists a symmetric positive definite matrix A_{hom} such that for every continuous $f:\Omega\to\mathbb{R}$ the sequence ρ^ε of solutions to

$$-\left(\mathcal{F}^\varepsilon\rho^\varepsilon\right)_i := -\sum_{j\sim i}\left(\rho_j^\varepsilon-\rho_i^\varepsilon\right)=f(P_i^\varepsilon)\,, \quad (35)$$

converges in $L^2(\Omega)$ to the solutions ρ of $-\nabla\cdot(A_{\text{hom}}\nabla\rho)=f$, where we interpret ρ^ε as a function that is constant on every cell Ω_i^ε. Hence, G-convergence and convergence of the SQRA-operator are more or less equivalent conditions on the tessellation. In recent years, G-convergence (or eq. 27) has been proved for random operators

$$\left(\mathcal{F}_\omega^\varepsilon\rho\right)(x_i) := \frac{1}{\varepsilon^2}\sum_{j\sim i}\omega_{ij}\left(\rho(x_j)-\rho(x_i)\right) \quad (36)$$

on the grid $\varepsilon\mathbb{Z}^n$ for a broad range of random coefficients ω_{ij} (see the overview in[28]). However, for stationary and ergodic tessellations, the recent results in[19,30] seem to be the only ones.

In conclusion, we showed that the convergence in eq. 23 holds on the rectangular grid for sufficiently smooth functions ρ. The calculations suggest that the result also holds on more

general grids. However, on such more general grids, the mathematics behind the convergence (eq. 23) becomes much more involved and is thus shifted to the article[19]. The results there, are though more general as they state that solutions of $\mathcal{L}^\varepsilon \rho^\varepsilon = f^\varepsilon$ converge to solutions of $\mathcal{L}\rho = f$ provided $f^\varepsilon \to f$ in $L^2(\boldsymbol{Q})$.

III. DISCRETIZATION ERROR

A. Relation between transition probability and rate matrices

The Markovian property of the transition probability matrix $\mathbf{T}(\tau)$, i.e. the discretized version of the transfer operator $\mathcal{T}(\tau)$, is guaranteed only by a proper discretization of the space[3,31,32]. For example, assume a discretization of the space into three disjoint sets A, B, and C. If the system is in the state $\mathbf{x} \in A$, it will jump to a set B or C with different probabilities, depending on the position inside the set A. Because the position inside the set A depends on the previous position, the Markovian property is lost, on the level of the set A.

Note, that a fine enough discretization of the space prevents the loss of the Markovian property. Alternatively, it can be proven that for a large enough value of the lag time τ, the Chpaman-Kolmogorov condition $\mathbf{T}(n \cdot \tau) = \mathbf{T}(\tau)^n$ holds[3], guarantying the Markovianity of the process.

With regard to the matrix $\mathbf{Q}$, two problems arise:

- If τ is too small, the matrix $\mathbf{T}(\tau)$ could not describe a Markovian process and the matrix $\mathbf{Q}$ cannot be considered a proper generator of $\mathbf{T}(\tau)$.
- If τ is large enough to guarantee the Markovianity of $\mathbf{T}(\tau)$, then the generator $\mathbf{Q}$ is the correct generator, but it is not physically meaningful. A proper generator is defined for $\tau \to 0$, in other words for instantaneous transitions that occur between neighboring sets. If τ is too big, then $\mathbf{Q}$ would describe instantaneous transition rates between non-neighboring sets, that are not physical if we are considering a time-continuous dynamics.

In conclusion, the matrix $\mathbf{Q}$, obtained by square root approximation (eq. 20) is the Galerkin discretization of the infinitesimal generator $\mathcal{Q}$, but it is not the correct generator of the transition probability matrix $\mathbf{T}(\tau)$.

B. Flux estimation

The entries of the matrix $\mathbf{Q}$ (eq. 20) are written as the product of the term $\tilde{Q}_{ij} = \sqrt{\frac{\pi_j}{\pi_i}}$ and the flux $\hat{\Phi}$ that is assumed to be constant:

$$Q_{ij} = \sqrt{\frac{\pi_j}{\pi_i}} \cdot \hat{\Phi} = \tilde{Q}_{ij} \cdot \hat{\Phi}\,.$$

While the first term can be estimated analytically from the potential energy function of the system, the factor $\hat{\Phi}$ is unknown. Thus, we can estimate only the matrix $\tilde{\mathbf{Q}}$, that represents the correct rates up to the scaling factor $\hat{\Phi}$. Nonetheless, the eigenvectors of the matrix $\tilde{\mathbf{Q}}$ are a correct approximation of the eigenfunctions of the continuous operator $\mathcal{Q}$, while the eigenvalues $\tilde{\theta}_i$, are scaled by the factor $\hat{\Phi}$ as well, such that $\theta_i \approx \tilde{\theta}_i \cdot \hat{\Phi}$, where θ_i are the correct eigenvalues of $\mathcal{Q}$.

Because the eigenvalues of the transfer operator $\lambda_i(\tau)$ are associated to the eigenvalues of the infinitesimal generator θ_i by the relation

$$\exp(\tau\,\theta_i) = \lambda_i(\tau) \quad \forall i > 1\,, \tag{37}$$

one could estimate the value of the flux, by comparing the eigenvalues of the rate matrix $\tilde{\mathbf{Q}}$, with the eigenvalues of the matrix $\mathbf{T}(\tau)$ obtained by MSM. Unfortunately, because the matrix $\mathbf{Q}$ is not the correct infinitesimal generator of $\mathbf{T}(\tau)$, following this route would lead to a wrong result.

Molecular systems are characterized by n_c *conformations* in the space, i.e. metastable subsets of the state space where the system stays for a time significantly longer then some macroscopic time span. The matrices $\mathbf{Q}$ and $\mathbf{T}(\tau)$ can be reduced to the $n_c \times n_c$ matrices of the conformations $\mathbf{Q}^c$ and $\mathbf{T}^c(\tau)$ that satisfy

$$\exp(\tau\,\mathbf{Q}^c) = \mathbf{T}^c(\tau)\,. \tag{38}$$

Thus, the flux can be obtained from the eigenvalues of the matrices of the conformations. The derivation and the mathematical proof of eq. 38 is given in the appendix B.

Here, we propose a simple scheme to estimate $\hat{\Phi}$ based on eq. 38. Firstly, one constructs the matrix $\tilde{\mathbf{Q}}$ by SQRA and the matrix $\mathbf{T}(\tau)$ by MSM. Afterward, the two matrices are reduced respectively to $\tilde{\mathbf{Q}}^c$ and $\mathbf{T}^c(\tau)$ by PCCA+ and the flux is estimated from the respective eigenvalues as

$$\hat{\Phi}_i = \frac{\log \lambda_i^c(\tau)}{\tau\,\tilde{\theta}_i^c} \quad \forall i \in (1, n_c]\,. \tag{39}$$

In eq. 39 the subscript i denotes that the flux $\hat{\Phi}_i$ has been estimated from the ith pair of eigenvalues $\{\lambda_i^c(\tau),\, \widetilde{\theta}_i^c\}$. Actually, $\hat{\Phi}$ should not depend on the choice of the eigenvalues, but, in our numerical experiments, different values of $\hat{\Phi}_i$ have been found for different pairs of eigenvalues. The result improves, i.e. the difference reduces, if the Voronoi cells are more homogeneously distributed. Thus, estimating the flux from different eigenvalues (eq. 39), and the respective standard deviation can be used as a test to evaluate the quality of the SQRA.

IV. METHODS

A. Two dimensional system

We consider the two-dimensional diffusion process governed by the stochastic differential equation:

$$\begin{cases} \mathrm{d}x_t = -\nabla_x V\left(x_t, y_t\right) + \sigma \mathrm{d}B_t^x \\ \mathrm{d}y_t = -\nabla_y V\left(x_t, y_t\right) + \sigma \mathrm{d}B_t^y \end{cases}, \tag{40}$$

where B_t^i denotes a standard Brownian motion in the direction $i = x, y$, σ is the volatility and $V\left(x_t, y_t\right)$ is a two-dimensional potential energy surface given by the function:

$$V(x,y) = 4\left(x^3 - \frac{3}{2}x\right)^2 - x^3 + x + 2 + 2y^2\,. \tag{41}$$

In principle, we could estimate the rate matrix of the system by SQRA, with no need to integrate the equation of motion. We could generate a set of random points uniformly distributed on $\mathbb{R}^2$, then discretize the space by a Voronoi tessellation and apply the SQRA formula (eq. 20). On the other hand, only a subset of $\mathbb{R}^2$ is relevant for the dynamics of the system, thus we solve numerically the equation of motion in order to sample the conformational space. A discretized trajectory is also useful to build a MSM and to estimate a correct value of the flux.

We have numerically integrated eq. 40 with the Euler-Maruyama scheme, producing trajectories of 4×10^7 time-steps with a time step $\Delta t = 0.001$, for several values of the volatility σ.

Afterward, we have partitioned the sampled space with a Voronoi tessellation, picking random points from the trajectories, such that the minimum distance between two points, is

the distance r, an input parameter that represents the minimum diameter of the cells. Both the parameter r and the volatility σ affect the quality of the Voronoi tessellation and the number of cells. A simulation at high volatility, samples a larger subset of the state space, thus the Voronoi cells are more homogeneously distributed and approximately of the same size. We have produced trajectories with $\sigma = 1.0, 1.5, 2.0, 2.5$ and built Voronoi tessellation with $r = 0.1, 0.15, 0.2$.

We point out that it is not necessary to know the complete Voronoi tessellation to build the SQRA, but only the adjacency matrix that identifies the neighboring cells. Thinking of the Voronoi diagram in terms of convex polyhedra[21,33] permits to write a Linear Program to estimate the adjacency matrix, improving the efficiency compared to usual algorithms.

To estimate the flux of the system, we have constructed MSMs with enforced detailed balance[34] for each trajectory. The MSMs have been constructed on the same tessellation used for the SQRA, choosing a lag time range from 100 to 1000 time steps.

The PCCA+ analysis has been realized using three conformations as input parameter.

To study the dependence of the flux on the potential energy, we have perturbed the potential energy function (eq. 41) with the function

$$U(\kappa, x) = \kappa x \tag{42}$$

where κ is a parameter that tunes the strength of the perturbation.

B. Alanine dipeptide

We studied alanine dipeptide in explicit water, built as Acetyl-alanine-methylamide (Ac-A-NHMe) capped with an acetyl group on the N-terminus and n-methylamide on the C-terminus (Ac-Ala-NHMe), in order to simulate the dynamics of the torsion angles within a peptide chain.

The rate matrix has been constructed on the two relevant coordinates, the backbone torsion angles ϕ and ψ. Thus, the potential energy function $V(\mathbf{x})$ has been replaced by the free energy profile $F(\phi, \psi)$ on torsion angles in the SQRA formula. Because an analytical function for $F(\phi, \psi)$ is unknown, a MD simulation was necessary to estimate the free energy profile from the histogram of the trajectory projected on ϕ and ψ.

We carried out simulations with the GROMACS 5.0.2 simulation package[35], with the force field AMBER ff-99SB-ildn[36] and the TIP3P water model[37]. A velocity rescale thermostat[38]

has been applied to control the temperature and a leap-frog integrator[39] has been used to integrate the equation of the motion with a timestep of 2 fs. We have performed simulations in a NVT ensemble, at temperature of 300 and 900 K. The length of each simulation was 600 ns and we printed out the positions every nstxout=500 time steps, corresponding to 1 ps.

The space on relevant coordinates $\{\phi, \psi\} = [-\pi, \pi] \times [-\pi, \pi]$ has been discretized with a $2\pi \times 2\pi$-periodic Voronoi tessellation. To study the quality of the SQRA as a function of the size of the cells, we used as minimum diameter $r = 0.1, 0.14, 0.17$ rad.

The trajectories used to sample the free energy profile has been used also to build the MSMs and to estimate the flux. The MSMs have been built with enforced detailed balance on the same Voronoi tessellation of the rate matrix, with a lag-time range of [0:300] ps.

V. RESULTS AND DISCUSSION

A. Two dimensional system

As first application, we illustrate the method for a two dimensional diffusion process. The potential energy function (eq. (41), fig. 3-A) has three minima respectively at (-1.12,0), (0.05, 0) and (1.29,0), separated by two barriers, whose highest points are approximatively at (-0.83, 0) and (0.61,0).

Because the potential energy function is known and the system is two-dimensional, one could build the discretized generator by SQRA, without producing any trajectory, but using random points uniformly distributed on the space $\mathbb{R}^2$. This approach is not possible for high-dimensional systems, in which the accessible state space, at a given temperature T, makes up only a small fraction of the total state space. In high-dimensional systems, the accessible state space has to be identified by a molecular simulation. Therefore we have numerically solved the equation of motion to produce a discretized trajectory of the two dimensional system and sample the most characteristic states of the space. Moreover, we used the trajectory to select random states as centers of the Voronoi cells Ω_i, whose Boltzmann weight π_i have been estimated as arithmetic mean of the unnormalized Boltzmann densities

of all the points of the trajectory falling in the cell Ω_i:

$$\pi_i = \left(\sum_{k=1}^{\mathsf{nsteps}} \mathbf{1}_{\Omega_i}(x_k, y_k) \right)^{-1} \cdot \sum_{k=1}^{\mathsf{nsteps}} \mathbf{1}_{\Omega_i}(x_k, y_k) \, \exp\left(-\beta V(x_k, y_k)\right) \quad \forall \, \text{cell} \, \Omega_i \,, \tag{43}$$

where $\{x_k, y_k\}$ are the coordinates of the kth point of the trajectory, $\mathbf{1}_{\Omega_i}(x_n, y_n)$ is the indicator function of the Voronoi cell Ω_i and nsteps is the length of the trajectory. The quantity $\sum_{k=1}^{\mathsf{nsteps}} \mathbf{1}_{\Omega_i}(x_k, y_k)$ represents the number of times that the trajectory has visited the cell Ω_i.

We first discuss the results obtained from a simulation with volatility $\sigma = 2.0$ and a partition of the space in 1725 Voronoi cells, realized with $r = 0.1$ as minimum diameter of the cells (fig. 3-D).

Fig. 3-E shows the first three left eigenvectors of the matrix $\tilde{\mathbf{Q}}$, i.e. of the matrix $\mathbf{Q}$ scaled by the factor $\hat{\Phi}$. The first left SQRA eigenvector, associated to the eigenvalue $\theta_1 = 0$ has only positive entries and represents the Boltzmann distribution. The dominant eigenvectors, associated to eigenvalues $\theta_i < 0$, have positive and negative values and represent kinetic exchanges between regions with different sign. In particular, the second eigenvector describes the slowest kinetic process between the region that includes the first and second minimum (blue area in fig. 3-E) and the third minimum (red area in fig. 3-E), through the highest barrier of the potential energy function. The third eigenvector represents the second slowest transition, between the middle mininum and the two on the sides. All the other eigenvectors (data not shown) describe faster dynamic exchanges inside the metastable regions. The left SQRA eigenvectors are in great agreement with the left MSM eigenvectors (data not shown) and are an excellent approximation of the eigenfunctions of the infinitesimal generator.

The respective eigenvalues θ_i of the generator are associated to the eigenvalues of the transfer operator (eq. 6) and contain information about the implied timescales associated to the kinetic processes of the system. Thus, from the eigenvalues of the rate matrix, we can obtain a valid approximation of the implied timescales of the system according to eq. 12. The advantage of estimating the implied timescales from the eigenvalues of the rate matrix (eq. 12), respect to the eigenvalues of the transition probability matrix (eq. 9), is that it is not necessary to verify the convergence of the implied timescales as in MSMs[3]. On the other hand, if we do not know the value of $\hat{\Phi}$, then we can only know the eigenvalues $\tilde{\theta}_i$ of the matrix $\tilde{\mathbf{Q}}$, that are correct up to the scaling factor $\hat{\Phi}$. The eigenvalues $\tilde{\theta}_i$ are useful anyway to evaluate how much a dominant process is faster than another one. For example,

if the second eigenvector is associated to a timescale of $t_2 = 70.53\,\hat{\Phi}^{-1}$ time steps, while the third eigenvector is associated to a timescale of $t_3 = 19.14\hat{\Phi}^{-1}$ time steps, then the process associated to the third eigenvector is 3.68 times faster than the process associated to the second eigenvector (tab. I and II).

B. Estimation of the flux

To estimate the value of the flux $\hat{\Phi}$, we have built MSMs and the matrices of the conformations $\tilde{\mathbf{Q}}^c$ and $\mathbf{T}^c(\tau)$ by PCCA+. Because the system has three metastable states, the matrices $\tilde{\mathbf{Q}}^c$ and $\mathbf{T}^c(\tau)$ are 3×3 and the flux $\hat{\Phi}$ has been estimated comparing the second and third eigenvalues of the matrices, i.e. $\{\tilde{\theta}_i^c,\ \lambda_i^c(\tau);\ i = 2, 3\}$. In each table that we present (tabs. III, IV, V and VI), $\hat{\Phi}_2$ denotes the flux estimated comparing the second eigenvalues, $\hat{\Phi}_3$ denotes the flux estimated comparing the third eigenvalues, $\bar{\Phi}$ is the average flux between $\hat{\Phi}_2$ and $\hat{\Phi}_3$, "std" is the standard deviation and "rel. err." is the relative error.

We have first studied how the flux depends on the volatility of the system, then we have produced four trajectories respectively with $\sigma = 1.0$, 1.5, 2.0 and 2.5 and built four rate matrices by SQRA and four transition probability matrices by MSM. The Voronoi tessellation of the space has been realized with $r = 0.15$. The trajectories for $\sigma = 1.0$, $\sigma = 1.5$ and $\sigma = 2.0$ and the respective partitions of the space are presented in fig. 3-(B, C, D).

Increasing the volatility, that is linked to the temperature of the environment, the trajectory samples a larger subset of the state space. Because the Voronoi tessellation is realized picking random points from the trajectories, at high volatility, the tessellation consists of a large number of cells, homogeneously distributed and approximately of the same size. The average flux increases linearly with the volatility (tab. III, col. $\hat{\Phi}$), because high volatility corresponds to a faster dynamics: a given cell is visited for a short amount of time, consequently, the number of times that a cell border is crossed rises. We also observe that the error on the flux, i.e. the difference between $\hat{\Phi}_2$ and $\hat{\Phi}_3$ reduces significantly increasing the volatility (tab. III, col. "rel. err."). Thus, we deduce that the quality of the SQRA is intrinsically linked to the quality of the Voronoi tessellation and the error on the measure reduces when the cells are homogeneously distributed.

Afterward, we have studied how the flux depends on the size of the cells (parameter r,

tab. IV). Keeping the volatility constant ($\sigma = 2.0$), but reducing the minimum distance between centers ($r = 0.2$, 0.15 and 0.1), a single cell is visited for a shorter time and the number of transitions through the intersecting surface, i.e. the flux, grows. We also note a significant reduction of the relative error, that confirms the convergence of the rate matrix to the continuous generator for small Voronoi cells.

Finally, we have studied how a perturbation (eq. 42 with $\kappa = 0$, 0.5, 1) of the potential energy function affects the flux. The effect of such perturbation is to tilt the potential energy function along the axis x and to modify respectively the Boltzmann weights. The experiment has been repeated with $\sigma = 1.5$ and $\sigma = 2.0$ and the results are collected respectively in tab. V and VI. In both the cases the perturbation does not affect the average flux, confirming the initial assumption that the flux does not depend on the potential energy function.

C. Alanine dipeptide

As high dimensional system, we have studied alanine dipeptide (Ac-A-NHMe) in explicit water. In principle, one could estimate the rate matrix using the full potential energy function, that is parametrized by the forcefield[36], but the resulting high-dimensional rate matrix would be computationally intractable. We have constructed the rate matrix and the MSM on two relevant coordinates, the backbone dihedral angles ϕ and ψ, that capture the main dynamical properties of the system. Running a MD simulation was necessary only to sample the free energy landscape, which can be recovered by a normalized histogram of a long trajectory projected on the dihedral angles ϕ and ψ. If the two-dimensional space $\{\phi, \psi\}$ is discretized by a Voronoi tessellation, then the Boltzmann weight of each cell is proportional to the number of times that the system has visited the cell Ω_i divided by the length of the trajectory:

$$\pi_i(\phi, \psi) = \lim_{\mathsf{nsteps}\to+\infty} \frac{\sum_{k=1}^{\mathsf{nsteps}} \mathbf{1}_{\Omega_i}(\phi_k, \psi_k)}{\mathsf{nsteps}} \quad \forall\, \text{cell}\, \Omega_i \tag{44}$$

where $\{\phi_k, \psi_k\}$ are the coordinates of the system at time step k and nsteps is the length of the trajectory. Consequently, the free energy profile of the cell Ω_i reads

$$F_i(\phi, \psi) = -\frac{1}{k_B T} \log \pi_i(\phi, \psi) + \mathrm{C}\,, \tag{45}$$

where C is a negligible constant.

We have first studied the rate matrix built on free energy profile obtained from a simulation at 300 K. In this case, the MD simulation does not sample the full state space and large regions of the space $\{\phi, \psi\}$, are never visited (figs. 4-A,B). In particular, few trajectory points are found in the barrier regions at $\phi \sim 0$, resulting large Voronoi cells in these regions. We have built the Voronoi tessellation, on the same trajectory, with $r = 0.1$ (figs. 4-A) and $r = 0.17$ (figs. 4-B). In both the cases the cells have significant different sizes in the minima and barrier regions. The only way to improve the discretization, i.e. to have small cells homogeneously distributed, is to increase the temperature to permit a better sampling of the state space. Fig. 4-C shows a trajectory at temperature 900 K, that covers a larger subspace of the state space, with a much more homogeneous Voronoi tessellation. From the two dimensional system and from alanine dipeptide, we have learnt that simulations at high temperatures (high volatilities), yield a homogeneous Voronoi discretization. Furthermore, at high temperatures the flux can be estimated with much higher confidence, than at low temperatures. This suggests that the Voronoi discretization for the SQRA should be based on a high temperature simulation, even if the goal is to model the dynamics at room temperature. The realistic magnitude of the implied timescales can be estimated from the high temperature simulation in a second step. Indeed, the Boltzmann weights can be obtained from the high temperature simulation by first calculating the free energy profile via eq. 45 and then converting F_i into the Boltzmann weights at room temperature via eq. 46. In summary, we propose a strategy in which a model of the dynamics at room temperature is obtained entirely from a simulation at high temperature.

Fig. 4-D shows the dominant left eigenvectors of the rate matrix built on the trajectory sampled at 900 K. The first eigenvector represents the Boltzmann distribution with the typical conformational states (β region, L_α region, and R_α region). The second eigenvector represents a kinetic exchange between the L_α-minimum ($\phi > 0$) and the α-helix and β-sheet minima ($\phi < 0$). The associated implied timescale is $146\hat{\Phi}^{-1}$ ps. The third eigenvector represents a transition β-sheet $\longleftrightarrow$ α-helical conformation, i.e. a torsion around ψ, and is associated to a timescale of $40\hat{\Phi}^{-1}$ ps. The eigenvectors are the same obtained from a MSM[25].

Even though the free energy profile was built on a trajectory produced at temperature $T = 900$ K, the eigenvectors are a valid approximation of the eigenvectors of the system at $T = 300$ K. Indeed, the simulation at $T = 900$ K was used only to build the free energy

profile according to eq. 45, but the Boltzmann weights for the SQRA have been estimated by the approximation

$$\pi_i \approx \exp\left(-\beta F_i(\phi,\, \psi)\right) \ . \tag{46}$$

where $\beta = \frac{1}{K_B T}$ has been set after the simulation with $T = 300$ K. Instead of this simple approximation to get the free energy profile, higher-order reweighting schemes can be applied as well[40].

To estimate the value of the flux, we have constructed a MSM and the conformation matrices assuming the existence of three metastable states (β-sheet, Lα-helix and Rα-helix). Using a free energy profile obtained from a simulation at $T = 900$ K, the gap between $\hat{\Phi}_2$ and $\hat{\Phi}_3$ is statistically acceptable. If the Voronoi tessellation is built with $r = 0.2$, the error was 8.58% (tab. VII, first row). Reducing the size of the cells ($r = 0.17$), the error reduces to 2%, confirming the results obtained also for the two dimensional system (tab. VII, second row).

By contrast, if the free energy was obtained from a simulation at temperature $T = 300K$, the difference between $\hat{\Phi}_2$ and $\hat{\Phi}_3$ is not negligible. The relative error is greater than 100%, and reducing the size of the cells ($r = 0.17$, 0.14 and 0.1) does not improve significantly the result (table VII, third, forth and fifth row). The reason for these results is that an insufficient sampling leads to an inhomogeneous Voronoi tessellation.

VI. CONCLUSION

The paper contributes to the classical molecular simulation community in three ways. It provides an easy way to estimate the rates between metastable molecular conformations. It shows that this type of discretization converges to a Fokker-Planck-operator. Finally, it shows that there is an easy mathematical relation between the discretized generator of the molecular process and the potential energy landscape.

Since many years the concept of transfer operator, well known in thermodynamics and quantum mechanics, has been established inside the classical molecular simulation community[1–3] and new methods, such as Markov State Models[1–9] have been developed to provide a discretized version of the transfer operator, in order to reduce the complexity and study conformational transition networks of molecular systems. The concept of transfer operator is connected to the concept of generator, which is simply the time-derivative of the

transfer operator. While the spatial discretization of the transfer operator is a transition probability matrix of a Markov chain, the spatial discretization of the generator is a rate matrix, which is, in general, hard to extract from time-discretized simulation data.

Our method simply uses the Boltzmann distribution of states for discretize the generator. The first underlying assumption is that we can define a continuity equation for the time-derivative of the transfer operator. Then, exploiting the Gauss theorem, we write the rate between two neighbor states as a surface integral of the flux, weighted by the Boltzmann density of the intersecting surface. The second assumption is a constant flux, i.e, the flux does not depend on the potential energy but on the discretization of the space. Instead of computing the Boltzmann weight of the intersecting surface of two adjacent Voronoi cells, here, it is estimated as geometric average of the Boltzmann weight of the cells. This we denoted as square root approximation (SQRA).

After having described in detail how to derive the SQRA, we have provided a mathematical proof that the rate matrix converges to the generator of the Smoluchowski equation[19] for infinitely small subsets of the conformational space. The validity of the theoretical assumptions has been confirmed also by numerical experiments. We have seen that the error on the measure of the flux decreases, reducing the size of the Voronoi cells, i.e. that the quality of the SQRA depends on the discretization of the state space. Moreover, we have demonstrated that an external perturbation to the potential energy function does not affect the value the flux, according to the second assumption about the independence of the flux on the potential energy function.

While for low dimensional systems, the SQRA can be linked directly to the potential energy function of the system; for high dimensional systems it is convenient to reduce the dimensionality to relevant coordinates and to replace the potential energy function with a free energy profile in few dimensions. In this paper, for Alanine dipeptide, we have performed MD simulations at different temperatures in order to produce a discretized trajectories of the system. Afterward, we have recovered the free energy profile from the histogram of the trajectories projected on the backbone dihedral angles. The results have shown that the quality of the SQRA improves using the free energy profile built from the simulation realized at high temperature, which provides a better sampling of the state space.

The SQRA can be improved implementing enhanced sampling techniques like metadynamics[41,42] or umbrella sampling[43], which offer a double advantage. Firstly, the MD

simulation time is notably reduced; secondly, they provide an analytical function for the free energy profile.

An important further application of the square root approximation, is the possibility to study the effect of Hamiltonian perturbation on the dynamics of molecular systems. Like other reweighting methods[44], SQRA can be useful to improve the parametrization of force fields[25] or to test the influence of restraining potentials[45,46] on the dynamics of the system. Furthermore, the method can be used to study the sensitivity of the dominant eigenspace on the degrees of freedom of the system[47,48].

In conclusion, we believe that the square root approximation can become a fundamental tool for the study of the dynamics of molecular systems and can expands its borders of applicability in different ways that will be treated in future works.

Appendix A: Gauss theorem

The Gauss theorem can be used to rewrite the non-diagonal entries of the matrix $\mathbf{Q}$ as a function of the flux and the stationary distribution.

Gauss theorem. Given a Voronoi tessellation of the state space $\Gamma = \cup_{i=1}^{n} \Omega_i$ and the discretized transfer operator $\mathbf{T}(\tau)$, the matrix $\mathbf{Q} := \frac{\partial \mathbf{T}(\tau)}{\partial \tau}\Big|_{\tau=0}$ satisfies

$$Q_{ij} = \frac{1}{\pi_i} \oint_{\partial\Omega_i \partial\Omega_j} \Phi(\mathbf{z})\, \pi(\mathbf{z}) \mathrm{d}S(\mathbf{z}) \tag{A1}$$

where $\partial\Omega_i\partial\Omega_j$ is the common surface between the cell Ω_i and Ω_j, π_i is the Boltzmann density of the cell i and $\Phi(\mathbf{z})$ denotes the flux of the configurations $\mathbf{z} \in \partial\Omega_i\partial\Omega_j$, through the infinitesimal surface $\partial\Omega_i\partial\Omega_j$.

Proof The conditional probability density $p(\mathbf{x}, \mathbf{y}; \tau)$ denotes the probability of observing the system in the state $\mathbf{y}$, after a time τ, given that it has been in $\mathbf{x}$. Because the system will always assume a thermodynamic state, it yields $\int_\Gamma p(\mathbf{x}, \mathbf{y}; \tau)\mathrm{d}\mathbf{y} = 1$. Thus, the conservation of the conditional probability density, can be associated to the mass conservation of a fluid, that moves in the state space Γ, transporting the properties of the system and we can introduce the continuity equation:

$$\frac{\partial p(\mathbf{x}, \mathbf{y}; \tau)}{\partial \tau}\bigg|_{\tau=0} = -\nabla_{\mathbf{y}} \cdot \mathbf{j} \tag{A2}$$

where $\mathbf{j} = p(\mathbf{x}, \mathbf{y}; \tau)\mathbf{v}(\mathbf{x})$ is the density flux and $\mathbf{v}(\mathbf{x})$ is the flow velocity. We interpret the flux of the probability density as the probability per unit area per unit time, that a trajectory passes through a surface. While the flow velocity vector represents the velocity with which the system moves from the state $\mathbf{x}$ to $\mathbf{y}$.

We now use the continuity equation, to rewrite $\mathbf{Q}$:

$$
\begin{aligned}
Q_{ij} &:= \left.\frac{\partial T_{ij}(\tau)}{\partial \tau}\right|_{\tau=0} \\
\text{(a)} &= \left.\frac{\partial}{\partial \tau}\left[\frac{1}{\pi_i}\int_{\Omega_j}\int_{\Omega_i} p(\mathbf{x},\mathbf{y};\tau)\pi(\mathbf{x})\mathrm{d}\mathbf{x}\mathrm{d}\mathbf{y}\right]\right|_{\tau=0} \\
&= \frac{1}{\pi_i}\int_{\Omega_j}\int_{\Omega_i} \left.\frac{\partial p(\mathbf{x},\mathbf{y};\tau)}{\partial \tau}\right|_{\tau=0} \pi(\mathbf{x})\mathrm{d}\mathbf{x}\mathrm{d}\mathbf{y} \\
\text{(b)} &= \frac{1}{\pi_i}\int_{\Omega_j}\int_{\Omega_i} -\nabla_{\mathbf{y}}\cdot\mathbf{j}|_{\tau=0}\ \pi(\mathbf{x})\mathrm{d}\mathbf{x}\mathrm{d}\mathbf{y} \\
\text{(c)} &= \frac{1}{\pi_i}\int_{\Omega_j}\oint_{\partial\Omega_i} -\mathbf{j}|_{\tau=0}\cdot\mathbf{n}_i\ \pi(\mathbf{x})\mathrm{d}S(\mathbf{x})\mathrm{d}\mathbf{y} \\
\text{(d)} &= \frac{1}{\pi_i}\int_{\Omega_j}\oint_{\partial\Omega_i} -\delta_{\mathbf{x}=\mathbf{y}}\mathbf{v}(\mathbf{x})\cdot\mathbf{n}_i\ \pi(\mathbf{x})\mathrm{d}S(\mathbf{x})\mathrm{d}\mathbf{y} \\
\text{(e)} &= \frac{1}{\pi_i}\oint_{\partial\Omega_i\partial\Omega_j} \Phi(\mathbf{z})\ \pi(\mathbf{z})\mathrm{d}S(\mathbf{z})
\end{aligned}
\tag{A3}
$$

where we have used:

(a) The discretized version of the transfer operator in eq. (8).

(b) The continuity equation.

(c) The divergence theorem. The vector $\mathbf{n}_i$ is the unit vector orthogonal to the surface $\partial\Omega_i$.

(d) Because $\tau = 0$, we have

$$p(\mathbf{x},\mathbf{y};\tau) = \delta_{\mathbf{x}=\mathbf{y}} \tag{A4}$$

Then the density flux is $\mathbf{j}|_{\tau=0} = \delta_{\mathbf{x}=\mathbf{y}}\mathbf{v}(\mathbf{x})$.

(e) If $\tau = 0$, only instantaneous transitions between neighbor cells have to be taken into account. Thus, the only points that satisfy $\mathbf{x} = \mathbf{y}$, are the points on the intersecting surface $\partial\Omega_i\partial\Omega_j$. The quantity $\Phi(\mathbf{z})$ denotes the flux of the configurations $\mathbf{z}$ trough the infinitesimal surface $\partial\Omega_i$. Note that $\Phi(\mathbf{z}) = -\delta_{\mathbf{x}=\mathbf{y}}\mathbf{v}(\mathbf{x})\cdot\mathbf{n}_i = \delta_{\mathbf{x}=\mathbf{y}}\mathbf{v}(\mathbf{x})\cdot\mathbf{n}_j$ where $\mathbf{n}_j$ is the unit vector normal to the surface $\partial\Omega_j$.

□

Appendix B: Transition matrices in the space of conformations

In the following section, we explain why the relation $\exp(\tau\,\mathbf{Q}^c) = \mathbf{T}^c(\tau)$ (eq. 38) is true.

We consider a partition of the state-space Γ into n_c overlapping metastable conformations. We now introduce a set of n_c membership functions $\chi = \{\chi_1, ..., \chi_{n_c}\}$ such that the function $\chi_i(\mathbf{x}) : \Gamma \to [0, 1]$ provides the probability that a state $\mathbf{x} \in \Gamma$ belongs to the conformation C_i: The membership functions meet the partition of unity property, i.e. $\forall \mathbf{x} \in \Gamma,\ \sum_i^{n_c} \chi_i(\mathbf{x}) = 1\ \forall i$. Thus the membership functions determine a standard n_c-simplex.

Because of metastability of the conformations, a state $\mathbf{x}$ tends to not leave its starting conformation C_i. Thus, the product between the generator $\mathcal{Q}$ and the membership function χ_i is almost zero for each conformation i:

$$\mathcal{Q}\chi_i \approx 0 \quad \forall i = 1, ..., n_c \tag{B1}$$

For the identification of the conformations, it can be assumed, that the function χ_i spans the same linear space as the leading first n_c right eigenfunctions $\mathcal{F}_i$ of the generator $\mathcal{Q}$, associated to eigenvalues θ_i near zero[31]. Thus, we can define an invertible transformation matrix $\mathbf{A}$ of size $n_c \times n_c$, such that $\chi = \mathcal{F}\mathbf{A}$, then

$$\mathcal{Q}(\mathcal{F}\,\mathbf{A})_i = \theta_i(\mathcal{F}\,\mathbf{A})_i \approx 0 \tag{B2}$$

The transformation matrix $\mathbf{A}$ is finally used to prove that if $\mathcal{Q}$ is the infinitesimal generator of $\mathcal{T}(\tau)$, then $\mathbf{Q}^c$ is the generator of $\mathbf{T}^c(\tau)$.

Lemma[49,50] If the n_c eigenfunctions $\mathcal{F} = \{\mathcal{F}_1, ..., \mathcal{F}_{n_c}\}$ of $\mathcal{Q}$, associated to eigenvalues $\theta_i \approx 0$, are π-orthonormal and $\chi = \mathcal{F}\mathbf{A}$ is a regular basis transformation of these eigenfunctions, then

$$\text{if}\ \ \exp(\tau\,\mathcal{Q}) = \mathcal{T}(\tau)\ \Rightarrow\ \exp(\tau\,\mathbf{Q}^c) = \mathbf{T}^c(\tau)$$

Proof. The eigenfunctions $\mathcal{F}_i$ of $\mathcal{Q}$ are eigenfunctions also of $\mathcal{T}(\tau)$ with eigenvalues $\lambda_i(\tau) = \exp(\tau\,\theta_i)$ (semigroup property). Thus it yields

$$\begin{aligned} \mathcal{T}(t)\mathcal{F}_i &= \lambda_i(\tau)\mathcal{F}_i = \exp(\tau\,\theta_i)\mathcal{F}_i \\ \mathcal{Q}\,\mathcal{F}_i &= \theta_i\,\mathcal{F}_i \end{aligned} \tag{B3}$$

The matrix $\mathbf{T}^c(\tau)$ of the conformations is the Galerkin discretization of the operator $\mathcal{T}(\tau)$ on the basis of the membership functions χ_i. Since the membership functions are not

orthogonal, the matrix $\mathbf{T}^c(\tau)$ is the product of two matrices generated by the corresponding inner products:

$$\mathbf{T}^c(\tau) = \left(\langle \chi, \chi \rangle_\pi\right)^{-1} \langle \chi, \mathcal{T}(\tau)\, \chi \rangle_\pi \tag{B4}$$

Replacing $\chi = \mathcal{F}\mathbf{A}$ in eq. B4, then

$$\begin{aligned}
\mathbf{T}^c(\tau) =& \left(\langle \chi, \chi \rangle_\pi\right)^{-1} \langle \chi, \mathcal{T}(\tau)\, \chi \rangle_\pi \\
=& \left(\mathbf{A}^\top \langle \mathcal{F}^\top,\, \mathcal{F} \rangle_\pi\, \mathbf{A}\right)^{-1}\, \mathbf{A}^\top \langle \mathcal{F}^\top,\, \mathcal{T}(\tau)\, \mathcal{F} \rangle_\pi\, \mathbf{A} \\
=& \left(\mathbf{A}^\top\, \mathbf{A}\right)^{-1}\, \mathbf{A}^\top \langle \mathcal{F}^\top,\, \Lambda(\tau)\, \mathcal{F} \rangle_\pi\, \mathbf{A} \\
=& \mathbf{A}^\top \langle \mathcal{F}^\top,\, \mathcal{F} \rangle_\pi\, \Lambda(\tau) \mathbf{A} \\
=& \mathbf{A}^\top\, \Lambda(\tau)\, \mathbf{A}\,.
\end{aligned} \tag{B5}$$

It follows that

$$\begin{aligned}
\mathbf{T}^c(\tau) =& \mathbf{A}^\top\, \Lambda(\tau)\, \mathbf{A} \\
=& \mathbf{A}^\top\, \exp(\tau\, \Theta)\, \mathbf{A} \\
=& \exp(\tau\, \mathcal{Q})\,.
\end{aligned} \tag{B6}$$

where the matrices Θ and $\Lambda(\tau)$ denote respectively the diagonal matrices $n_c \times n_c$ of the eigenvalues θ_i and $\lambda(\tau)_i$. Then $\mathbf{Q}^c$ is an infinitesimal generator of $\mathbf{T}^c(\tau)$. □

In practice, one can exploit the partition of unity property to determine the transformation matrix $\mathbf{A}$ using the Robust Perron Cluster Analysis (PCCA+)[26]. The eigenfunctions $\mathcal{F}$ are unknown, thus one can use the eigenvectors of the matrix $\mathbf{Q}$ estimated by square root approximation.

ACKNOWLEDGMENTS

This research has been funded by Deutsche Forschungsgemeinschaft (DFG) through grant CRC 1114 *Scaling Cascades in Complex Systems*, Projects A05 *Probing scales in equilibrated systems by optimal nonequilibrium forcing*, B05 *Origin of the scaling cascades in protein dynamics* and C05 *Effective models for interfaces with many scales.*

REFERENCES

[1]C. Schütte, A. Fischer, W. Huisinga, and P. Deuflhard, *Journal of Computational Physics* **151**, 146 (1999).

[2]C. Schütte, W. Huisinga, and P. Deuflhard, *ZIB Report* **36**, SC 99 (1999).

[3]J.-H. Prinz, H. Wu, M. Sarich, B. Keller, M. Senne, M. Held, J. D. Chodera, C. Schütte, and F. Noé, *J. Chem. Phys.* **134**, 174105 (2011).

[4]P. Deuflhard, W. Huisinga, A. Fischer, and C. Schütte, *Linear Algebra Appl.* **315**, 39 (2000).

[5]W. C. Swope, J. W. Pitera, and F. Suits, *J. Phys. Chem. B* **108**, 6571 (2004).

[6]J. D. Chodera, N. Singhal, V. S. Pande, K. A. Dill, and W. C. Swope, *J. Chem. Phys.* **126**, 155101 (2007).

[7]N.-V. Buchete and G. Hummer, *J. Phys. Chem. B* **112**, 6057 (2008).

[8]B. Keller, X. Daura, and W. F. Van Gunsteren, *J. Chem. Phys.* **132**, 074110 (2010).

[9]B. Keller, P. Hünenberger, and W. F. van Gunsteren, *J. Chem. Theory Comput.* **7**, 1032 (2011).

[10]O. Lemke and B. G. Keller, *J. Chem. Phys.* **164104**, 1 (2016).

[11]F. Nüske, B. Keller, G. Perez-Hernandez, A. S. J. S. Mey, and F. Noé, *J. Chem. Theory Comput.* **10**, 1739 (2014).

[12]V. A. Voelz, G. R. Bowman, K. A. Beauchamp, and V. S. Pande, *J. Am. Chem. Soc.* **132**, 1526 (2010).

[13]G. D. Fabritiis, N. Stanley, and S. Esteban-mart, *Nat. Commun.* **5**, 5272 (2014).

[14]G. R. Bowman, E. R. Bolin, K. M. Hart, B. C. Maguire, and S. Marqusee, *Proc. Natl. Acad. Sci. U.S.A.* **112**, 2734 (2015).

[15]N. Plattner and F. Noé, *Nat. Commun.* **6**, 7653 (2015).

[16]L. Zhang, I. C. Unarta, P. P.-H. Cheung, G. Wang, D. Wang, and X. Huang, *Accounts Chem. Res.* **49**, 698 (2016).

[17]J. Witek, B. G. Keller, M. Blatter, A. Meissner, T. Wagner, and S. Riniker, *J. Chem. Inf. Model.* **56**, 1547 (2016).

[18]B. Øksendal, *Stochastic Differential Equations: An Introduction with Applications*, Springer Verlag, Berlin, 6th edition, 2003.

[19]M. Heida, *WIAS Preprint Nr.* .

[20]D. J. Bicout and A. Szabo, *J. Chem. Phys.* **109**, 10.1063/1.476800 (1998).

[21]H. C. Lie, K. Fackeldey, and M. Weber, *SIAM. J. Matrix Anal. Appl.* **34**, 738 (2013).

[22]A. Schild, *Electron Fluxes During Chemical Processes in the Electronic Ground State*, PhD thesis, Freie Universität Berlin, Berlin, 2013, http://www.diss.fu-berlin.de/diss/receive/FUDISS_thesis_000000095279.

[23]P. D. Dixit, A. Jain, G. Stock, and K. A. Dill, *J. Chem. Theory Comput.* **11**, 5464 (2015).

[24]J. Vymětal and J. Vondrášek, *The Journal of Physical Chemistry B* **114**, 5632 (2010).

[25]F. Vitalini, A. S. J. S. Mey, F. Noé, B. G. Keller, F. Vitalini, A. S. J. S. Mey, F. Noé, and B. G. Keller, *J. Chem. Phys.* **142**, 084101 (2015).

[26]P. Deuflhard and W. Marcus, *Linear Algebra and its Applications* **398**, 161 (2004).

[27]J.-P. Bouchaud and A. Georges, *Phys. Rep.* **195**, 127 (1990).

[28]M. Biskup, *Probab. Surv.* **8**, 294 (2011).

[29]V. V. Jikov, S. M. Kozlov, and O. A. Oleĭnik, *Homogenization of differential operators and integral functionals*, Springer-Verlag, Berlin, 1994, Translated from the Russian by G. A. Yosifian [G. A. Iosif′yan].

[30]R. Alicandro, M. Cicalese, and A. Gloria, *Archive for Rational Mechanics and Analysis* **200**, 881 (2011).

[31]M. Weber, *A Subspace Approach to Molecular Markov State Models via a New Infinitesimal Generator*, Habilitation thesis, Freien Universität Berlin, Zuse Institute Berlin, 2011.

[32]S. Kube and M. Weber, *AIP Conference Proceedings* **593** (2008).

[33]K. Fukuda, Frequently asked questions in polyhedral computation, 2004.

[34]G. R. Bowman, V. S. Pande, and F. Noé, editors, *An Introduction to Markov State Models and Their Application to Long Timescale Molecular Simulation*, volume 797 of Advances in Experimental Medicine and Biology, Springer, Heidelberg, 2014.

[35]D. Van Der Spoel, E. Lindahl, B. Hess, G. Groenhof, E. Mark, A., and J. Berendsen, H., *J. Comput. Chem.* **26(16)**, 1701 (2005).

[36]K. Lindorff-Larsen, S. Piana, K. Palmo, P. Maragakis, J. Klepeis, R. Dror, and E. Shaw, D., *Proteins* **78**, 1950 (2010).

[37]W. L. Jorgensen, J. Chandrasekhar, J. D. Madura, R. W. Impey, and M. Klein, *J. Chem. Phys.* **79**, 926 (1983).

[38]G. Bussi, D. Donadio, and M. Parrinello, *J. Chem. Phys.* **126**, 014101 (2007).

[39]R. W. Hockney, S. P. Goel, and J. Eastwood, *J. Comp. Phys.* **14**, 148 (1974).

[40]V. Durmaz, K. Fackeldey, and M. Weber, A rapidly-mixing monte carlo method for the simulation of slow molecular processes, in *Applications of Monte Carlo Methods in Biology, Medicine and Other Fields of Science*, edited by C. J. Mode, chapter 11, pages 399–424, InTech, 2011.

[41]T. Huber, A. E. Torda, and W. F. van Gunsteren, *J. Comput. Aided Mol. Des.* **8**, 695 (1994).

[42]A. Laio and M. Parrinello, *Proc. Natl. Acad. Sci. U.S.A.* **99**, 12562 (2002).

[43]G. Torrie and J. Valleau, *J. Comput. Phys* **23**, 187 (1977).

[44]L. Donati, C. Hartmann, and B. G. Keller, *J. Chem. Phys.* **146**, 244112 (2017).

[45]A. Cesari, A. Gil-Ley, and G. Bussi, *J. Chem. Theory Comput.* **12**, 6192 (2016).

[46]B. Keller, M. Christen, C. Oostenbrink, and W. F. Van Gunsteren, *J. Biomol. NMR* **37**, 1 (2007).

[47]A. Tsourtis, Y. Pantazis, M. Katsoulakis, and V. Harmandaris, *J. Chem. Phys.* **143**, 014116 (2015).

[48]G. Arampatzisa, M. Katsoulakis, and L. Rey-Bellet, *J. Chem. Phys.* **144**, 104107 (2016).

[49]S. Kube and M. Weber, *ZIB Report* **35** (2006).

[50]M. Weber, *ZIB Report* **611** (2009).

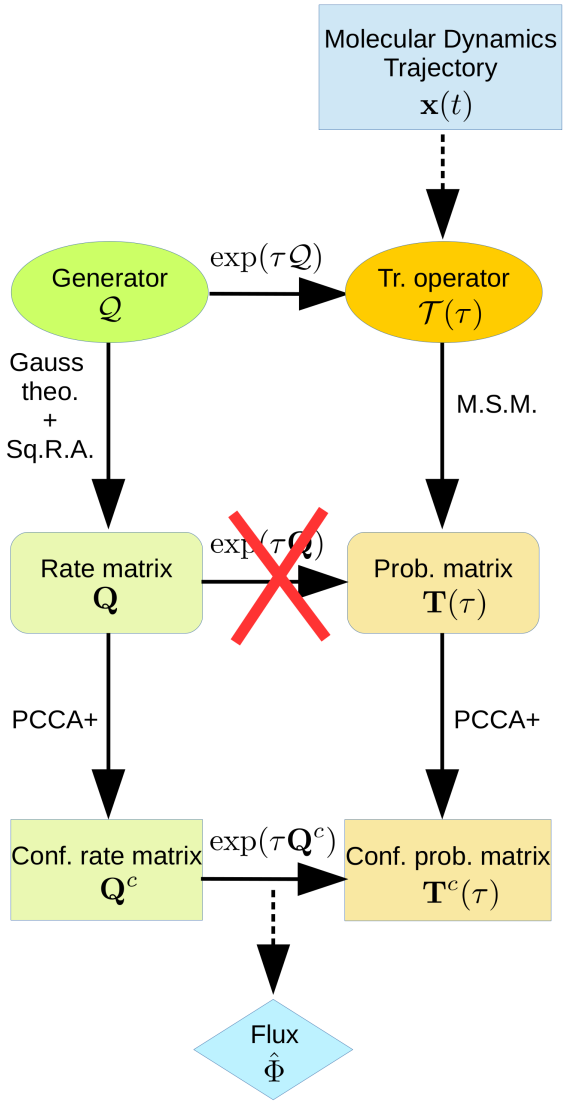

FIG. 1. Scheme summarizing the theory of the transfer operator, the generator and the associated transition matrices.

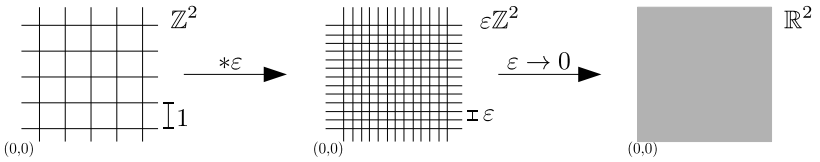

FIG. 2. The role of the parameter in the case $\varepsilon\mathbb{Z}^2$. As $\varepsilon \to 0$, the grid becomes finer and finer and approximates the whole of $\mathbb{R}^2$.

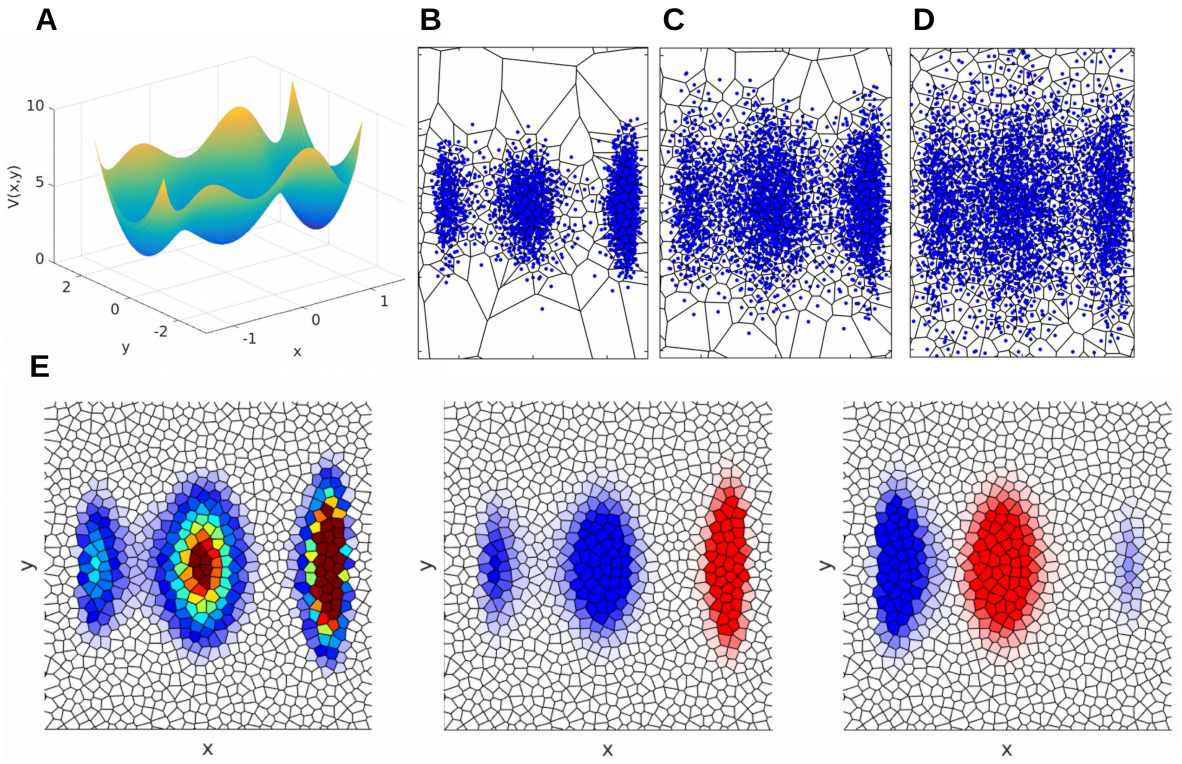

FIG. 3. Two-dimensional system. (A) Potential energy function. (B) Trajectory generated with $\sigma = 1.0$. (C) Trajectory generated with $\sigma = 1.5$. (D) Trajectory generated with $\sigma = 2.0$. (E) First three left eigenvectors of the rate matrix

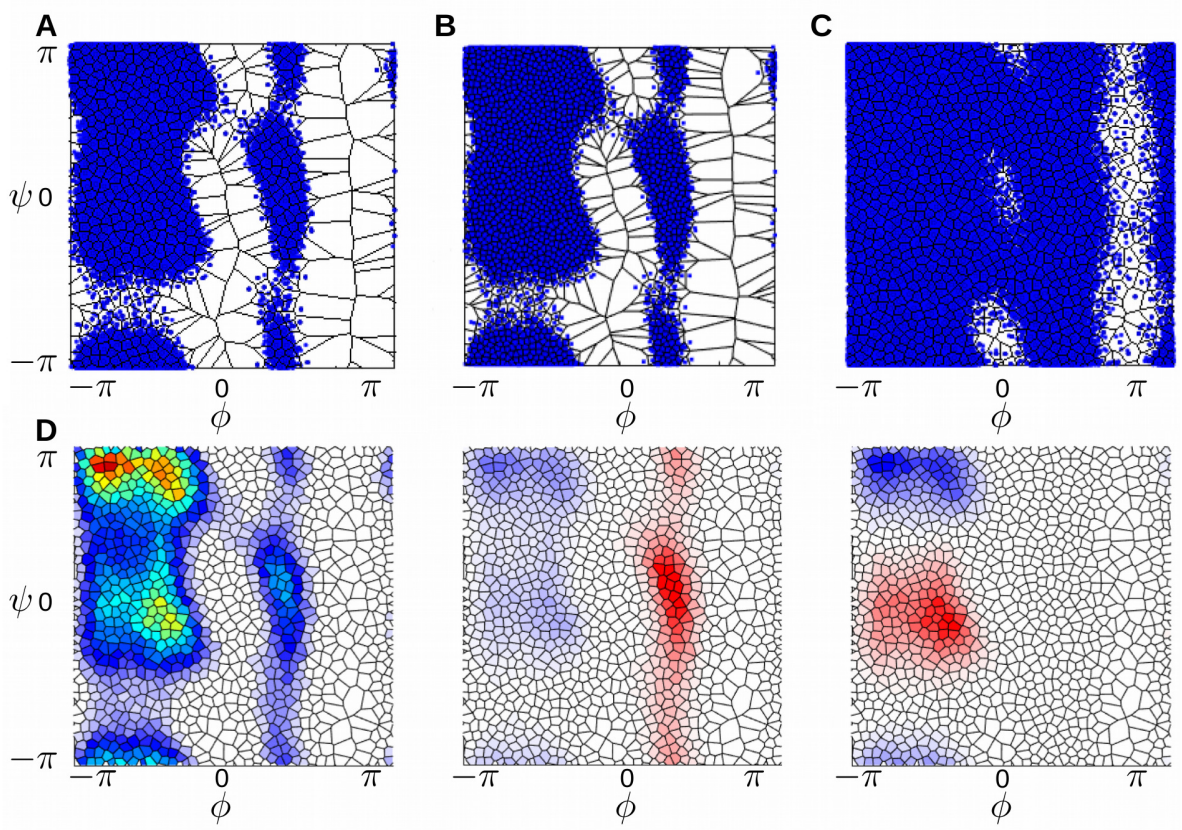

FIG. 4. Alanine dipeptide. (A) Trajectory (ϕ_n, ψ_n) generated at temperature 300 K, Voronoi tessellation with $r = 0.17$. (B) Trajectory (ϕ_n, ψ_n) generated at temperature 300 K, Voronoi tessellation with $r = 0.1$. (C) Trajectory (ϕ_n, ψ_n) generated at temperature 900 K, Voronoi tessellation with $r = 0.17$. (D) First three left eigenvector of the rate matrix.

i	θ_i	I.T.S. (time steps)
1	0	-
2	-0.0142	$70.5319\,\hat{\Phi}^{-1}$
3	-0.0522	$19.1482\,\hat{\Phi}^{-1}$
4	-0.0738	$13.5452\,\hat{\Phi}^{-1}$
5	-0.0871	$11.4772\,\hat{\Phi}^{-1}$
6	-0.1252	$7.9900\,\hat{\Phi}^{-1}$

TABLE I. Two dimensional system. First five eigenvalues and implied timescales as function of the flux. The volatility was set equal to 1.5 and the minimum distance between the centers of neighbor cells was set equal to $r = 0.1$.

i \ j	2	3	4	5	6
2	1.00	3.68	5.20	6.14	8.82
3	0.27	1.00	1.41	1.66	2.39
4	0.19	0.70	1.00	1.18	1.69
5	0.16	0.59	0.84	1.00	1.43
6	0.11	0.41	0.58	0.69	1.00

TABLE II. Two dimensional system. Ratio ITS_i/ITS_j between the first five implied timescales of table I. The volatility was set equal to 1.5 and the minimum distance between the centers of neighbor cells was set equal to $r = 0.1$.

σ	ncells	$\hat{\Phi}_2$	$\hat{\Phi}_3$	$\bar{\Phi}$	std	rel. err.
1.0	740	0.0080	0.0161	0.0121	0.0057	47,11%
1.5	1258	0.0461	0.0523	0.0492	0.0044	8.94%
2.0	1725	0.0913	0.0931	0.0922	0.0013	1.41%
2.5	2205	0.1427	0.1372	0.1400	0.0039	2.79%

TABLE III. Two dimensional system. Variation of the flux as function of the volatility σ. The minimum distance between the centers of neighbor cells was set equal to $r = 0.1$.

r	ncells	$\hat{\Phi}_2$	$\hat{\Phi}_3$	$\bar{\Phi}$	std	rel. err.
0.20	456	0.0207	0.0248	0.0227	0.0029	12.87%
0.15	784	0.0396	0.0425	0.0410	0.0021	5.12%
0.10	1725	0.0913	0.0931	0.0922	0.0013	1.41%

TABLE IV. Two dimensional system. Variation of the flux as function of the minimum distance between the centers of neighbor cells. The volatility was set equal to 2.0.

κ	ncells	$\hat{\Phi}_2$	$\hat{\Phi}_3$	$\bar{\Phi}$	std	rel. err.
0.0	1258	0.0461	0.0523	0.0492	0.0044	8.94%
0.5	1235	0.0459	0.0502	0.0480	0.0030	6.25%
1.0	1225	0.0449	0.0526	0.0487	0.0055	11.29%

TABLE V. Two dimensional system. Variation of the flux as function of an external perturbation. The volatility was set equal to 1.5 and $r = 0.1$.

κ	ncells	$\hat{\Phi}_2$	$\hat{\Phi}_3$	$\bar{\Phi}$	std	rel. err.
0.0	1725	0.0913	0.0931	0.0922	0.0013	1.41%
0.5	1722	0.0927	0.0922	0.0924	0.0003	0.36%
1.0	1720	0.0904	0.0926	0.0915	0.0015	1.64%

TABLE VI. Two dimensional system. Variation of the flux as function of an external perturbation. The volatility was set equal to 2.0 and $r = 0.1$.

Temp. (K)	r	ncells	$\hat{\Phi}_2$	$\hat{\Phi}_3$	$\bar{\Phi}$	std	rel. err.
900	0.20	740	11.4390	12.9166	12.1778	1.0448	8.58%
900	0.17	1005	17.0914	16.5862	16.8388	0.3572	2.12%
300	0.17	566	0.1238	2.5672	1.3455	1.7277	128.41%
300	0.14	792	0.1645	3.0356	1.6000	2.0301	126.88%
300	0.10	1423	0.3090	6.4278	3.3684	4.3266	128.45%

TABLE VII. Alanine dipeptide. Variation of the flux as function of the temperature and the parameter r.

Chapter 9

Conclusion and outlook

In this thesis we have presented several techniques [41, 59, 57] to improve the study of the dynamics of molecular systems. The high sensitivity exhibited by molecules subjected to external perturbations [6], has requested a deeper investigation of the models used in MD simulations, in order to improve the development of forcefields, i.e. the collection of parameters that rule the interaction between atoms in an MD simulation.

The first part of the thesis focused on MSMs and on how one would be possible to implement a reweighting scheme to build the MSM of a perturbed system, from the trajectory produced by MD simulation of an unbiased system.

The answer was provided by the Girsanov theorem [42], that permits a correct reweighting of MSMs [40, 41]. The method is based on the concept of path probability that is strictly dependent on the potential energy function of the system. The Girsanov theorem guarantees, under certain conditions, the existence of the ratio between two path probability densities, arisen from two different potential energy functions. This ratio permits the reweighting of path ensemble averages, like time-lagged correlation functions and consecutively of MSMs.

Such reweighting scheme has become necessary, because studying perturbations directly from MD simulations is extremely expensive from a computational point of view. Thus the main advantage of the method is to reduce the time to investigate the dynamical effects of a perturbation, through MD and MSMs analysis.

Girsanov reweighting is very versatile and could be implemented also with other MD techniques like variational and milestoning approaches [55, 83, 84, 85, 86], because they are based on path ensemble averages like MSMs.

A different research area of interest, where Girsanov reweighting could be useful, is the development of enhanced sampling methods, like metadynamics [43, 44, 45, 46] and umbrella sampling [29, 30]. Typically, such methods, where the Hamiltonian is perturbed by a bias, are used to explore the phase space and to build the free energy profile on few relevant coordinates. However, the bias of such techniques destroys the dynamics of the system and does not permit to build the MSM of the unbiased molecule. Girsanov reweighting can be used to recover the correct dynamical properties and to build the proper MSM. We have successfully implemented the method for metadynamics simulation [59, 81], for low dimensional diffusion processes and for full atomistic simulations. This has permitted to reduce the time necessary to build the MSM of a molecular system.

On the other hand, as for other reweighting schemes [37, 38, 39, 35, 36], the method is limited by the strength of the perturbation and on the choice of the lag time used to build the MSM. The error on the measure can indeed grow sharply, in particular on the estimation of the implied timescales. Thus a better understanding of the conditions

and the limitations of the Girsanov reweighting is necessary and will be treated in future works.

Another technique studied in this thesis is the so called Square Root Approximation [60, 57], which is used to estimate a discretization of the infinitesimal generator, i.e. a transition rate matrix. The rate matrix studies the dynamics of molecules in terms of rates between adjacent microsets of the state space, which are estimated as the product between the geometric average of their Boltzmann weights and the flux of configurations through the intersecting surface. The relevance of the method lies in the fact, that it does not depend on time-lagged correlation function as MSMs, but it directly depends on the potential energy function of the system. This characteristic is fundamental because it offers a simple scheme to reweight the generator when the system is externally perturbed, both by changing the temperature or modifying the potential energy function. If our insight is correct, this new method will close the gap in the reweighting methods for dynamical operators, offering a valid solution also from the point of view of the infinitesimal generator.

Bibliography

[1] J. M. Haile, *Molecular Dynamics Simulations: Elementary Methods*, vol. 797 of Advances in Experimental Medicine and Biology. New York: Wiley-Interscience, 1997.

[2] D. Frenkel and B. Smit, *Understanding Molecular Simulation: From Algorithms to Applications*. San Diego: Academic Press, 2nd ed., 2002.

[3] D. Bhella, "The role of cellular adhesion molecules in virus attachment and entry," *Philos. Trans. Royal Soc. B*, vol. 370, p. 20140035–20140035, 2014.

[4] S. Bhatia, L. C. Camacho, and L. C. xHaag, "Pathogen Inhibition by Multivalent Ligand Architectures," *J. Am. Chem. Soc.*, vol. 138, p. 8654–8666, 2016.

[5] C. T. Varner, T. Rosen, J. T. Martin, and R. S. Kane, "Recent Advances in Engineering Polyvalent Biological Interactions," *Biomacromolecules*, vol. 16, p. 43–55, 2014.

[6] F. Vitalini, A. S. J. S. Mey, F. Noé, and B. G. Keller, "Dynamic properties of force fields," *J. Chem. Phys.*, vol. 142, p. 084101, 2015.

[7] A. Ramanathan and P. K. Agarwal, "Computational identification of slow conformational fluctuations in proteins," *J. Phys. Chem. B*, vol. 113, p. 16669–16680., 2009.

[8] D. E. Shaw, M. M. Deneroff, R. O. Dror, J. S. Kuskin, R. H. Larson, J. K. Salmon, C. Young, B. Batson, K. J. Bowers, J. C. Chao, M. P. Eastwood, J. Gagliardo, J. Grossman, C. R. Ho, D. J. Ierardi, I. Kolossváry, J. L. Klepeis, T. Layman, C. McLeavey, M. A. Moraes, R. Mueller, E. C. Priest, Y. Shan, J. Spengler, M. Theobald, B. Towles, and S. C. Wang, "Anton, A Special-Purpose Machine For Molecular Dynamics Simulation," *Commun. ACM*, vol. 51, pp. 91–97, 2008.

[9] D. E. Shaw, R. O. Dror, J. K. Salmon, J. Grossman, K. M. Mackenzie, J. A. Bank, C. Young, M. M. Deneroff, B. Batson, K. J. Bowers, E. Chow, M. P. Eastwood, D. J. Ierardi, J. L. Klepeis, R. H. Kuskin, Jeffrey S.and Larson, K. Lindorff-Larsen, P. Maragakis, M. A. Moraes, S. Piana, Y. Shan, and B. Towles, "Millisecond-scale molecular dynamics simulations on Anton," *SC '09: Proceedings of the Conference on High Performance Computing Networking, Storage and Analysis*, vol. 39, pp. 1–11, 2009.

[10] A. Lasota and M. C. Mackey, *Chaos, Fractals and Noise, volume 97 of Applied Mathe- matical Sciences*. New York: Springer, 2nd ed., 1994.

[11] C. Schütte, A. Fischer, W. Huisinga, and P. Deuflhard, "A Direct Approach to Conformational Dynamics Based on Hybrid Monte Carlo," *J. Comput. Phys.*, vol. 151, pp. 146–168, 1999.

[12] C. Schütte, W. Huisinga, and P. Deuflhard, "Transfer operator approach to conformational dynamics in biomolecular systems," in *Ergodic Theory, Analysis, and Efficient Simulation of Dynamical Systems* (B. Fiedler, ed.), pp. 191–223, Berlin: Springer, 2001.

[13] J.-H. Prinz, H. Wu, M. Sarich, B. Keller, M. Senne, M. Held, J. D. Chodera, C. Schütte, and F. Noé, "Markov models of molecular kinetics: generation and validation.," *J. Chem. Phys.*, vol. 134, p. 174105, 2011.

[14] S. Klus, F. Nüske, P. Koltai, H. Wu, I. Kevrekidis, C. Schütte, and F. Noé, "Data-Driven Model Reduction and Transfer Operator Approximation," *J. Nonlinear Sci.*, vol. 28, p. 985–1010, 2018.

[15] P. Deuflhard, W. Huisinga, A. Fischer, and C. Schütte, "Identification of almost invariant aggregates in reversible nearly uncoupled Markov chains," *Linear Algebra Appl.*, vol. 315, no. 1-3, pp. 39–59, 2000.

[16] W. C. Swope, J. W. Pitera, F. Suits, M. Pitman, M. Eleftheriou, B. G. Fitch, R. S. Germain, A. Rayshubski, T. J. C. Ward, Y. Zhestkov, and R. Zhou, "Describing Protein Folding Kinetics by Molecular Dynamics Simulations. 2. Example Applications to Alanine Dipeptide and a -Hairpin Peptide †," *J. Phys. Chem. B*, vol. 108, pp. 6582–6594, 2004.

[17] J. D. Chodera, N. Singhal, V. S. Pande, K. A. Dill, and W. C. Swope, "Automatic discovery of metastable states for the construction of Markov models of macromolecular conformational dynamics.," *J. Chem. Phys.*, vol. 126, p. 155101, 2007.

[18] N.-V. Buchete and G. Hummer, "Coarse master equations for peptide folding dynamics.," *J. Phys. Chem. B*, vol. 112, no. 19, pp. 6057–6069, 2008.

[19] B. Keller, X. Daura, and W. F. Van Gunsteren, "Comparing geometric and kinetic cluster algorithms for molecular simulation data.," *J. Chem. Phys.*, vol. 132, no. 7, p. 074110, 2010.

[20] B. Keller, P. Hünenberger, and W. F. van Gunsteren, "An Analysis of the Validity of Markov State Models for Emulating the Dynamics of Classical Molecular Systems and Ensembles," *J. Chem. Theory Comput.*, vol. 7, pp. 1032–1044, 2011.

[21] G. R. Bowman, V. S. Pande, and F. Noé, eds., *An Introduction to Markov State Models and Their Application to Long Timescale Molecular Simulation*, vol. 797 of Advances in Experimental Medicine and Biology. Heidelberg: Springer, 2014.

[22] V. A. Voelz, G. R. Bowman, K. A. Beauchamp, and V. S. Pande, "Molecular Simulation of Ab Initio Protein Folding for a Millisecond Folder NTL9 (1- 39)," *J. Am. Chem. Soc.*, vol. 132, pp. 1526–1528, 2010.

[23] G. D. Fabritiis, N. Stanley, and S. Esteban-martõ, "Kinetic modulation of a disordered protein domain by phosphorylation," *Nat. Commun.*, vol. 5, p. 5272, 2014.

[24] G. R. Bowman, E. R. Bolin, K. M. Hart, B. C. Maguire, and S. Marqusee, "Discovery of multiple hidden allosteric sites by combining Markov state models and experiments.," *Proc. Natl. Acad. Sci. U.S.A.*, vol. 112, pp. 2734–9, 2015.

[25] N. Plattner and F. Noé, "Protein conformational plasticity and complex ligand-binding kinetics explored by atomistic simulations and Markov models," *Nat. Commun.*, vol. 6, pp. 7653–10, 2015.

[26] L. Zhang, I. C. Unarta, P. P.-H. Cheung, G. Wang, D. Wang, and X. Huang, "Elucidation of the Dynamics of Transcription Elongation by RNA Polymerase II using Kinetic Network Models," *Accounts Chem. Res.*, vol. 49, pp. 698–694, 2016.

[27] J. Witek, B. G. Keller, M. Blatter, A. Meissner, T. Wagner, and S. Riniker, "Kinetic Models of Cyclosporin A in Polar and Apolar Environments Reveal Multiple Congruent Conformational States," *J. Chem. Inf. Model.*, vol. 56, pp. 1547–1562, July 2016.

[28] S. Kumar, J. M. Rosenberg, D. Bouzida, R. H. Swendsen, and P. A. Kollman, "The weighted histogram analysis method for free-energy calculations on biomolecules. I. The method.," *J. Comp. Chem.*, vol. 13, no. 8, p. 1011–1021, 1992.

[29] G. Torrie and J. Valleau, "Nonphysical Sampling Distributions in Monte Carlo Free-Energy Estimation: Umbrella Sampling," *J. Comput. Phys*, vol. 23, pp. 187–199, 1977.

[30] J. Kästner and W. Thiel, "Bridging the gap between thermodynamic integration and umbrella sampling provides a novel analysis method: "Umbrella inegration"," *J. Chem. Phys.*, vol. 123, p. 144104, 2005.

[31] M. Souaille and B. Roux, "Extension to the weighted histogram analysis method: combining umbrella sampling with free energy calculations," *Comp. Phys- Comm.*, vol. 135, no. 1, p. 40–57, 2001.

[32] J.-H. Prinz, J. D. Chodera, V. S. Pande, W. C. Swope, J. C. Smith, and F. Noé, "Optimal use of data in parallel tempering simulations for the construction of discrete-state Markov models of biomolecular dynamics," *J. Chem. Phys.*, vol. 134, pp. 244108–14, June 2011.

[33] J. D. Chodera, W. C. Swope, F. Noé, J.-H. Prinz, M. R. Shirts, and V. S. Pande, "Dynamical reweighting: Improved estimates of dynamical properties from simulations at multiple temperatures," *J. Chem. Phys.*, vol. 134, pp. 244107–15, June 2011.

[34] D. D. L. Minh and J. D. Chodera, "Optimal estimators and asymptotic variances for nonequilibrium path-ensemble averages," *J. Chem. Phys.*, vol. 131, pp. 134110–10, Oct. 2009.

[35] P. Tiwary and M. Parrinello, "From Metadynamics to Dynamics," *Phys. Rev. Lett.*, vol. 111, p. 230602, 2013.

[36] R. Casasnovas, V. Limongelli, P. Tiwary, P. Carloni, and M. Parrinello, "Unbinding Kinetics of a p38 MAP Kinase Type II Inhibitor from Metadynamics Simulations," *J. Am. Chem. Soc.*, vol. 139, pp. 4780–4788, 2017.

[37] H. Wu, A. S. J. S. Mey, E. Rosta, and F. Noé, "Statistically optimal analysis of state-discretized trajectory data from multiple thermodynamic states," *J. Chem. Phys.*, vol. 141, p. 214106, 2014.

[38] H. Wu, F. Paul, C. Wehmeyer, and F. Noé, "Multiensemble Markov models of molecular thermodynamics and kinetics.," *Proc. Natl. Acad. Sci. U.S.A.*, vol. 113, pp. E3221–30, 2016.

[39] E. Rosta and G. Hummer, "Free Energies from Dynamic Weighted Histogram Analysis Using Unbiased Markov State Model," *J. Chem. Theory Comput.*, vol. 11, pp. 276–285, Dec. 2014.

[40] C. Schütte, A. Nielsen, and M. Weber, "Markov state models and molecular alchemy," *Mol. Phys.*, vol. 113, pp. 69–78, 2015.

[41] L. Donati, C. Hartmann, and B. G. Keller, "Girsanov reweighting for path ensembles and markov state models," *J. Chem. Phys.*, vol. 146, no. 24, p. 244112, 2017.

[42] B. Øksendal, *Stochastic Differential Equations: An Introduction with Applications*. Berlin: Springer Verlag, 6th ed., 2003.

[43] T. Huber, A. Torda, and W. van Gunsteren, "Local elevation: A method for improving the searching properties of molecular dynamics simulation," *J. Comput. Aided Mol. Des.*, vol. 8, pp. 695–708, 1994.

[44] A. Laio and M. Parrinello, "Escaping free-energy minima.," *Proc. Natl. Acad. Sci. U.S.A.*, vol. 99, pp. 12562–6, 2002.

[45] A. Barducci, G. Bussi, and M. Parrinello, "Well-tempered metadynamics: A smoothly converging and tunable free-energy method.," *Phys. Rev. Lett.*, vol. 100, p. 020603, 2008.

[46] A. Barducci, M. Bonomi, and M. Parrinello, "Metadynamics," *Wiley Interdisciplinary Reviews: Computational Molecular Science*, vol. 1, p. 826–843, 2011.

[47] S. Nosé, "A molecular dynamics method for simulations in the canonical ensemble," *Mol. Phys.*, vol. 52, p. 255, 1984.

[48] S. Nosé, "A unified formulation of the constant temperature molecular dynamics methods," *J. Chem. Phys.*, vol. 81, p. 511, 1984.

[49] W. G. Hoover, "Canonical dynamics: Equilibrium phase-space distributions ," *Phys. Rev. A*, vol. 31, p. 1695, 1985.

[50] D. A. McQuarrie, *Statistical Mechanics*. University Science Books, 2000.

[51] J. Sethna, *Statistical Mechanics: Entropy, Order Parameters, and Complexity*. Oxford: Oxford University Press, 2006.

[52] C. W. Gardiner, *Handbook of Stochastic Methods*. Berlin: Springer Verlag, 2nd ed., 1997.

[53] B. O. Koopman, "Hamiltonian dynamics and transformations in Hilbert space," *Proc. Nat. Acad. Sci.*, vol. 17, p. 315–318, 1931.

[54] H. Risken, *The Fokker-Planck Equation. Methods of Solution and Applications.* Berlin: Springer Verlag, 2nd ed., 1989.

[55] F. Nüske, B. Keller, G. Perez-Hernandez, A. S. J. S. Mey, and F. Noe, "Variational Approach to Molecular Kinetics," *J. Chem. Theory Comput.*, vol. 10, pp. 1739–1752, 2014.

[56] B. G. Keller, S. Aleksic, and L. Donati, "Markov state models in drug design," in *Biomolecular Simulations in Structure-based Drug Discovery* (F. L. Gervasio, ed.), p. 67, Weinheim: Wiley-Interscience, 2018.

[57] L. Donati, M. Heida, B. G. Keller, and M. Weber, "Estimation of the infinitesimal generator by square-root approximation," *J. Phys. Condens. Matter*, accepted, online 7 september 2018.

[58] I. V. Girsanov, "On transforming a certain class of stochastic processes by absolutely continuous substitution of measures," *Theory Probab. Appl.*, vol. 5, no. 3, pp. 285–301, 1960.

[59] L. Donati and B. G. Keller, "Girsanov reweighting for metadynamics simulations," *J. Chem. Phys.*, vol. 149, p. 072335, 2018.

[60] H. C. Lie, K. Fackeldey, and M. Weber, "A square root approximation of transition rates for a markov state model," *SIAM. J. Matrix Anal. Appl.*, vol. 34, pp. 738–756, 2013.

[61] D. J. Bicout and A. Szabo, "Electron transfer reaction dynamics in non-Debye solvents," *J. Chem. Phys.*, vol. 109, p. 10.1063/1.476800, 1998.

[62] P. D. Dixit, A. Jain, G. Stock, and K. A. Dill, "Inferring Transition Rates of Networks from Populations in Continuous-Time Markov Processes," *J. Chem. Theory Comput.*, vol. 11, pp. 5464–5472, 2015.

[63] E. Fischer, "Einfluss der configuration auf die wirkung der enzyme. ii," *Ber. Dtsch. Ges.*, vol. 27, no. 3, pp. 3479–3483, 1894.

[64] J. Monod, J. Wyman, and J.-P. Changeux, "On the Nature of Allosteric Transitions: A Plausible Model," *J. Mol. Biol.*, vol. 12, pp. 88–118, 1965.

[65] D. E. Koshland, G. Namethy, and D. Filmer, "Comparison of experimental binding data and theoretical models in proteins containing subunits," *ACS Biochem.*, vol. 5, no. 1, pp. 365–385, 1966.

[66] S. Mukherjee, G. A. Pantelopulos, and V. A. Voelz, "Markov models of the apo-MDM2 lid region reveal diffuse yet two-state binding dynamics and receptor poses for computational docking," *Sci. Rep.*, vol. 6, no. 1, p. 1038, 2016.

[67] R. Takahashi, V. A. Gil, and V. Guallar, "Monte Carlo Free Ligand Diffusion with Markov State Model Analysis and Absolute Binding Free Energy Calculations," *J. Chem. Theory Comput.*, vol. 10, no. 1, pp. 282–288, 2013.

[68] Q. Bai, H. Pérez-Sánchez, Y. Zhang, Y. Shao, D. Shi, H. Liu, and X. Yao, "Ligand induced change of β2 adrenergic receptor from active to inactive conformation and its implication for the closed/open state of the water channel: insight from molecular dynamics simulation, free energy calculation and Markov state model analysis," *Phys. Chem. Chem. Phys.*, vol. 16, no. 30, pp. 15874–15885, 2014.

[69] K. J. Kohlhoff, D. Shukla, M. Lawrenz, G. R. Bowman, D. E. Konerding, D. Belov, R. B. Altman, and V. S. Pande, "Cloud-based simulations on Google Exacycle reveal ligand modulation of GPCR activation pathways," *Nat. Chem.*, vol. 6, pp. 15–21, 2014.

[70] D. Shukla, Y. Meng, B. Roux, and V. S. Pande, "Activation pathway of Src kinase reveals intermediate states as novel targets for drug design," *Nat. Commun.*, vol. 5, p. 3397, 2014.

[71] S. Gu, D.-A. Silva, L. Meng, A. Yue, and X. Huang, "Quantitatively Characterizing the Ligand Binding Mechanisms of Choline Binding Protein Using Markov State Model Analysis," *PLoS Comput. Biol.*, vol. 10, no. 8, p. e1003767, 2014.

[72] N. Stanley, L. Pardo, and G. De Fabritiis, "The pathway of ligand entry from the membrane bilayer to a lipid G protein-coupled receptor," *Sci. Rep.*, pp. 1–8, 2016.

[73] G. Zhou, G. A. Pantelopulos, S. Mukherjee, and V. A. Voelz, "Bridging microscopic and macroscopic mechanisms of p53-MDM2 binding using molecular simulations and kinetic network models," *Biophys. J.*, vol. 113, no. 4, pp. 785–793, 2017.

[74] I. Hassan, L. Donati, B. G. Keller, T. Stensitzk, K. Heyne, and P. Imhof, "The vibrational spectrum of the hydrated alanine-leucine peptide in the amide region from ir experiments and first principles calculations," *Chem. Phys. Lett.*, vol. 698, p. 227, 2018.

[75] P. Deuflhard and W. Marcus, "Robust perron cluster analysis in conformation dynamics," *Linear Algebra and its Applications*, vol. 398, pp. 161–184, 2004.

[76] D. Marx and J. Hutter, *Ab Initio Molecular Dynamics: The Virtual Laboratory Approach*. Cambridge University Press, 2010.

[77] A. Tsourtis, Y. Pantazis, M. Katsoulakis, and V. Harmandaris, "Parametric sensitivity analysis for stochastic molecular systems using information theoretic metrics," *J. Chem. Phys.*, vol. 143, p. 014116, 2015.

[78] G. Arampatzisa, M. Katsoulakis, and L. Rey-Bellet, "Efficient estimators for likelihood ratio sensitivity indices of complex stochastic dynamics," *J. Chem. Phys.*, vol. 144, p. 104107, 2016.

[79] Y. Sugita and Y. Okamoto, "Replica-exchange multicanonical algorithm and multicanonical replica-exchange method for simulating systems with rough energy landscape," *Chem. Phys. Lett.*, vol. 329, pp. 261–270, 2000.

[80] P. Eastman, M. S. Friedrichs, J. D. Chodera, R. J. Radmer, C. M. Bruns, J. P. Ku, K. A. Beauchamp, T. J. Lane, L.-P. Wang, D. Shukla, T. Tye, M. Houston, T. Stich, C. Klein, M. R. Shirts, and V. S. Pande, "Openmm 4: A reusable, extensible, hardware independent library for high performance molecular simulation.," *J. Chem. Theory Comput.*, vol. 9(1), pp. 461–469, 2013.

[81] J. Quer, L. Donati, and B. G. Keller, "An automatic adaptive importance sampling algorithm for molecular dynamics in reaction coordinates," *SIAM J. Sci. Comput.*, vol. 40, p. A653–A670, 2018.

[82] M. Heida, "Convergences of the squareroot approximation scheme to the fokker–planck operator," *Math. Models Methods Appl. Sci.*, accepted, 14 July 2018.

[83] F. Nüske, F. Schneider, F. Vitalini, and F. Noe, "Variational tensor approach for approximating the rare-event kinetics of macromolecular systems," *J. Chem. Phys.*, vol. 144, p. 054105, 2016.

[84] F. Vitalini, F. Noe, and B. G. Keller, "A Basis Set for Peptides for the Variational Approach to Conformational Kinetics," *J. Chem. Theory Comput.*, vol. 11, pp. 3992–4004, 2015.

[85] C. Schütte, F. Noé, J. Lu, M. Sarich, and E. Vanden-Eijnden, "Markov state models based on milestoning," *J. Chem. Phys.*, vol. 134, no. 20, 2011.

[86] O. Lemke and B. G. Keller, "Density-based cluster algorithms for the identification of core sets," *J. Chem. Phys.*, vol. 164104, no. 145, pp. 1–36, 2016.